THE ELECTROCHEMICAL REDUCTION OF DICHROMATE

Thesis submitted to the
University of Newcastle upon Tyne

for the Degree of Doctor of Philosophy

by

W. MAKEPEACE, B.Sc.

SEPTEMBER, 1973

ABSTRACT

The reduction of dichromate to chromic ion has been studied in sulphuric and perchloric acid solutions in connection with the possible use of dichromate as a depolariser in a primary battery. Gold and pyrolytic graphite electrodes have been used.

At a gold electrode the current increases rapidly to a limiting value. Potential-sweep experiments and electron diffraction studies indicate that the rate of reduction is controlled by the properties of a surface film. The nature of this film is altered by potential and is also modified by addition of foreign anions.

On a pyrolytic graphite electrode in perchloric acid, film deposition and modification again considerably modify the rate of reduction. In sulphuric acid solutions, however, the form of the current-potential curves obtained is not determined primarily by the properties of a surface film. Under these conditions it was shown that dimeric CrVI species are reduced at more positive potentials than the monomeric species. The kinetics of the reduction of the monomeric species has been investigated.

INDEX

1. INTRODUCTION

The aim of this research was to study the kinetics and mechanism of the electrochemical reduction of the dichromate ion to Cr III in acid solutions. In most of the work, graphite or gold was employed as the electrode material in solutions containing either perchloric or sulphuric acid as background electrolyte. In order to investigate the effect of dichromate concentration under conditions of constant ionic strength, the solutions employed were normally about 1 M in background electrolyte and between 10^{-4} and 10^{-2} M in Cr VI. The effect of changing the H^+ concentration was also investigated, using background electrolytes containing both the acid and its sodium or potassium salt to maintain constant ionic strength. The effect of additions of other foreign ions was studied briefly.

Although there have been many previous studies of the reduction of dichromate, much of the published work has been concerned with the mechanism of chromium plating. The behaviour observed in the concentrated solutions (c.a. 3 M in Cr VI) normally used in this process, is more complex than in dilute solutions. This complexity is mainly due to the formation of inhibiting films on the electrode surface. Other studies have been concerned with the processes occurring at a dropping mercury electrode in neutral and alkaline media. Relatively few papers report measurements under conditions comparable with those employed here. Reported studies in these

three composition ranges are discussed in separate sections below.

At least five different chromium-containing species may be present in dichromate solutions, their relative concentrations varying with both the total concentration of Cr VI and the pH. A proper understanding of the electrode reactions occurring in such media necessitates a knowledge of these concentrations. The equilibria involved are discussed below.

1.1 Species present in dichromate solutions

The equilibria existing in acidic solutions of Cr VI have been studied by several workers[1.1-1.7]. With the exception of Neuss and Rieman[1.1], who measured the hydrogen ion activity in dichromate solutions using a glass electrode, all other workers obtained the equilibrium constants by spectrophotometric methods.

The equilibria believed to exist in perchloric acid solutions and the values of the equilibrium constants obtained are given in table 1.1.

The evaluation of K_3 from the results reported in references 1.4, 1.5 and 1.6 may be made in two ways, depending on whether or not the protonation of $Cr_2O_7^=$ is taken into account. Unfortunately, there is no direct evidence for the presence or absence of $HCr_2O_7^-$. Equilibrium constants (in terms of concentrations) based on the assumption that $HCr_2O_7^-$ is not present are given in square brackets.

TABLE 1.1

Reaction		Equilibrium Constant					
		Ref. 1.1	Ref. 1.2	Ref. 1.3	Ref. 1.4, 1.5	Ref. 1.6	Ref. 1.7
$2HCrO_4^- \rightleftharpoons Cr_2O_7^= + H_2O$	K_1/litre mole^{-1}	(43.5)	(33)	(34)	93(33.2)	-	-
$HCrO_4^- \rightleftharpoons H^+ + CrO_4^=$	K_2/mole litre^{-1}	(3.2×10^{-7})	-	-	-	-	(3.0×10^{-7})
$HCrO_4^- + H^+ \rightleftharpoons H_2CrO_4$	K_3/litre mole^{-1}	3.45	-	-	0.83[0.24]	[0.2]	-
$HCr_2O_7^- \rightleftharpoons H^+ + Cr_2O_7^{2-}$	K_4/mole litre^{-1}	-	-	-	0.85	-	-

Thermodynamic constants are given in parentheses.

TABLE 1.2

Acid	Equilibria	Equilibrium Constant
H_2SO_4	$HSO_4^- + HCrO_4^- \rightleftharpoons CrSO_7^= + H_2O$	K_5 = 4.1 litre mole^{-1}
HCl	$H^+ + Cl^- + HCrO_4^- \rightleftharpoons CrO_3Cl^- + H_2O$	K_6 = 17 litre mole^{-1}
H_3PO_4	$H_3PO_4 + HCrO_4^- \rightleftharpoons H_2CrPO_7^- + H_2O$	K_7 = 9.4 litre mole^{-1}
	$H_2PO_4^- + HCrO_4^- \rightleftharpoons HCrPO_7^= + H_2O$	K_8 = 2.9 litre mole^{-1}

The values of K_1 and K_3 reported by Neuss and Rieman[1.1] are not in agreement with those obtained by the more direct spectrophotometric measurements, and are therefore suspect.

Haight et al.[1.6] have studied the monomolecular Cr VI species present in solutions containing acids other than perchloric acid. In sulphuric, hydrochloric and phosphoric acids additional equilibria exist; these are listed in table 1.2. No new species were found in the presence of nitric or acetic acids.

The concentrations of the Cr VI species present in both perchloric and sulphuric acid solutions are shown as a function of the total chromium concentration in Figs. 1.1 to 1.4. Figs. 1.1 and 1.2 both refer to 0.5 M H_2SO_4, in the former $H\,Cr_2O_7^-$ was assumed to be present, while this species is ignored in the latter. Tables of the concentrations of the various Cr VI species in the solutions employed in the present work are presented in Appendix I.

The equilibrium constants used in calculating these concentrations were those of Tong and King[1.4] (K_1, K_3 and K_4), Howard et al.[1.7] (K_2) and Haight et al.[1.6] (K_5). Since K_2 is very small, the concentration of CrO_4^- is negligibly small in solutions where $[H^+] > 10^{-3}$ M. This species has therefore been ignored in the present work.

1.2 Reduction in neutral and alkaline media

Over the pH range 6.5-13, in dilute solutions of Cr VI ($< 10^{-2}$ M), the current-potential curve obtained

at a dropping mercury electrode may display up to three well defined waves and a pre-wave.

In such solutions, the Cr VI exists almost exclusively as the ions $CrO_4^=$ and $HCrO_4^-$. Since the reaction

$$HCrO_4^- \rightleftharpoons CrO_4^= + H^+$$

has a pK of 6.8, the $CrO_4^=$ ion predominates.

Lingane and Kolthoff[1.8], using a neutral, unbuffered KCl solution, obtained three well defined waves corresponding to the reduction of Cr VI to Cr III, Cr II and Cr (0) respectively. The first wave (A), was preceded by a pre-wave which had the form of a rounded maximum, insensitive to the usual suppressors. Only wave A and the pre-wave need concern us further. The amplitude of the pre-wave, but not wave A, decreased as the solution was made more alkaline. The relative amplitude of the maximum decreased linearly with decrease in the chromate concentration.

Lingane and Kolthoff considered that the pre-wave and wave A were in reality one wave corresponding to the reduction of $CrO_4^=$ to Cr III. The decrease in current, which gives the wave the appearance of a pre-wave and main wave, was attributed to inhibition of the reduction by a film of chromium hydroxide. While this suggestion explains many of the observations it has a number of shortcomings[1.10]; in particular the current oscillations did not show the irregularities which normally accompany film formation.

Green and Walkley[1.9] studied the reduction reaction in bicarbonate buffers over the pH range 6.56 to 12.50. On the basis of their results they offered two alternative explanations of the observed phenomena.

In the first, the polarogram is considered to consist not of a pre-wave and main wave but of two waves, the first of which has a maximum of a type not suppressible with the usual reagents. The plateau current of the first wave was independent of the height of the mercury column suggesting that it was kinetically controlled. Green and Walkley assumed that a singly charged anion would be more readily reduced than a doubly charged one at the negatively charged mercury surface. They therefore suggested that the first wave corresponds to the reduction of $HCrO_4^-$, its concentration at the electrode being largely determined by the rate of the preceding chemical step

$$CrO_4^{=} + H^+ \longrightarrow HCrO_4^- \qquad (1.1)$$

The second wave was attributed to the reduction of $CrO_4^{=}$. The change in the relative heights of the two waves with pH was readily explicable on this basis.

The alternative explanation advanced by these authors, like that of Lingane and Kolthoff, is based on the assumption that the polarogram consists of only one wave, its distorted shape being attributed to electrostatic repulsion effects. Thus at potentials more negative than the maximum in the curves, the mercury surface becomes negatively charged and exerts a repulsive force on the negatively

charged electroactive ion. This causes a reduction in the number of ions reaching the electrode surface and hence in the current. The electroactive ion was still considered to be the $HCrO_4^-$ ion, produced by a preceding chemical step as described previously.

In a detailed study of the reaction, Gierst et al.[1.10] confirmed many of the previous findings. They concluded that the mechanism is probably a combination of the two mechanisms suggested by Green and Walkley. Thus the pre-wave probably corresponds to the reduction of $HCrO_4^-$, produced by the preceding chemical step of equation (1.1). The maximum in this pre-wave appears to be the result of double-layer effects. The $CrO_4^=$ ion is specifically adsorbed on the mercury surface but the amount adsorbed decreases as the potential is made more negative. Since the $HCrO_4^-$ ion can be produced from both adsorbed $CrO_4^=$ and $CrO_4^=$ in the solution, a decrease in the amount of adsorbed $CrO_4^=$ would lead to a decrease in the current. The main wave was attributed to the reduction of the $CrO_4^=$ by a slow electron-transfer process.

None of the foregoing explanations, however, will account for all the experimental results on the maximum in the pre-wave. In particular the maximum current can be considerably higher than that predicted from the Ilkovic equation.

Further studies of this reaction[1.11,1.12] have essentially confirmed the mechanism suggested by Gierst et al. Some further complexities have however been noted. It

has been shown, for example, that whereas the maximum observed in unbuffered halide solutions is unaffected by gelatin, that observed in buffer solutions is suppressed by the addition of gelatin.

It appears therefore that the main processes occurring in these solutions are:

1) The initial reduction of $HCrO_4^-$, its concentration at the electrode being determined by the rate of the preceding chemical step

$$CrO_4^{2-} + H^+ = HCrO_4^-,$$

occurring both in the solution and also involving CrO_4^{2-} adsorbed on the electrode surface.

2) The subsequent reduction of CrO_4^{2-}, by a slow electron transfer process.

1.3 Reduction in acid solutions

The behaviour observed in acid dichromate solutions depends upon the relative concentrations of CrVI and added acid, the nature of the acid, and the electrode material used.

1.3.1 Pure chromic acid solutions

When foreign acids are either wholly absent or present in very small concentration, the reduction process is seriously inhibited at all metal electrodes[1.13]. Thus, for example, with platinum and gold[1.14,1,15], although their open circuit potentials are close to the equilibrium potential for the reaction

$$H_2CrO_4 + 6H^+ + e = Cr^{3+} + 4H_2O, \quad E_H^o = 1.36 \text{ V}$$

no significant current flows on cathodic polarisation until the potential is approximately -0.4 V. The process occurring under these conditions is almost exclusively hydrogen evolution. At very negative potentials small amounts of oxygen-containing chromium (black chromium) is produced[1.13].

It is generally accepted that this inhibition of dichromate reduction is caused by the presence of a film of some chromium compound. The nature and properties of this film are, however, incompletely understood.

Müller[1.14] suggested that the film was an insoluble and unreducible chromi-chromate, which resulted from reaction between the cathodically-produced lower valent chromium ions and CrVI. He also postulated that the film was semi-permeable, allowing H^+ and H_2, but not

chromic acid, to pass through it. This view received considerable support[1.16,1.17] but little experimental evidence was available until more recently.

Evidence for the existence of a film on gold electrodes has been provided by double-layer capacitance measurements[1.15]. Potentiostatic, current-time curves[1.15,1.18] have also shown that with gold and platinum an initial layer, 1-2 molecules thick, is produced very rapidly. This conclusion has been confirmed from galvanostatic, potential-time curves[1.19], which also showed that reduction of the noble metal oxide preceded formation of the film.

Gerischer and Käppel[1.15] found that under constant potential conditions, the film on gold thickens slowly. Electron diffraction patterns were obtained with sufficiently thick films. Although the patterns were not characterised, they showed that the structure and chemical composition of the film depend on the potential at which it is formed.

These thick films were shown to be impervious to mercury and to possess high electronic conductivity. Unfortunately, the range of potentials over which conducting films are formed was not reported. Since the potential of the layer-covered electrode varied with the partial-pressure of oxygen, it was concluded that the layer probably consists of chromium oxides. If a mixture of valency states is present, as is likely over at least part of the available potential range,

the layer would be expected to show semiconducting properties and hence a low electrical resistance.

Gerischer and Käppel argued that because the current-time transients indicated that the layer was formed rapidly, any holes would be expected to be closed quickly and hence the layer is unlikely to be semi-permeable. They consider that the fact that the layer inhibits the reduction of CrVI but still allows hydrogen evolution to occur is consistent with the established selectivity of semiconductor electrodes toward electrode reactions.

Relatively few studies have been made of the film produced on non-noble metals. Sysoev et al.[1.21], using chemical analysis, showed that the films formed on copper and stainless steel consist essentially of only $Cr(OH)_3$. This conclusion receives support from the electron-diffraction studies[1.22] of the films formed on Fe, Ni, Cr, Cu and Ag, where only ~~CrO_3~~ $Cr(OH)_3$ could be detected. Since, however, these films were produced at high current densities they were presumably formed at very negative potentials where almost complete reduction of the film to $Cr(OH)_3$ is to be expected. Indeed Sysoev et al. observed that a thin layer of metallic chromium was always formed beneath the film.

It is of interest that the films produced by Sysoev et al., on an iron electrode, were not permeable to Walkers reagent and that no pores could be detected at a magnification of x4,500. The films were only slowly

dissolved by mineral acids at room temperature but when heated to 80-90°C were dissolved by 6N H_2SO_4.

Graphite electrodes behave very differently from metals. Potential-sweep measurements[1.15] show that the current rises steadily from E_H = 1.20 V reaching a maximum value of about 500 mA cm^{-2} at 0.50 V. Severe inhibition of the reduction reaction occurs near 0.0 V but the initial activity is regained at about 0.70 V on the return sweep. These results have been largely substantiated in galvanostatic experiments[1.23]. When high current densities were employed the reduction process rapidly suffered complete inhibition, the potential falling to a value characteristic of hydrogen evolution. At lower current densities the reduction process occurs at potentials in the neighbourhood of 1.0 V. Even under these conditions, however, some inhibition of the reaction is apparent. Thus at a current density of 20 mA cm^{-2} the potential fell from an initial value of 1.20 V to 1.00 V after a period of about seven minutes. Since this partial inhibition was removed by mild anodic polarisation or by resting on open circuit, but was produced by strong anodic polarisation in either chromic or sulphuric acid solutions, it was attributed to a change in the state of the surface oxides on the carbon.

No explanation for the marked difference in behaviour between metal and graphite electrodes seems to have been suggested.

1.3.2 Solutions containing "foreign" anions

The reduction of CrVI to CrIII and indeed to metallic chromium is possible on metal and carbon electrodes in chromic acid solutions containing foreign anions. A wide variety of anions, including[1.16,1.20] sulphate, chloride, fluoride, borofluoride, silicofluoride, nitrate and perchlorate, has proved to be satisfactory in this respect. The detailed behaviour observed depends upon the nature of the foreign anion, the relative concentration of chromic acid and added anion, the pH and the nature of the cathode.

Most of the reported work has been concerned with solutions containing chloride, sulphate and perchlorate. Since in the present work detailed studies were made only in the presence of the latter two species, the following review is restricted to investigations involving these solutions. Gold and carbon electrodes were used in the present work because the reduction of CrVI to CrIII occurs most readily on these materials. Previous studies with these electrodes are described in detail later. A general account of the reduction process is given below.

The reduction process in general

The current potential curves obtained with metallic electrodes, in chromic acid solutions containing sulphate or perchlorate, are not continuous, but, as first shown by Liebreich[1.24] may consist of up to four branches (Fig. 1.5). Under potentiostatic conditions these

branches are separated from one another by limiting current regions, generally followed by current minima. The processes occurring in the four branches are believed to be:

Branch I - reduction of CrVI to CrIII; this branch is not observed with all metals.

Branch II - reduction of CrVI to CrIII

Branch III - hydrogen evolution, possibly accompanied by reduction of CrVI but without chromium deposition. This stage is observed only with metals such as Pt and Pd which have a low hydrogen overpotential.

Branch IV - chromium deposition accompanied by hydrogen evolution.

Since, irrespective of the electrode material employed, the final stage occurs on a chromium surface, this stage of the reduction occurs over the same potential range with all metals. It begins at about E_H = -750 mV. The potentials at which the other branches occur depend upon the nature of the metal used.

Weiner[1.17] has pointed out that the potentials at which the second branch of the curve occurs are in the same order as the electromotive series of the metals employed. He considers that, because of the high potential of the CrVI/CrIII couple, all metals will undergo anodic dissolution to some extent when immersed in a chromic acid solution. Since cathodic polarisation will

destroy any passivating films produced by the chromic acid, cathodic deposition of the metal ions will be the main potential-determining reaction. The potential should therefore be close to that of the metal/metal ion couple involved. Weiner also points out that the first branch of the curve is obtained only with those metals which have more than one stable oxidation state.

Kabasakaloglu and Uneri[1.25,1.26], found that with Pt, Rh and Ir electrodes in sulphate containing solutions, the reduction of CrVI occurred at the potential where the surface oxide on the metal was reduced. Okada et al.[1.19] have also shown that reduction of the surface oxide on Pt and Au occurs prior to reduction of CrVI. With these metals, therefore, the first branch of the current-potential curve probably occurs close to the potential at which reduction of their surface oxides begins. Weiner recognised this possibility and his views, as presented above, refer to bare metals.

The termination of each of these first three stages, and the subsequent current minima, apparently result from the formation of passivating layers on the electrode surface. The nature of these layers has been discussed frequently but experimental work on their structure and content is not extensive. Furthermore, much of this work has been carried out under constant current conditions, the potential often varying with time during the experiments.

With silver, nickel and chromium in sulphate containing solutions the nature of the layer formed under constant current conditions varies with the duration of the electrolysis[1.27]. Electron microscopy showed that a thin (0.02 μ) coherent film is first produced, presumably during the second branch of the curve. Continued polarisation, probably resulting in the potential shifting to the third branch of the curve, causes the development of larger crystallites in this layer until eventually almost the whole electrode surface is covered with a thick (0.1 μ) but porous layer of crystals. Electron diffraction studies[1.17] have shown that the electrode metal is present, at least to a small extent in these films. Similar results on iron have been reported by Saiddington and Hoey[1.28] using optical microscopy. They detected an amorphous film formed during the third branch of the curve; at more negative potentials, where chromium deposition begins, this film disintegrates and is replaced by a viscous layer which may consist of a colloidal suspension of solid particles. The rate of formation of the amorphous film was greater the lower the concentration of sulphuric acid. This suggests that the film results from the solution near the electrode becoming more alkaline. The formation of an amorphous film on steel has also been observed by Okada and Yamamoto[1.29].

In a fairly comprehensive series of experiments Solov'eva et al.[1.30] analysed the layers formed on

chromium plated copper. Solutions containing different amounts of CrO_3 and sulphuric acid were employed and the layers were formed at a current density of 250 or 500 mA cm^{-2}. The potential was not stated, but it must have been more negative than E_H = -400 mV[1.16]. In contrast to the film formed in the absence of sulphuric acid[1.21], which was thin and dissolved only in concentrated acids, the films produced in sulphate containing solutions were thick and dissolved easily in dilute chromic or sulphuric acid. These latter films contained CrVI, CrIII and SO_4^{2-}, the relative amounts varying with the solution composition and current density.

It appears therefore that with the non-noble metals the nature of the film on the electrode surface varies with the solution composition and the electrode potential. In the absence of added anions a thin unreactive film is formed, the ratio of CrVI to CrIII in this film decreasing as the potential is made more negative. In the presence of sulphate three types of film appear to be formed. At more positive potentials a non-porous thin film is formed akin to that produced in the absence of sulphate. At more negative potentials the film is porous, thick and easily dissolved. It contains sulphate ions as well as CrVI and CrIII, their relative proportions depending on the solution composition and electrode potential. At potentials where deposition of chromium occurs this latter film becomes replaced by a viscous, possibly colloidal layer.

Reduction on a gold electrode

The detailed form of the current-potential curve obtained with a gold electrode in solutions containing perchloric or sulphuric acid depends on the ratio of the concentrations of chromic acid and the foreign acid. Whenever measurable currents flow, however, all four branches of the current-voltage curve may be observed in quasi-steady state measurements[1.13]. The potentials at which the steeply rising sections of the curves occur depend somewhat on the composition of the solution. The first branch occurs near to E_H = 1200 mV in 3 M CrVI, 0.01 M H_2SO_4[1.16] and as shown by Okada et al.[1.19] may well correspond to the reduction of the surface oxide on the gold. It has not, however, been studied in any detail.

The second branch has received much more attention. The potential at which it occurs and its shape depend upon the concentrations of both the chromic and foreign acid. In sulphuric acid solutions containing excess chromic acid[1.13] this stage begins in the neighbourhood of 600-700 mV. After reaching a maximum value the current decreases and, depending on the solution composition, may fall almost to zero. Clearly some type of passivating layer is produced under these conditions. The maximum current obtained in such solutions is linearly dependent on the concentration of sulphuric acid employed, showing that it is limited by the rate of diffusion of sulphuric acid to the electrode[1.13]. This linear relationship,

however, extends only over a limited range of sulphuric acid concentrations. Thus with 0.3 M CrO_3, the linearity is maintained up to about 0.1 M H_2SO_4; further increase in the sulphuric acid concentration causes the current to pass through a maximum value (in 0.5 M H_2SO_4) and then decrease slowly[1.13]. Perchloric acid is much less effective in promoting the reduction than is sulphuric acid, no significant current being observed in 0.3 M CrO_3 until the perchloric acid concentration is 1.5 M. The current reaches its maximum value in 2 M $HClO_4$, decreasing again with further increase in $HClO_4$ concentration[1.13].

When excess sulphuric or perchloric acid is employed, the current reaches a limiting value and remains at that value over a fairly wide potential range. Thus with 1 M H_2SO_4, containing 0.016 M CrO_3, this plateau extended from E_H = 800 to 50 mV. As the CrO_3 concentration was increased the length of the plateau decreased and it was terminated by a sharp fall in the current, indicating that passivation was again occurring. The magnitude of the limiting current increased linearly with chromic acid concentration up to 0.24 M CrO_3 in 1 M H_2SO_4[1.20], but only up to 0.1 M CrO_3 in 0.1 M H_2SO_4. Although a narrower range of conditions was employed, solutions containing $HClO_4$ behaved in a very similar manner. The slope of the limiting current/CrO_3 concentration relation was the same for both solutions, showing that this plateau-

current is limited by the rate of diffusion of CrO_3 to the electrode surface.

Nature of the layers formed on gold electrodes

To explain the discontinuous nature of the current-potential curve, Reinkowski and Knorr[1.16] suggested that the reduction process involves the participation of a surface film. Their theory is a modification of that suggested earlier by Liebreich[1.24]. They postulate this film to be produced, in the first instance, by reduction of CrVI and oxidation of the electrode material. When formed in the presence of foreign anions, this film is capable of further reduction; the reduced form is presumably re-oxidisable by CrVI with the formation of CrIII. As the potential is made more negative the rate of film reduction will increase, whereas its rate of re-oxidation becomes limited by the rate of supply of CrVI. A given stage in the current-potential curve ends when the rate of reduction of the film exceeds its rate of re-oxidation. The existence of subsequent branches in the current-potential curve is attributed to the film adopting different oxidation states with change in potential.

Gerischer and Kappel[1.15,1.31] also suggested that the reduction process involves participation of the surface film. Their evidence for the existence of a film in the absence of foreign anions has been presented in Section 1.3.1. Since the double-layer capacitance behaviour of the electrode and its resistance to

amalgamation were unaltered by the presence of sulphate ions, they infer that a similar film is again present.

These authors propose that the reduction occurs in two steps. The first step involves the rapid formation of an oxide layer according to the reaction,

$$\frac{1}{2}\,HCr_2O_7^- + me^- \xrightarrow{H^+} CrO(3 - \tfrac{m}{2})_{ads} + x\,H_2O \qquad 1.2$$

the composition of this layer depending on the potential. In the absence of foreign anions no further reaction is possible, whereas in their presence a second step occurs. This involves reduction of the oxide layer, with the assistance of the foreign anions, through a soluble chromium complex to CrIII, the oxide film being continuously regenerated according to equation 1.2. The shape of the current-potential curve is attributed to the fact that the oxide layer participates in the electrode reaction and suffers modification as a consequence of changing the potential. In contrast to Reinkowski and Knorr, Gerischer and Käppel do not suggest that the nature of the oxide film is altered by the presence of foreign anions.

Fiegl et al.[1.13,1.20] suggest that in the presence of foreign anions a passivating layer of the type found in pure CrO_3 is produced only between +1300 and +800 mV. At more negative potentials a porous film of limited thickness is produced, which allows the reduction reaction to occur.

Fiegl and Knorr[1.13] observed the formation of a red-brown layer on the electrode at the beginning of the falling section of the second branch (in 0.3 M CrO_3, 3×10^{-3} M H_2SO_4). The composition of this layer (produced in 3 M CrO_3, 0.5 M H_2SO_4) was investigated using spot tests and found to consist of chromium III-chromate. Analysis of the solution showed the presence of a hexa-aquo CrIII complex and two sulphate-free chromium complexes, probably containing hydroxyl groups. The formation of these basic CrIII complexes is presumably due to depletion of H^+ at the electrode surface. Since these CrIII hydroxy-complexes are precursors in the formation of CrIII hydroxide, they must play an important role in layer formation at the cathode since the latter species polymerise in aqueous media and can react with chromate ions to form the chromi-chromate complex.

Since the limiting current density of the second stage was proportional to sulphuric acid concentration, the magnitude of this current must depend on the rate diffusion of SO_4^{2-} to the electrode.

These observations led Fiegl and Knorr to suggest that H_2SO_4 (and other foreign species) can exert two effects on the layer.

(i) If they are acidic they will increase the H^+ concentration and thus inhibit the formation of the basic CrIII hydroxy-complexes.

(ii) If the anion is capable of forming a complex with CrIII it will again deplete the concentration of the CrIII hydroxy-complexes.

Supporting evidence for the dual role of the foreign species was obtained from comparing the behaviour of $HClO_4$ and H_2SO_4. The concentration of $HClO_4$ required to obtain a given current was much larger than that of H_2SO_4. This is consistent with the fact that ClO_4^- does not complex with CrIII and hence the sole effect of adding $HClO_4$ is to increase the acidity of the solution.

Direct evidence as to whether or not the layer is porous is not available. Gerischer and Käppel[1.15] showed that the film prevented amalgamation of the gold by mercury, but this may mean only that the pores have too small a diameter to allow penetration of the mercury. Weiner and Schiele[1.27], using metals other than gold, have shown by electron microscopy that the layer formed at potentials negative to that corresponding to the maximum of the second branch is porous. In order to explain the effects produced by adding reducible metal ions to chromic acid solutions, Fiegl, Kandler and Reinhold[1.20] found it necessary to assume that the layer produced on gold is porous. Addition of $Fe_2(SO_4)_3$ to 1 M CrO_3 caused an increase in the current in the rising section of the second branch, i.e. between E_H = +750 to +300 mV, attributable to the reduction of Fe^{3+}. At potentials negative to the current maximum, however

i.e. +300 to -300 mV, the presence of Fe^{3+} resulted in a lower current than that observed in the presence of an equivalent amount of Na_2SO_4. When the electrode was held at -250 mV, addition of Fe^{3+} or Cu^{2+} to the solution caused a decrease of 15 and 10% respectively in the current. Addition of Ag^+ under the same conditions, however, caused an increase in the current proportional to the amount of Ag^+ added. Similar results were obtained earlier by Kolthoff and Shams El Din[1.18]. Fiegl et al. attributed the lower currents to precipitation of $Fe(OH)_3$ or $Cu(OH)_2$ in pores in the surface layer. Since many H^+ are consumed in the reduction of CrVI according to

$$H_2CrO_4 + 6H^+ + 3e \longrightarrow Cr^{3+} + 4H_2O$$

a rise in pH at the electrode surface and within the pores would be expected. These workers argued that if the pH of the solution in the pores was between 6.1 and 8.9, precipitation of $Fe(OH)_3$ and $Cu(OH)_2$ would occur, but not that of AgOH. Gerischer and Käppel[1.15], however, argued that results of this type can be explained on the basis of the established selectivity of semiconductor electrodes toward electrode reactions.

In connection with Fiegl and Knorrs' suggestion that added foreign species play a dual role in promoting the reduction of CrVI, it is of interest that the reduction of Fe^{3+} could not be observed in the potential range +1100 to -250 mV in solutions of $Fe(ClO_4)_3$ in 1 M CrO_3.

This indicates that ClO_4^-, in contrast to SO_4^{2-}, does not prevent the formation of a passivating film.

Confirmation[1.20] that chromi-chromate rather than $Cr(OH)_3$ would be deposited on the electrode in the pH range 6.1 to 8.9 was obtained by titrating (a) $Cr_2(SO_4)_3$ and (b) $Cr_2(SO_4)_3 + CrO_3$ (mole ratio 1:1) with NaOH. The titration curve obtained with solution (a) showed a plateau in the pH range 5.5 to 5.8 resulting from the precipitation of $Cr(OH)_3$. With solution (b) the plateau lay between pH 6.0 to 6.4 and a precipitate, presumably of chromi-chromate, was produced; no precipitate of $Cr(OH)_3$ was obtained at lower pH values. It follows therefore that the CrIII ion must be complexed by chromate to give a soluble complex which would be precipitated under the conditions of pH existing at the electrode surface.

A different view as to the role of foreign anions has been presented by Weiner[1.17] who has suggested that the film is formed less readily in the presence of foreign ions because of the increased solubility of the film-forming material. Consequently, the film is produced only when the rate of formation of the film-forming material is high and the concentration near the electrode exceeds the solubility of the material.

It is generally agreed, therefore, that in pure CrO_3 solutions the reduction of CrVI is inhibited by the presence of a surface film. This film appears to be an oxide, containing chromium in a variety of valence states and has high electrical conductivity.

In the presence of foreign ions the same film probably exists over the potential range +1300 to +800 mV. At more negative potentials the film either dissolves[1.17], undergoes modification, allowing the reduction of CrVI to occur[1.13,1.16,1.20], or is able to take part in the electrode reaction[1.15].

Reduction on a carbon electrode

Very little work on the reduction of CrVI on carbon electrodes has been reported. Sternberg and Bagotskii[1.23] obtained potential-time curves for the reduction of CrVI under galvanostatic conditions. The solutions employed were normally 0.5 M in H_2SO_4 and between 0.5 and 7.0 M in CrO_3; additions of other salts were made to some solutions. At a current density of 20 mA cm^{-2} the initial potential was always in the neighbourhood of E_H = +1200 to +1300 mV. The value of this potential was made more positive by increasing either the CrO_3 or the H^+ concentration. The potential remained in this neighbourhood for a time which depended on the solution composition, subsequently falling to a lower value which was constant over the duration of the experiment. The authors termed this fall in potential "partial passivation". In no case, however, was this lower potential below E_H = +950 mV. The upper plateau was longer the greater the CrO_3 or H^+ concentration.

In a solution containing 3 M CrO_3, 0.5 M H_2SO_4 the addition of 4.5 gm equiv. l^{-1} $Cr_2(SO_4)_3$ virtually eliminated the upper plateau, the potential falling

within two minutes to approximately +1000 mV. Additions of equivalent amounts of Na_2SO_4 or $NaClO_4$ also shortened the upper plateau, but to a lesser extent, the potential again falling to approximately +1000 mV.

Since the addition of CrIII had no effect on the potentials of the upper and lower plateaux, Sternberg and Bagotskii argued that the fall in potential is not due to the formation of a layer of a sparingly soluble CrIII compound. This conclusion is perhaps questionable since the fall to the lower plateau occurred more rapidly in the presence of CrIII.

These workers attribute the phenomenon of partial passivation to a change in the state of the oxide layers on the electrode surface. This is consistent with their observation that all factors which increased the potential of the upper plateau also increased its length. Further evidence supporting their interpretation was obtained from the results of experiments involving pretreatment of the electrode. Previous cathodic polarisation of the electrode in CrO_3 solution, followed by a short period on open circuit, resulted in the disappearance of the upper plateau on subsequent polarisation. The normal behaviour of the electrode was restored, however, after a long period on open circuit. If, instead of resting the electrode on open circuit, it was subjected to "slight" anodic polarisation, its normal behaviour was rapidly restored. Prior "strong" anodic polarisation, even in pure H_2SO_4, produced a partially

passivated electrode. Such an electrode apparently could not be reactivated. These results were interpreted by suggesting that in its active state the electrode is covered by one form of oxide which gradually undergoes a change of state on cathodic polarisation. This produces a change in the mechanism of reduction of CrVI. Resting on open circuit or "slight" anodic polarisation restores the oxide to its initial condition.

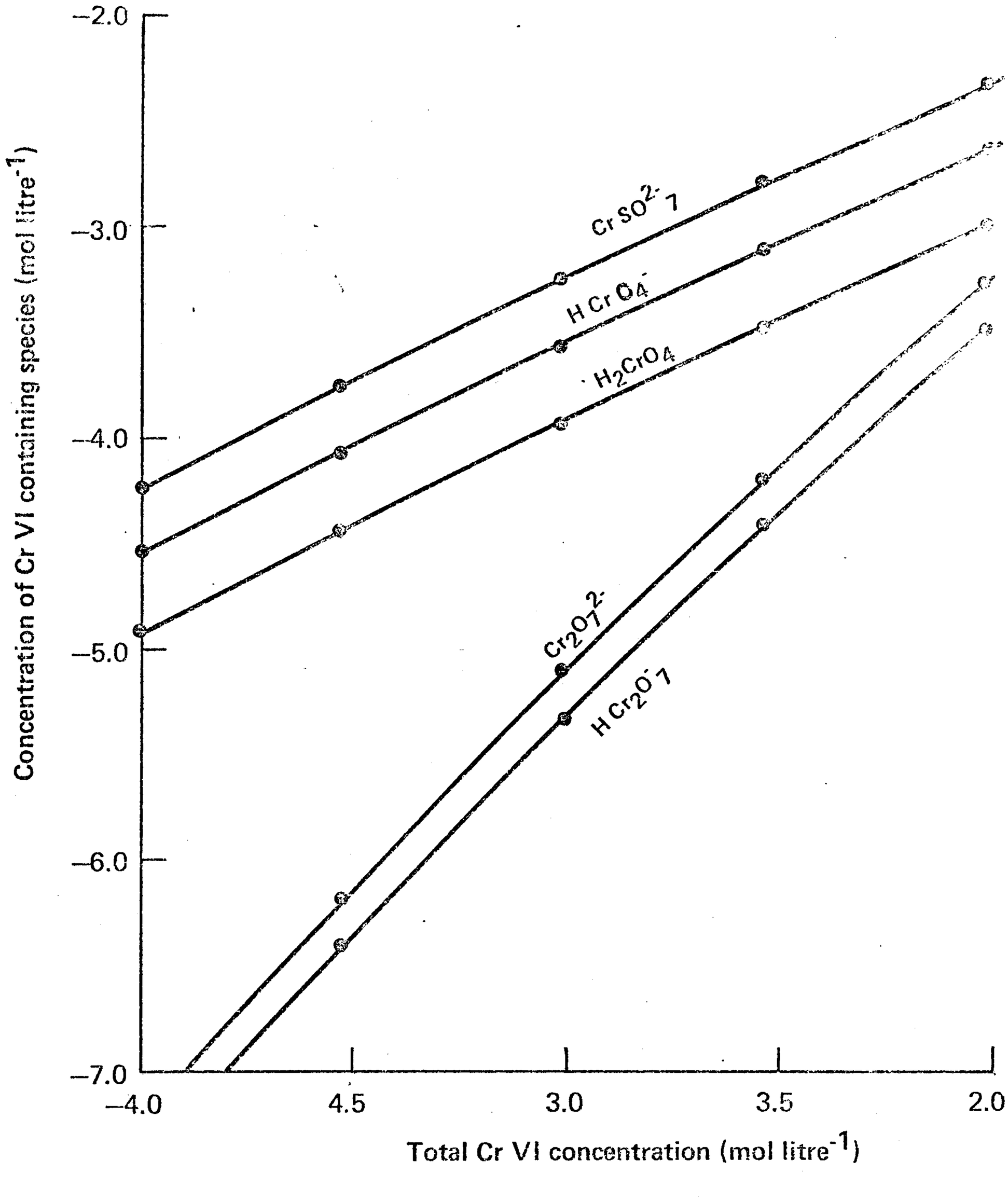

Fig. 1.1

CONCENTRATION OF CrVI SPECIES PRESENT IN 0.5M H_2SO_4($HCr_2O_7^-$ assumed present)

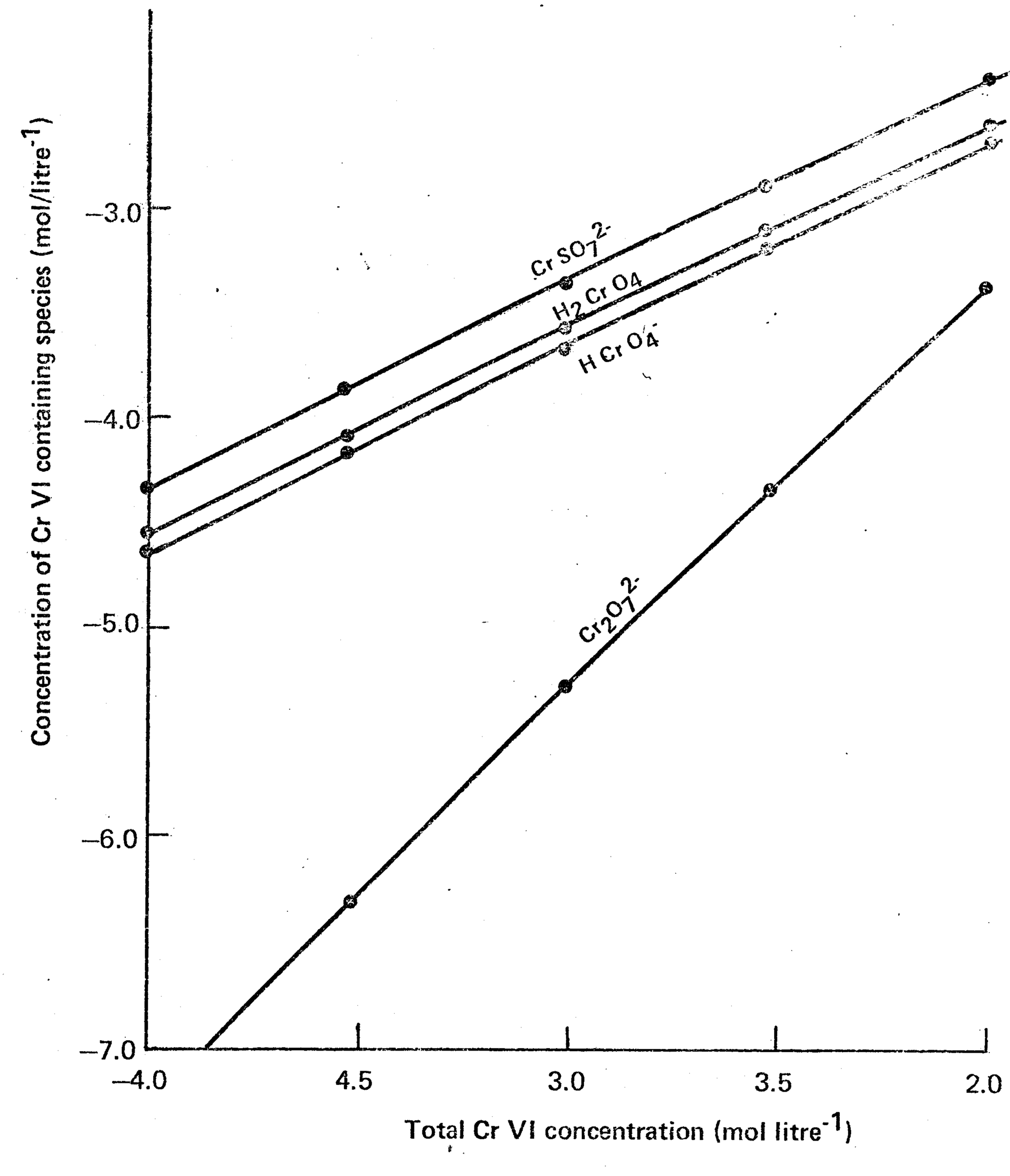

Fig. 1.2

CONCENTRATION OF Cr VI SPECIES PRESENT IN 0.5M H_2SO_4

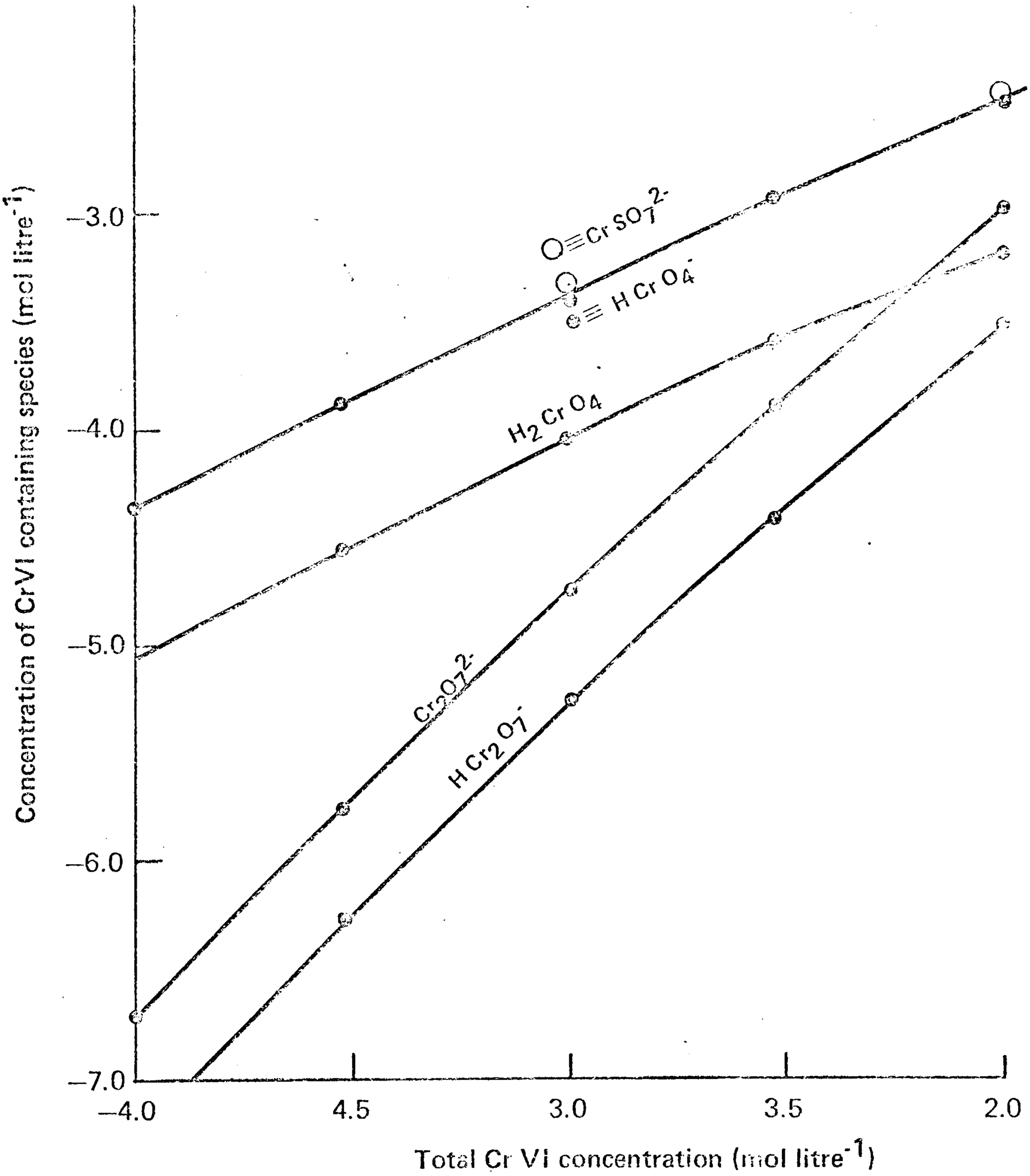

Fig. 1.3

CONCENTRATION OF Cr VI SPECIES PRESENT IN 0.25M H_2SO_4, 0.25M Na_2SO_4

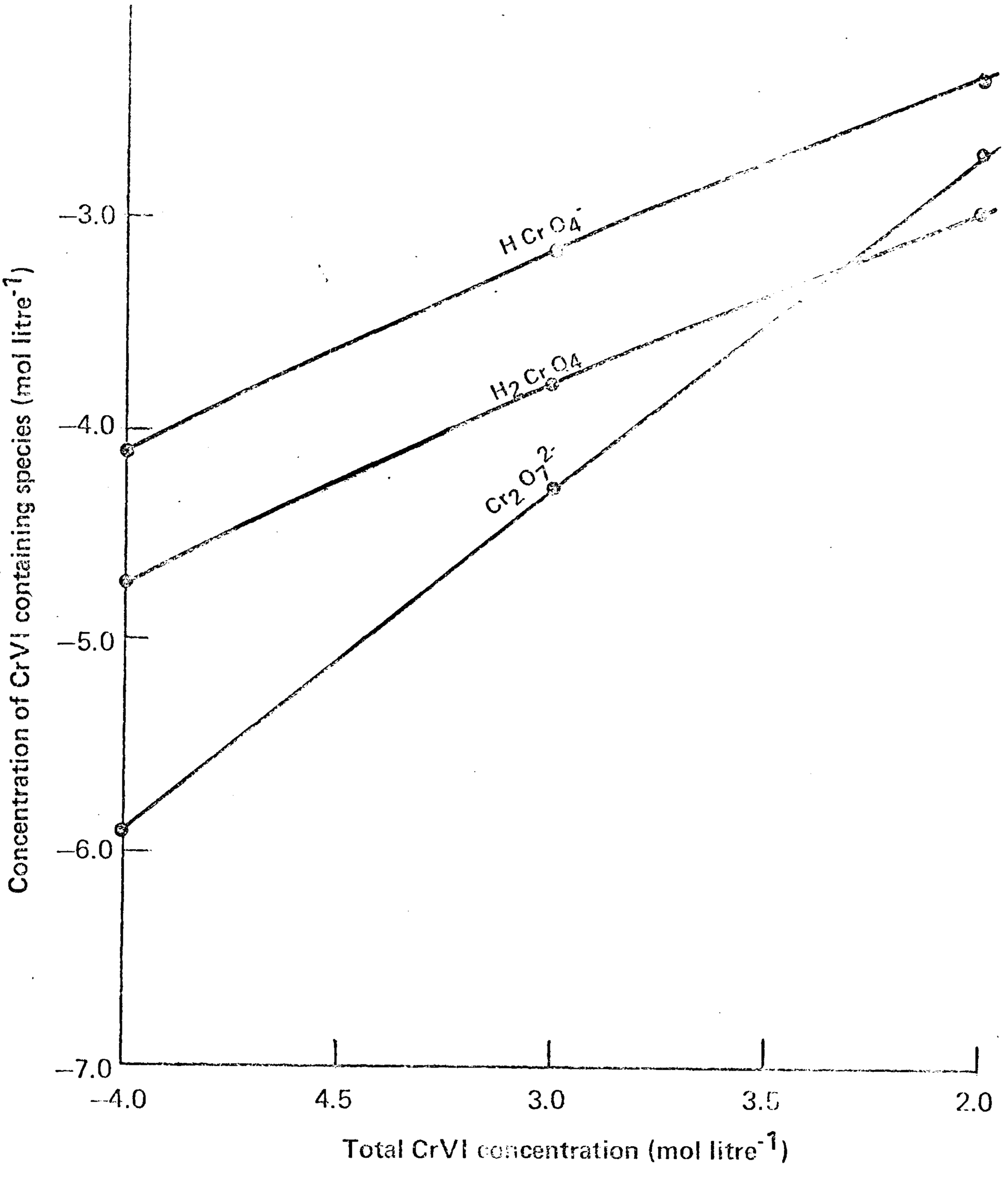

Fig. 1.4

CONCENTRATION OF CrVI SPECIES PRESENT IN IM$HClO_4$ (No H $Cr_2O_7^-$ assumed present)

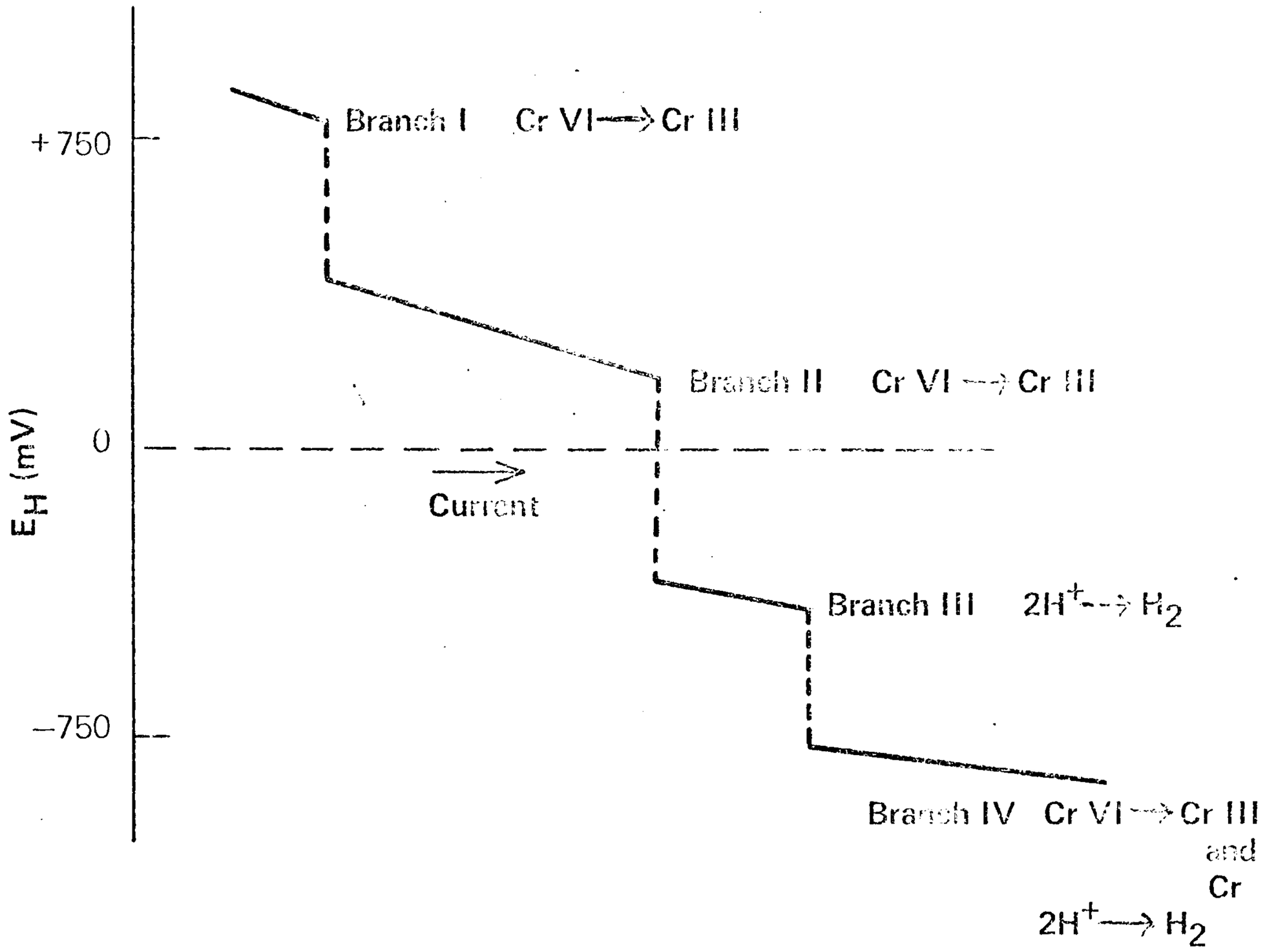

Fig. 1.5
SCHEMATIC CURRENT-POTENTIAL CURVE FOR REDUCTION OF Cr VI

CHAPTER 2

THEORY

2.1 Basic Electrode Kinetics

Considering the simple electrode reaction

$$O + ne \underset{k_{-1}}{\overset{k_1}{\rightleftharpoons}} R \qquad 2.1$$

in which the rate determining step and the overall reaction are one and the same process. When O is being consumed, the transport of O from the bulk of the solution to the electrode surface and transport of R from the electrode to the bulk must also occur. The rates of these mass transfer processes can influence the rate of electrode reaction (as will be discussed later). For the present it will be assumed that the solution is stirred sufficiently rapidly for the surface and bulk concentrations to be effectively equal.

Under these conditions, the dependence of the current for the reduction reaction on electrode potential can be derived using the Transition State Theory[2.1]. Providing that the total concentration of the solution is reasonably high, so that double-layer effects may be ignored, this leads to the relationship

$$i = nFA\left(k_1 c_o^b \exp-\frac{\beta nFE}{RT} - k_{-1} c_R^b \exp\frac{(1-\beta)nFE}{RT}\right) \qquad 2.2$$

In this expression A is the area of the electrode, the k's are the rate constants for the forward and reverse reactions, while c_o^b and c_R^b are the concentrations of O and R respectively in the bulk of the solution. β is the

symmetry factor for the cathodic reaction, n the number of electrons involved in the reaction and E the potential of the electrode with respect to the reference electrode. When the rate determining step and the overall reaction are not the same, but the reaction is still first order in R and O, this expression becomes,

$$i = nFA\left(k_1 c_o^b \exp-\frac{\alpha n_a FE}{RT} - k_{-1} c_R^b \exp\frac{(1-\alpha)n_a FE}{RT}\right) \qquad 2.3$$

Here, α the transfer coefficient is related to β, but unlike the latter quantity is not limited in its range of possible values. $n_a = {}^{n}/_{v}$, where v, the stoichiometric number, is the number of times the rate determining step must occur for the transfer of n electrons in the overall process.

At the reversible potential, the two terms on the R.H.S. of Equation 2.3 are equal. When the potential is sufficiently negative to the reversible value, however, (c.a. 60 mV) the second exponential in Equation 2.3 becomes much smaller than the first, so that it may be ignored. Making this approximation and taking logarithms gives

$$\log i = \log nFAk_1 c_o^b - \frac{\alpha n_a FE}{RT} \qquad 2.4$$

A corresponding relation applies to the anodic process. This is the Tafel equation; its use allows the values of $nFAk_1 c_o^b$ and αn_a to be obtained from a graph of log i against the potential.

2.2 Influence of Mass Transport

Up to the present it has been assumed that the solution was sufficiently well stirred so that the surface and bulk concentrations are effectively equal. This will be true only for very slow electrode reactions. In general the following mechanism will apply

$$O_b = O_s \qquad 2.5$$

$$O_s + ne = R_s \qquad 2.6$$

$$R_s = R_b \qquad 2.7$$

where the subscript b refers to the bulk of the solution and s refers to near the electrode surface (but still at the potential of the bulk).

When a net reduction reaction occurs, O is consumed and R produced

$$c_o^s < c_o^b \qquad \text{and} \qquad c_R^s > c_R^b$$

where the superscripts s and b refer to the surface and bulk respectively. The values of c_o^s and c_R^s will depend on the current.

Since the rate equation, at sufficiently negative potentials, should now be written as

$$i = nFAk_1 c_o^s \exp -\alpha n_a FE/RT$$

$$\text{or} \quad i/c_o^s = nFAk_1 \exp -\alpha n_a FE/RT \qquad 2.8$$

the value of c_o^s must be evaluated before a meaningful Tafel plot can be constructed.

The movement of reactants and products to and from the electrode can occur by three main processes;

(1) migration, if charged species are involved,

(2) convection, due to mechanical stirring or thermal gradients,

(3) diffusion, as a result of concentration gradients.

Migration is unimportant when there is a large concentration of inert electroactive ions in solution. Natural convection is difficult to treat theoretically and to control experimentally and is therefore normally minimised by controlled stirring. When a reproducible form of stirring is used and the solution contains an excess of inert electrolyte mass transport occurs as a result of forced convection and diffusion.

Assuming that diffusion provides the sole means of mass transport and that steady-state conditions prevail, the rate of supply of material, to unit area of the electrode surface from the solution, is obtained from Fick's first law[2.2] as

$$j_{x=0} = D\left(\frac{\delta c}{\delta x}\right)_{x=0} \qquad 2.9$$

where $\frac{\delta c}{\delta x}$ is the concentration gradient in the solution,

j the flux to the electrode,

D the diffusion coefficient of the species concerned

and x the distance from the electrode surface.

Since $\left(\frac{\delta c}{\delta x}\right)_{x = 0}$ is the limiting slope of the relation between concentration and distance, we can write

$$\left(\frac{\delta c}{\delta x}\right)_{x = 0} = \frac{c_o^b - c_o^s}{\delta} \qquad 2.10$$

where δ is the thickness of an imaginary layer called the diffusion layer.

Under steady-state conditions, the rate of supply of material (i.e. the flux) is equal to its rate of consumption in the electrode reaction

$$\therefore \quad j_{x = 0} = \frac{i}{nFA} \qquad 2.11$$

From Equations 2.9, 2.10 and 2.11 we can obtain

$$i = \frac{nFAD}{\delta}(c_o^b - c_o^s) \qquad 2.12$$

The value of δ depends on the geometry of the electrode, or when stirring (i.e. forced convection) is employed on the type and rate of stirring. When the rotating disc is used δ depends on a number of experimental parameters.

2.3 The Rotating Disc Electrode (R.D.E.)

The R.D.E. offers a very reproducible form of stirring and satisfies the following important requirements:

(a) The current is steady with time, that is a steady rate of stirring is provided.

(b) The rate of supply of material (i.e. the flux) is uniform over the electrode surface.

(c) The thickness of the "diffusion layer" and its dependence on the rate of stirring is known.

Levich has shown theoretically[2.3] that the diffusion layer thickness is given by

$$\delta = kD^{1/3} v^{1/6} w^{-1/2} \qquad 2.13$$

where D is the diffusion coefficient of the species considered, v the kinematic viscosity of the solution and w the angular velocity of the electrode (radian sec^{-1}).

v is defined as : $v/cm^2 s^{-1} = \frac{\text{viscosity (poise)}}{\text{density (g cm}^{-3})}$ 2.14

Gregory and Riddiford[2.4] evaluated k as:

$$k = 1.6125 + 0.5704 \left(\frac{D}{v}\right)^{0.36} \qquad 2.15$$

The second term in 2.15 is normally small compared with the first, and may usually be neglected so that 2.13 simplifies to

$$\delta = 1.61\, D^{1/3} v^{1/6} w^{-1/2} \qquad 2.16$$

Combining 2.12 and 2.16 we get

$$i = 0.620 nFAD^{2/3} v^{-1/6} (c_o^b - c_o^s)\, \omega^{1/2} \qquad 2.17$$

which may be conveniently rewritten as

$$i = Bw^{1/2}(c_o^b - c_o^s) \qquad 2.18$$

where $B = 0.620\ nFAD^{2/3} v^{-1/6}$.

When the current is diffusion limited, $c_o^s = 0$ and therefore Equation 2.18 becomes

$$i_d = Bw^{1/2} c_o^b \qquad 2.19$$

where i_d is the diffusion limited current. Combination of Equations 2.18 and 2.19 gives

$$c_o^s = \left(\frac{i_d - i}{i_d}\right) c_o^b \qquad 2.20$$

allowing c_o^s to be calculated from a knowledge of i_d, i and c_o^b.

It also follows from Equation 2.19 that a graph of either $^1/i_d$ against $^1/w^{1/2}$ or of i_d against $w^{1/2}$ should be linear and pass through the origin. It also follows that plots of c_o^b/i_d against $^1/w^{1/2}$, corresponding to different bulk concentrations should superimpose.

2.4 Determination of reaction order

For a reaction of order p with respect to the oxidised species, which can be studied at potentials where the reverse reaction is unimportant, we have

$$i = nFAk_1(c_o^s)^p \exp -\alpha n_a FE/RT$$

Consequently, at constant electrode potential,

$$\log i = \log k_1' + p \log c_o^s \qquad 2.21$$

where $k_1' = nFAk_1 \exp -\alpha n_a FE/RT$. Since c_o^s may be evaluated from Equation 2.20, a graph of log i against log c_o^s allows the reaction order to be determined.

2.5 Causes of plateaux and inflexions

The foregoing treatment applies to the situation where the current-voltage relation is a smooth curve, the current finally becoming limited by the rate of diffusion of the reactant. Since a limiting current can also result from causes other than diffusion limitation, criteria for distinguishing a diffusion-limited current from other types

of limiting current are required. These criteria are deduced below.

In many cases, the current-voltage curve displays one or more inflexions. Such inflexions are often ill-defined plateaux resulting from the superimposition of a second electrode process on a process approaching a limiting rate. Methods of determining the value and nature of the limiting current associated with such inflexions are also described below.

Plateaux and inflexions can be caused by the following:

(a) The rate of the reaction becoming diffusion limited.

(b) The reaction rate becoming limited by the rate of a preceding chemical step (p.c.s.).

(c) The rate being determined by adsorption of a reactant or desorption of a product.

(d) Deposition of inhibiting material limiting the rate.

(e) Alteration in the Ψ_2 potential.

If (d) is the cause of a plateau or inflexion, peaks in the current-potential curve caused by deposition or removal of this material are normally observed when a rapid, linear potential sweep is employed. Some hysteresis would normally also be expected between the positive and negative-going sweeps. Alteration in the Ψ_2 potential (e) would be likely to cause a plateau only in the neighbourhood of the potential of zero charge and when the concentration of background electrolyte is low.

Thus plateaux resulting from the last two causes can be easily recognised. However it is more difficult to differentiate between plateaux caused by reasons (a), (b) or (c). When an inflexion results from any of these causes, it is an ill-defined plateau as described above. The theory is conveniently presented in two stages, that corresponding to well-defined plateaux and that corresponding to ill-defined plateaux where the plateau current is not directly measurable. The treatment presented applies when a rotating-disc electrode is employed.

2.5.1 Well-defined plateaux

a) Diffusion limitation

The theoretical treatment of this condition has already been presented in Section 2.3. Thus the diffusion limited current is given by Equation 2.19

$$i_d = Bw^{1/2}c_o^b \qquad 2.19$$

and graphs of i_d against $w^{1/2}$ or of $^1/i_d$ against $^1/w^{1/2}$ should both be linear and pass through the origin.

b) Limitation by the rate of a chemical step

The simplest situation to treat is that where a species A present in the solution does not undergo direct reduction in the potential range considered, but is first converted by a chemical reaction into the reducible species B, i.e.

$$A \xrightarrow{k} B + ne \longrightarrow \text{Products.} \qquad 2.22$$

A rigorous derivation of the resulting equation for the current has been given by Delahay[2.5]. A less rigorous,

but for the present purposes sufficiently precise treatment, assumes that conversion of A into B occurs almost entirely within a thin layer of solution adjacent to the electrode, called the reaction layer. Under these circumstances the rate of production of B at the electrode surface (in mole cm^{-2} s^{-1}), as a result of the p.c.s. is given in terms of its concentration c^B by

$$[\delta N_B\ (x,t)/\delta t]_{x\,=\,0} \;=\; \mu[\delta c^B\ (x,t)/\delta t]_{x\,=\,0}$$

where x is the distance measured from the electrode surface. The reaction layer, of thickness μ, is defined as the layer of solution in which all molecules of z produced by reaction 2.22 are subsequently reduced at the electrode surface. Consequently

$$[\delta c^B\ (x,t)/\delta t]_{x\,=\,0} \;=\; k[c^A\ (x,t)]_{r.l.}$$

and hence

$$[\delta N_B\ (x,t)/\delta t]_{x\,=\,0} \;=\; \mu k[c^A\ (x,t)]_{r.l.}$$

where $[c^A\ (x,t)]_{r.l.}$ is the concentration of A in the reaction layer. This quantity is normally assumed to be essentially constant throughout the reaction layer so that, in the steady state

$$[c^A\ (x,t)]_{r.l.} \;=\; c_s^A$$

where c_s^A represents the surface concentration of A.

If the equilibrium concentration of B in the solution is negligibly low, diffusion of B to the electrode may be neglected so that the kinetic current (i_k) is given by

$$\frac{i_k}{nFA} = \left[\frac{\delta N_B\ (x,t)}{\delta t}\right]_{x\ =\ 0} = \mu k c_s^A \qquad 2.23$$

The rate of supply of A to the electrode by mass transport must equal its rate of consumption so that

$$\mu k c_s^A = \frac{B w^{1/2}}{nFA}\left(c_b^A - c_s^A\right)$$

and hence

$$c_s^A = \frac{B w^{1/2} c_b^A}{B w^{1/2} + nFA\mu k} \qquad 2.24$$

Substituting for c_s^A in Equation 2.23 from Equation 2.24 gives

$$i_k = \frac{nFA\mu k B w^{1/2} c_b^A}{B w^{1/2} + nFA\mu k} \qquad 2.25$$

or

$$\frac{1}{i_k} = \frac{1}{nFA\mu k c_b^A} + \frac{1}{B w^{1/2} c_b^A} \qquad 2.26$$

Consequently under these conditions the relation between i_k and $w^{1/2}$ is not linear (Equation 2.25). That between $1/i_k$ and $1/w^{1/2}$ is linear but should show an intercept at $w = \infty$ (Equation 2.26).

If a significant concentration of B exists in the solution, the limiting current is equal to the sum of the diffusion limited current for B and i_k. The rotation speed dependence of i_l is therefore more complex than i_k, that is

$$i_l = \frac{nFA\mu k B w^{1/2} c_b^A}{B w^{1/2} + nFA\mu k} + B w^{1/2} c_b^B \qquad 2.27$$

and graphs of $^1/i_l$ against $^1/w^{1/2}$ are no longer linear.

c) Adsorption of reactant rate-limiting

If the species A is adsorbed onto the electrode surface and then suffers reduction, i.e.

$$C_s^A \underset{k_{-1}}{\overset{k_1}{\rightleftharpoons}} c_{Ads}^A \xrightarrow{k_2} \text{Product (soln.)}$$

If the second step in this mechanism is irreversible, the current is given by

$$i = k_2 \theta$$

where k_2 is a potential dependent constant and θ is the fraction of the surface covered with adsorbed material. Since

$$\frac{d\theta}{dt} = k_1 c_s^A (1 - \theta) - k_{-1}\theta - k_2\theta = 0$$

in the steady state

$$\therefore \quad \theta = \frac{k_1 c_s^A}{k_1 c_s^A + k_{-1} + k_2}$$

Substituting for θ in the expression for the current gives

$$i = \frac{k_1 k_2 c_s^A}{k_1 c_s^A + k_{-1} + k_2}$$

when $k_2 \gg k_1 c_s^A$ and k_{-1} the process becomes independent of potential because adsorption becomes the rate determining step

$$\text{i.e.} \quad i_l = k_1 c_s^A \qquad 2.28$$

Since in the steady state the rate of transport of A to the surface equals its rate of adsorption,

$$\frac{dc_s^A}{dt} = Bw^{1/2}(c_b^A - c_s^A) - k_1 c_s^A = 0$$

so that

$$c_s^A = \frac{Bw^{1/2} c_b^A}{Bw^{1/2} + k_1} \qquad 2.29$$

substituting 2.29 into 2.28 gives

$$i_l = \frac{k_1 Bw^{1/2} c_b^A}{Bw^{1/2} + k_1} \qquad 2.30$$

or $$\frac{1}{i_l} = \frac{1}{k_1 c_b^A} + \frac{1}{Bw^{1/2} c_b^A} \qquad 2.31$$

Thus a graph of i_l against $w^{1/2}$ will not be linear, while one of $1/i_l$ against $1/w^{1/2}$ will be linear but show an intercept at $w = \infty$.

If it were possible to observe the diffusion-limited rate of this process, it would be given by

$$i_d^A = Bw^{1/2} c_b^A .$$

Combination of this expression with Equation 2.29 gives

$$i_l = \frac{k_1 i_d^A}{Bw^{1/2} + k_1}$$

showing that i_l must be smaller than i_d^A.

d) Desorption of product rate-limiting

Here we assume that species A after being adsorbed on the electrode surface is reduced to the adsorbed species R which is subsequently desorbed, i.e.

$$c_s^A \underset{k_{-1}}{\overset{k_1}{\rightleftharpoons}} c_{Ads}^A \;(\theta_1) \xrightarrow{k_2} c_{Ads}^R \;(\theta_2) \xrightarrow{k_3} c_s^R$$

The particular case considered is that where the electrochemical step, with potential dependent rate-constant k_2, is irreversible. The constants k_1, k_{-1} and k_3 are independent of potential.

If desorption is rate determining then:

$$i = k_3\theta_2 = k_2\theta_1$$

so that

$$\theta_2 = \frac{k_2\theta_1}{k_3}$$

In the steady state,

$$\frac{d\theta_1}{dt} = k_1 (1 - \theta_1 - \theta_2)c_s^A - k_{-1}\theta_1 - k_2\theta_1 = 0$$

and

$$k_1 \left(1 - \theta_1 - \frac{k_2\theta_1}{k_3}\right) c_s^A - k_{-1}\theta_1 - k_2\theta_1 = 0$$

therefore

$$\theta_1 = \frac{k_1k_3c_s^A}{(k_1k_3 + k_1k_2)\, c_s^A + k_{-1}k_3 + k_2k_3}$$

and

$$i = \frac{k_1k_2k_3c_s^A}{(k_1k_3 + k_1k_2)\, c_s^A + k_{-1}k_3 + k_2k_3}$$

For desorption to be rate determining, $k_3 \ll k_2$ and for potential independence $k_2 \gg k_{-1}$

$$\therefore \quad i = \frac{k_1 k_2 k_3 c_s^A}{k_1 k_2 c_s^A + k_2 k_3} = \frac{k_1 k_3 c_s^A}{k_1 c_s^A + k_3}$$

For desorption to be rate determining, $k_3 \ll k_1 c_s^A$

$$\therefore \quad i_l = k_3 \qquad 2.32$$

i.e. the current is independent of rotation speed and concentration.

It is now possible to differentiate between the different mechanisms proposed.

(i) By considering the dependence of the plateau current on w.

If the plateaux are caused by the reaction rate becoming diffusion limited, then at a potential which is on the plateau at all rotation speeds, a plot of $^1/i$ against $^1/w^{½}$ will be linear and give zero intercept.

However if the plateau were caused by the rate being limited by a p.c.s. or the rate being determined by adsorption of reactant, an intercept would be obtained. If desorption were rate limiting the current would be independent of rotation speed.

A plot of i_m against $w^{½}$ will be linear for a true diffusion limited plateau and show curvature if adsorption or a preceding chemical step limits the rate.

(ii) If the plateau is an intermediate one and the final plateau current (i_d) is diffusion limited, the ratio of the current for the first plateau (i_l) to i_d varies as follows.

For a diffusion limited plateau

$$\frac{i_l}{i_d} = \frac{n_A c^A}{n_A c^A + n_B c^B}$$

where the solution is assumed to consist of two species A and B with bulk concentrations c^A and c^B, the numbers of electrons involved in the reduction of A and B being n_A and n_B respectively. This expression, and those given below, is based on the assumption that the diffusion coefficients of the two species are similar.

For a plateau resulting from a p.c.s.

$$\frac{i_l}{i_d} > \frac{n_B c^B}{n_A c^A + n_B c^B}$$

This follows from Equation 2.27, since $i_d^B < i_l$.

For adsorption limiting the rate,

$$\frac{i}{i_d} < \frac{n_A c^A}{n_A c^A + n_B c^B}$$

since as shown earlier $i_l < i_d^A$.

Finally, if desorption is rate determining, i_l is independent of c^A.

2.5.2 Ill-defined plateaux

a) Diffusion limitation

An ill-defined diffusion-limited plateau may result if two or more species are present in the solution and are reduced in different potential regions. If the rate of reduction of the second species (B) becomes significant

before that of the first species (A) has become diffusion limited an ill-defined plateau will be observed within the wave. The current at this plateau will normally exceed the true diffusion limited current for reduction of species A.

If the processes occurring prior to the intermediate plateau become diffusion limited at sufficiently negative potentials, then in this potential range the observed current (i_m) equals the sum of the required diffusion-limited current (i_l) and the current due to the subsequent process (i_c), i.e.

$$i_m = i_l + i_c$$

If this subsequent process is straightforward and of first order

$$i_c = k_B c_s^B \qquad 2.33$$

where k_B is a potential dependent constant. Introducing the equation for mass transport of B

$$i_c = B_B w^{1/2} (c_b^B - c_s^B) \qquad 2.18$$

and combining this with Equation 2.33 gives

$$c_s^B = \frac{B_B w^{1/2} c_b^B}{k_B + B_B w^{1/2}}$$

Substitution of this expression into Equation 2.33 gives

$$i_c = \frac{k_B B_B w^{1/2} c_b^B}{k_B + B_B w^{1/2}}$$

Since

$$i_l = B_A w^{1/2} c_b^A$$

then

$$i_m = B_A w^{1/2} c_b^A + \frac{k_B B_B w^{1/2} c_b^B}{k_B + B_B w^{1/2}}$$

Rearrangement of this equation gives

$$i_m k_B + i_m B_B w^{1/2} - B_A B_B w c_b^A = k_B (B_A w^{1/2} c_b^A + B_B w^{1/2} c_b^B)$$

$$= k_B i_d$$

where i_d is the total diffusion-limited current for the whole wave.

Consequently

$$\frac{i_m}{w^{1/2}} = B_A c_b^A + \frac{k_B}{B_B} \left(\frac{i_d - i_m}{w}\right) \qquad 2.34$$

Providing therefore that the reduction of B is first-order and straightforward and the reduction of A becomes diffusion limited, a graph of $i_m/w^{1/2}$ against $(i_d - i_m)/w$ should be linear. Moreover the intercepts of such graphs at potentials where the reduction of A is diffusion-limited should be the same and equal to $B_A c_b^A$.

Since

$$i_l = B_A c_b^A w^{1/2}$$

determination of the value of this intercept allows the true value of the first diffusion limited current to be calculated.

An alternative cause of an ill-defined diffusion-limited plateau, particularly the final plateau, is that hydrogen evolution begins before the reduction current has reached its limiting value. If a number of reducible species (A, B and C) are present in the solution and the potential is sufficiently negative that their rates of reduction are all diffusion limited, the observed current will be given by

$$i_m = w^{1/2}(B_A c_b^A + B_B c_b^B + B_C c_b^C) + i_H \qquad 2.35$$

where i_H is the current due to hydrogen evolution. Since in sufficiently acid solutions, i_H should be independent of w, it follows from Equation 2.35 that a graph of i_m against $w^{1/2}$ should be linear with intercept i_H. Thus the true value of the diffusion-limited current can be found by subtracting i_H from the measured value. It should also be noted that Equation 2.35 predicts that a graph of $1/i_m$ against $1/w^{1/2}$ will not be linear.

b) Diffusion limitation plus a preceding chemical step (p.c.s.)

This condition can only be the cause of a plateau within a curve, and not the final limiting current. To ensure that the theory developed here has maximum relevance to the results discussed in Section 8.8, a p.c.s. of the type

$$Cr_m + Cr_m \xrightarrow{k} Cr_d \qquad 2.36$$

is considered. The symbol Cr_m refers to a monomeric chromium species while Cr_d refers to a dimeric species.

To simplify the treatment it is necessary to assume that all the monomers behave in a closely similar manner.

Using the reaction layer treatment[2.5] again the rate of production of dimer at the electrode surface (mole cm^{-2} s^{-1}) as a result of the p.c.s. is given in terms of its concentration c^d by

$$[\delta N_d\ (x,t)/_{\delta t}]_{x\,=\,0} = \mu[\delta c^d\ (x,t)/_{\delta t}]_{x\,=\,0}$$

Since in the reaction layer all dimer molecules produced by reaction 2.36 are reduced at the electrode,

$$[\delta c^d\ (x,t)/_{\delta t}]_{x\,=\,0} = k[c^m\ (x,t)]^2_{r.l.}$$

hence

$$[\delta N_d\ (x,t)/_{\delta t}]_{x\,=\,0} = \mu k[c^m\ (x,t)]^2_{r.l.}$$

where $[c^m\ (x,t)]_{r.l.}$ is the concentration of monomer in the reaction layer.

In the normal reaction-layer treatment, it is assumed that the concentration of monomer is essentially constant within the reaction layer. In the present treatment this assumption has been made even at potentials where the monomer itself is reduced; some error will be introduced in this way. Making this assumption gives $[c^m\ (x,t)]_{r.l.} = c^m_s$ i.e. the surface concentration of monomers. Since the dimers are supplied to the electrode by diffusion as well as by the p.c.s. and are removed by reduction, then under conditions where the diffusion process has reached its limiting value,

$$\left[\delta N_d\ (x,t)/_{\delta t}\right]_{x\,=\,0} = \mu k(c_s^m)^2 + \frac{B^d w^{1/2} c_b^d}{6FA} - \frac{i_l}{6FA} = 0 \qquad 2.37$$

where i_l is the limiting current for dimer reduction (not diffusion-limited, but both diffusion plus p.c.s.) and it is assumed that 6 electrons are involved in the reduction of one dimer molecule.

The rate of supply of monomers to the electrode surface, at a potential such that dimer reduction is at its limiting rate, is given by

$$\left[\delta N_m\ (x,t)/_{\delta t}\right]_{x\,=\,0} = \frac{B^m w^{1/2}}{3FA}\,(c_b^m - c_s^m) - 2\mu k(c_s^m)^2 - \frac{i_c}{3FA} = 0 \qquad 2.38$$

where $\frac{B^m w^{1/2}}{3FA}\,(c_b^m - c_s^m)$ is the rate of supply by diffusion, assuming the Levich equation to apply, $2\mu k(c_s^m)^2$ is the rate of consumption by the p.c.s. and $\frac{i_c}{3FA}$ is the rate of reduction.

The observed current i_m is related to i_c and i_l by the expression

$$i_m = i_c + i_l$$

The two relevant equations are, therefore,

$$6FA\mu k(c_s^m)^2 + B^d w^{1/2} c_b^d - i_l = 0 \qquad 2.39$$

$$B^m w^{1/2}(c_b^m - c_s^m) - 6FA\mu k(c_s^m)^2 - i_c = 0 \qquad 2.40$$

Adding 2.39 and 2.40 gives

$$B^d w^{1/2} c_b^d + B^m w^{1/2}(c_b^m - c_s^m) = i_l + i_c = i_m$$

$$\therefore\ B^m w^{1/2} c_s^m = B^d w^{1/2} c_b^d + B^m w^{1/2} c_b^m - i_m = i_d - i_m$$

where i_d is the total diffusion-limited current, it being assumed that the current is eventually limited by the rate of diffusion of monomers to the electrode. Consequently

$$c_s^m = \frac{i_d - i_m}{B^m w^{1/2}} \qquad 2.41$$

Assuming that $i_c = k' c_s^m$

then

$$i_c = \frac{k'}{B^m} \left(\frac{i_d - i_m}{w^{1/2}}\right) \qquad 2.42$$

Also by substituting for c_s^m from Equation 2.41 into Equation 2.39 we obtain

$$i_l = B^d w^{1/2} c_b^d + 6FA\mu k \left(\frac{i_d - i_m}{B^m w^{1/2}}\right) \qquad 2.43$$

and since $i_m = i_l + i_c$

combination of Equations 2.42 and 2.43 gives

$$i_m = B^d w^{1/2} c_b^d + 6FA\mu k \left(\frac{i_d - i_m}{B^m w^{1/2}}\right)^2 + \frac{k'}{B^m} \left(\frac{i_d - i_m}{w^{1/2}}\right)$$

or

$$\frac{i_m}{w^{1/2}} = B^d c_b^d + \frac{6FA\mu k}{B_m^2} \left(\frac{i_d - i_m}{w^{3/2}}\right)^2 + \frac{k'}{B_m} \left(\frac{i_d - i_m}{w}\right) \qquad 2.44$$

In the absence of a p.c.s. the following equation was obtained

$$\frac{i_m}{w^{1/2}} = B_A c_b^A + \frac{k_B}{B_B} \left(\frac{i_d - i_m}{w}\right) \qquad 2.34$$

Therefore if a p.c.s. is important, a plot of $\frac{i_m}{w^{1/2}}$ against $\left(\frac{i_d - i_m}{w}\right)$ should be curved.

c) Adsorption of reactant rate-limiting

If two species A and B are present in the solution, the reduction of A occurring via an adsorbed state as described in Section 2.5.1(c), then the limiting current for this process will be as given by Equation 2.30

$$i_l = \frac{k_1 B_A w^{1/2} c_b^A}{B_A w^{1/2} + k_1} \qquad 2.30$$

In this expression, k_1 is independent of potential. Assuming as before that the reduction of B obeys the equation

$$i_c = k_B c_s^B = B_B w^{1/2} (c_b^B - c_s^B)$$

then

$$c_s^B = \frac{i_d^B - i_c}{B_B w^{1/2}} \qquad 2.45$$

since

$$i_m = i_l + i_c \qquad 2.46$$

and on the final plateau where the reduction of B becomes diffusion limited

$$i_d = i_l + i_d^B$$

$$i_d^B - i_c = i_d - i_m$$

Substituting this expression into 2.45 and then substituting for c_s^B in the equation for i_c we obtain

$$i_c = k_B \frac{(i_d - i_m)}{B_B w^{1/2}} \qquad 2.47$$

Finally, combining 2.30, 2.46 and 2.47 and rearranging gives

$$\frac{i_m}{w^{\frac{1}{2}}} = \frac{k_1 B_A c_b^A}{B_A w^{\frac{1}{2}} + k_1} + \frac{k_B (i_d - i_m)}{B_B w} \qquad 2.48$$

Once more therefore a plot of $i_m/w^{\frac{1}{2}}$ against $(i_d - i_m)/w$ should not be linear.

d) Desorption of a product rate-limiting

An analogous treatment to that described above, but with

$$i_1 = k_3 \qquad 2.32$$

gives

$$\frac{i_m}{w^{\frac{1}{2}}} = k_3 + \frac{k_B (i_d - i_m)}{B_B w} \qquad 2.49$$

In this case therefore linear plots should be obtained but the intercept should be independent of the concentration of A.

2.6 Practical considerations necessary to satisfy the R.D.E. theory

The relationship derived by Levich between the diffusion layer thickness and the rotation speed of a R.D.E., applies to laminar solution flow over a planar disc of infinite size, rotating about an axis perpendicular to its surface in a solution of infinite extent. The actual sizes and shapes of the electrode and cell needed to give agreement with these equations have been discussed by Riddiford[2.3].

The important requirement concerning the disc size is that its overall diameter must be large compared with

the thickness of the Prandtl layer. This is the layer of liquid dragged round with the disc and its thickness is approximately equal to $2.7\ (\nu/w)^{1/2}$.

The theoretical disc has no thickness, whereas the edges of a practical disc can cause turbulence. This is best minimised by embedding the disc in an annulus of an inert insulator with tapered edges. The use of this annulus also allows small electrode areas to be employed without contravening the requirement discussed in the last paragraph. Local turbulence also results if irregularities in the disc surface are comparable in depth to the thickness of the Prandtl layer. When this occurs, e.g. with unpolished, flaked pyrolytic graphite, the Levich theory is no longer quantitatively correct. In the case of the pyrolytic graphite curved $1/i \,/\, 1/w^{1/2}$ plots were obtained.

A further cause of turbulence is the use of too high a rotation speed. If, however, the rotation speed is too low, natural convection becomes important and the theory is again inapplicable. The limits of application of the theoretical equations are conveniently expressed by the corresponding values of the Reynolds number (R_e), given by

$$R_e = \frac{r\,w}{\nu}$$

where r is the overall radius of the disc. The theory applies when $10^2 < R_e < 5 \times 10^4$.

The electrode must be centred accurately on the driving shaft which must be free from whip. If these

conditions are not met, the area swept out by the disc differs from its geometric area.

The requirement that the solution should be of infinite volume arises from the need to ensure that no interference to fluid flow is produced by the cell walls. In practice it is found that this condition is satisfied providing that the cell walls are at least 0.5 cm from the periphery and surface of the disc.

The Luggin capillary must also be located with care. It is best arranged to be vertical as it approaches the disc and to be directly below the centre of the disc. Ideally the tip of the capillary should be at least 0.5 cm from the disc but this may result in an unacceptably large iR drop.

CHAPTER 3

EXPERIMENTAL

3.1 The Potentiostat

A Chemical Electronics, Model TR70, 2A, potentiostat was used for the majority of the work.

Two signals were applied to the inputs of the amplifier. One signal, either a steady potential from a potentiometer or a linear voltage sweep supplied from a function generator, was the potential to be impressed on the working electrode (W.E.). The second signal was the difference in potential between the W.E. and the reference electrode (R.E.). The difference between the two input signals was amplified, and applied via the output stage, to the subsidiary electrode (S.E.) and the W.E. of the cell. This resulted in a current being driven through the cell in a direction such that the potential of the W.E. tended towards the required value.

3.2 The Rotating Disc Electrode (R.D.E.) drive

The R.D.E. was driven by a motor controlled by a velodyne servo-amplifier (Fig. 3.1). A generator mounted on the same shaft as the motor produced a voltage which is ideally directly proportional to motor speed. A fraction of this voltage was compared with a reference voltage obtained from a zener diode stabilised source. Any difference was amplified by the C450 and 2N3741 transistors and the signal applied to the motor field coils, which, in turn, increased the motor speed until the generated voltage was equal and opposite to the reference voltage.

To minimise variations in motor speed as a result of changing motor temperatures it is necessary to maintain a constant current through the generator field coils. A constant voltage supply is unsatisfactory because the resistance of these coils varies with temperature, leading to variation in the magnetic field in the generator and hence in the output voltage at a given rotation speed. The current to the generator field coil was stabilised using the circuit shown in Fig. 3.1. (Ref. 3.1). The potential on the base of the AUY 10 transistor was fixed by the 330 and 160 Ω resistor chain. If the current passing through the field coils decreased, the potential of the collector decreased so that the base-collector potential difference would become greater thus restoring the current to its original value.

The variation in the motor speed with temperature was about 1% per degree. At constant temperature the reproducibility was within the timing error.

A small magnet attached to the top of the motor shaft caused a reed switch (Radiospares 6RSR) to close twice for every revolution of the shaft. This switch was connected via the circuit shown in Fig. 3.1 to a Harwell scaling unit type 1221C. This counted the number of pulses and hence the number of revolutions in a given time.

3.3 The function generator

The function generator was constructed as described in Ref. 3.2: linear potential sweeps between 0 and $\pm$ 3 V at rates between 1 mV and 900 V sec^{-1} were possible.

3.4 Recording arrangements

In the steady-state potentiostatic experiments, the current was measured either on a calibrated Cambridge Unipivot galvanometer or from the voltage drop across a standard resistor measured with a Digital Voltmeter.

When a voltage sweep was applied to the system the resulting current-potential curve was recorded on either an X-Y plotter or an oscilloscope. The current was measured as the potential developed across a 0.1% standard resistor in series with the electrolysis cell, while the potential was fed directly from the output of the function generator. The X-Y recorders used were a Bryans 21000 series or a Bryans 26000 series; the latter, having a much faster response time, was used when rapid transients were obtained. For very fast sweeps a Tektronix type 502A Dual Beam Oscilloscope was used.

3.5 Cells

All cells were made from pyrex glass, the taps being of the liquid-sealed type. The electrolysis cell was thermostated at 25 $\pm$ 0.1 ^{o}C in a water bath.

3.5.1 Electrolysis cell

The design of this cell was such as to satisfy the requirements of the Levich theory of the rotating disc

electrode as completely as possible[3.3]. It is illustrated in Fig. 3.2. The main compartment had a volume of approximately 50 cm^3 and was filled with tubes to enable gas to be passed through the electrolyte or over its surface. The disc electrode passed through a "Hostaflon" cone mounted in the B24 socket. A platinum counter electrode was located in a separate compartment isolated from the main compartment by a glass sinter. An external hydrogen reference electrode connected via a liquid-sealed tap and Luggin capillary to the main compartment.

The potential difference required in potentiostatic experiments is that between the W.E. and a point in solution outside the electrical double layer. The experimentally measured potential difference is that between the W.E. and the tip of the Luggin capillary. It has been shown[3.4,3.5], that the ohmic potential drop resulting from the flow of current through the solution is minimal if the tip of the capillary is placed close to and directly below the disc. In order to satisfy these requirements and also ensure that the hydrodynamic flow of material to the electrode was not disturbed, the tip of the Luggin capillary was located about 0.5 cm directly below the disc. The high conductivity of the solutions and the low current densities employed ensured that iR effects were small.

3.5.2 The pre-electrolysis cell

This cell had a total volume of approximately 1 litre. The solution was contained in a glass vessel 7 cm in diameter and 25 cm long. A two-way liquid-sealed tap, sealed to the bottom of the vessel, enabled the solution to be transferred directly into the electrolysis cell. Nitrogen was passed through a sinter in a B24 socket into the solution. A B50 socket carrying an exit bubbler for nitrogen and two 3 cm square, lightly-platinised, platinum electrodes fitted into the top of the cell. One of the electrodes, normally made the anode, was positioned near the sinter and 12 cm above the other.

3.6 Electrodes

3.6.1 Noble metal cathodes

The rotating-disc electrodes are shown in Fig. 3.3 A. They consisted of a precision-ground silver-steel shaft $^1/_4$" diameter and 25 cm long, to one end of which a 1 cm length of platinum or gold rod was silver soldered. The noble metal was machined into a cone shape with the lower surface 0.5 cm in diameter, so that its tip ran true to within $\pm$ 0.003 cm when 17 cm of the shaft protruded from a chuck. The electrode was encased in a 12.5 cm long "Hostaflon" tube which screwed into a threaded collar on the steel shaft so that only the upper part of the shaft, and the lower face of the noble metal was exposed. The hole in the lower end of the "Hostaflon" tube was tapered to fit the conical sides of the noble metal to obtain a leak-free seal. The "Hostaflon" was finally

machined to the shape shown in Fig. 3.3a. The surface of the electrode was polished by grinding on a series of emery papers, finishing with a 6"o" grain size. A mirror finish was then imparted by wet-grinding with alumina powders on selvyt cloth, finishing with γ alumina powder. The alumina was removed by immersion in dilute sulphuric acid. The area of the exposed noble metal was 0.132 cm^2 for platinum and 0.135 cm^2 for gold.

3.6.2 Carbon cathodes

In the preliminary work with pyrolytic graphite electrodes, polythene, araldite and laconite were tried as insulators. Araldite was poured into a glass mould surrounding the electrode, and cured by heating at 100°C for 48 hours. Laconite was painted on to the sides of the electrode and dried at room temperature for 48 hours. Heat-shrinkable polythene tubing was heated with hot air while surrounding the electrode. None of these materials proved entirely satisfactory, see Chapter 7.

An electrode (Fig. 3.3b) was therefore designed using "Hostaflon" as insulator. This design was used to investigate the behaviour of different types of graphite in the background electrolytes. It also protected the edges of the layer planes in pyrolytic graphite. A graphite cylinder of the same diameter as the stainless steel shaft was cemented to the shaft with conducting araldite. The final 2 mm of the central hole in the "Hostaflon" insulator was of slightly smaller

diameter than the graphite cylinder so that it could be screwed home tightly against the graphite, thus forming a leak-tight seal.

This design of electrode, although satisfactory in many respects, did not satisfy the conditions for laminar flow of the solution. In all of the work in chromium containing solutions, an electrode with a moulded PTFE insulator was used. This electrode was prepared by placing a 0.6 cm diameter $1^{1}/_{2}$ cm thick, P.G. core in the centre of a steel mould. PTFE powder (Grade G3, I.C.I. Ltd.) was added and compressed at 2 ton in^{-2}. After releasing the pressure, the mould was heated to 375°C, the above pressure again applied and the mould allowed to cool to room temperature. An axial hole was drilled through the resulting PTFE cylinder up to the enclosed surface of the graphite. A stainless steel shaft, inserted in this hole, was cemented to the graphite with conducting araldite. The final electrode could then be machined to any desired shape, although the simple cylinder was found to be perfectly satisfactory.

In the experiments involving electron-optical examination of the graphite surface, heat-shrinkable PTFE was used as insulating material. Initial experiments with one variety of this material (Hellashrink, Hellermann Electric Ltd.) had shown that it did not adhere to the electrode sufficiently well to prevent leakage. More recently a new variety "Flo-tite" tubing

(Pope Scientific Inc.) has become available. This consists of an outer sheath of heat-shrinkable PTFE and an inner tube of F.E.P. On heating, the inner tube melts and adheres to the sides of the electrode, providing a very satisfactory seal.

With either moulded or heat-shrunk insulators, a fresh graphite surface could be produced by machining away a little of the PTFE surface and flaking off the exposed graphite with a clean, sharp razor-blade. Such a surface, however, was not sufficiently flat to satisfy the requirements of the Levich theory (see Chapter 2). A satisfactorily smooth surface could be produced by machining the freshly exposed surface and carefully removing the debris with tissue paper. Alternatively, the electrode could be held at 0.7 V in 1 x 10^{-2} M Cr VI, 1 M $HClO_4$ for 15 minutes and the surface then polished with tissue paper. Repetition of this treatment, at least three times, produced a smooth surface as shown in Fig. 3.4.

3.7 Bearing for the R.D.E.

The bearings for the electrode shaft, Fig. 3.3, were ball races of 0.25" internal diameter mounted in a brass tube attacked to a brass back plate. A B24 "Hostaflon" cone screwed onto the bottom of the brass tube and compressed a PTFE "o" ring onto the steel shaft of the electrode so that a gas-tight seal was achieved. A steel rod, mounted in a second bearing assembly, also attached to the back plate, was connected to the motor

shaft with polythene tubing. The electrode was driven via two nylon gears, one fitted to the driver shaft and the other to the electrode. Electrical contact to the electrode was made via a nickel wire dipping into a mercury pool in a small hole in the top of the electrode shaft. A PTFE cap with a small central hole prevented the mercury from escaping.

3.8 Reference electrodes

A hydrogen reference electrode immersed in the background electrolyte was used in all experiments and potentials are quoted with respect to this electrode. The electrodes were platinised by a modification of the method described by Popoff et al[3.6].

The electrode was first cleaned by anodic polarisation in concentrated HCl, followed by cathodic polarisation in hot, strong NaOH and washed in doubly distilled water. It was then platinised by cathodic deposition at 13 mA cm^2 for 5 minutes from a solution of 3% chloroplatinic acid made 5×10^{-3} M in lead acetate. After washing, it was polarised cathodically in cold dilute NaOH for 15 seconds and in 1 M H_2SO_4 for 30 seconds, finally being stored in doubly distilled water.

"White spot" hydrogen (B.O.C. Ltd.) was used without further purification.

3.9 Cleaning of glassware and electrodes

The cells, and associated glassware, were cleaned by immersion for at least 12 hours in a freshly prepared

mixture of equal volumes of concentrated nitric and sulphuric acids. After steeping, the glassware was washed in distilled water, followed by several washings in doubly distilled water, to remove the excess acid.

The noble metal electrodes were cleaned by immersion in concentrated H_2SO_4 and then washed in doubly distilled water. Glassy-carbon electrodes were cleaned by abrasion with fine grade wet and dry paper, followed by alumina on selvyt cloth. They were then immersed in dilute sulphuric acid and rinsed in doubly distilled water. The preparation of the pyrolytic graphite surface has already been described. No chemical cleaning agents were found suitable for use with this graphite.

3.10 Preparation of purified water

During the initial work triply distilled water was used. This was prepared by normal distillation of tap water followed by distillation from a very dilute solution of potassium permanganate and then from a dilute phosphoric acid solution. It appeared, however, that traces of phosphoric acid in this water were affecting the results (see Chapter 1). Powers[3.7], has shown that water obtained in this manner is normally contaminated, probably due to droplet entrainment, with permanganate and phosphoric acid.

This contamination can be avoided[3.7] by using the still design shown in Fig. 3.5. The still pot was a 10 litre Pyrex flask, connected to the condenser by a 35/50 ball joint. This ball joint, and the others on the still,

were lubricated only with water. Provision was made in the flask for the introduction of feed water and of purified gas through a fritted bubbler. The pot was heated with an Electrothermal heating mantle.

The fused-silica condenser consisted of a vertical section $1^{3}/_{4}$" in diameter and 18" long, joined to a $^{1}/_{2}$" diameter re-entrant tube which could be water cooled over a 15" length. The vertical section was thermally lagged with asbestos tape to reduce transport by surface creep[3.8].

The fused-silica still head provided means for measuring the electrical conductivity of the distillate and either accepting the distillate into a receiver or rejecting it. When the Teflon-bore stopcock located beneath the conductivity cell was closed, the water level rose in the still head and distillate was rejected. Continuous sampling of the distillate was possible by opening the cock partially. The gas bubbled through the still pot was vented through a water trap.

Ordinary distilled water in the still pot was held at a temperature just under the boiling point for 16 to 24 hours. During this time purified oxygen was bubbled through the water to oxidise any organic impurities. Distillation was then carried out at rates of up to 1 litre per hour in the presence of oxygen or an inert gas. The usual practice was to operate the condenser without water cooling until about 1 litre of water had been removed from the pot. This ensured that the condenser and still head were thoroughly cleaned with steam. About 2 litres were then rejected before collecting the water.

The oxygen gas was passed through a purification train to remove any organic impurities. This train consisted of four 0.5 litre gas-washing bottles containing respectively, concentrated H_2SO_4, water, concentrated NaOH, and water. The head of each bottle was fitted with a coarse grade, fritted, cylindrical gas-dispersion tube. Gas passed through the train at a rate of 2 to 3 litres per hour. Flexible connections were made with polythene tubing.

Conductivities as low as 9×10^{-8} ohm^{-1} cm^{-1} have been obtained when using this still.

3.11 Solutions

The background electrolytes were "Aristar" grade perchloric or sulphuric acids. Solutions containing Cr VI were prepared initially from Analar CrO_3 but this was difficult to purify further and triply recrystallised Analar K_2CrO_7 was used in the later experiments. Where required, Analar Na_2SO_4 and $NaClO_4$ were used with no further purification.

Ionic impurities in solution can be removed by pre-electrolysis on auxiliary electrodes, while non-ionic species may be adsorbed on platinised platinum or active charcoal. In the present work the solutions to be used with noble metal electrodes were purified by pre-electrolysis, while active charcoal was employed when graphite electrodes were to be used. These procedures were adopted because the impurities likely to affect a particular electrode material are ~~not~~ most likely to be removed onto similar material.

Thus perchloric acid, used in work with gold electrodes, was pre-electrolysed at constant current for 48 hours in the cell described in Section 3.5.2. The purity of the sulphuric acid used was already high and was not significantly improved by this technique.

Purified active charcoal was added to all background electrolytes used with carbon electrodes. After adding the charcoal, the solution was well shaken then allowed to stand for 30 minutes before use. The charcoal was removed before adding K_2CrO_7.

3.12 Preparation of purified active charcoal

A highly absorbing active carbon of mesh 14-22 (Speakmann and Sutcliffe Ltd.) was used. It was purified by extracting with frequently renewed constant-boiling hydrochloric acid in a Soxhlet for six weeks, followed by extracting with successive portions of doubly distilled water, until acidified silver nitrate solution added to the water gave no precipitate.

3.13 Identification of surface film on gold and graphite

The gold electrode used was in the form of a cylinder, radius 0.5 cm, length 0.4 cm, suitable for mounting in an electron microscope. The face to be observed was abraded on a fine grade wet and dry paper followed, in some experiments, by polishing with alumina on selvyt cloth. The alumina was removed with dilute and concentrated sulphuric acid and the electrode washed in acetone, followed by doubly distilled water.

The pyrolytic graphite electrode is described in section 3.6.2. Samples for examination were removed by flaking off thin sections from the electrode using a clean, stainless steel blade.

Both gold and graphite were examined by glancing-incidence, high-energy electron diffraction. The pyrolytic graphite was also examined using scanning electron microscopy, X-ray probe analysis and mass spectrometry.

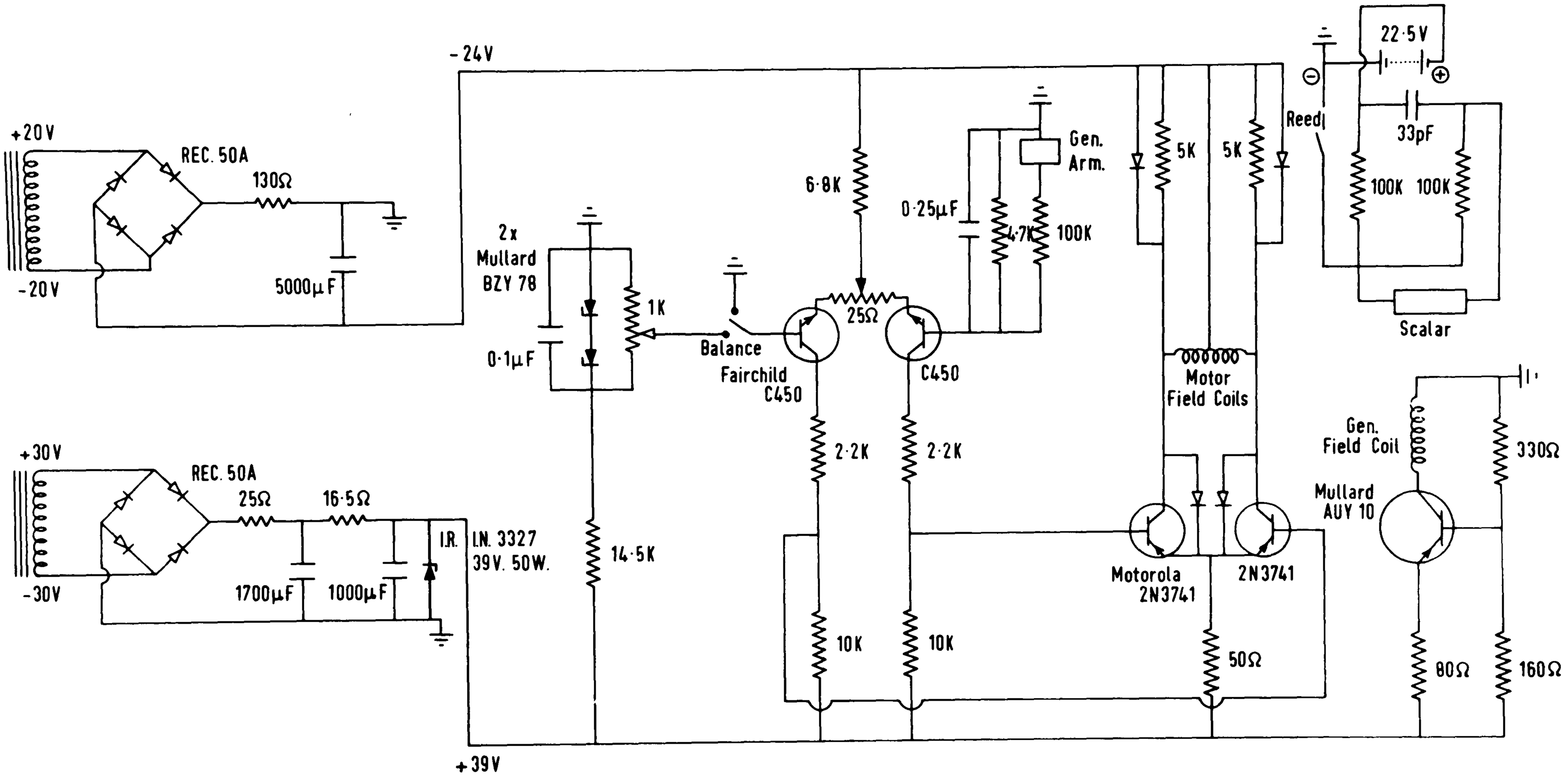

VELODYNE AMPLIFIER

Fig. 3.1

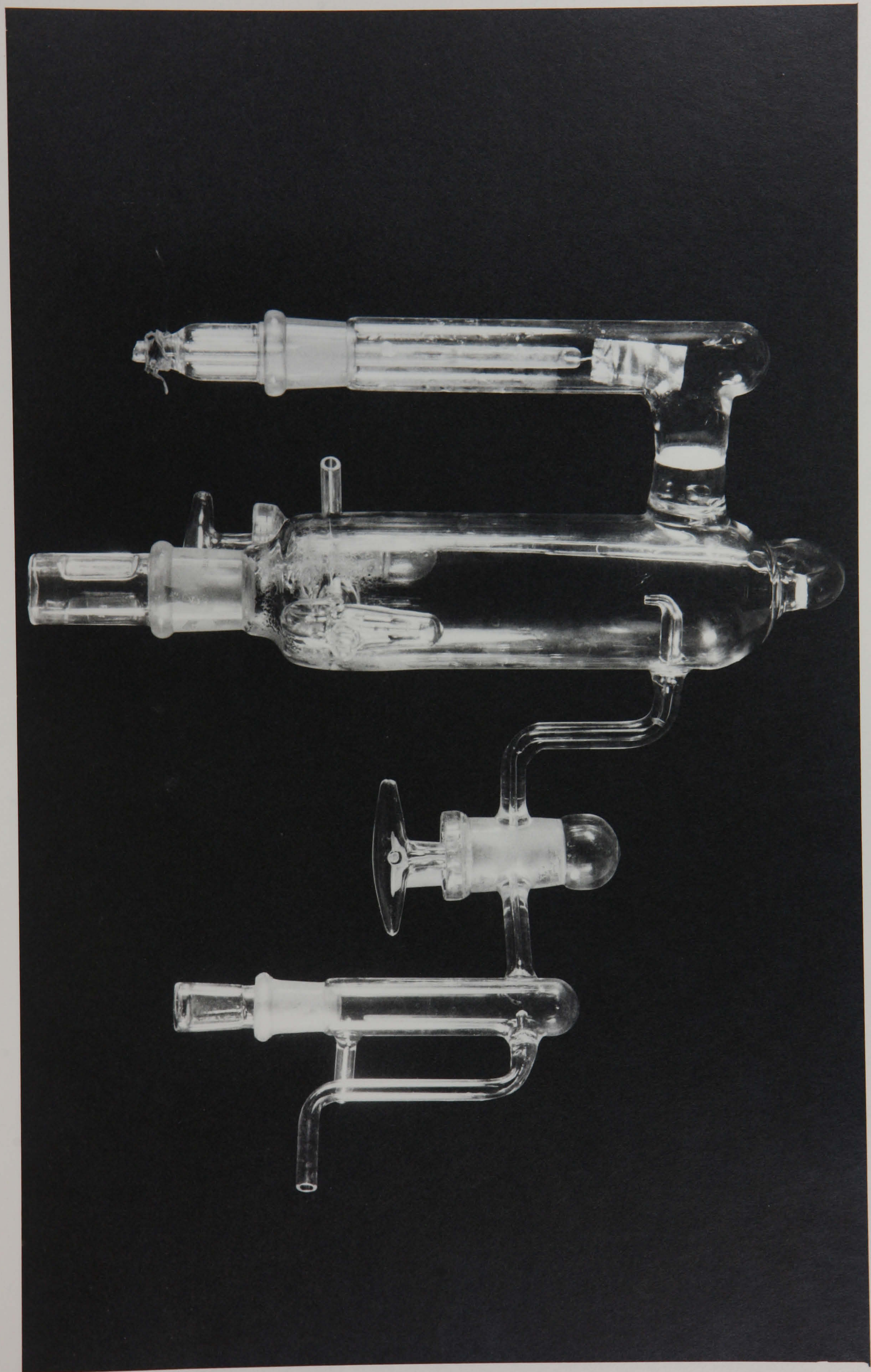

Fig. 3.2 The Electrolysis Cell

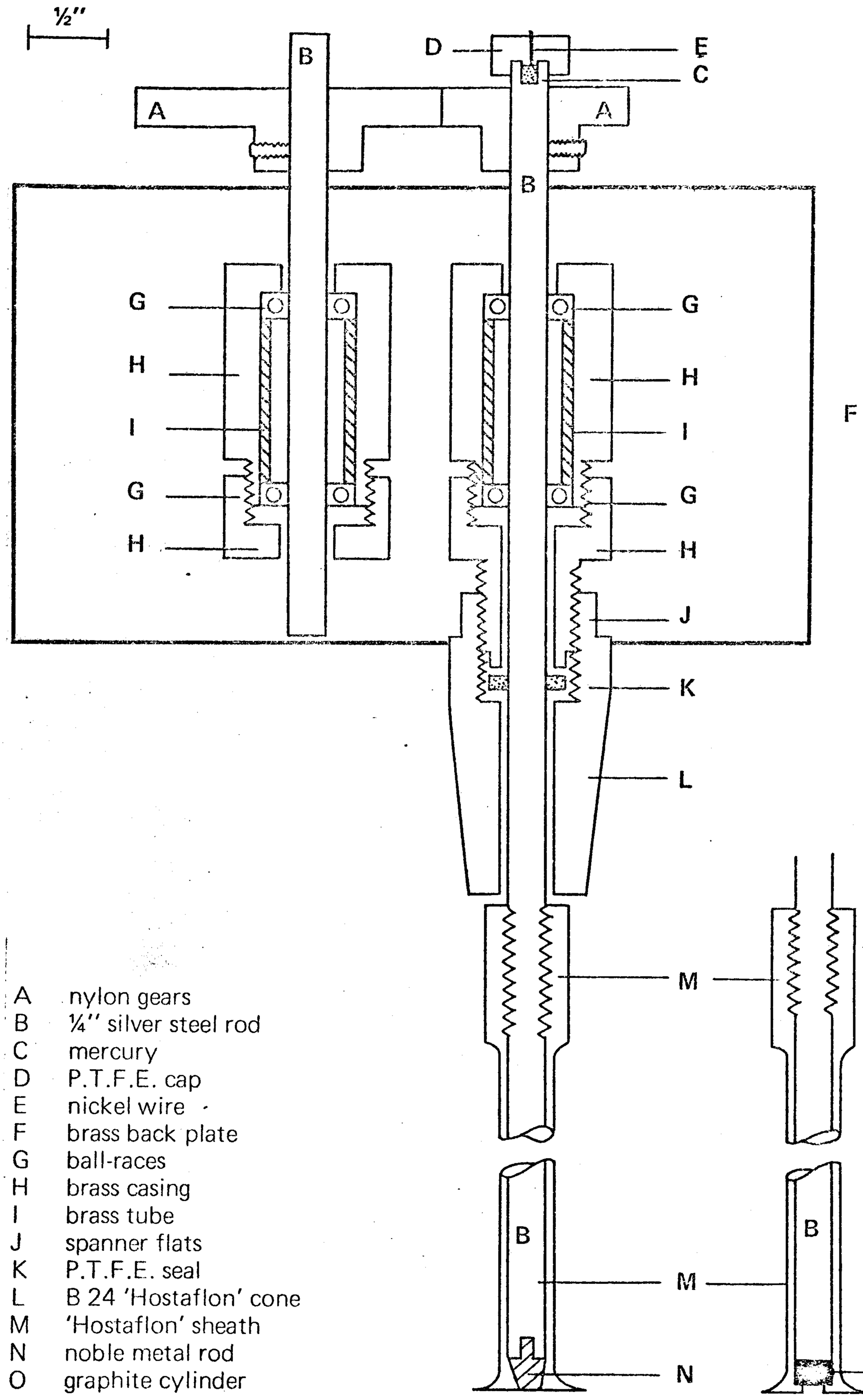

- A nylon gears
- B ¼" silver steel rod
- C mercury
- D P.T.F.E. cap
- E nickel wire
- F brass back plate
- G ball-races
- H brass casing
- I brass tube
- J spanner flats
- K P.T.F.E. seal
- L B 24 'Hostaflon' cone
- M 'Hostaflon' sheath
- N noble metal rod
- O graphite cylinder

Fig. 3.3
THE ROTATING DISC ELECTRODES AND BEARING ASSEMBLY

(a) Flaked P.G. surface x 100

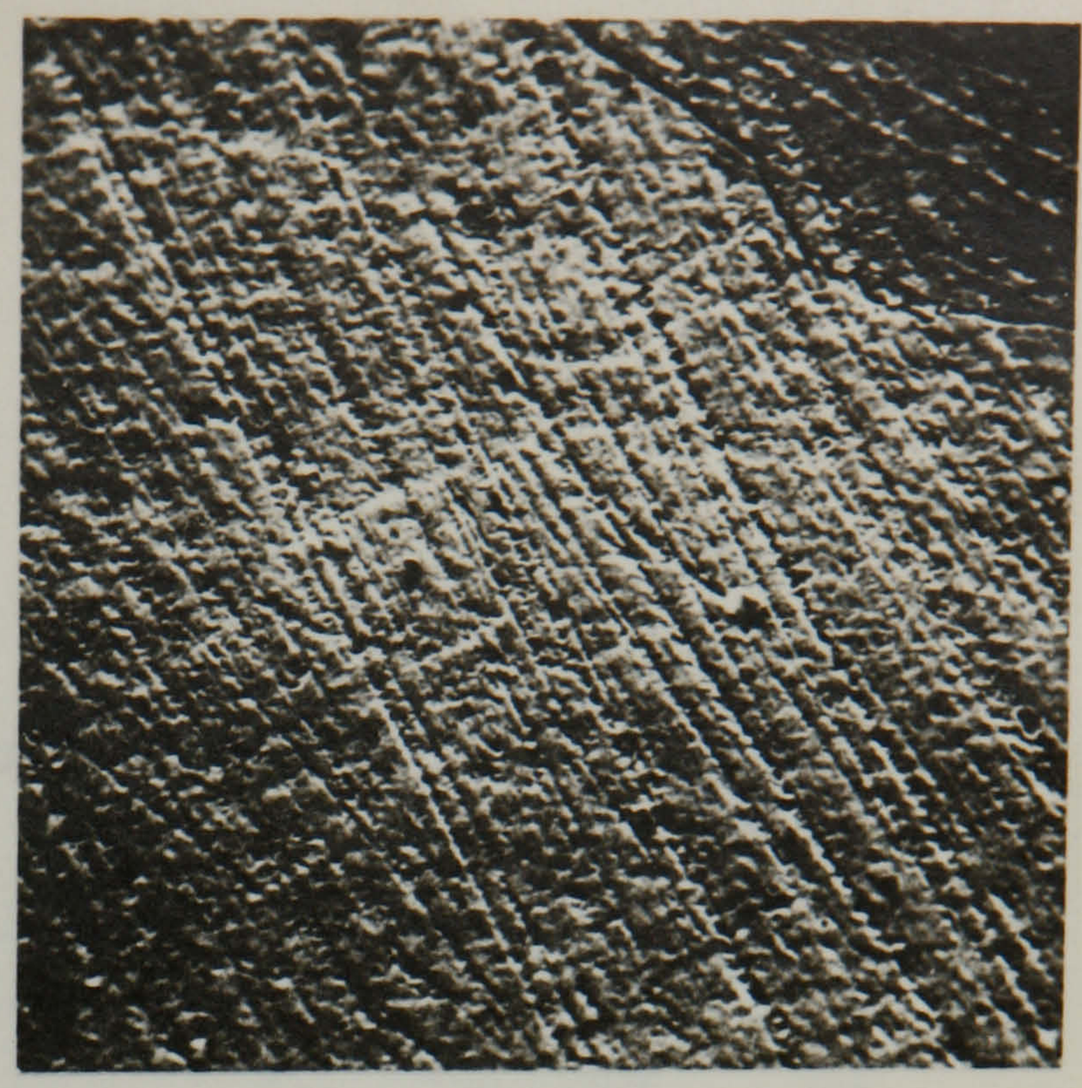

(b) P.G. surface following machining, electrochemical pretreatment and polishing x 100

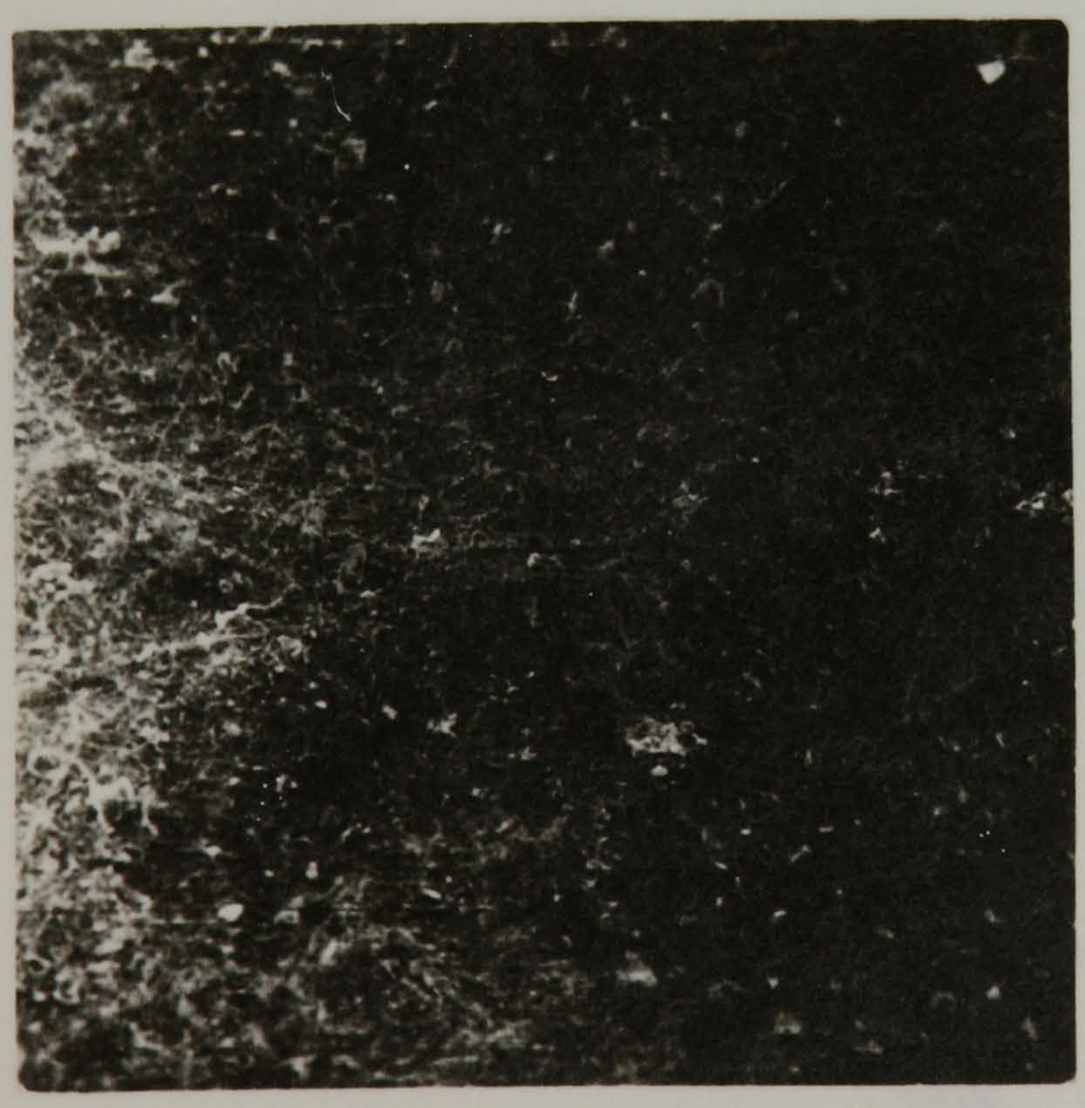

(c) Flaked P.G. electrode following 30 minutes pretreatment at 0.7v, 1×10^{-2} M Cr VI, IM $HClO_4$. x 100

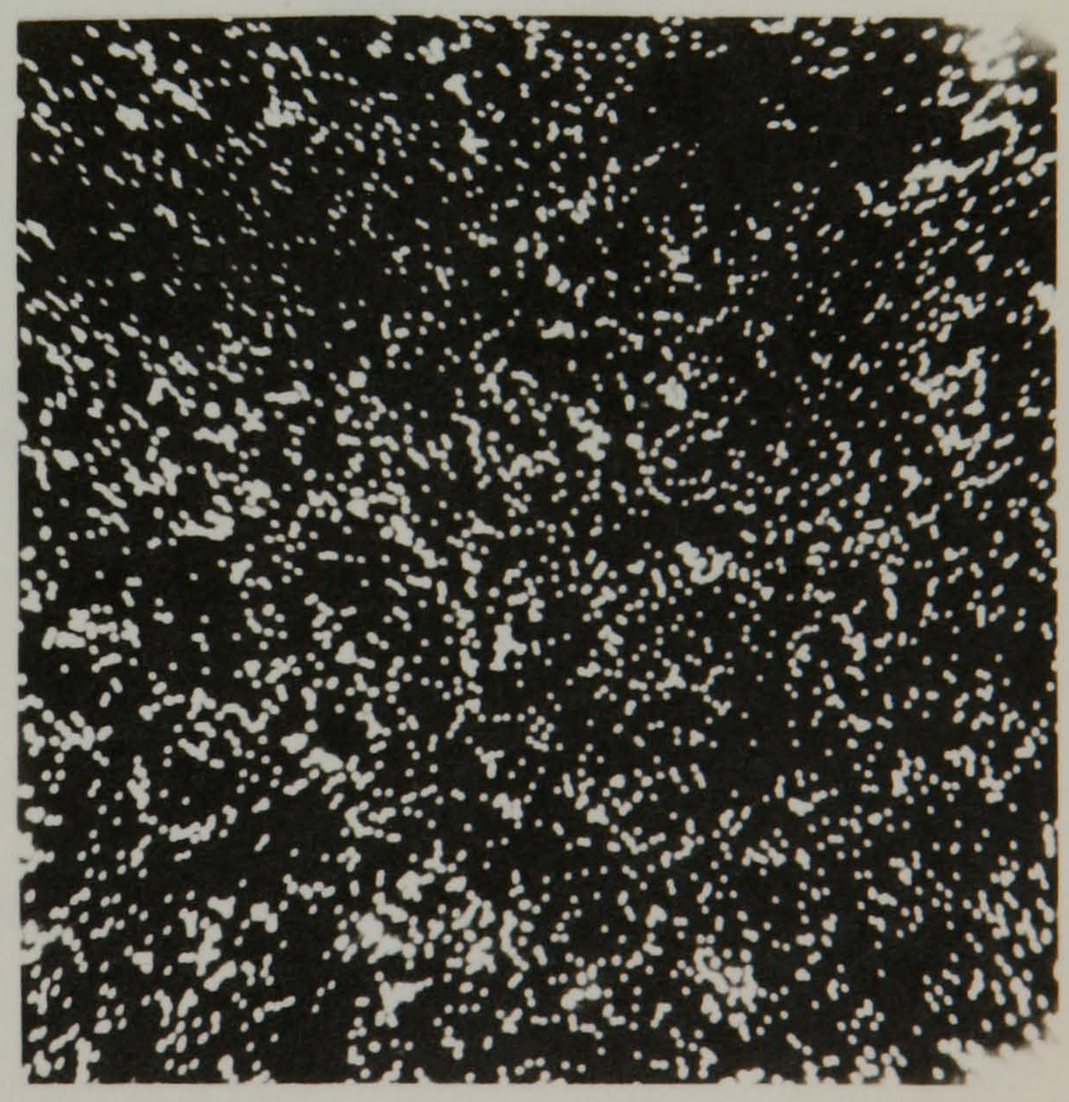

(d) Flaked P.G. electrode following 30 minutes pretreatment at 0.7v, 1×10^{-2} M Cr VI, IM $HClO_4$; X-ray emission. x 500

Fig. 3.4 SCANNING ELECTRON MICROSCOPE PICTURES OF PYROYTIC GRAPHITE

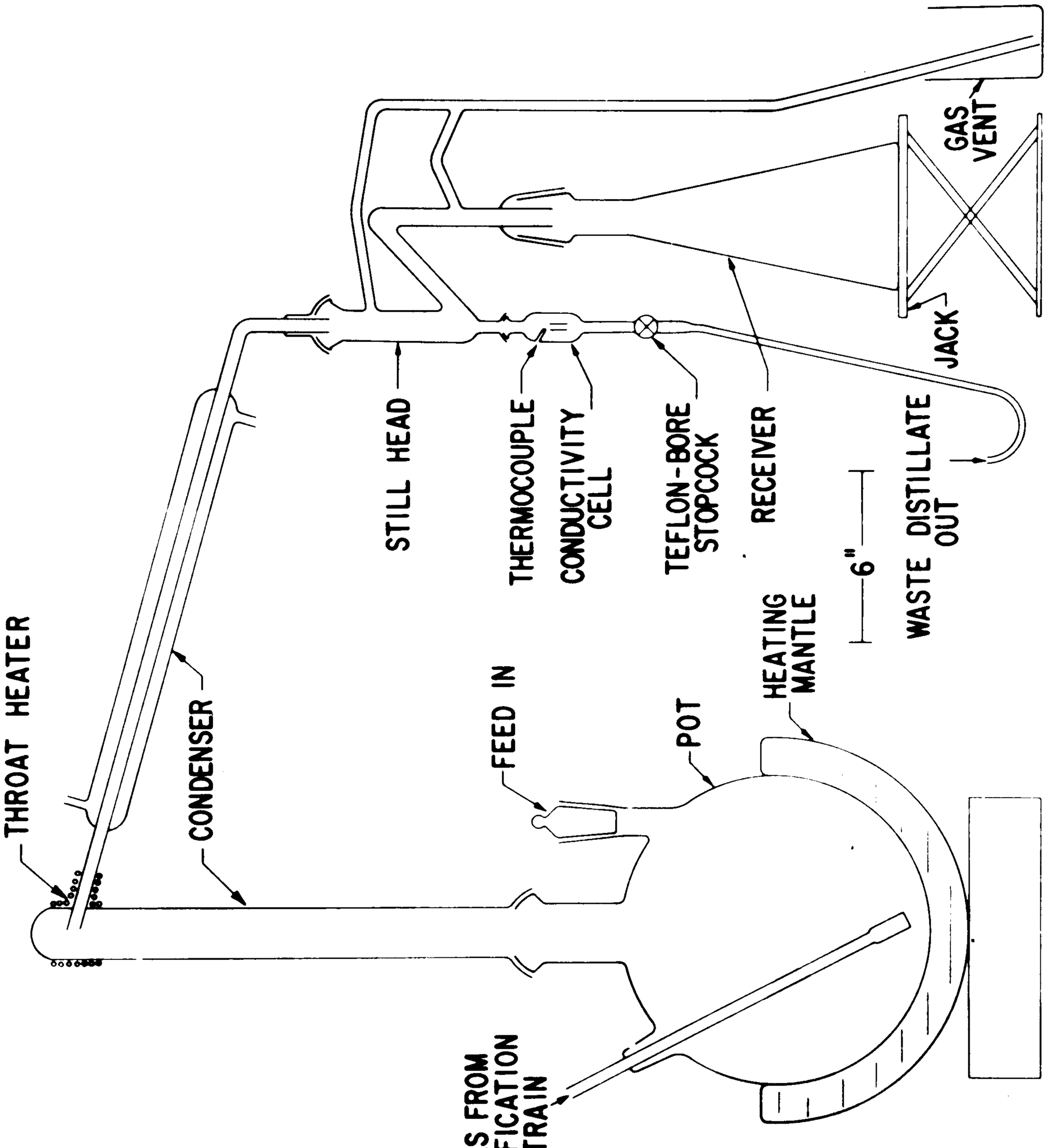

Fig. 3.5 Still for preparation of very pure water

CHAPTER 4

COULOMETRIC EXPERIMENTS

4.1 Introduction

In order to define the potential range over which Cr VI is reduced to Cr III it was necessary to determine the number of electrons involved in the reduction process. With pyrolytic graphite the current-potential relation consisted of three steps and coulometric experiments were necessary to establish whether or not the reduction was taking place in three one-electron steps.

4.2 Experimental

The experiments consisted of recording the current-time relation during constant-potential electrolysis of Cr VI solutions. Integration of this relation gave the quantity of electricity passed during the electrolysis. The initial and final concentrations of Cr VI and Cr III in the catholyte were determined by colorimetric procedures. If the whole of the current is used in the reduction of Cr VI to Cr III, the quantity of electricity passed should equal that calculated from Faraday's Law and the quantity of Cr III produced, while the decrease in Cr VI concentration should equal the increase in Cr III concentration.

The current-time relation was recorded on a Servoscribe Y-t recorder. An accurate value of the quantity of electricity passed was obtained by cutting out and weighing the relevant area of chart paper. Comparison

of this weight with that of a known number of squares gave the area under the curve.

After electrolysis, 10 ml samples of the solution were analysed either for Cr VI or for Cr III as described below.

4.2.1 Analysis for Cr III

Analysis for tervalent chromium was performed using the method described by Fuhrman and Latimer[4.1]. The Cr III was separated from Cr VI by precipitation as the hydrous oxide, with $Zn(OH)_2$ as a carrier. The hydrous oxide was collected by centrifuging, washed with water at pH 10 and dissolved in perchloric acid. The Cr III solution was then complexed with 1,2-diaminocyclo-hexanetetra-acetic acid (CDTA) at pH 3 and the absorbance of the resulting solution measured at 540-550 mμ. The Cr III concentration was then obtained from a calibration graph.

This graph was obtained initially as a result of complexing a known amount of chromic perchlorate with CDTA and analysing the resulting solution. Chromic perchlorate, however, is hygroscopic, making an accurate calibration impossible. More satisfactory results were obtained by using two other sources of Cr III. Thus either potassium chromate was dissolved in 1 M perchloric acid or a standard solution of potassium dichromate in 1M perchloric acid was reduced using excess hydrogen peroxide[4.1]. The calibration graphs obtained by the two latter methods were identical.

A quantity of Cr III was always found in the freshly prepared electrolyte. The concentration varied from 3 to 5 x 10^{-4} M Cr III in a 1 x 10^{-2} M solution of Cr VI. The analytical results were corrected for this background concentration of Cr III.

4.2.2 Analysis for Cr VI

The concentration of Cr VI was determined by the absorbance of the solution at 351 mμ. A calibration graph obtained with a range of standard solutions of Cr VI was used to calculate the concentration. Since the relation between concentration and absorbance was non-linear[4.2] it was necessary to use standard solutions with concentrations close to that of the solution being analysed.

4.2.3 The coulometric cells

Two coulometric cells were employed. Cell 1 was a single compartment design containing a maximum of 15 cm^3 of electrolyte. It was preferred for work at more positive potentials where the quantity of electricity passed was small. A platinum cylinder approximately 2 cm^2 in area served as an anode. The cathode was insulated with shrink-fit polythene, since an electrode of small external diameter was required. The hydrogen reference electrode was separated from the main compartment by a liquid-sealed tap. Cell 2 had a maximum volume of 50 cm^3 so that the usual R.D.E. design could be used. Two subsidiary electrodes were provided, an internal platinum cylinder 2 cm^2

in area and a platinum wire coil located in a low volume ($3\ cm^3$) side-arm connected to the main compartment via a porous sinter.

4.3 Results

4.3.1 Pyrolytic graphite

Experiments were conducted at a range of potentials in a solution of 1 M in $HClO_4$ and 10^{-2} M in Cr VI. Under all circumstances, the amount of Cr VI consumed by electrolysis was equal to the amount of Cr III produced, and three electrons were required to reduce one atom of Cr VI. The actual results are reported in table 4.1.

It appears therefore that over the potential range 0.95 to 0 V the electrode process may be represented by the equation

$$Cr\ VI + 3e = Cr\ III \qquad (4.1)$$

It should be noted that the oxidation of Cr III to Cr VI can occur on platinum at sufficiently positive potentials. Consequently erroneous results are obtained if the internal counter-electrode is used under these conditions.

4.3.2 Gold

It was not possible to conduct experiments at potentials other than those corresponding to the plateau of the current-potential curve; the amount of Cr III produced at more positive potentials was too small for an accurate analysis. The results obtained at potentials

from 0.4 to 0.1 V are shown in table 4.2. They again indicate that the process occurring on the plateau of the curve is accurately represented by equation 4.1.

Similar results were obtained with sulphuric acid as background electrolyte using both pyrolytic graphite and gold electrodes.

TABLE 4.1

Reduction of Cr VI on Pyrolytic Graphite

Potential (V)	Quantity of Electricity (coulomb)	Concentration of Cr III produced (mol litre^{-1})	Current efficiency (%)
0.00	119.8	5.50×10^{-4}	97 ± 3
0.30	112.2	6.50×10^{-4}	103 ± 3
0.65	70.2	3.50×10^{-4}	102 ± 3
0.85	20.8	1.35×10^{-4}	94 ± 12
0.90	54.5	2.75×10^{-4}	97 ± 5
0.925	39.6	1.95×10^{-4}	103 ± 8
0.95	53.4	1.73×10^{-4}	94 ± 6

TABLE 4.2

Reduction of Cr VI on Gold

Potential (V)	Quantity of Electricity (coulomb)	Concentration of Cr III produced (mol litre^{-1})	Current efficiency (%)
0.4	57.7	3.7×10^{-4}	99 ± 3
0.2	53.0	3.5×10^{-4}	99 ± 3
0.1	73.5	4.3×10^{-4}	98 ± 3

4.4 Discussion

Although these results indicate that, over the potential ranges investigated, the final product of the reduction reaction is Cr III, this is not conclusive evidence that the electrode process is always represented by equation 4.1. It is possible, for example, that the first step in the current-potential curve obtained with pyrolytic graphite actually corresponds to the process

$$3\ Cr\ VI + 3e = 3\ Cr\ V \qquad (4.2)$$

Providing this were followed by the disproportionation of the unstable Cr V species according to

$$3\ Cr\ V = 2\ Cr\ VI + Cr\ III \qquad (4.3)$$

the overall reaction would still be given by equation 4.1.

In the absence of any evidence for such processes, however, it has been assumed that the stages in the curve do not correspond to the transfer of differing numbers of electrons, but to the participation of different solution species in the electrode reaction.

CHAPTER 5

THE BEHAVIOUR OF GOLD IN ACID SOLUTIONS

5.1 Introduction

As an aid to interpreting the current-potential curves for the reduction of dichromate, the behaviour of gold in the various background electrolytes has been studied.

The surface oxidation of gold in acid solutions has been studied previously using both galvanostatic and potentiostatic techniques. The oxidation ultimately leads to the formation of chemisorbed oxygen[5.1,5.5,5.7] or gold oxide[5.1-5.6,5.8-5.10] with the initial formation of this film occurring at about 1.28 - 1.36 V w.r.t. a standard hydrogen electrode. Reduction of the film commences at potentials between 1.20 and 1.30 V. The potentials of film formation and reduction vary by $-2.3 \frac{RT}{F}$ per unit pH[5.3-5.5,5.8,5.9]. About a monolayer of Au_2O_3 is formed but at potentials more anodic than 1.8 - 1.95 V a thick oxide film forms[5.7,5.8,5.10].

The behaviour at potentials between 0.0 and 1.2 V is less well established. El Wakkad and Shams El Din[5.4] obtained inflections in the charging curves which they attributed to the successive formation of Au_2O and AuO, but their results have not been reproduced by later workers. Deborin and Ershler[5.2], after heating the gold in air, observed an anodic arrest at 0.70 V and a corresponding cathodic arrest at 0.4 V. These processes were subsequently shown to result from contamination of the gold by iron[5.6].

More definite evidence for the occurrence of a process, other than double-layer charging, in this potential region has now been reported[5.11,5.12]. This process is characterised by a maximum in the electrode capacity at $\simeq$ 0.6 V, or an abrupt increase in the quantity of electricity needed to reduce surface species after polarisation to potentials above about 0.7 V. Comparable changes in the relative phase retardation have also been observed using ellipsometry[5.12,5.13]. These phenomena have been attributed to the formation of AuOH or AuO (called "chemisorbed oxygen")[5.11,5.14,5.15].

5.2 Experimental

The measurements were made in the electrolysis cell (Section 3.5.1). A rotating disc electrode was used and was cleaned either by immersion in concentrated sulphuric acid or by etching in aqua regia. It was then washed several times in doubly distilled water. Prior to cleaning by the first method the electrodes were normally polished with γ-alumina on selvyt cloth (Section 3.6.1). The chemicals used are described in Section 3.11.

The electrode potential was swept at a known scan rate over the range to be investigated and the resulting current-potential curve was recorded on a Bryans X-Y recorder.

5.3 Results and Discussion

5.3.1 $HClO_4$ solution

The current-potential relationship obtained with a stationary electrode in oxygen-free 1 M Aristar $HClO_4$ is shown as curve a, Fig. 5.1. Rotation of the electrode produced marked changes in the curve (curve b, Fig. 5.1) suggesting the presence of electroactive impurities in the solution. In accord with this view, the magnitude of the effect depended on the batch of perchloric acid employed. These impurities were not removed by active charcoal, nor by oxidation either by boiling the concentrated perchloric acid, or by the addition of small amounts of $K_2Cr_2O_7$. However, after pre-electrolysis of the solution for 18 hours (see Section 3.11) the current-potential curve was insensitive to rotation of the electrode (Fig. 5.2) indicating that the impurities had now been removed. The current maxima observed in this latter curve must therefore be associated with modification of the electrode surface. The potentials at which these processes begin and the quantity of electricity under the maxima are reported in Table 5.1.

TABLE 5.1

Anodic maxima		Cathodic maxima	
Beginning at	Quantity of Electricity ($\mu C\ cm^{-2}$)	Beginning at	Quantity of Electricity ($\mu C\ cm^{-2}$)
c.a. 0.65 V	450	c.a. 0.75 V	450
c.a. 1.3 V	1350	c.a. 1.3 V	1350

Scans over a limited potential range (Fig. 5.3) clearly demonstrate the relationship between the two smaller peaks and between the two larger peaks. The anodic and cathodic processes occurring at the more positive potential have been observed in all previous studies of the electrochemical behaviour of gold. Since the reversible potential of the Au/Au_2O_3 electrode in 1 M $HClO_4$ is 1.36 V these current maxima have been attributed to the formation and reduction of Au_2O_3 on the gold surface. The quantity of electricity passed in the more anodic maxima is comparable to that reported by previous workers and corresponds approximately to the formation and reduction of a monolayer of Au_2O_3. The complex shape of the anodic curve suggests however that the process may be more complicated than this.

Processes akin to those occurring during the less positive maxima have been observed by Schmid and O'Brien[5.11] and Sirohi and Genshaw[5.12] and attributed to the formation and reduction of AuO and AuOH. Since a number of other workers had failed to observe these processes, it seemed possible that they originated from impurities. Although

a variety of cleaning procedures including polishing the electrode with γ-alumina and washing in acetone or in an equivolume mixture of concentrated sulphuric and nitric acids failed to remove the maxima, they were almost removed by etching the gold for two hours in fresh aqua regia, Fig. 5.4. This suggests that they do in fact originate from impurities in the gold surface.

Since the gold was at least 99.95% pure, it was unlikely that the impurity originated from within the gold. The great difficulty experienced in removing this impurity allied to the failure to remove the effect by more careful control of the experimental conditions suggested that the inclusions were introduced during abrasion with emery paper (see Section 3.6.1). In accord with this, a sample of gold identical with that used in previous experiments but not polished with emery paper gave the curve shown in Fig. 5.5. Confirmation of this conclusion is also provided by the fact that only those previous workers who polished their electrodes with emery paper observed these processes[5.11,5.12]. (Compare for example reference 5.16).

Since the behaviour in chromium containing solutions was substantially unaltered by the presence or absence of these inclusions and a polished electrode was preferred, most of the measurements reported subsequently refer to electrodes polished with emery paper.

5.3.2 H_2SO_4 solutions

The addition of 2×10^{-3} M H_2SO_4 to 1 M $HClO_4$ produced some interesting changes in the form of the current-potential curves (fig. 5.6). While the reduction peak at about 1.16 V is unaffected, the onset of surface oxidation of the gold at 1.28 V is moved about 100 mV more positive. The shape of this section of the curve is also modified. It is also of interest that the maxima attributed to contaminants now occur at 0.8 and 0.7 V rather than at 0.9 and 0.55 V.

In 0.5 M H_2SO_4 essentially the same curve is obtained as described above (fig. 5.7). The quantities of electricity passed in the oxidation and reduction of the gold surface are very close to those observed in perchloric acid solution. It is probable that the interpretation of these curves given in Section 5.3.1 is again applicable.

In 0.25 M H_2SO_4/0.25 M Na_2SO_4 and 0.05 M H_2SO_4/ 0.45 M Na_2SO_4 solutions, after correcting for the changes in hydrogen ion concentration, the curves were identical with those obtained in 0.5 M H_2SO_4.

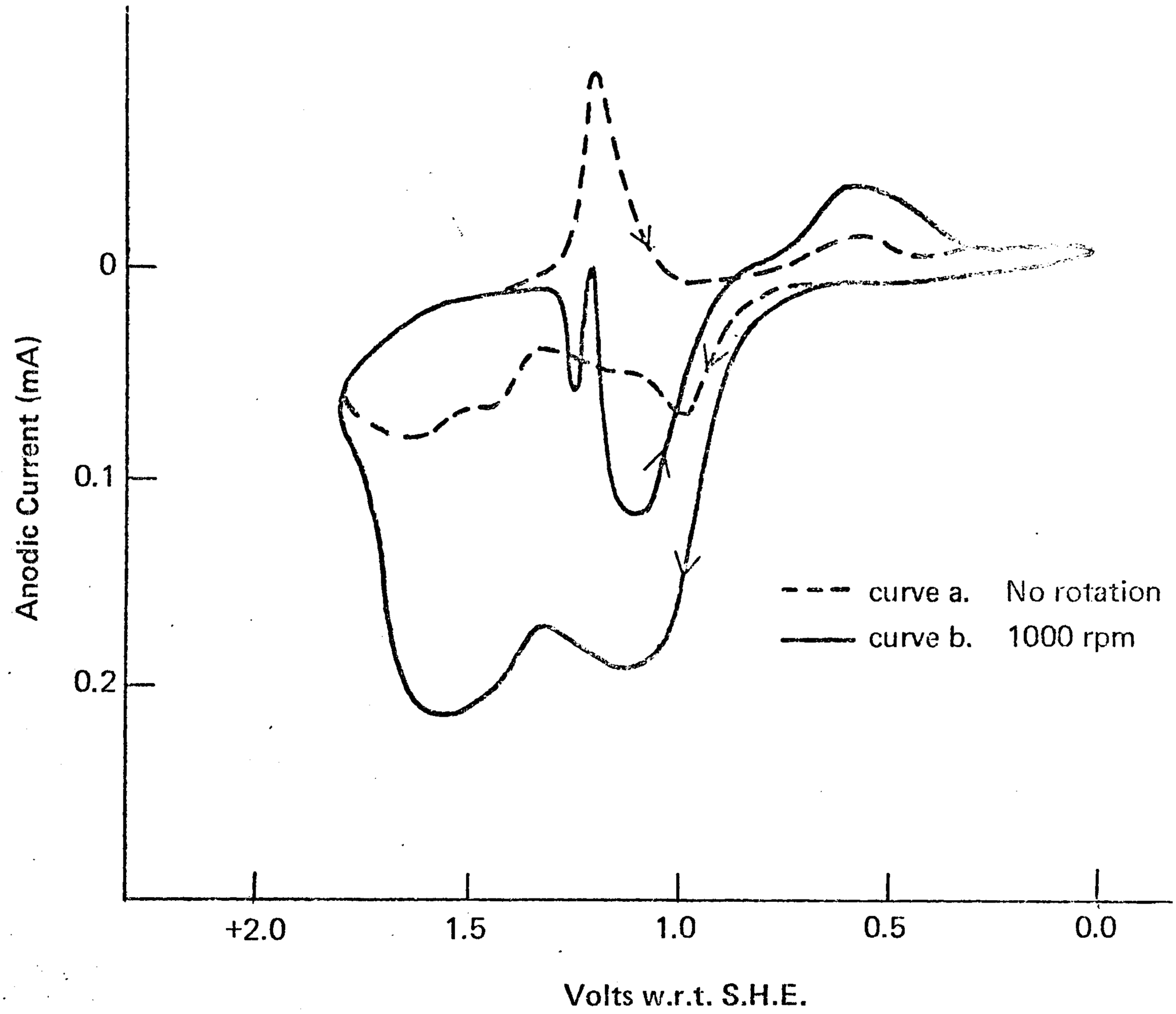

Fig. 5.1

CURRENT POTENTIAL RELATION, GOLD IN IM HC104, SWEEP RATE 100mV sec^{-1}

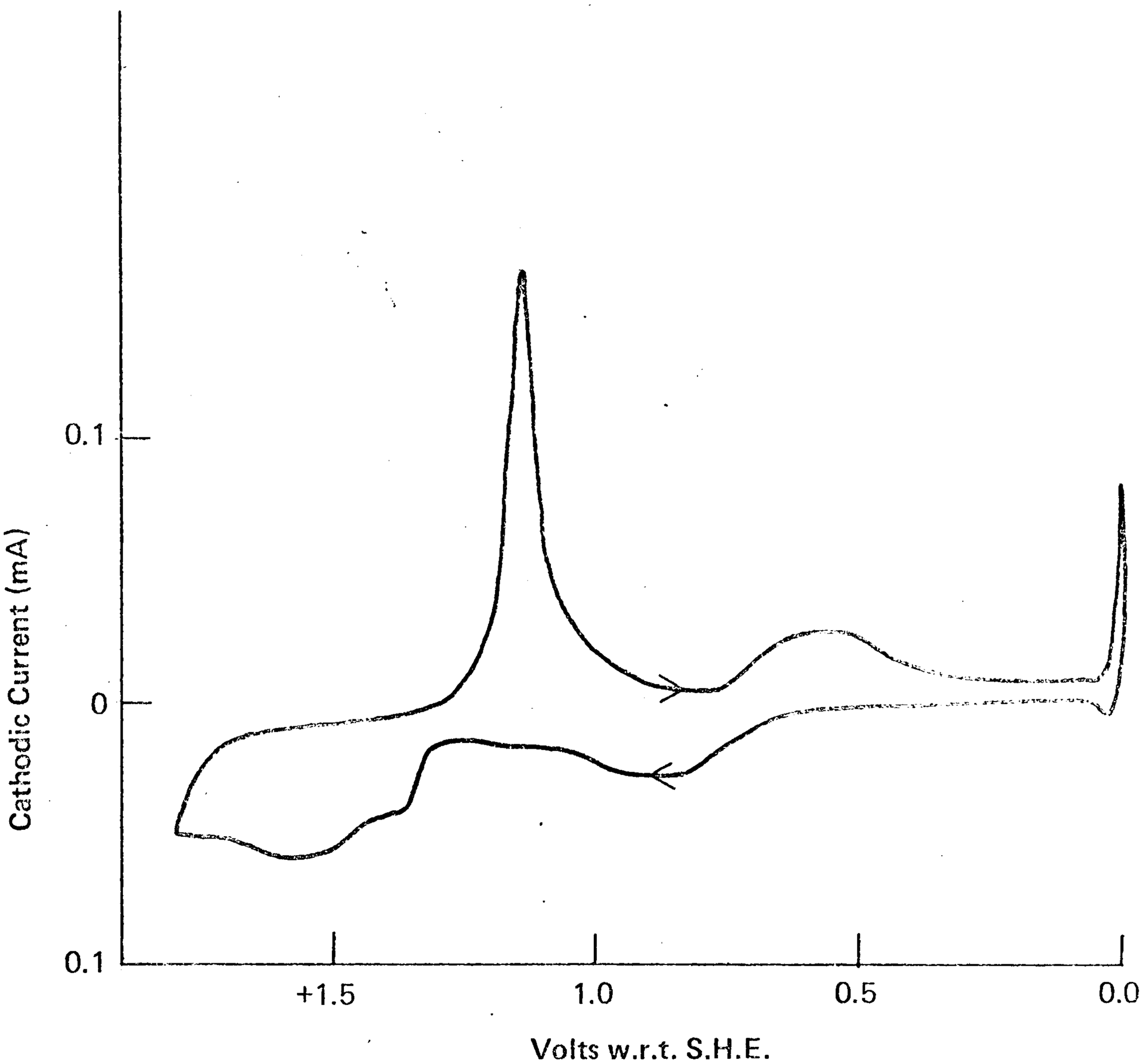

Fig. 5.2

CURRENT–POTENTIAL RELATION, GOLD (polished) IN 1M $HClO_4$, 1000 rpm, 100 mV sec^{-1}

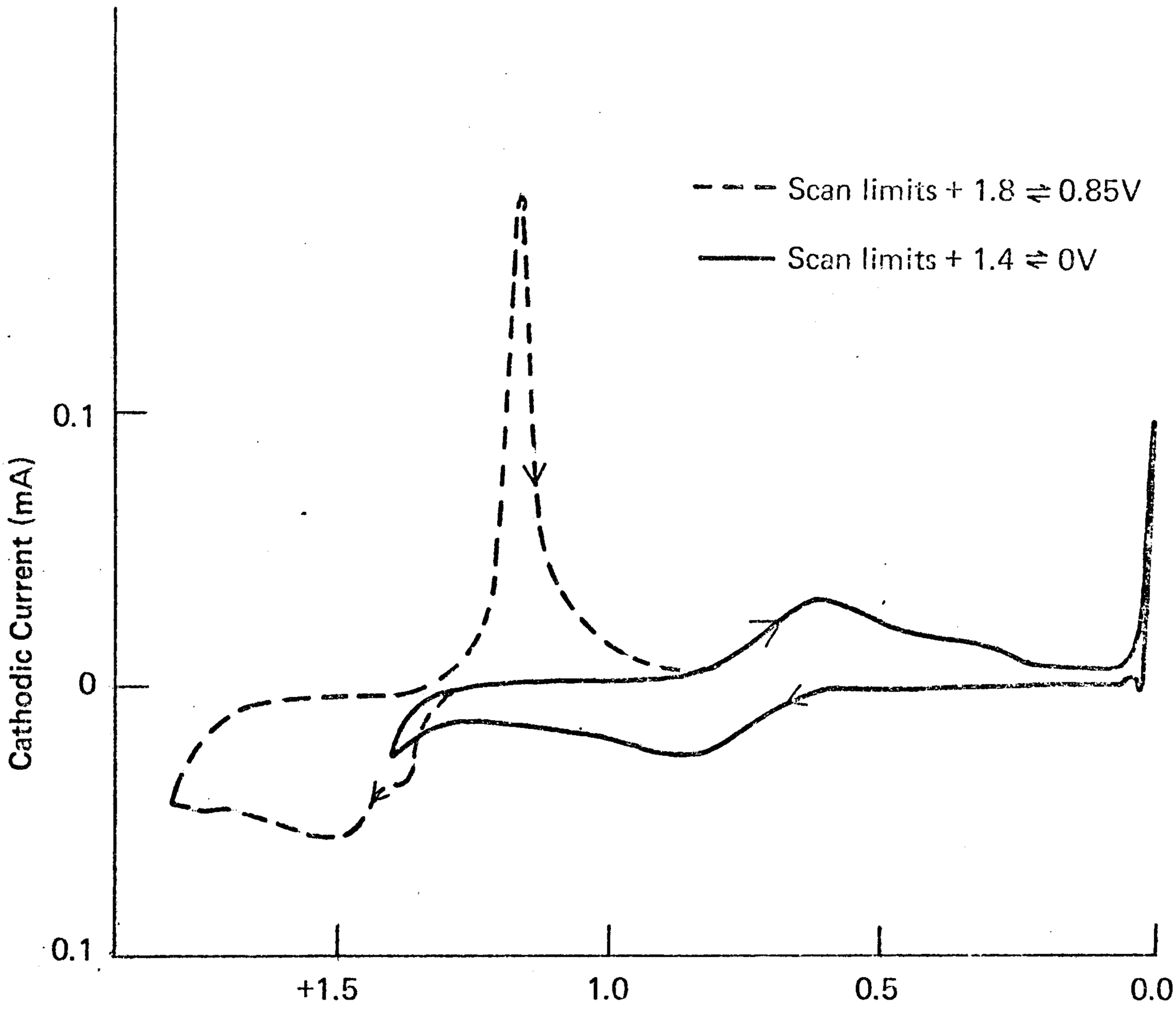

Fig. 5.3

CURRENT–POTENTIAL RELATION, GOLD (polished) IN IM $HClO_4$, 1000 rpm, 100 mV sec^{-1}

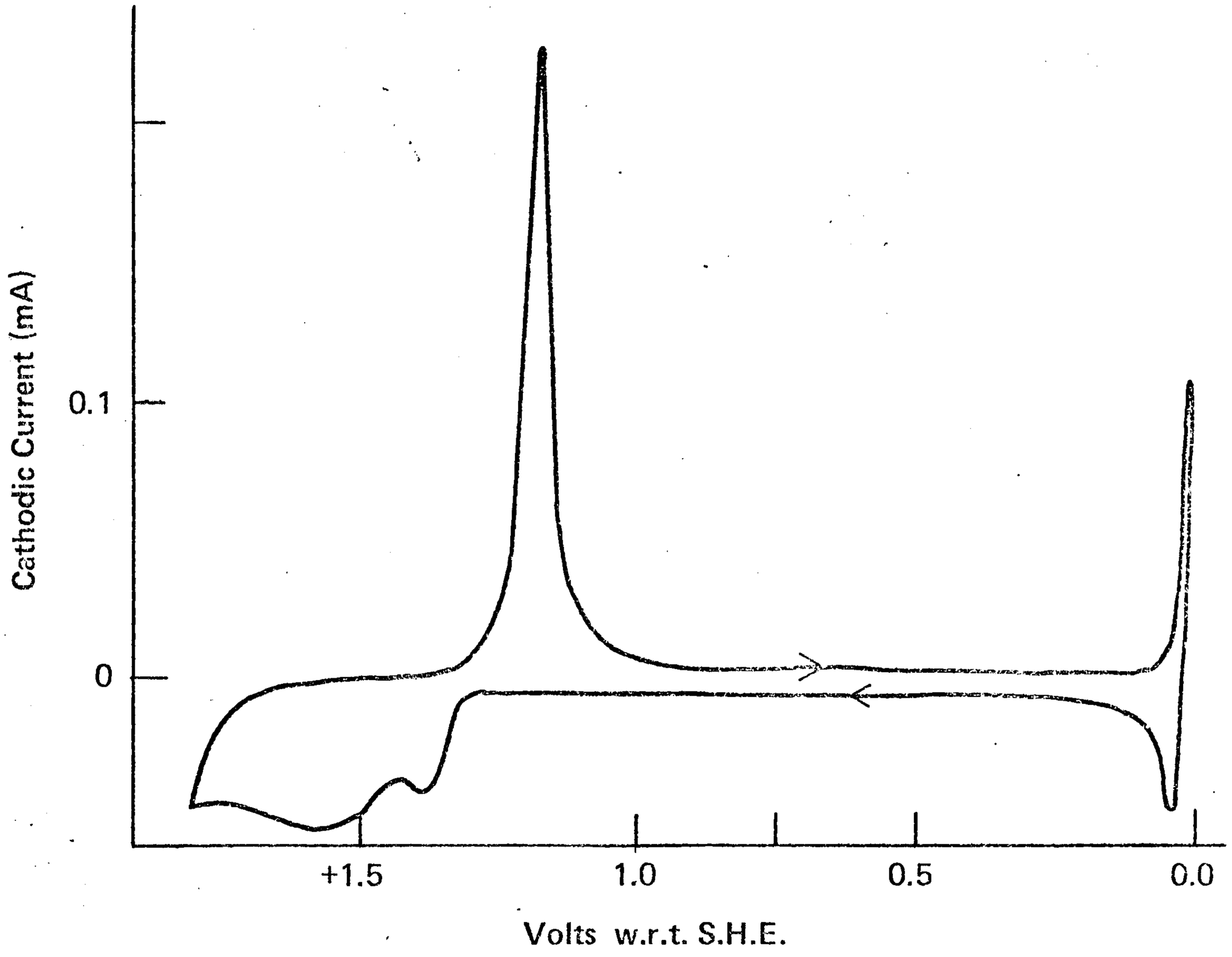

Fig. 5.4

CURRENT–POTENTIAL RELATION, GOLD (etched) IN IM $HClO_4$, 1000 rpm, 100 mV sec^{-1}

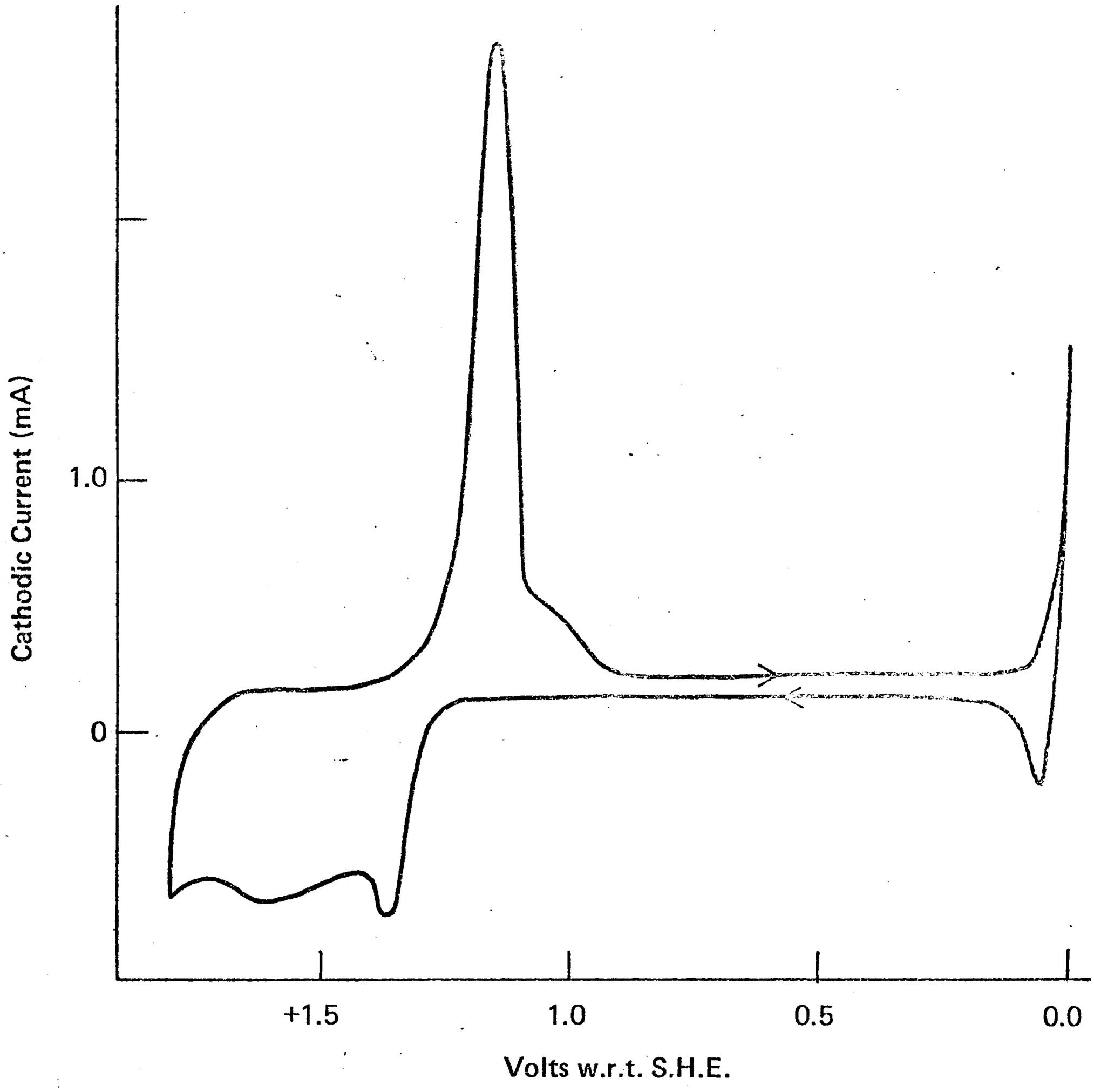

Fig. 5.5

CURRENT–POTENTIAL RELATION, GOLD IN IM $HClO_4$, SWEEP RATE 100mV sec^{-1}

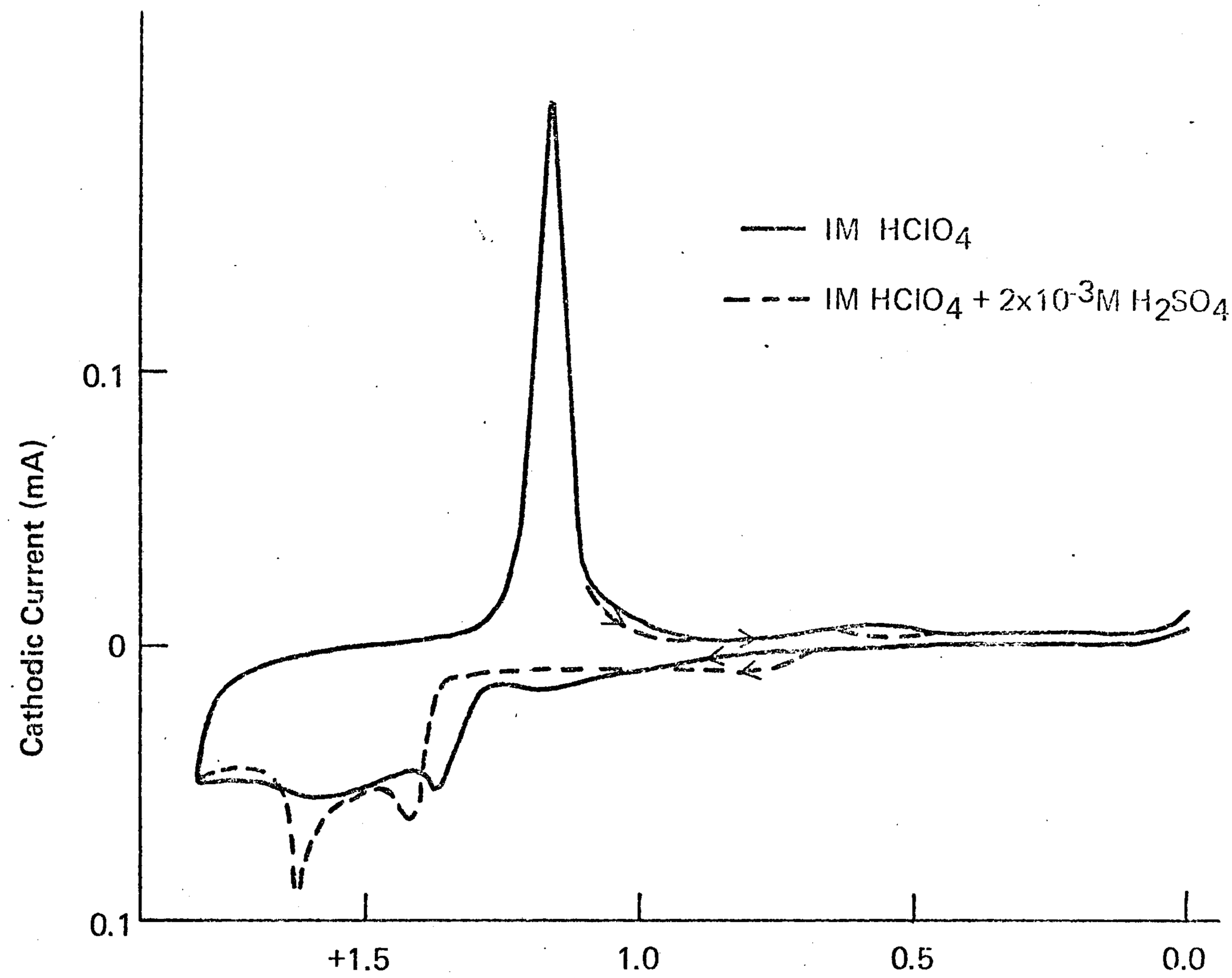

Fig. 5.6
CURRENT–POTENTIAL RELATION, GOLD (etched), 1000 rpm, 100 mV sec^{-1}

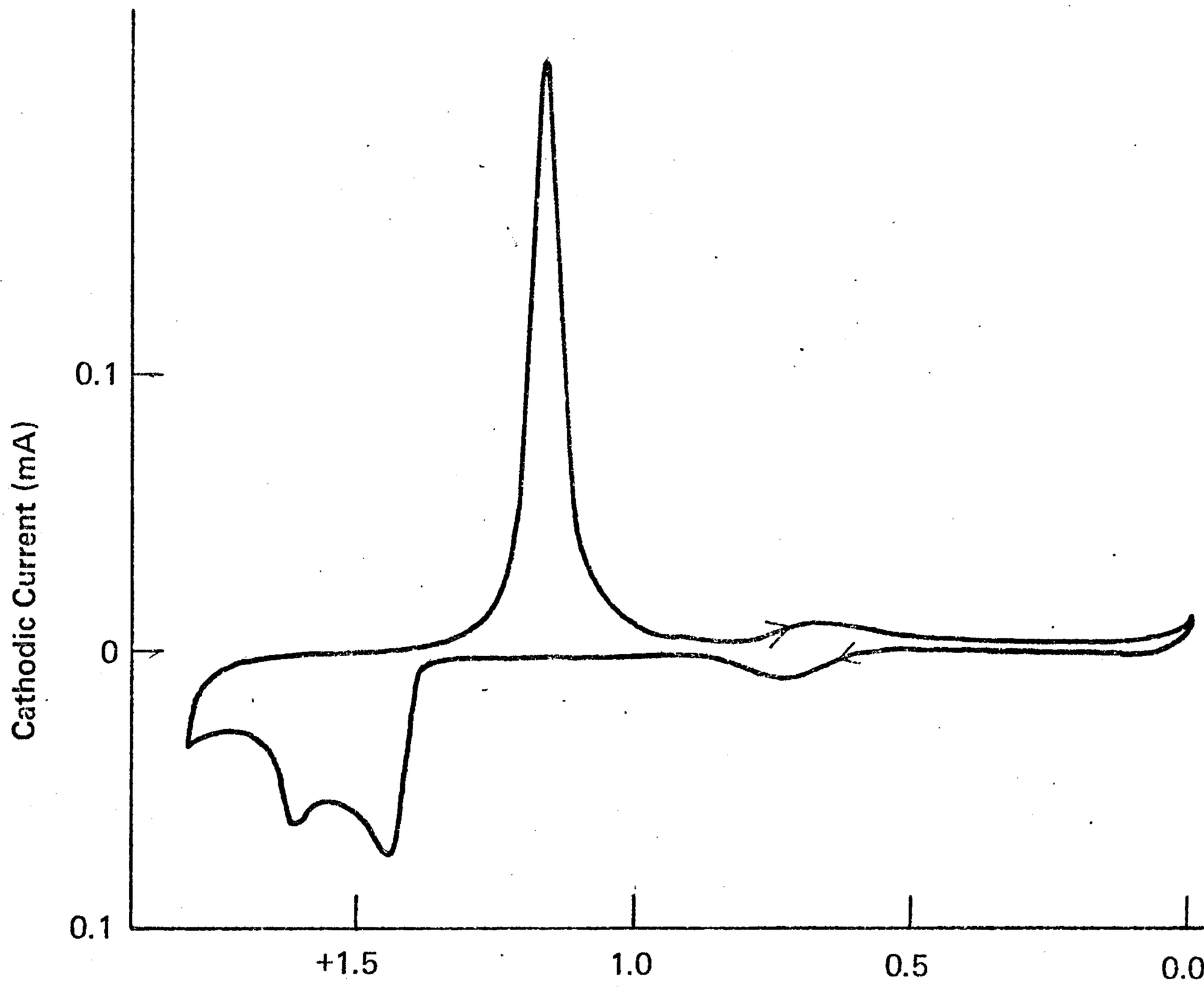

Fig. 5.7

CURRENT–POTENTIAL RELATION, GOLD (etched) IN 0.5 MH_2SO_4, 1000 rpm, 100 mV sec^{-1}

CHAPTER 6

REDUCTION OF CrVI IN PERCHLORIC AND SULPHURIC ACID SOLUTIONS ON A GOLD ELECTRODE

6.1 Introduction

The object of this work was to study the kinetics and mechanism of the reduction of CrVI on a gold electrode. As described in Section 1.1, the use of perchloric acid as background electrolyte ensured that only four CrVI-containing species were present in solution. Work in sulphuric acid solutions is reported later.

Using a R.D.E. the current-potential curves at constant rotation speed, the current-rotation speed relation at constant potential, and the dependence of the current on the concentration of $HClO_4$, H_2SO_4 and the reacting ions was observed. Both steady-state and potential-sweep techniques were employed. Electrochemical evidence for the formation of surface films was obtained and their presence confirmed by electron diffraction.

6.2 Experimental

The reduction of CrVI in $HClO_4$ at noble metal electrodes is very sensitive to the presence of other ions so that careful solution purification was necessary. Sulphate and phosphate ions had particularly marked effects. Since phosphate appeared to be present in triply distilled water, the alternative method of water purification, described in Section 3.10, was adopted. In the earlier work in $HClO_4$ solutions both the cell

and electrodes were cleaned using concentrated Analar sulphuric acid and this led to traces of the acid being present in the experimental solutions. After the effect of H_2SO_4 was recognised all experiments were carried out in sulphate-free solutions.

The solutions contained between 5×10^{-5} and 1×10^{-2} M CrVI and were 1 M in ClO_4^- or 0.5 M in SO_4^{2-} as appropriate. The pH of the solutions was varied by altering the ratio of $HClO_4$ to $NaClO_4$, or of H_2SO_4 to Na_2SO_4. The perchloric acid was of Aristar grade; for the sweep measurements it was further purified by pre-electrolysis. Analar $NaClO_4$, Aristar sulphuric acid and Analar Na_2SO_4 were used without further purification. Triply recrystallised Analar $K_2Cr_2O_7$ was used as the source of CrVI.

All potentials are with respect to a hydrogen electrode in the background solution.

6.3 Steady-state results

6.3.1 Results in $HClO_4$ solutions

Steady-state measurements were made by holding the electrode at the chosen potential until the current became almost constant. This process did not normally take more than two minutes although, as discussed later, prolonged treatment at more negative potentials caused the current to fall slowly with time. In the present work, the potential was not held long enough for this fall to occur. A polished electrode was used in all these steady-state measurements.

A typical steady-state current-potential curve obtained in a solution 10^{-2} M in CrVI and 1 M in $HClO_4$ and $NaClO_4$ is shown in Fig. 6.1 (curves a and a'). On making the potential more negative, no significant current is observed until the potential is about 0.65 V. The current then increases slowly up to a potential of about 0.5 V when it rises very abruptly. A limiting current is obtained at more negative potentials. When the potential is changed in the reverse direction, the limiting current is maintained up to about 0.6 V. At more positive potentials the current falls abruptly, and is close to zero at 0.65 V. This marked hysteresis is also observed in more dilute dichromate solutions but the potentials at which the abrupt rise and fall of the current occur become more positive as the dichromate concentration is reduced. The curves obtained in a 10^{-3} M CrVI solution are shown as curves b and b' in Fig. 6.1. The difference in the plateau currents is discussed later. The mean potential between the current rise and fall decreases by about 250 mV for a tenfold increase in the concentration of CrVI. Curves of similar form were obtained in solutions containing more and less perchloric acid. The interpretation of these curves is discussed in Section 6.4.2.

Nature of the limiting current

A marked feature of these curves is the very flat plateau produced when the current reaches its limiting value. Such flat plateaux have been described previously

by Feigl and Knorr[1.13]. As described in Chapter 2, if this current is limited by mass transport, a plot of $^{c}b/_{i}$ against $w^{-\frac{1}{2}}$ should be linear and pass through the origin. Typical graphs obtained at 0.0 V with a variety of dichromate concentrations are shown in Figs. 6.2 and 6.3. The background electrolyte was 1 M $HClO_4$, 1 M $NaClO_4$ in Fig. 6.2 and 2 M $HClO_4$ in Fig. 6.3. The results obtained in 0.1 M $HClO_4$, 1.9 M $NaClO_4$ coincided with curve (c) of Fig. 6.2. The plots obtained at more positive potentials on the plateau were indistinguishable from these. It is important to note that in obtaining these results the potential was held at the chosen value for only about 2 minutes.

In both background electrolytes the plots are linear but appear to give small intercepts at $w^{\frac{1}{2}} = 0$. The cause of these intercepts is not clear. They may indicate that the current plateau is the result of a preceding chemical step (see Chapter 2) or they may be the result of a deposit on the electrode surface[6.1] as explained later. The slopes of these plots vary with the dichromate concentration, especially in the more acid solution. This variation in slope is equivalent to a departure from a first-order dependence of the limiting current on the dichromate concentration, as is apparent in Fig. 6.4. This diagram shows the relation between the logarithm of the dichromate concentration and the logarithm of the limiting current

which should be linear with a slope of unity if the current is diffusion controlled. The results obtained in the most dilute acid almost satisfy this requirement, as do those of Fiegl and Knorr[1.13], but those from the more concentrated acid solutions do not, the discrepancy being most marked in 2 M $HClO_4$.

Haight, Richardson and Coburn[1.6] reported that CrVI decomposes to CrIII in solutions more than 1 M in hydrogen ion, but they did not observe this phenomenon in less acid solutions. As reported in Chapter 4, a background concentration of CrIII was always detected in CrVI solutions containing 1 M $HClO_4$. Visual and spectrophotometric examination showed that solutions of CrVI in 1.0 and 2.0 M $HClO_4$ rapidly produced some CrIII, the amount being proportional to the concentration of perchloric acid but varied with the batch of perchloric acid employed. This suggests that some oxidisable impurity was present in the perchloric acid. As reported in Chapter 5, it was subsequently discovered that this material could be removed by pre-electrolysis of the solution. No decomposition was detected in solutions 0.1 M in $HClO_4$ and 1.9 M in $NaClO_4$.

When the concentration of CrVI, as determined by analysis, was used in place of the apparent concentration, the logarithmic plots corresponding to 2 M $HClO_4$ obeyed the first-order equation. It appears, therefore, that the limiting current for the reduction of CrVI in all the solutions studied varies linearly with the concentration of CrVI.

The results described above were obtained by holding the potential at the chosen value for only about 2 minutes. If the potential was held for longer periods, the current fell much more rapidly than would correspond to consumption of CrVI. The current could be raised to near its original value by anodic treatment, but a complete restoration of the original behaviour was obtained only by immersing the electrode in concentrated sulphuric acid, followed by extensive washing in doubly distilled water.

The relation between the current and rotation speed of the electrode obtained with an "inhibited" electrode is shown in Fig. 6.2, curve (d). The electrode used in this experiment had been held at 0 V for not more than 15 minutes. In contrast to the results described earlier, this graph is not linear. The section at lower rotation speeds is almost parallel to curve (c) but would extrapolate to give a larger intercept at $w = \infty$. At higher rotation speeds the line curves towards curve (c). Curves of this type have been shown by Landsberg et al.[6.1] to correspond to an electrode with a partially blocked surface. It seems probable, therefore, that a film is present on the electrode surface at potentials corresponding to the limiting current plateau, its amount increasing slowly with time. The intercepts in all the plots of $1/i$ against $1/w^{\frac{1}{2}}$ may therefore be caused by the presence of this film. Further evidence for this film and an investigation into its nature are described in Section 6.4.2.

6.3.2 Steady state results in H_2SO_4 containing solutions

True steady-state current-potential curves were difficult to obtain because prolonged changes in the current occurred over the potential dependent part of the curve. The detailed shape of the curves is therefore somewhat uncertain.

Typical current-potential curves obtained in 0.5 M H_2SO_4 with 1 x 10^{-2} and 1 x 10^{-3} M CrVI are illustrated in Fig. 6.5. On making the potential progressively more negative in 1 x 10^{-2} M CrVI the current began to rise at potentials more negative than 1.1 V, the final plateau being reached by 0.6 V. The positive-going current began to fall at 0.7 V, reaching zero at 1.1 V. In 1 x 10^{-3} M CrVI the behaviour was almost identical but the curve was shifted 50 mV more positive.

In more dilute H_2SO_4 solutions, the shape of the curve became more complex, Fig. 6.6. The potential-sweep results, reported in Section 6.4.2, indicate that this is almost certainly due to modification of a surface film with change in potential. In these more dilute H_2SO_4 solutions the rise in current moves to more negative values. This effect was also observed by Feigl and Knorr[1.13].

A comparison between Figs. 6.1 and 6.5 illustrates the following points of difference between the reduction behaviour in H_2SO_4 and $HClO_4$ solutions:

(i) At a given, constant CrVI concentration, the initial current rise occurs at more positive potentials, 1.1 V compared with 0.65 V in 1 x 10^{-2} M CrVI.

(ii) Less hysteresis is observed between the positive and negative-going sweeps.

(iii) The shift of the curve with increase in the CrVI concentration is much smaller. These observations are further investigated and discussed in Section 6.4.

Nature of the final plateau

Compared with the behaviour in $HClO_4$, the final plateau current, i_p, tended to fall at a faster rate, particularly in the more dilute H_2SO_4 solutions. Furthermore i_p was smaller in H_2SO_4 solutions than in $HClO_4$ and it decreased, at a given CrVI concentration, as the H_2SO_4 concentration was lowered. Addition of H_2SO_4 to a $HClO_4$ solution (Section 6.4.2) also lowered i_p.

Graphs of $^{c_b}/_{i_p}$ against $^{1}/_{w^{\frac{1}{2}}}$ obtained in the more dilute sulphuric acid solutions, Fig. 6.7, showed greater curvature and a more pronounced intercept than corresponding plots in $HClO_4$. These diagrams also show that with more dilute CrVI concentrations, $^{c_b}/_{i_p}$ decreased (i.e. i_p relatively increased). This did not occur in 0.5 M H_2SO_4, where a first order dependence of i_p on CrVI concentration was obtained, Fig. 6.8.

These results strongly suggest that at potentials corresponding to the final plateau, an inhibiting film is again present in sulphuric acid containing solutions. Since the plateau currents observed in sulphuric acid solutions were smaller and the intercepts of the $^{c}b/_{i_p}$ against $^{1}/_{w^{\frac{1}{2}}}$ plots were greater than those observed in perchloric acid solutions a more complete or more inhibiting film must be produced in the former case. In dilute acid solutions the extent of the inhibition increased as the CrVI concentration increased or the sulphuric acid concentration decreased.

6.4 Sweep measurements

6.4.1 Introduction

Insight into the processes occurring at potentials more positive than the final plateau was obtained by investigating the form of the current-potential curve obtained by applying a triangular potential sweep to the working electrode. These curves were obtained in solutions containing varying amounts of CrVI and showed features attributable to the formation and modification of a film on the electrode. A range of sweep speeds was employed initially but 100 mV sec^{-1} proved to be most satisfactory: lower sweep speeds generally gave curves in which the features of interest were not clearly obvious, while at higher sweep rates these features were magnified, but the resulting distortion in the overall shape of the curves made them difficult to interpret. Only slight variability between the

results from sweep to sweep were observed. The effect of varying the positive limit of the sweep and of holding the electrode at various potentials was also examined. Modifications to the current-potential relation in background electrolyte after treatment in chromium containing solutions were observed.

6.4.2 Sweep measurements in $HClO_4$ containing solutions

The current-potential curve obtained in pure 1 M $HClO_4$ is shown in Fig. 6.9 while the curves obtained after adding small amounts of CrVI to this solution are shown in Fig. 6.10. The section of the curve beginning at about 1.3 V on the positive-going sweep and attributed to the formation of a layer of Au_2O_3 on the gold surface, begins at the same potential and shows only slight changes in form when CrVI is added to the solution. However, the quantity of electricity required to oxidise the gold surface is decreased slightly. Since there is no evidence for the reduction of CrVI at these potentials and the quantity of electricity involved in the reduction of the surface oxide is not altered, it is possible that some oxidation of the gold surface by CrVI occurs. The maxima at about 0.5 V and 0.95 V on the negative and positive-going sweeps respectively do not appear to be affected by the addition of CrVI to the solutions, but some new peaks are observed. On the positive-going sweep there is the suggestion of a maximum at 1.15 V, while on the negative-going sweep a maximum of 0.88 V with a shoulder at 0.95 V (Fig. 6.10, curve (b)).

The curves observed in a solution containing 10^{-3} M CrVI have essentially the same form as described above (Fig. 6.11, curve (a)). The hysteresis between the positive and negative-going sweeps is however larger, while the maximum originally at 0.88 V is occurring near to 0.83 V. By restricting the anodic limit of the scan to 1.3 V, the complications introduced by oxidation of the electrode surface are avoided and the resulting curve, Fig. 6.11b, shows the features described above without those due to oxidation and reduction of the gold surface. In all other respects this curve is closely similar to that described earlier, Fig. 6.11a. The various maxima can be seen more clearly at a faster sweep rate (Fig. 6.12) but the overall current-potential relationship is more distorted.

A marked change in the form of the current-potential curve resulted from increasing the dichromate concentration to 1×10^{-2} M, Fig. 6.13. On the negative-going curve, reduction begins at about 1.1 V but this process suffers inhibition at about 0.95 V, the current falling to a lower value. This is presumably the first branch of the reduction process as described in Section 1.3. This inhibition is presumably due to the formation of a film (film A) which undergoes modification, to form film B, at about 0.6 V when the current rises abruptly to its limiting value. Evidence for the presence of film B will be discussed later; it must clearly be less inhibiting than film A. On the positive-going

sweep, the limiting current is maintained up to about 0.78 V when the current falls steeply to a very low value, probably as a consequence of the reformation of film A. Some of this film must be removed during the time the electrode is at more positive potentials, since the peak at 0.95 V is repeated on successive sweeps. The sharp peaks on the rising and falling sections of these curves are probably caused by a combination of overshoot of the recorder and current maxima for the layer modification processes.

A clearer understanding of the processes occurring was obtained by studying the effect of holding the electrode for 10 minutes at various anodic potentials, Fig. 6.14. The results were a little variable but the first negative-going curves obtained in these experiments clearly showed the following features.

(i) After pretreatment at 1.3 or 1.35 V almost identical curves were obtained. The shape of these curves along with the fact that in the absence of this pretreatment the electrode displayed the relatively inactive behaviour of Fig. 6.13, suggests that these pretreatments must remove film A. The reduction therefore probably occurs initially on a clean surface but some inhibition is observed at potentials below 0.93 V.

(ii) After pretreatment at 1.2 V the current between 1.2 and 0.9 V is again much higher than that obtained by continuous sweeping (Fig. 6.15) but rather lower than in the above cases. This suggests that the

inhibiting layer A is not completely removed at this potential. Moreover the reaction is much more seriously inhibited below 0.9 V, the current displaying a maximum at about 0.88 V and falling to a low value at 0.75 V. This inhibition is attributed to the formation of further amounts of film A. The subsequent reduction of A to B is observed at about 0.5 V.

(iii) After pretreatment at 1.1 V the electrode is much less active, only a small maximum in the current being obtained, but the activity was higher than observed with continuous sweeping. Pretreatment at 1.0 V produced a virtually inhibited electrode, the curve obtained being almost identical with that obtained by continuous sweeping.

(iv) Pretreatment at 1.4 V gives an apparently anomalous result but this may be associated with oxidation of the gold surface.

We can therefore conclude that in 1 x 10^{-2} M CrVI solutions the inhibiting layer (A) begins to be removed, presumably by reoxidation, between 1.0 and 1.1 V and that it is almost completely removed by 1.3 V. Under the conditions applying at a sweep rate of 100 mV per second reformation of this layer begins at potentials below about 0.93 V and the reformation is almost complete by 0.75 V. Reduction of this layer to a less inhibiting form (film B) occurs at potentials below about 0.65 V and is complete by 0.4 V, Fig. 6.14. A diagrammatic representation of these conclusions is

presented in Fig. 6.16A, where the broken lines represent deductions drawn from steady-state experiments and the continuous lines those from sweep measurements. Since the processes represented could not be studied in isolation from the reduction of dichromate, the potential limits are necessarily approximate.

The subsequent positive-going sweep was essentially independent of the pretreatment (Fig. 6.15). The current remains at the limiting value up to a potential of about 0.78 V and then falls rapidly, becoming almost zero by about 0.88 V. As suggested earlier this fall in the current probably corresponds to reoxidation of film B to A. Since some reoxidation could occur without the current falling from its limiting value, the potential at which it begins cannot be established from these results; it must however be almost complete by 0.88 V.

The next negative-going sweep was indistinguishable from subsequent sweeps for a given anodic limit of the potential scan, Fig. 6.15. With anodic potentials more positive than 1.2 V a small current maximum was observed at about 0.93 V indicating that some removal of film A occurs during sweeping to these more positive potentials. At 1.2 V and lower potentials the curve showed the electrode to be almost completely passivated. The contrast between these results and those obtained following holding the electrode at positive potentials shows that film removal is slow.

The conclusions on the layer formation and modification processes, illustrated in Fig. 6.16A, are in accord with the steady-state results reported in Section 6.3.1. The current rise beginning at about 0.65 V, Fig. 6.1, presumably corresponds to the onset of reduction of film A; this process is probably completed by 0.47 V when the current reaches its limiting value. Similarly the current fall beginning at 0.57 V is attributed to the reoxidation of B to A, which is complete by about 0.68 V. The onset of the reoxidation process during a potential sweep presumably also begins at 0.57 V.

The curves obtained in 1 x 10^{-3} M CrVI solutions can also be explained in terms of similar layer formation and removal processes. These processes are however less easy to identify because, as will be shown later, they occur over a much narrower potential range and the current involved in these surface processes was comparable to that involved in the reduction of CrVI.

The first negative-going curves obtained after holding the electrode for 5 minutes at different anodic potentials are shown in Fig. 6.17 and show the following features:

(i) The curves obtained after holding at 1.3 and 1.2 V are very similar and presumably correspond to initial reduction on a clean surface with some inhibition being seen at 0.99 V.

(ii) After holding at less positive potentials down to 0.95 V, the reduction of CrVI appears to be inhibited, the extent of the inhibition increasing as the potential is reduced.

(iii) The inhibition produced by holding at 0.90 V is slightly less than that at 0.95 V as shown by the somewhat higher value of the current at 0.90 V.

(iv) Little inhibition is evident after holding at 0.80 V.

(v) A cathodic peak is present on most of the curves; the magnitude of this peak increases as the pretreatment potential is decreased down to 0.95 V, and decreases again.

The results strongly suggest, as shown diagrammatically in Fig. 6.16B that an essentially film-free surface is produced by holding the electrode at 1.2 or 1.3 V. At potentials less positive than 1.2 V to 1.1 V an inhibiting film (A) must be slowly formed on the electrode surface as one product of the reduction process. This film can subsequently be reduced further to a less inhibiting form (B), giving rise to the peak in the current-potential curve and allowing the reduction current to rise rapidly. The subsequent reduction of the film presumably begins between 0.90 V and 0.95 V. This process is again not very rapid as shown by the drawn-out nature of the maxima and the fact that at 100 mV sec^{-1} scan rate the reduction is not complete until about 0.55 V, whereas under steady state conditions

it must be complete by 0.75 V (Fig. 6.1). As demonstrated later, this film or some further modification presumably remains on the electrode at more cathodic potentials.

The subsequent positive-going sweep after the initial curves described above, was independent of the previous anodic pretreatment (Fig. 6.18) and the next negative-going sweep was again reproducible, provided that a constant anodic limit was maintained. The ill-defined nature of these curves makes their detailed interpretation difficult but the following conclusions seem justified.

(i) Since the current fall on the positive-going curve occurs at potentials more positive than 0.8 V the oxidation of B to A must begin in this neighbourhood: it is probably complete by about 1.05 V.

(ii) The slight maximum, after sweeping to 1.3 V, between 1.15 and 1.05 V probably corresponds to the redeposition of film A, part of which has been removed in the positive-going sweep.

(iii) The peak occurring at about 0.85 to 0.8 V is associated with the reduction of A to B.

These conclusions, along with those drawn from the steady-state results, Fig. 6.1, are summarised in Fig. 6.16B. The pattern of behaviour is similar to that observed in 1 x 10^{-2} M CrVI solutions.

Evidence for the existence of a film at negative potentials

In the foregoing it has been assumed that a film is present on the electrode at potentials corresponding to the limiting current. The existence of a film would be consistent with the intercepts shown in Figs. 6.2 and 6.3. Evidence for the presence of a film, after holding the electrode for 5 minutes at 0.0 V, is shown in Fig. 6.19. The anodic maximum at approximately +1.15 V was present only on the first positive-going sweep following this treatment. It presumably corresponds to the oxidation and removal of a film produced by the cathodic polarisation.

Potential sweeps in the background electrolyte after cathodic polarisation at 0.0 V in 1 x 10^{-2} M CrVI, 1 M $HClO_4$ also showed the presence of an anodic maximum at approximately +1.15 V. In these experiments, after the cathodic polarisation, the electrode was switched to open circuit, removed from the cell and well washed with 2x distilled water prior to recording the current-potential relationship in the background electrolyte. The resulting curve is compared with that obtained with a clean gold electrode in Fig. 6.20. For clarity, the results shown were obtained with an etched gold electrode, but essentially similar results were observed with polished electrodes. The peak at +1.15 V is again apparent while the presence of a corresponding reduction process is indicated in the negative-going curve. The section of the curve corresponding to the

surface oxidation of gold is virtually identical in both curves. The cathodic process is more readily seen in experiments where the anodic sweep limit was restricted to +1.3 V, Fig. 6.21.

The anodic oxidation must convert the film to a soluble product since on rotating the electrode, while the first positive-going sweep showed the presence of a maximum, subsequent negative and positive-going sweeps were identical to those obtained with a clean gold electrode.

It would be attractive to associate the anodic maximum at 1.15 V with the oxidation and removal of film A. Since however the former oxidation and removal process occurred rapidly and did not lead to enhanced electrode activity (Fig. 6.19), this film (C) is probably additional to films A and B. The quantity of electricity in the anodic peak of Fig. 6.19 was only 750 $\mu C\ cm^{-2}$, indicating that only a small amount of reoxidisable material was present on the electrode surface, the greater part of the surface could still be covered by film B. The quantity of electricity involved in the corresponding anodic maximum in the background electrolyte, Fig. 6.20, was only 400 $\mu C\ cm^{-2}$ even though this followed longer pretreatment at 0.0 V. This is consistent with some oxidation and removal of C occurring while the electrode was on open circuit.

It is to be expected that during the period on open circuit film B present on the surface would be reoxidised to A. Since no peak attributable to the oxidation and removal of A was observed in the background electrolyte and yet the oxidation of gold was unaffected by previous cathodic pretreatment, it must be concluded that this film is either soluble in $HClO_4$ or is removed during the period the electrode was on open circuit.

The electron diffraction pattern obtained from a gold electrode after 90 minutes electrolysis at 0.2 V in 1 x 10^{-2} M CrVI, 1 M $HClO_4$ showed lines additional to those for gold, indicating the presence of a film. Modification of this film occurred after the same electrode was further electrolysed at 1.0 V for 60 minutes, Fig. 6.22.

Kinetics of the reduction process

Since in 1 x 10^{-2} M CrVI solutions, pretreatment at 1.3 or 1.35 V apparently allowed reduction of CrVI to occur initially on a bare surface, the first part of the subsequent potential sweep can be used to obtain kinetic data on the reduction process. Because the section of the curve employed lies near the foot of the wave the correction for mass transport should be small and has been omitted. A plot of log i against potential is shown in Fig. 6.23, curve (a), and is satisfactorily linear between 1.05 and 0.93 V. This line has a slope of approximately 100 mV per decade

implying a transfer coefficient of 0.59, which is consistent with the rate determining step being a simple single electron transfer process.

In 1 x 10^{-3} M CrVI solutions, as is obvious from Fig. 6.16(B), the reduction of CrVI is always accompanied by film formation or modification processes. Under these circumstances, part of the observed current will be due to these latter processes and consequently it is not possible to obtain a very good Tafel plot. As shown in Fig. 6.23 (curve (a)) the reaction rate is decreased by lowering the chromium concentration but the above considerations preclude any reliable determination of the order of the reaction.

6.4.3 Sweep measurements in H_2SO_4 containing solutions

The effects of adding small amounts of a concentrated H_2SO_4 solution to a solution of 1 x 10^{-2} M CrVI, 1 M $HClO_4$ are shown in Fig. 6.24. A noticeable consequence of adding H_2SO_4 was that the slight variability in the results obtained in pure $HClO_4$ was almost entirely removed. The maximum at 0.94 V, attributed in $HClO_4$ containing solutions to inhibition of the reduction by the formation of film A, is essentially unaltered in potential by the addition of H_2SO_4. However its height increases markedly from 0.20 mA in pure $HClO_4$ to 0.32 mA in a solution 5 x 10^{-4} M in H_2SO_4. Increase in the concentration of H_2SO_4 to 4 x 10^{-2} M. however, raised this current to only 0.40 mA (Fig. 6.24, curve (c)).

As observed in $HClO_4$ solutions (Section 6.4.2) anodic pretreatment (4 minutes at 1.4 V) increased the height of this maximum, Fig. 6.25, curve (b), compared with that obtained during sweeping, Fig. 6.25, curve (a), but in contrast to the results in $HClO_4$ solutions no peak for the reduction of gold oxide was obtained. However in H_2SO_4 containing solutions, oxidation of gold did not occur to a significant extent below 1.4 V, Fig. 5.6. More anodic pretreatment at 1.8 V, that is, at potentials where the gold is oxidised, lowered the height of this first maximum and inhibited the second rise in current, Fig. 6.25, curve (c). The same effect was observed in $HClO_4$ solutions following oxidation of the gold, and was attributed to slight differences in surface state following oxidation.

The potential at which the second rise in current occurs was very markedly affected by the addition of H_2SO_4, being moved more positive by about 150 mV by making the solution 5×10^{-4} M in H_2SO_4. Since the potential corresponding to the current fall on the positive-going sweep was largely unaffected, the hysteresis was therefore decreased.

Following addition of H_2SO_4 the plateau current was much lower than could be accounted for by simple dilution. Holding at 0.0 V caused a greater fall in current than observed in $HClO_4$ solutions, although the initial value could be restored by sweeping to 1.4 V

or leaving the electrode on open circuit. This observation reinforces the view expressed in Section 6.3.2 that when on the final plateau greater film deposition occurs, or a more inhibiting film is produced, in H_2SO_4 solutions.

These results can be interpreted in a similar manner to those obtained in $HClO_4$ solutions, that is initially reduction of CrVI occurs at potentials below 1.15 V, but is inhibited at about 0.95 V by film deposition. Subsequent reduction of this film (A'), to a less inhibiting form (B'), occurs at more negative potentials. The presence of sulphate or bisulphate ions must modify the properties of A', since as has been clearly shown, its reduction occurs very much more easily in sulphate containing solutions. The more reversible oxidation and reduction of A' accounts for the decreased hysteresis.

Reoxidation and removal of A' occurs slowly at more positive potentials, the surface coverage of A' being reduced for example by holding at 1.4 V for 4 minutes, Fig. 6.25, curve (b). Anodic pretreatment at potentials positive enough to oxidise the gold, adversely affects the condition of the electrode surface, as observed in $HClO_4$ solutions.

The fall in current observed if the electrode is held at potentials on the plateau, must be due to inhibition caused by the production either of large amounts of B' or of another reduction product (C') which inhibits the process.

The current-potential curve obtained in 1 x 10^{-3} M CrVI, 0.5 M H_2SO_4 at 100 mV sec^{-1} is shown in Fig. 6.26, curve (a). Following sweeping to 1.4 V the initial increase in current occurs at approximately 1.19 V, some inhibition is apparent at 1.1 V but a separate maximum is not observed because the second rise in current follows at 1.02 V. The fall in current from the plateau occurs at potentials more positive than 0.86 V. The maxima at about 0.6 and 0.8 V were present in the sweeps in 0.5 M H_2SO_4 alone, Fig. 5.7.

The behaviour following sweeping at different anodic limits is shown in Fig. 6.27. In these measurements a lower rotation speed was employed to improve the resolution of the curve. As observed at the higher rotation speed some inhibition presumably due to the formation of A' is observed at 1.1 V. This process merges with the reduction of A' to B' at approximately 1.0 V and consequently the negative limit of the production of A' cannot be established under these conditions. Reduction of A' to B' clearly begins at 1.0 V and is almost complete by about 0.75 V.

Oxidation of B' to A' does not begin until potentials more positive than 0.9 V, but must be complete by 1.1 V because the negative-going sweep is unaltered after sweeping to 1.2 V. Removal of A' appears to begin at potentials close to 1.1 V, since the negative-going curve rises above the positive-going one at this potential. Where this process ends is not clear because

sweeping to more positive potentials results in oxidation of the gold which introduces complications into the subsequent negative-going sweep. However, sweeping to 1.8 V (with a rotation speed of 1000 r.p.m.), Fig. 6.26b, shows that the area associated with the oxidation of gold is modified in the presence of CrVI, Fig. 6.26c. This modification is presumably caused by the progressive oxidation and removal of A'.

Better separation of the first current maximum is seen by using a sweep rate of 10 mV sec^{-1}, Fig. 6.28, the formation of A' occurring between 1.13 and 1.02 V. Removal of A' is not complete by 1.3 V, since sweeping to 1.4 V further increases the magnitude of the cathodic maximum at 1.1 V. The removal of A' therefore appears to be a slow process. Fig. 6.29 summarises the potentials at which these processes occur.

Evidence for the presence of a film at negative potentials was again obtained by recording the current-voltage curve in 0.5 M H_2SO_4 after holding the electrode at 0.0 V for 75 minutes in 1 x 10^{-3} M CrVI, 0.5 M H_2SO_4, Fig. 6.30. As observed in $HClO_4$, Section 6.4.2., when the potential was swept from 0.0 V an anodic peak was observed at 1.15 V. The peak height was proportional to sweep rate indicating that the process was a surface phenomenon and presumably corresponds to the oxidation of similar material to that produced under comparable conditions in $HClO_4$ solutions. In spite of the presence of this peak, sweeping to 1.8 V indicated that the

oxidation of gold was essentially the same as that obtained in 0.5 M H_2SO_4 alone, Fig. 6.26c. Since as shown in Fig. 6.26, the presence of A' modifies the section of the curve corresponding to the oxidation of gold and there is no evidence in Fig. 6.30 for the oxidation and removal of A', it must again be concluded that this substance is removed either during the period the electrode was on open circuit, or by dissolution in the background electrolyte.

Fig. 6.31 is a typical 100 mV sec^{-1} sweep obtained in 1 x 10^{-2} M CrVI, 0.5 M H_2SO_4. Compared with the behaviour of 1 x 10^{-2} M CrVI in 1 M $HClO_4$, Fig. 6.13 or 6.15, removal of film A' appears to be more difficult, since the cathodic current between 1.2 and 1.0 V is lower in the former case. However further reduction of A' to B' and the reverse reaction are much more reversible in H_2SO_4 solution.

The further formation of A' may be seen at approximately 1.1 V. Reduction of A' to B' has probably started by 0.95 V, this process being almost complete by 0.6 V. Reoxidation of B' to A' probably occurs over the potential range 0.8 to 1.0 V.

The potentials of film deposition and modification are summarised in Fig. 6.29A. They follow the trend established in $HClO_4$, of film formation and modification potentials moving more negative in more concentrated CrVI solutions.

In 1 x 10^{-3} M CrVI, 0.25 M H_2SO_4, 0.25 M Na_2SO_4, Fig. 6.32, at 10 mV sec^{-1} the reduction begins at 1.15 V and deposition of A' first modifies the rate at approximately 1.03 V. Reduction of A' to B' is superimposed on this at 0.95 V and is complete by 0.76 V. Reoxidation of P' to A' occurs at potentials more positive than 0.82 V and is complete by 1.0 V. At 100 mV sec^{-1}, Fig. 6.32, there is some evidence for the oxidation and removal of A' at potentials more positive than 1.2 V. Deposition of A' occurs more negative to 1.03 V and reduction of A' to B' at approximately 0.95 V being complete by 0.75 V. Oxidation of B' to A' takes place at 0.83 V and is complete by 1.05 V. Fig. 6.29 summarises these results.

6.5 Conclusions

The results in $HClO_4$ solutions show that after anodic pretreatment in a particular potential range an essentially film-free surface appears to be produced. Reduction of CrVI on this surface occurs readily but as the potential is made more negative an inhibiting film (A) begins to form. If this film is allowed to reach its equilibrium state it produces severe inhibition of the electrode reaction. At still more negative potentials however further reduction of this film to a less inhibiting form (B) apparently occurs which allows the reaction to proceed at a higher rate. At very negative potentials an additional

deposit (C) is slowly formed on the electrode surface and decreases the rate of the electrode reaction. On making the potential more positive, reoxidation of B to A occurs with a consequent fall in the current. Reoxidation and removal of films A and C takes place at sufficiently positive potentials. After prior anodic oxidation of the gold, reduction of the surface oxide and CrVI appear to occur simultaneously in dilute solutions of CrVI. In 1 x 10^{-2} M CrVI solutions however some interaction between gold oxide and film A is apparent, leading to a somewhat more inhibited electrode.

A similar pattern of behaviour was observed in H_2SO_4 solutions. This acid is, however, more effective than $HClO_4$ in promoting reduction of CrVI because the inhibiting layer (A') is converted to its less inhibiting form (B') at more positive potentials than in $HClO_4$ solutions (compare Figs. 6.16 and 6.29). Since addition of small amounts of H_2SO_4 to $HClO_4$ solutions caused a marked shift in the potential for the reduction of film A it is presumably the sulphate ion (or HSO_4^-), rather than the hydrogen ion, which is responsible for the easier reduction of this layer. This is confirmed by the fact that although the hydrogen ion concentration in 0.5 M H_2SO_4 is substantially lower than that in 1 M $HClO_4$, the reduction of the inhibiting film occurs at more positive potentials in the former case. The material produced at negative potentials (C')

may be the same substance as formed in $HClO_4$ solutions since it is oxidised at the same potential. However it produces greater inhibition in H_2SO_4 solutions as indicated by the lower i_p values and larger intercepts in the graphs of $^c b/_{i_p}$ against $^1/_{w^{\frac{1}{2}}}$. Since i_p increases as the H_2SO_4 concentration increases, it is likely that the hydrogen ion hinders the formation of this layer. By contrast, the sulphate ion must promote the formation of this layer or modify its structure since addition of H_2SO_4 to $HClO_4$ decreases i_p.

The current-potential curves obtained in the present work had the same general form as reported by many previous workers. In agreement with Okada et al.[1.19] it has been found that in more concentrated CrVI solutions oxidised gold is reduced prior to the reduction of CrVI. It appears however that the first branch of the current-voltage curve is due, not to the reduction of oxidised gold, but results from the inhibition of CrVI reduction by a surface film.

Although the solution compositions employed here were different from those used in most earlier work the theories propounded by previous authors, if they are to be generally applicable, should explain the present results.

With the exception of Weiner[1.17] all earlier workers agree that a film is present on the gold surface at all potentials; its nature varying with potential. This is in general agreement with the present results

although it appears that under certain conditions a film-free surface is obtained over a narrow potential range, Section 6.4.2. Weiner maintained that the film dissolved in solutions containing foreign anions; this view appears to be in complete conflict with the present work.

Reinkowski and Knorr[1.16] and Gerischer and Käppel[1.15] all suggest that the film participates in the electrode reaction; a view which is not shared by Fiegl and Knorr[1.13,1.20]. The results reported here indicate that film A or A' does not participate in the electrode reaction since the steady-state currents, obtained in its presence, are practically zero. No evidence is available to indicate whether films B and C (or B' and C') do or do not participate in the electrode reaction.

The role of foreign anions has been interpreted in the following ways:

(a) Reinkowskii and Knorr[1.16] suggest that the film formed in the presence of anions differs in composition from that produced in their absence and is capable of further reduction.

(b) Gerischer and Käppel[1.15] propose that foreign anions do not alter the composition of the film but are involved in its further reduction.

(c) Fiegl and Knorr[1.13,1.20] believe that added acids can inhibit the formation of the film as a consequence of both the increase in hydrogen ion concentration

and through the formation of soluble CrIII complexes; the sulphate ion but not the perchlorate ion was said to operate in this manner. No clear evidence has been obtained to support or reject (a) or (b). The hydrogen ion has been shown to inhibit the formation of film C (or C') whereas sulphate ion appears to promote the formation of these films, although it facilitates reduction of A or A'.

Differing views have been expressed as to whether the surface film is porous. Film A or A' is almost certainly not since it is capable of completely inhibiting the electrode reaction. No evidence is available as to the nature of film B or B'. Film C or C' appears to be porous since film A or A' can be removed from the surface without prior removal of C.

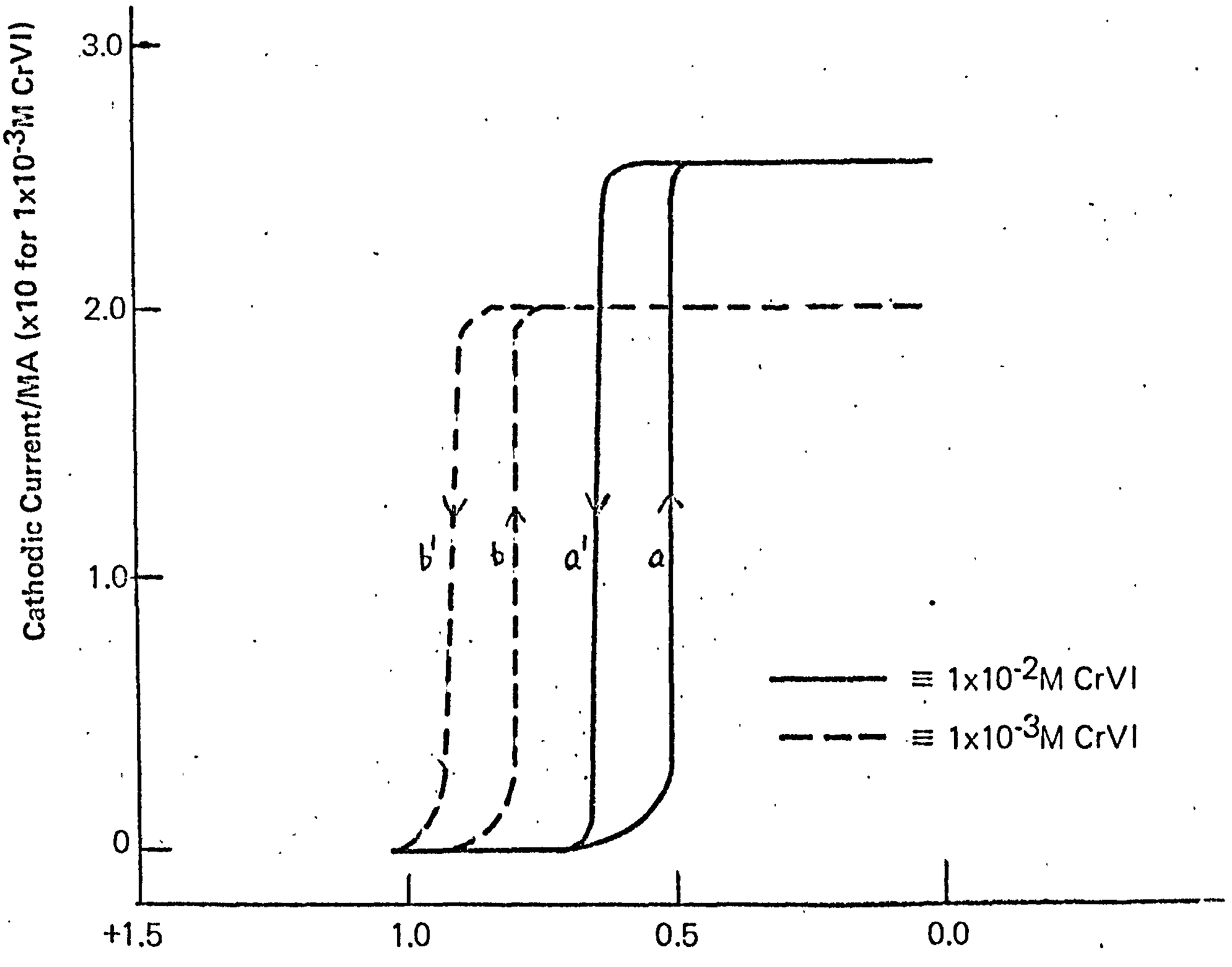

Fig. 6.1

STEADY-STATE CURRENT POTENTIAL CURVE IN IM $HClO_4$. IM $NaClO_4$, 1000 rpm

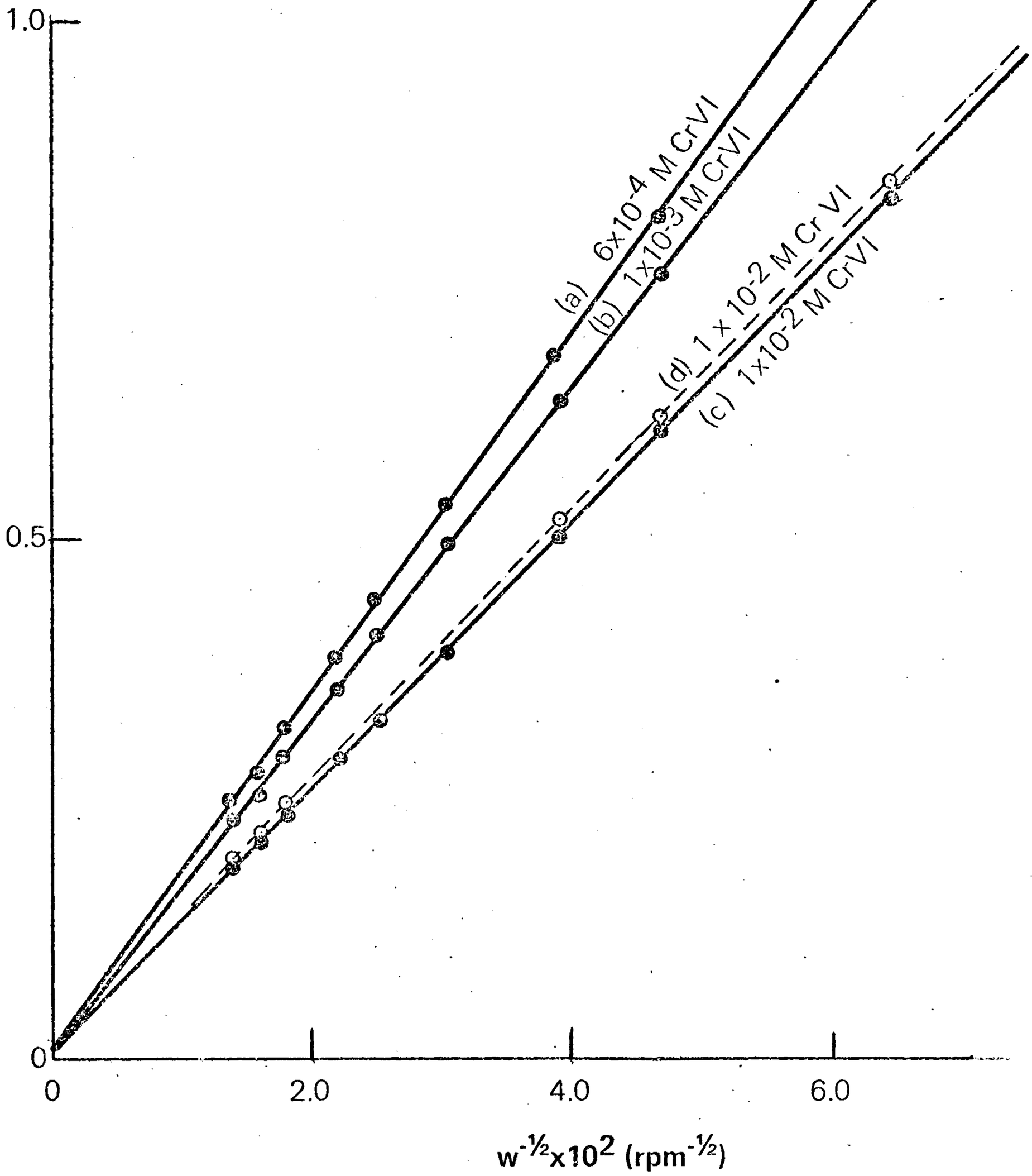

Fig. 6.2
PLOT OF $C^{b}/_{i}$ / $w^{-½}$ IN IM $HClO_4$, IM $NaClO_4$

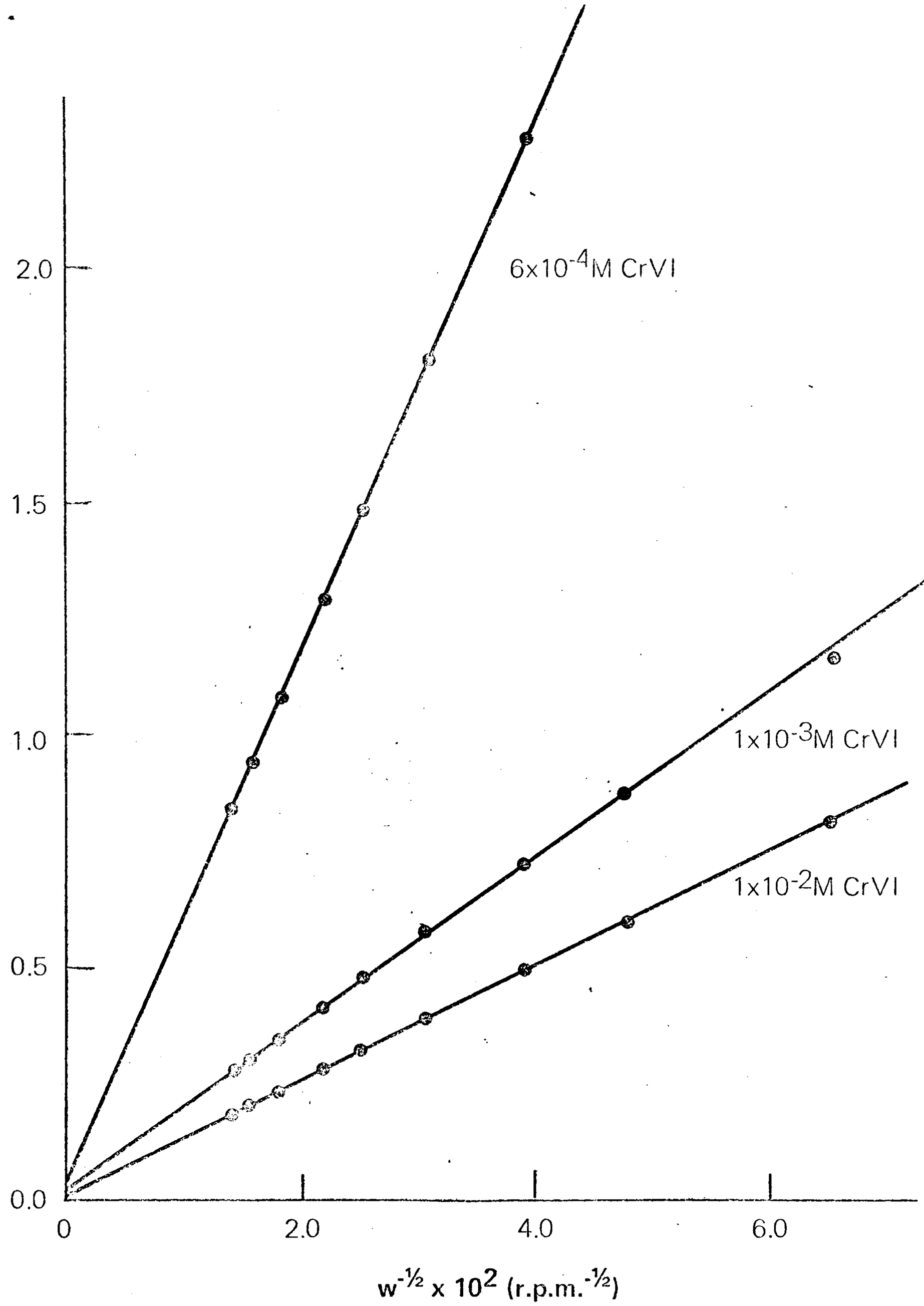

Fig. 6.3
PLOT OF $^{Cb}/_i$ / $w^{-½}$ IN 2M $HClO_4$

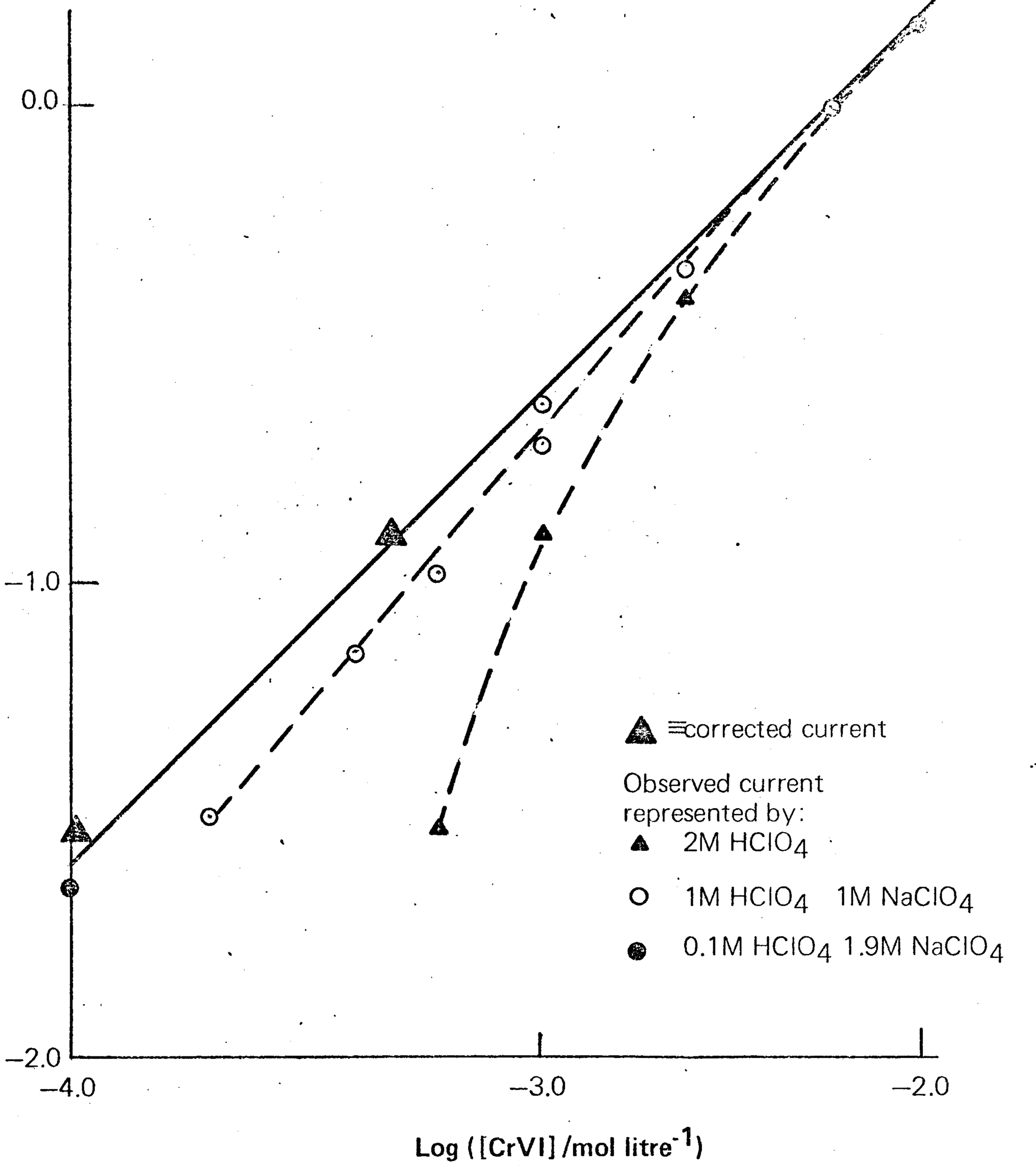

Fig. 6.4

REACTION ORDER PLOT

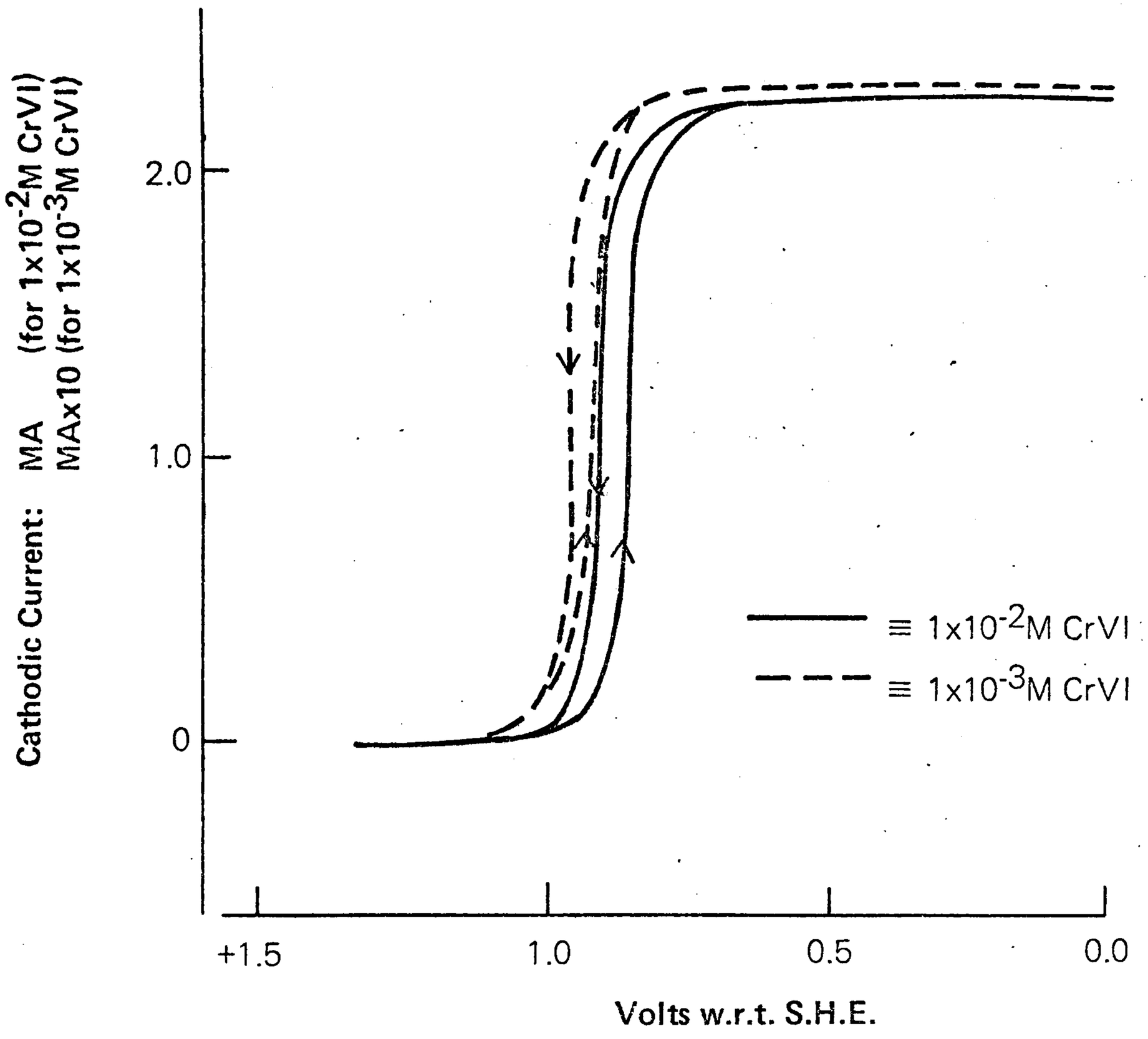

Fig. 6.5

STEADY-STATE CURRENT-POTENTIAL CURVE IN 0.5M H_2SO_4, 1000 rpm

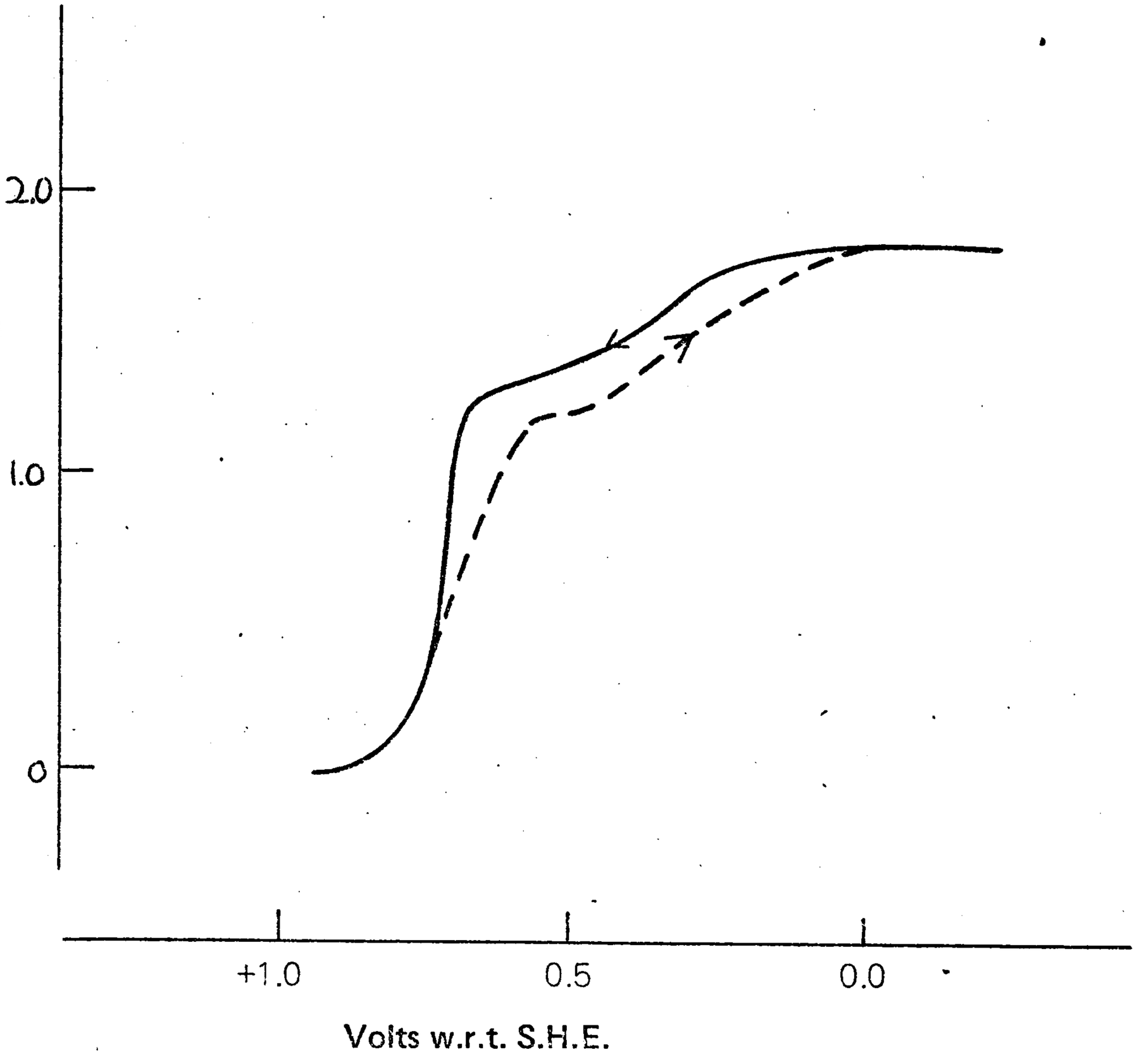

Fig. 6.6

STEADY-STATE CURRENT-POTENTIAL CURVE IN 0.25M H_2SO_4, 0.25M Na_2SO_4, 1000 rpm. 1×10^{-2}M CrVI

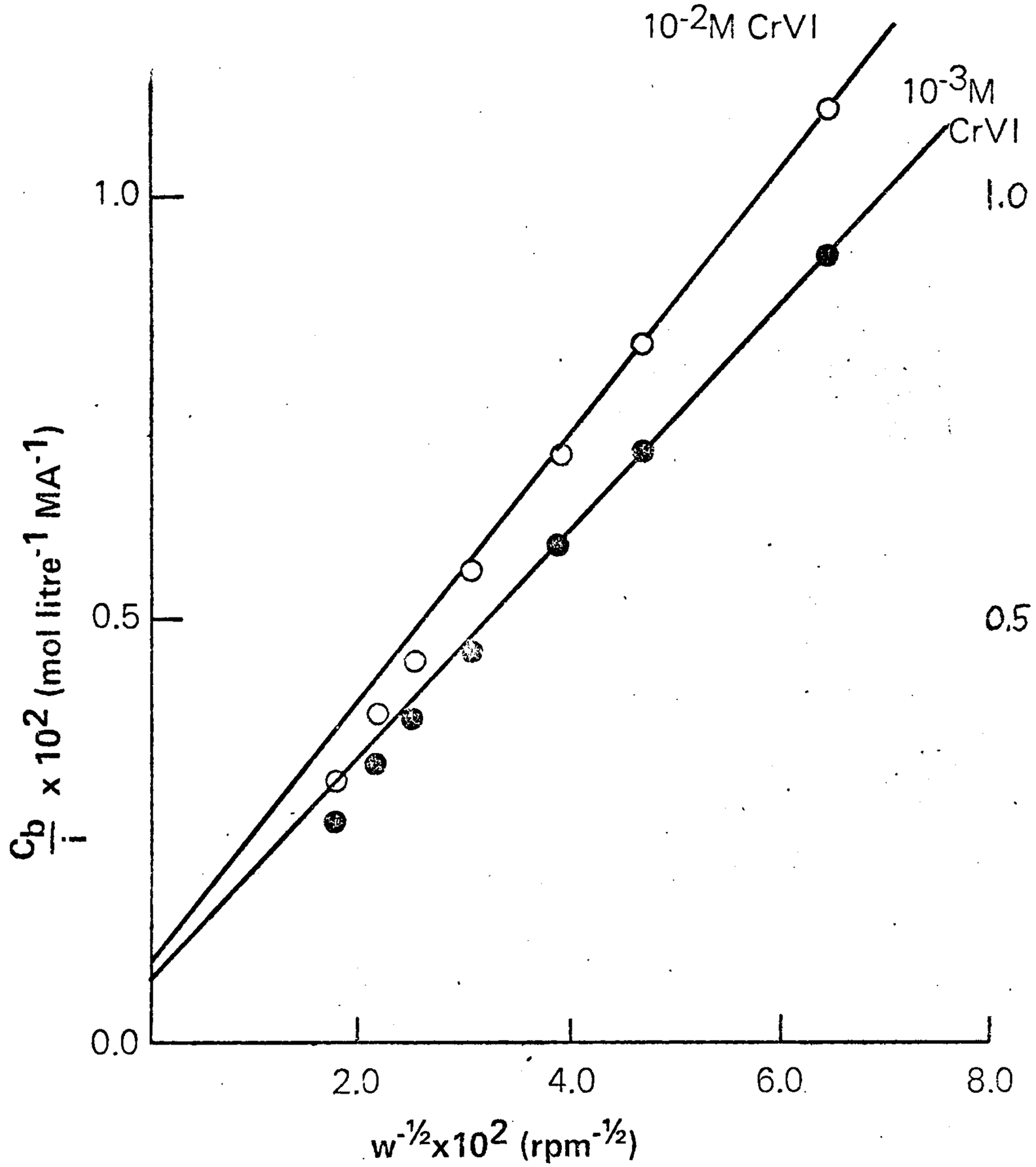

Fig. 6.7
PLOT OF $\frac{C_b}{i}/w^{-½}$ IN 0.25M H_2SO_4, 0.25M Na_2SO_4

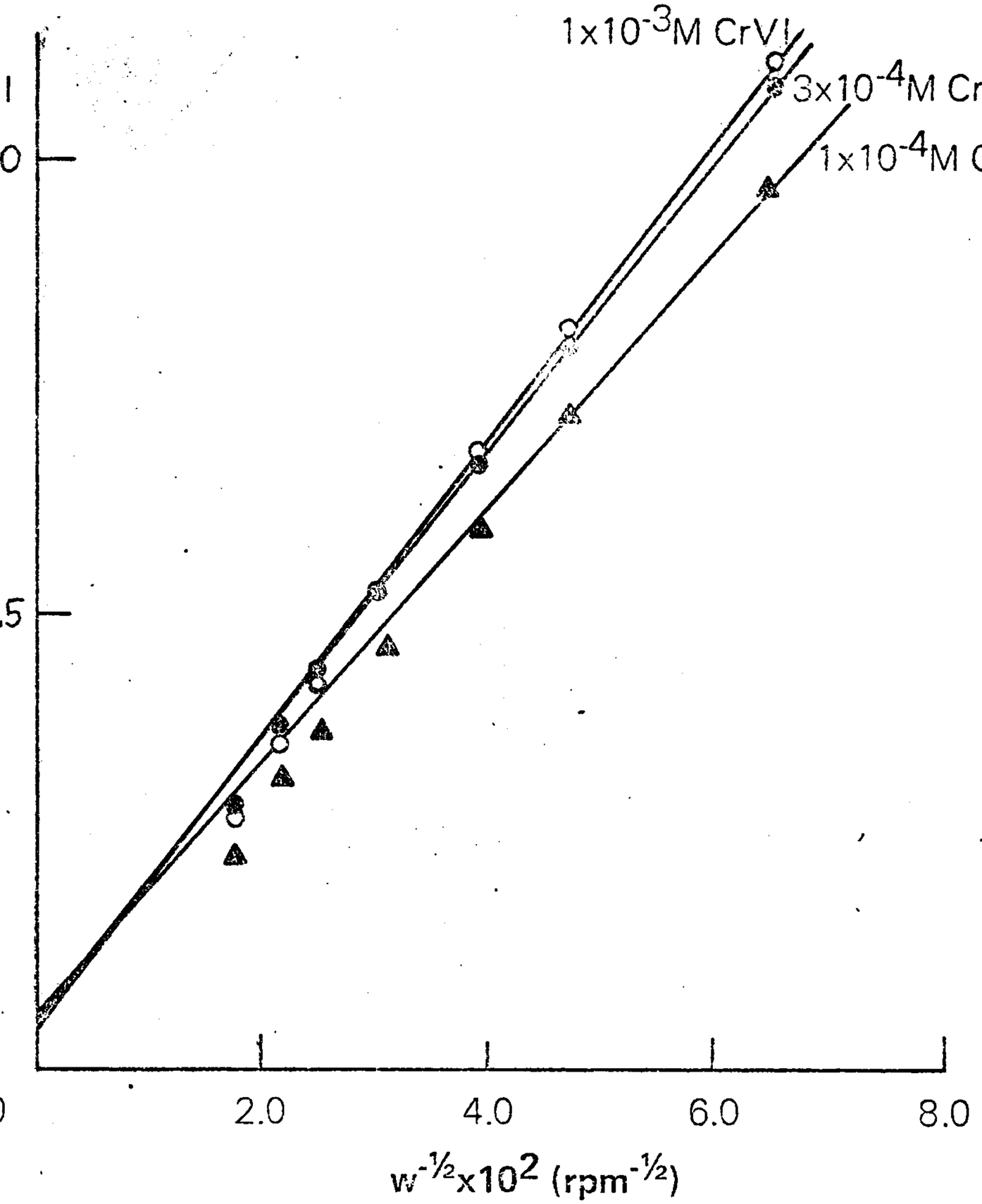

Fig. 6.7
PLOT OF $\frac{C_b}{i}/w^{-½}$ IN 0.05M H_2SO_4, 0.45M Na_2SO_4

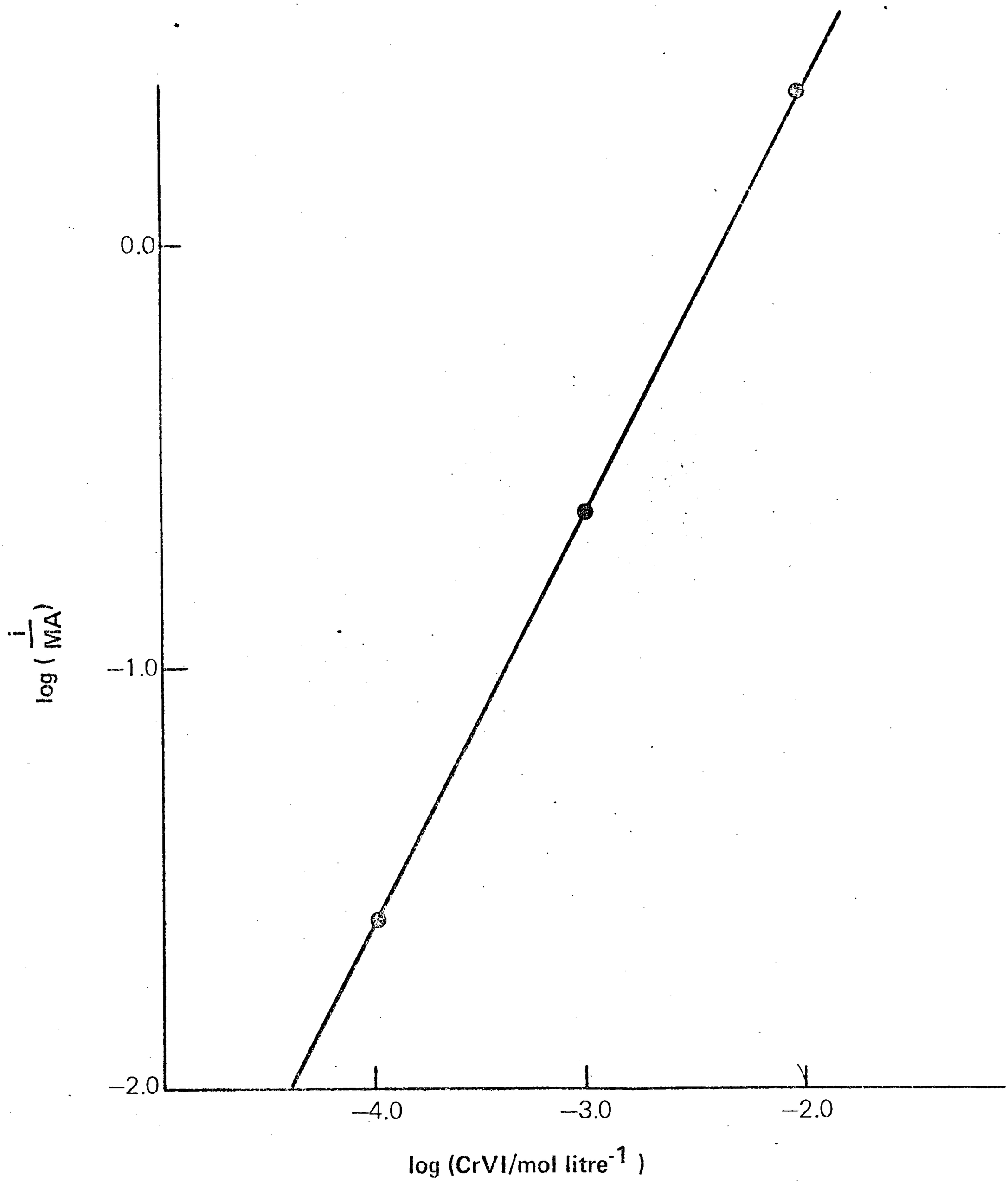

Fig. 6.8
REACTION ORDER PLOT 0.5M H_2SO_4

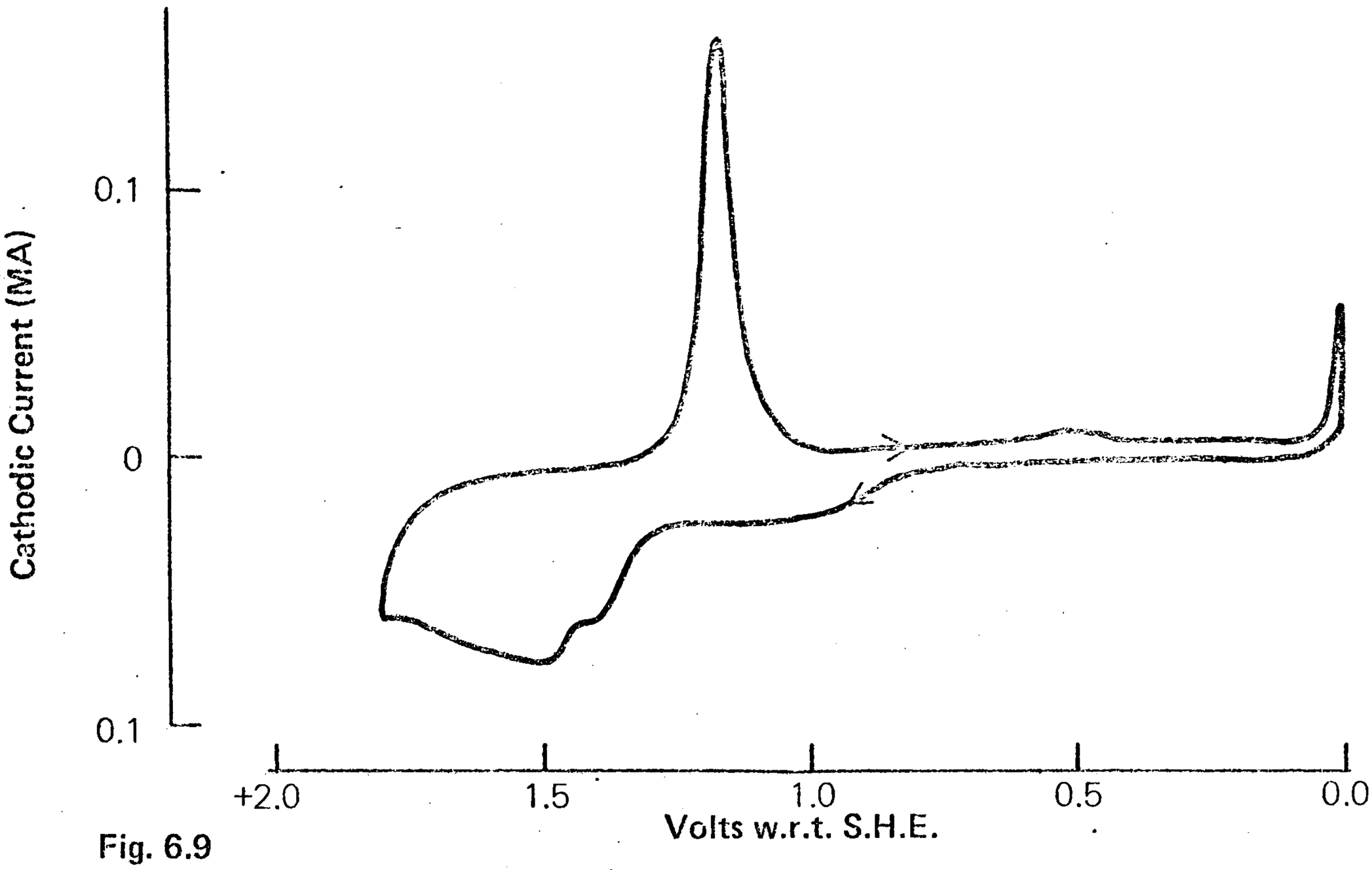

Fig. 6.9

CURRENT-POTENTIAL RELATION, GOLD IN IM $HClO_4$, ROTATION SPEED 1000 rpm, 100 mV sec^{-1} SWEEP

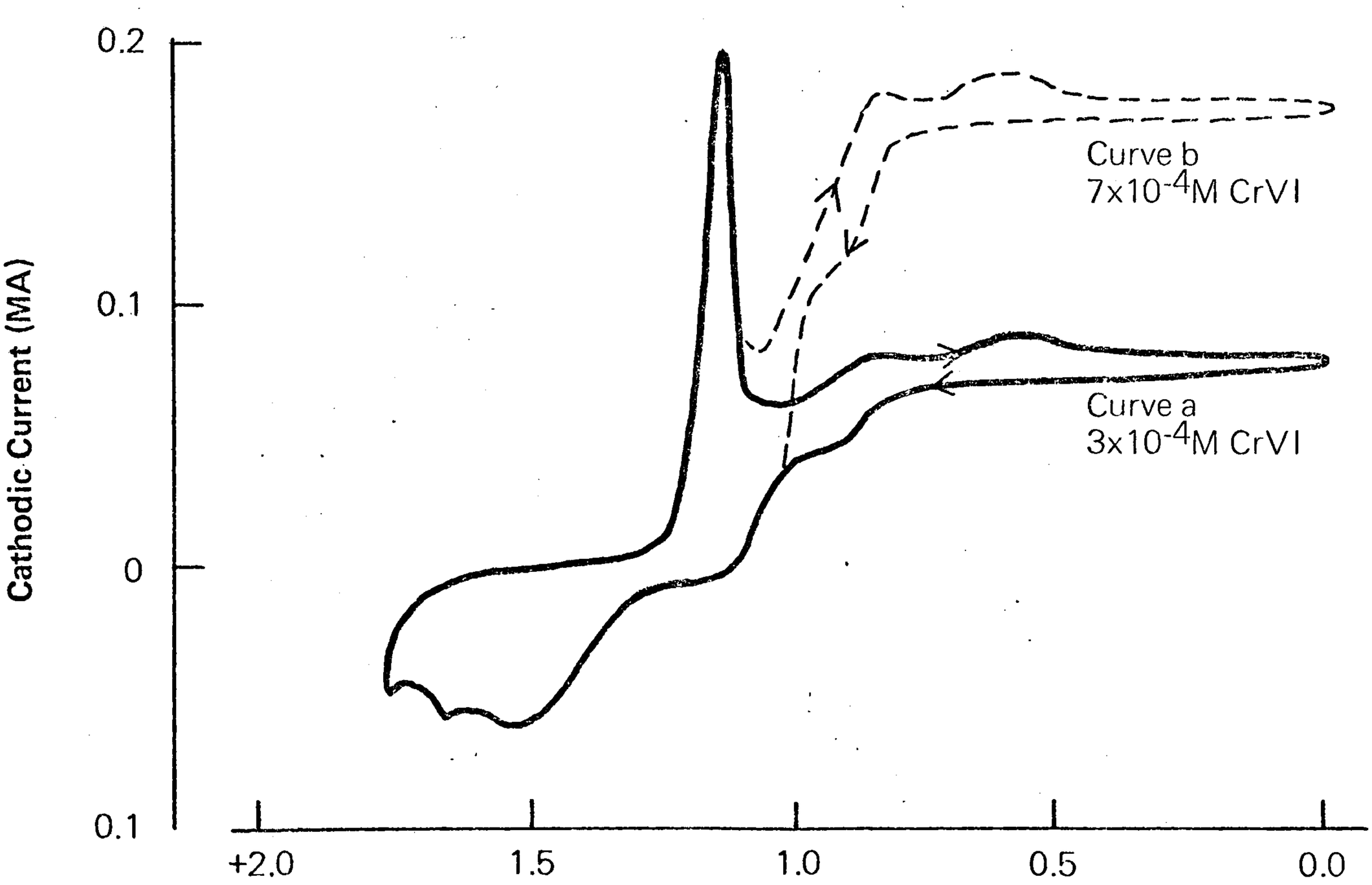

Fig. 6.10

CURRENT-POTENTIAL RELATION, GOLD ELECTRODE, IM $HClO_4$, 1000 rpm, 100 mV sec^{-1} SWEEP

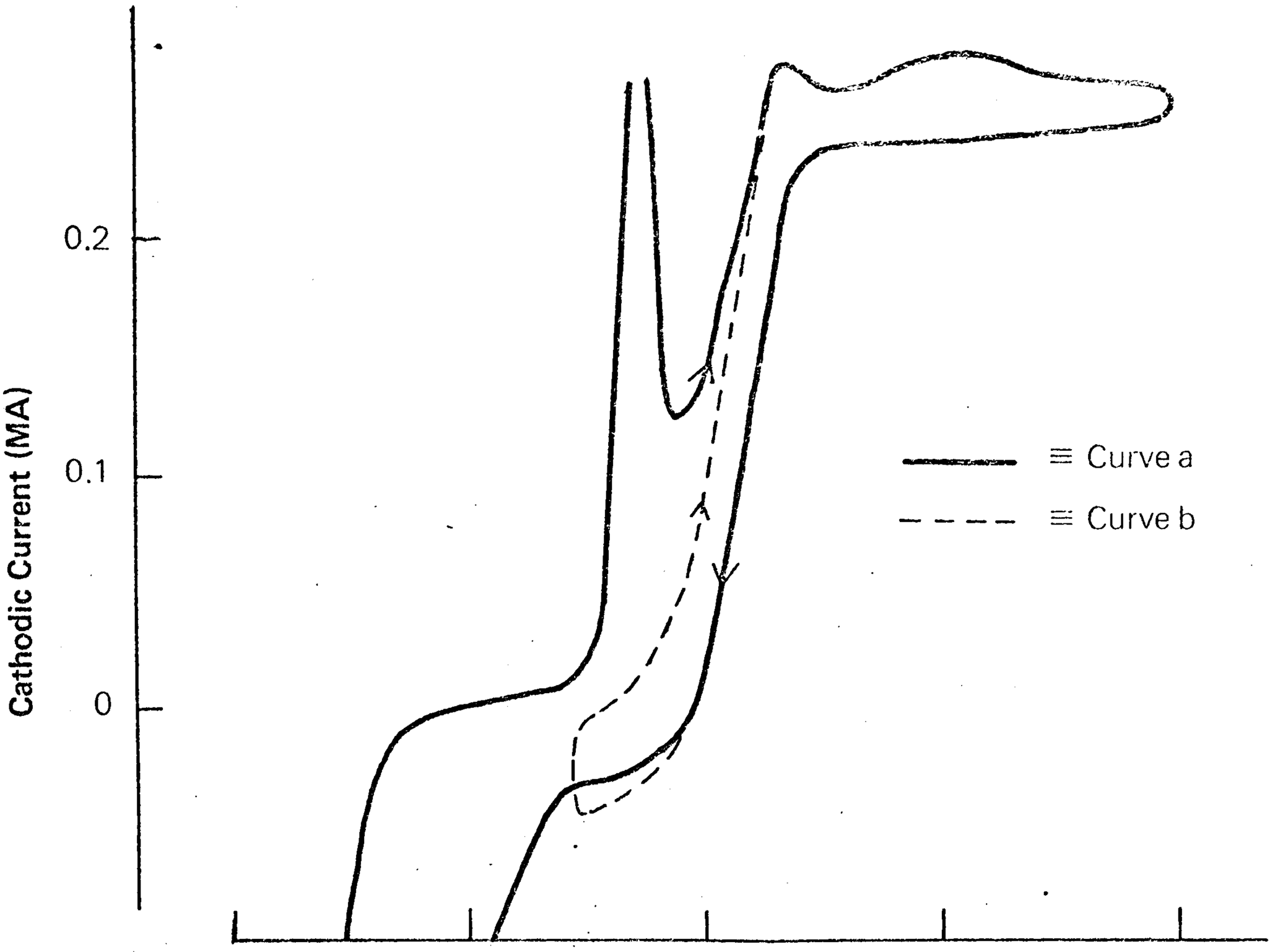

Fig. 6.11

CURRENT-POTENTIAL RELATION. GOLD ELECTRODE, 1×10^{-3}M CrVI, IM $HClO_4$, 1000 rpm, 100mV sec^{-1} SWEEP

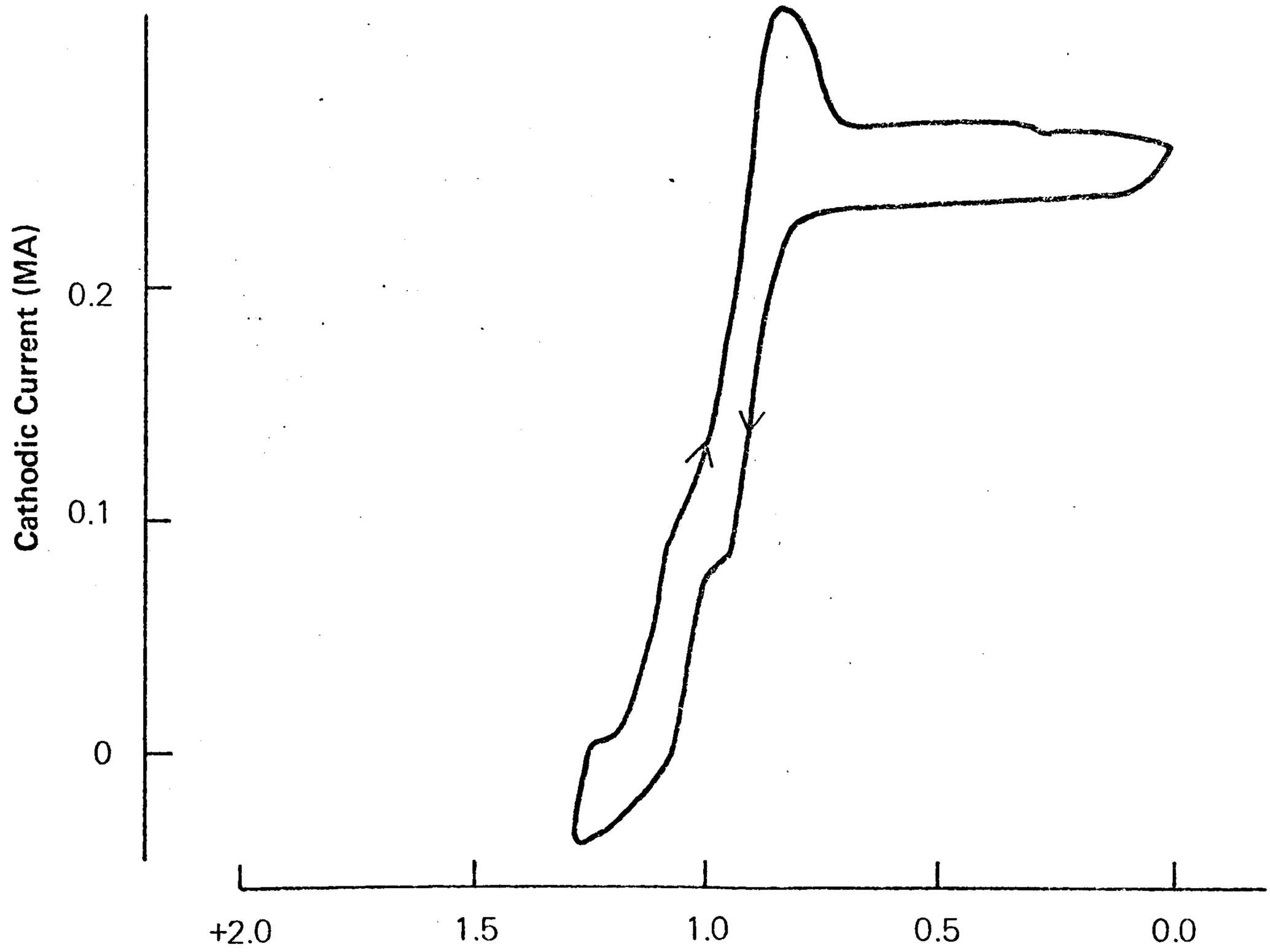

Fig. 6.12

ATION. GOLD ELECTRODE, 1×10^{-3}M CrVI, IM $HClO_4$

EP

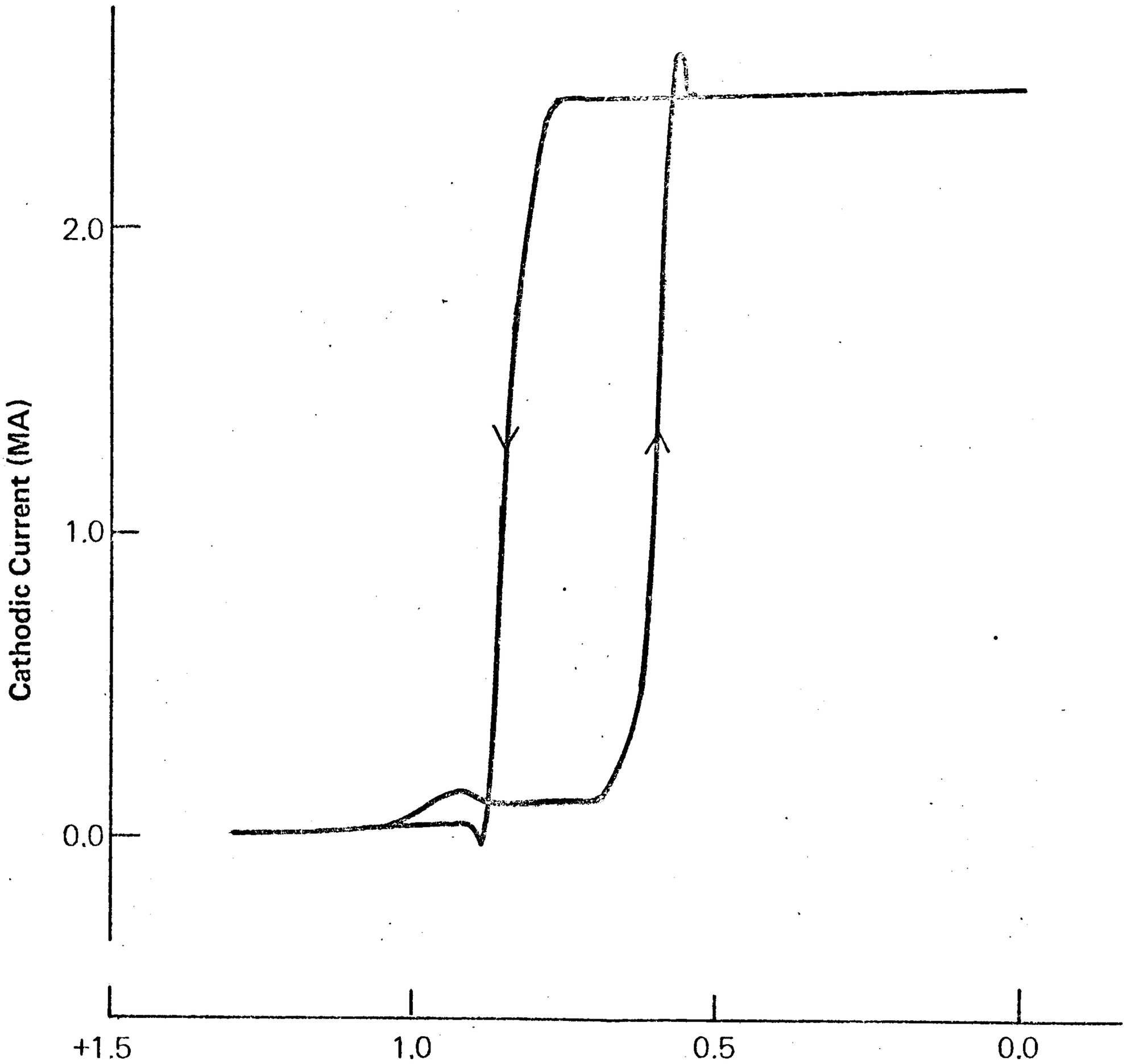

Fig. 6.13

CURRENT-POTENTIAL RELATION, GOLD ELECTRODE, 1×10^{-2}M CrVI, IM $HCLO_4$, 1000 rpm, 100 mV sec^{-1}

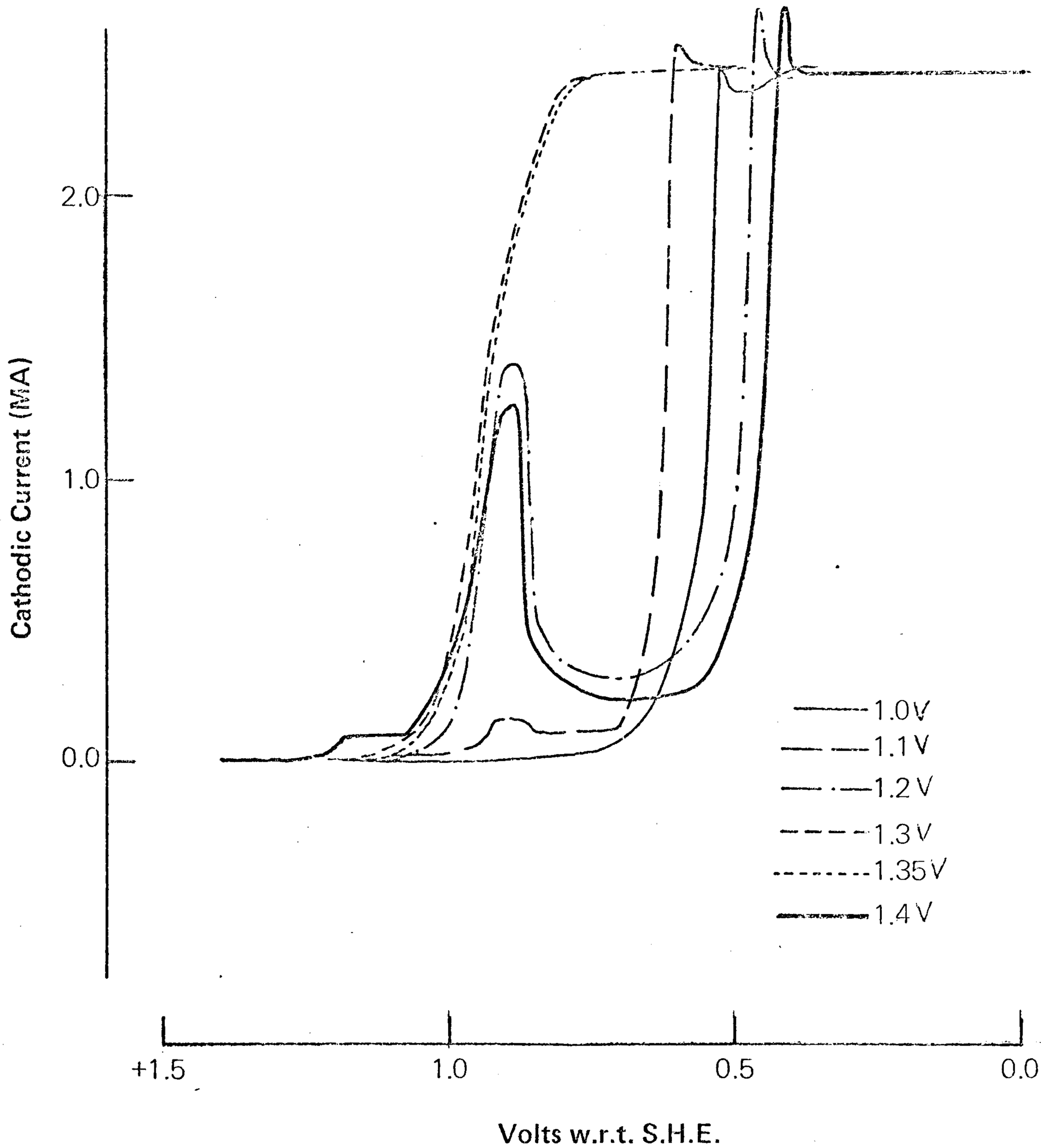

Fig. 6.14

NEGATIVE-GOING SWEEP AFTER HOLDING AT POSITIVE POTENTIALS FOR 10 min. GOLD ELECTRODE, 1×10^{-2}M CrVI, IM $HClO_4$, 1000 rpm, 100 mV sec^{-1}

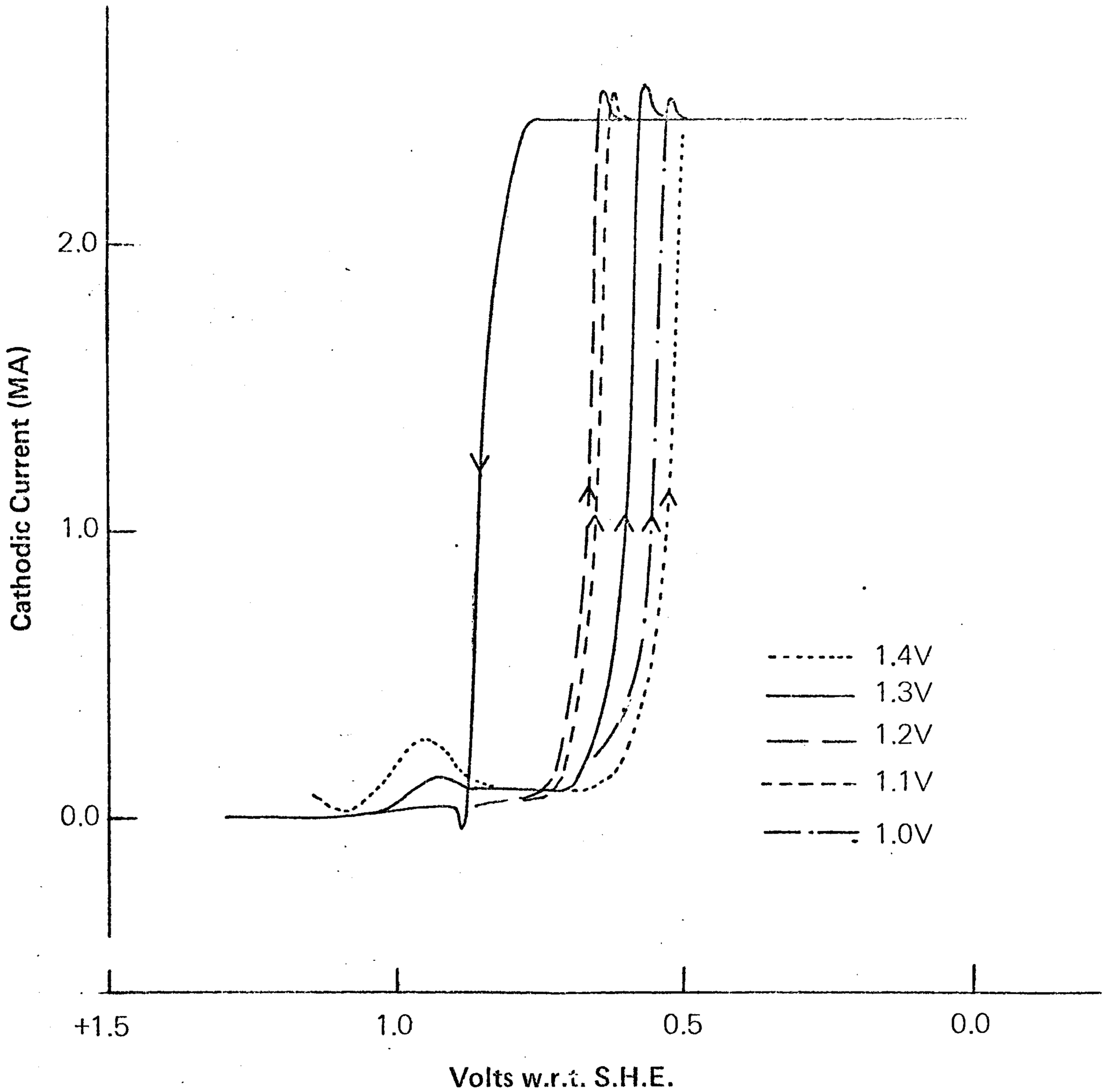

Fig. 6.15

CURRENT-POTENTIAL RELATIONSHIP OBTAINED BY CONTINUOUS SWEEPING FROM LIMITS SHOWN GOLD ELECTRODE, 1×10^{-2} M CrVI, IM $HClO_4$, 1000 rpm, 100 mV sec^{-1}

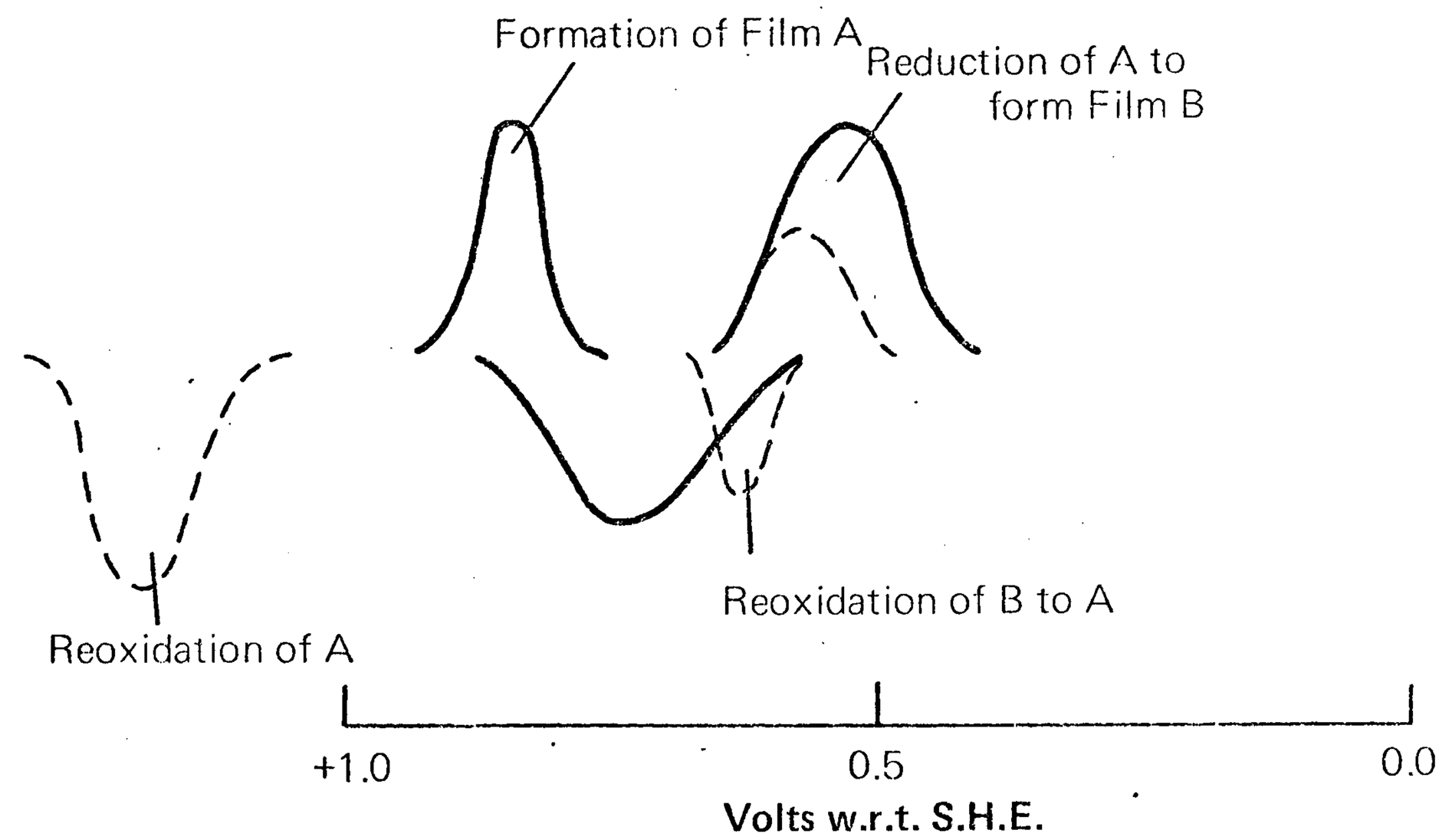

(A) SUMMARY OF CONDITION OF ELECTRODE SURFACE IN 1×10^{-2}M CrVI, IM $HClO_4$

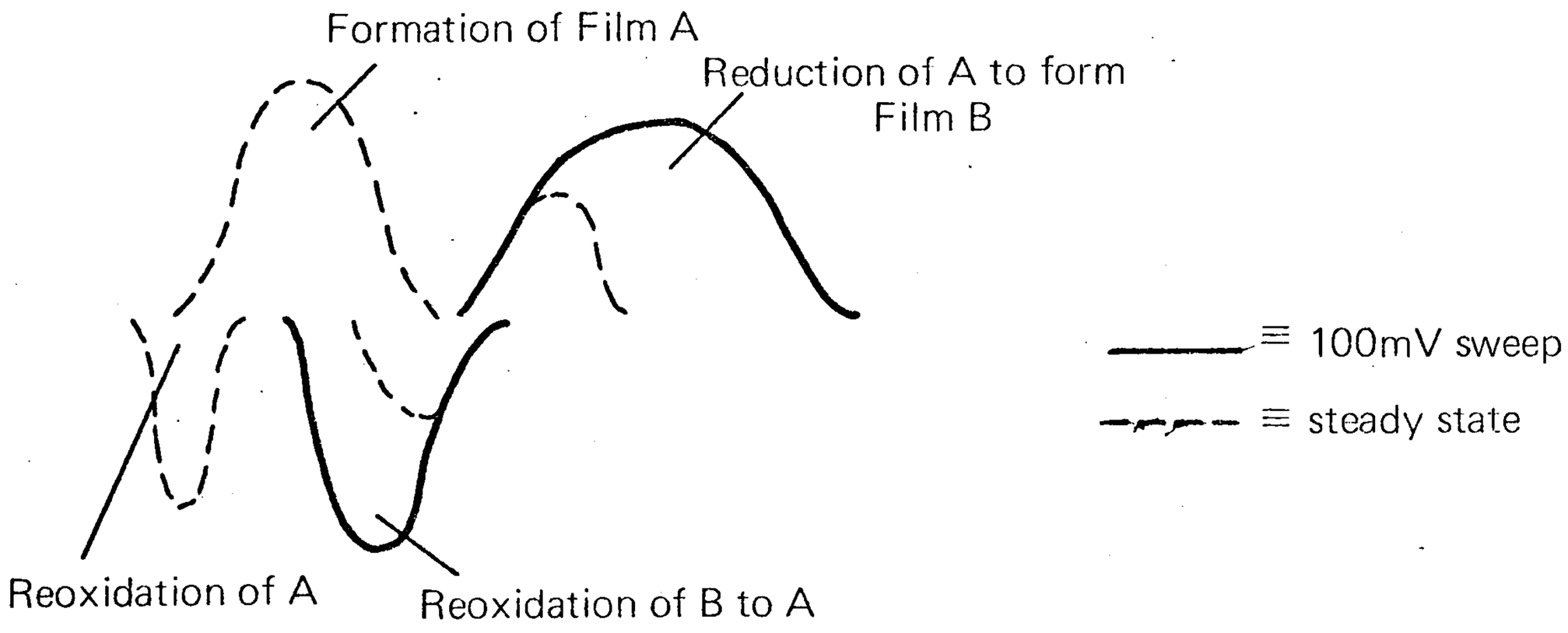

(B) SUMMARY OF CONDITION OF ELECTRODE SURFACE IN 1×10^{-3} M CrVI, IM $HClO_4$

Fig. 6.16
DIAGRAMMATIC REPRESENTATION OF LAYER FORMATION

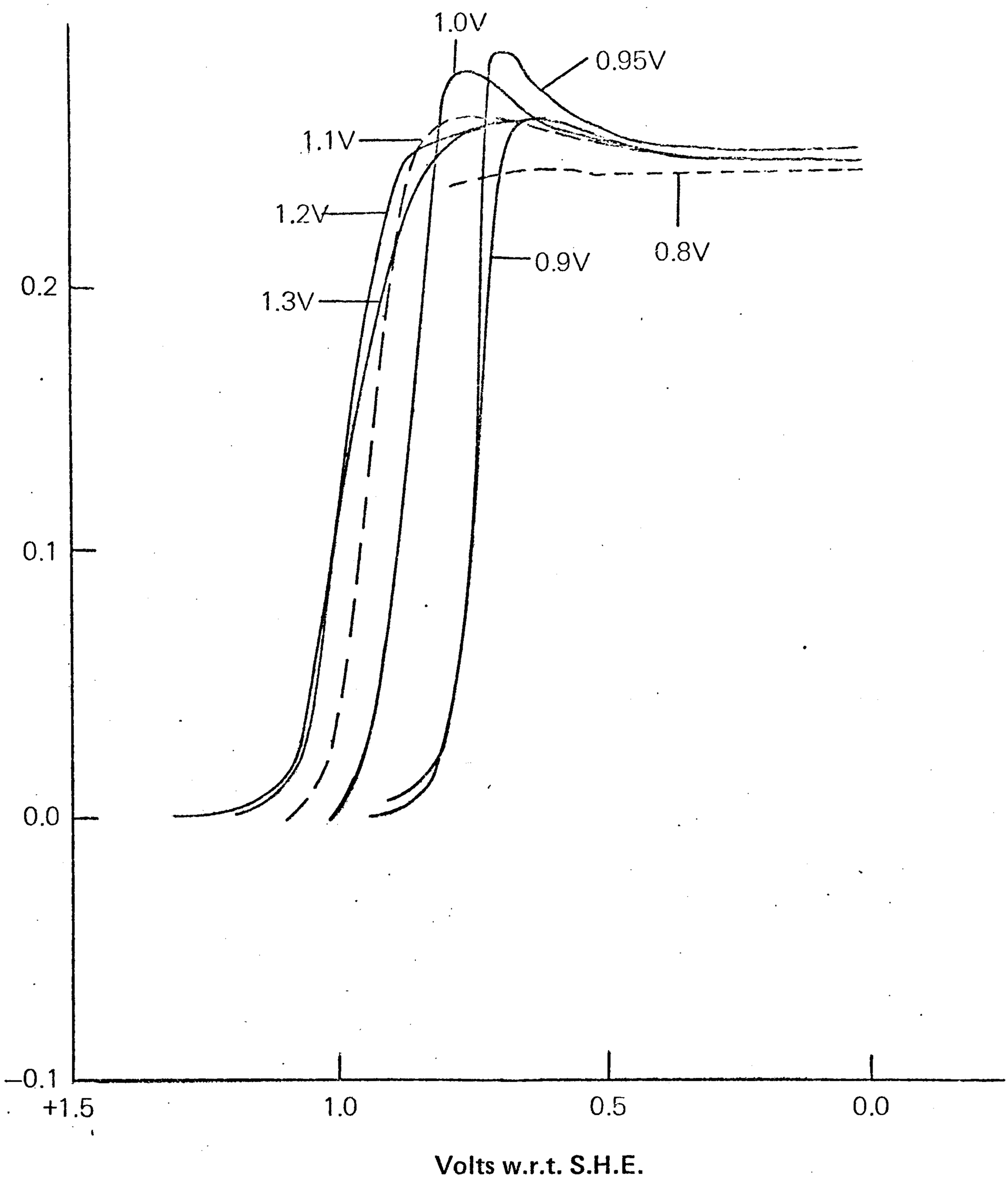

Fig. 6.17

NEGATIVE-GOING SWEEP AFTER HOLDING AT POSITIVE POTENTIALS FOR 5 min (10 min for +1.3V) GOLD ELECTRODE, 1×10^{-3}M CrVI, IM $HClO_4$, 1000 rpm, 100 mV sec^{-1}

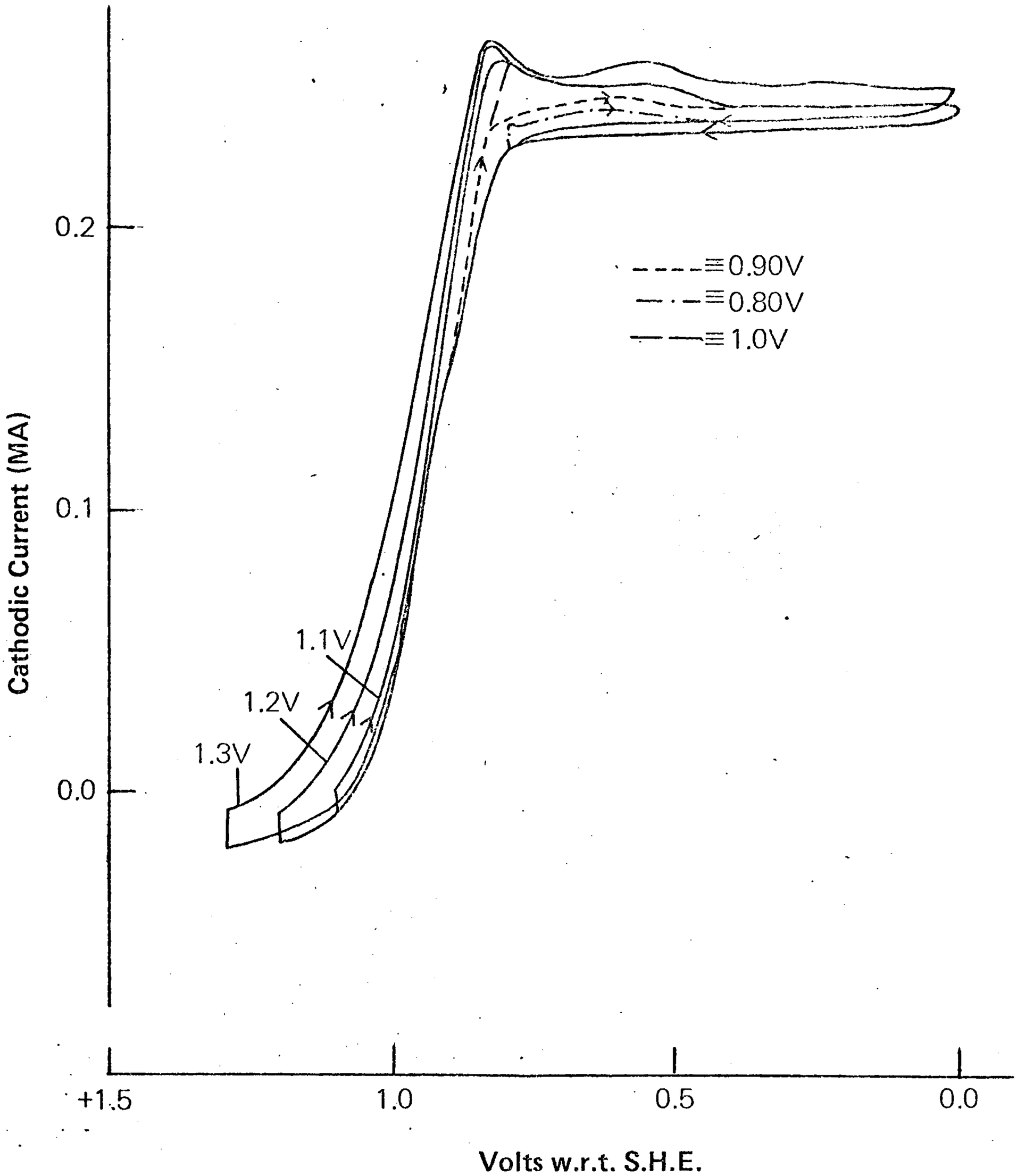

Fig. 6.18

CURRENT-POTENTIAL RELATION OBTAINED AFTER SWEEPING TO POTENTIAL LIMIT INDICATED. GOLD ELECTRODE, 1×10^{-3}M CrVI, IM $HClO_4$, 1000 rpm, 100mV sec^{-1}

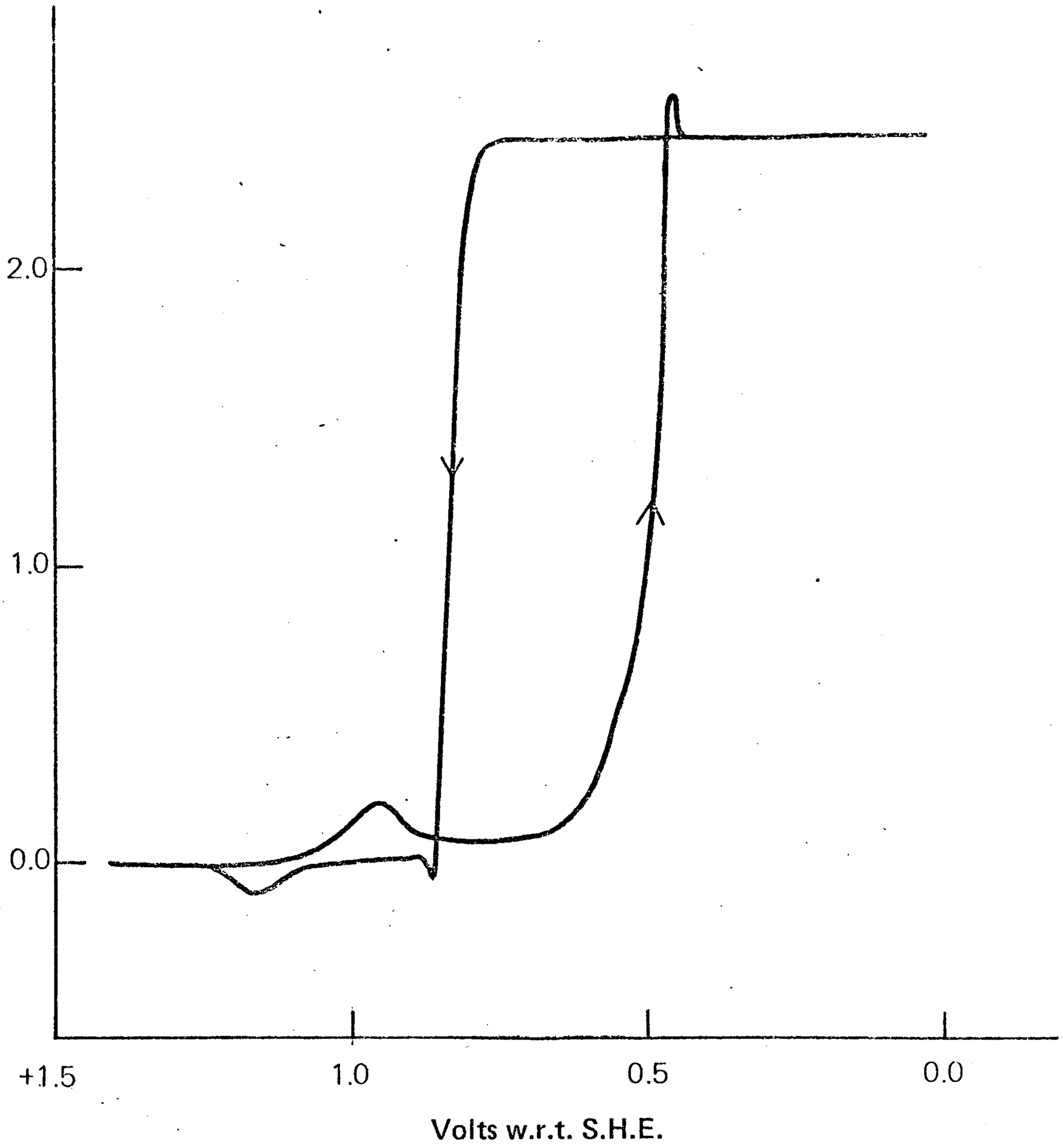

Fig. 6.19

CURRENT-POTENTIAL RELATION OBTAINED AFTER HOLDING THE ELECTRODE AT 0.0V FOR 5 MINUTES, GOLD ELECTRODE, 1×10^{-2}M CrVI, IM $HClO_4$, 1000rpm, 100 mV sec^{-1}

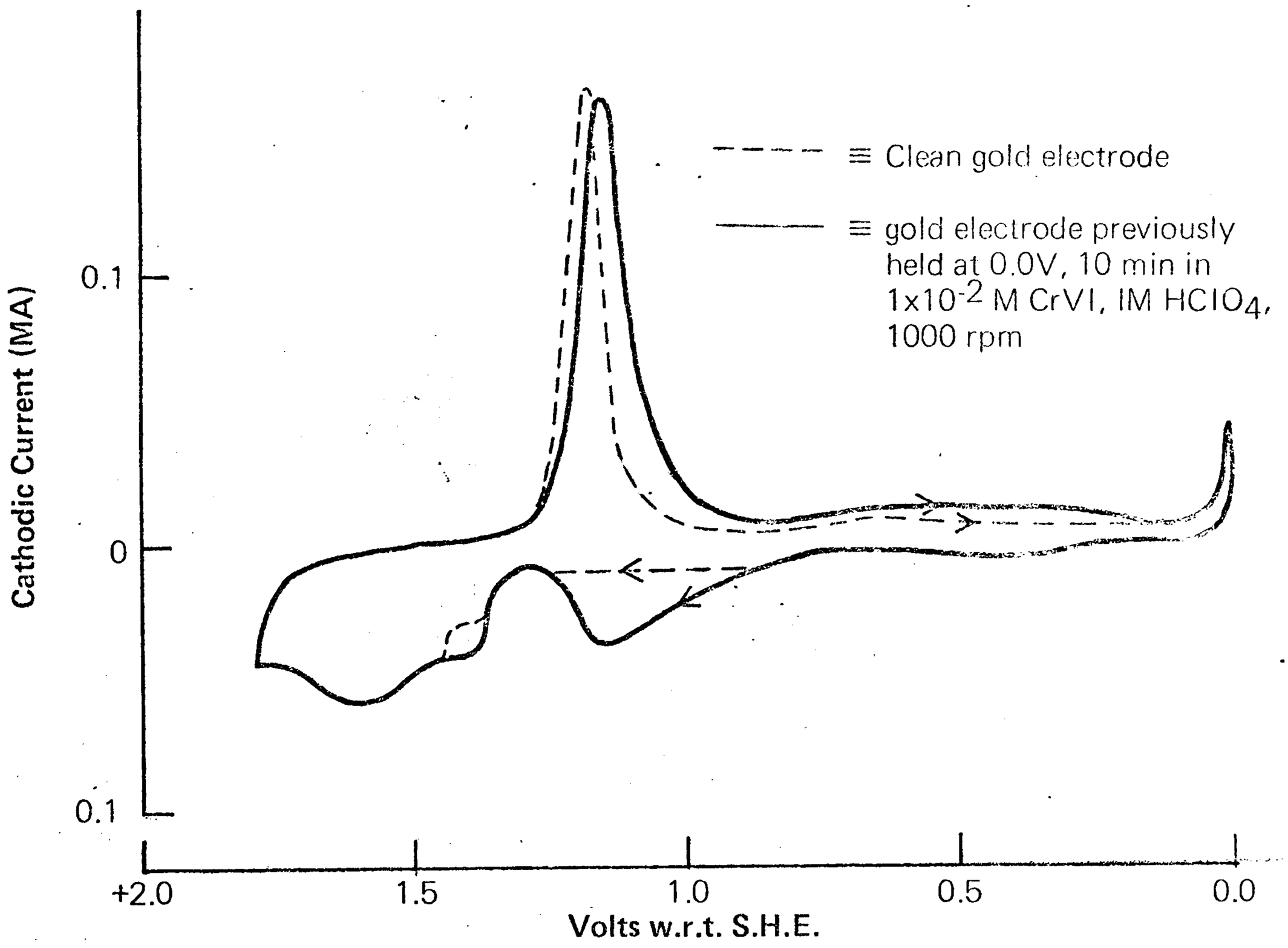

Fig. 6.20 CURRENT-POTENTIAL RELATION, ETCHED GOLD ELECTRODE, IM $HClO_4$, NO ROTATION, 100mV sec^{-1}

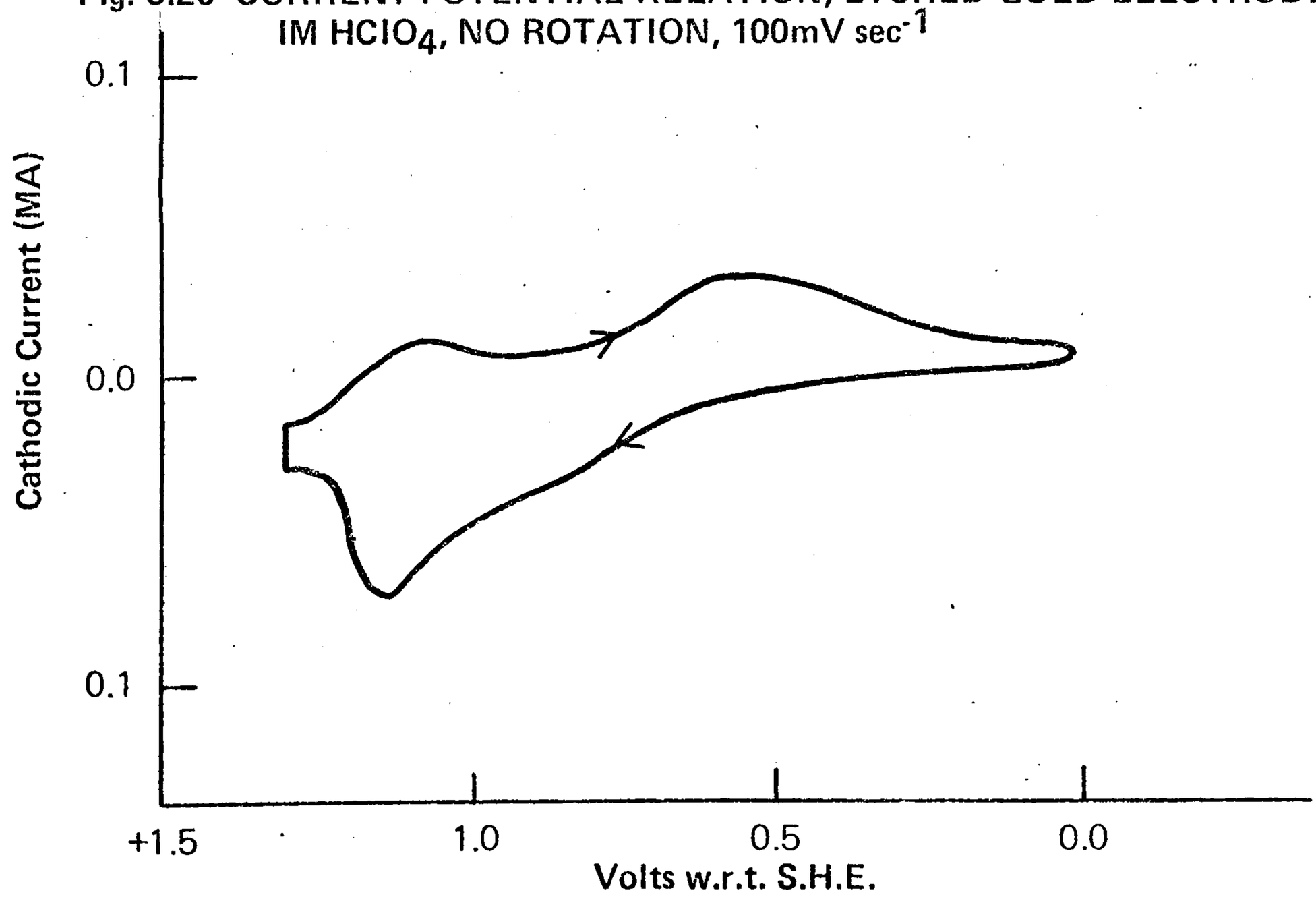

Fig. 6.21

CURRENT-POTENTIAL RELATION, POLISHED GOLD ELECTRODE, IM $HClO_4$, NO ROTATION, 100mV sec^{-1}, FOLLOWS POLARISATION FOR 25 min, AT 0.0V, IN $1x10^{-2}$M CrVI, IM $HClO_4$

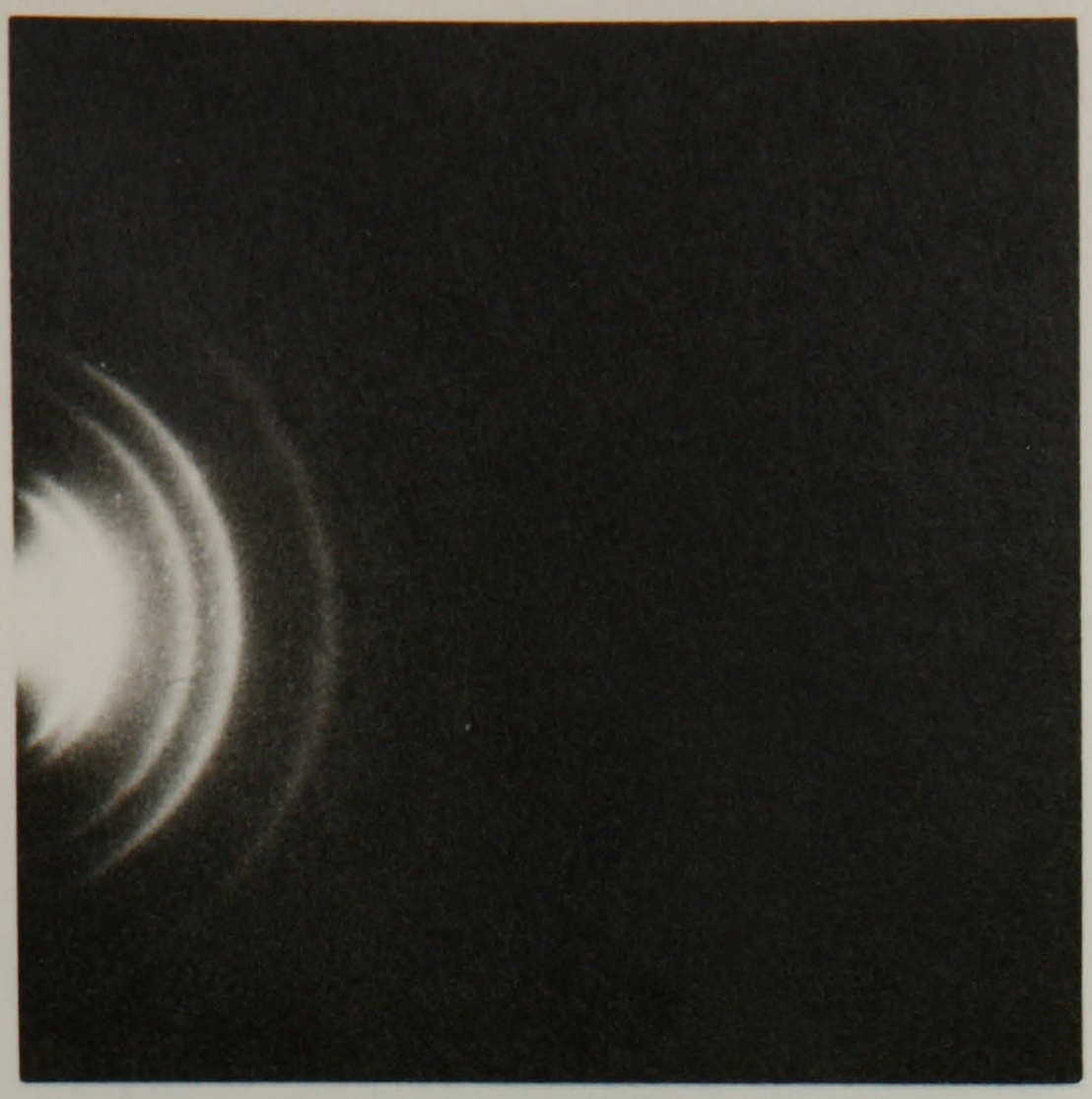

(a) Unpretreated gold electrode

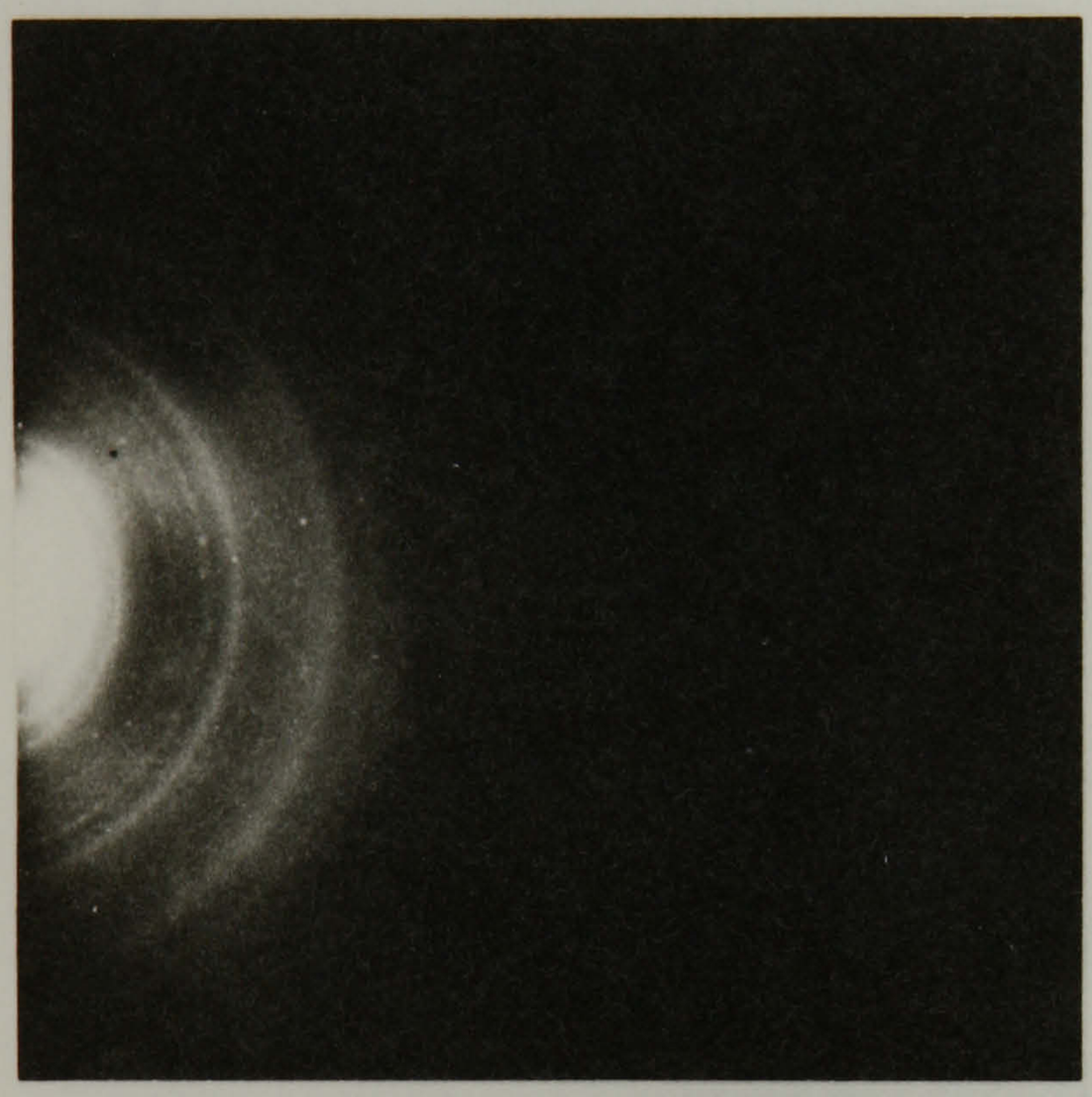

(b) Gold electrode following 90 min. prelectrolysis at 0.2v in 1×10^{-2} M Cr VI IM $HClO_4$

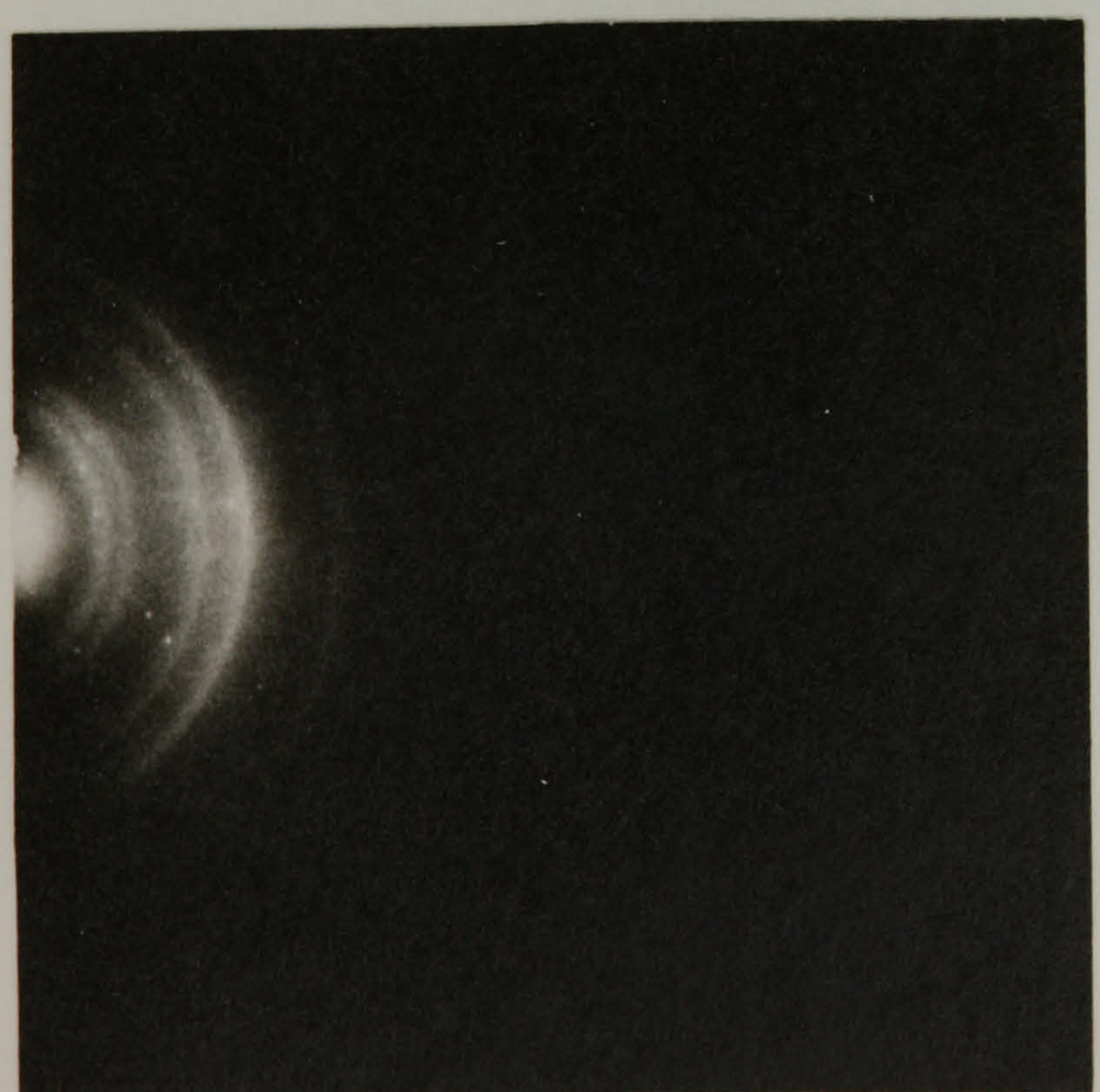

(c) Gold electrode pretreated as above, then pre-electrolysed a further 60 minutes at 1.0v in 1×10^{-2} M Cr VI, IM $HClO_4$

Fig. 6.22 ELECTRON DIFFRACTION PHOTOGRAPHS OF A GOLD ELECTRODE

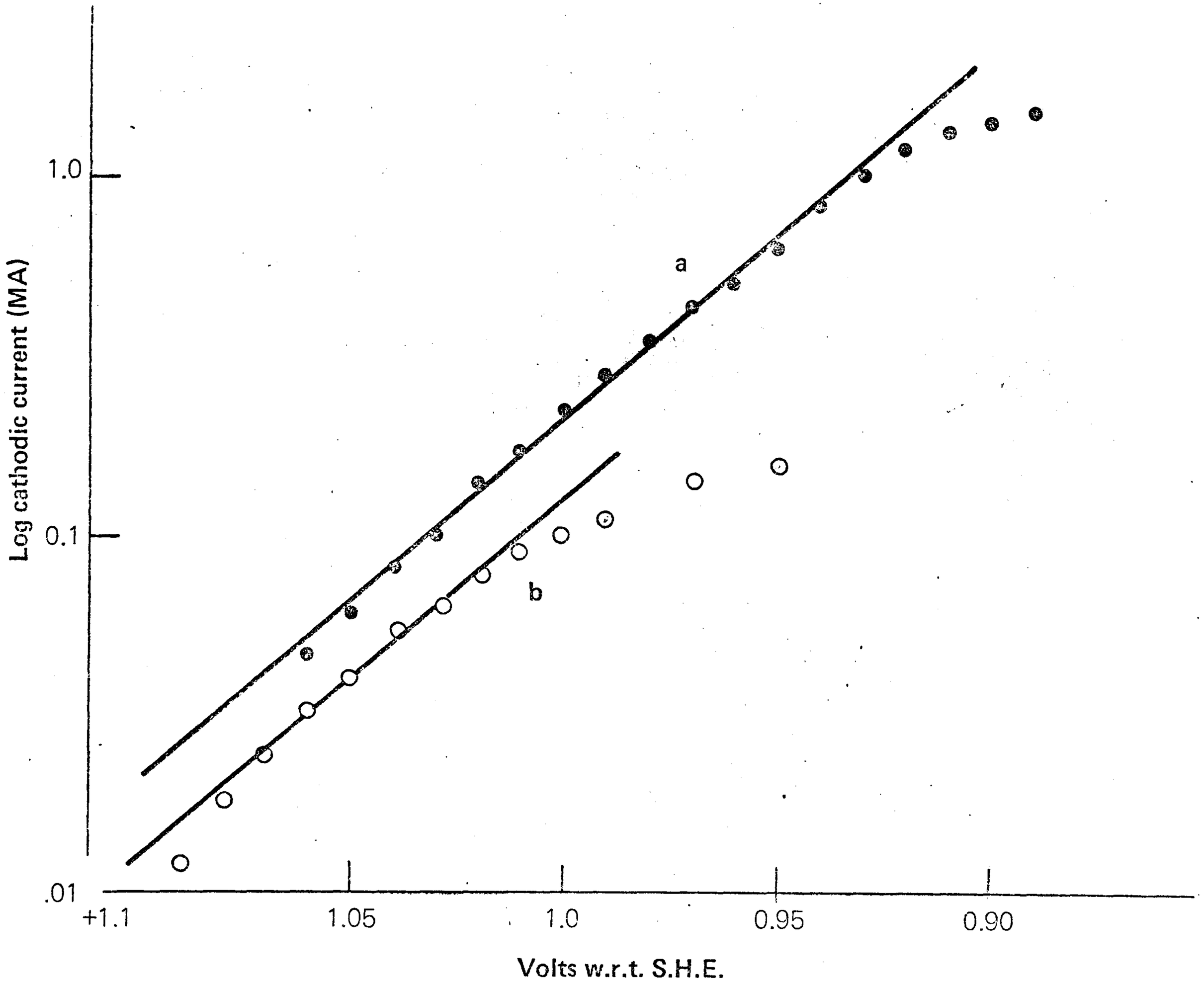

Fig. 6.23

PLOT OF LOG (Cathodic current)/POTENTIAL (a) $1x10^{-2}$M CrVI, IM $HClO_4$, 1000 rpm, 100mV sec^{-1}. gold electrode (b.) $1x10^{-3}$M CrVI IM $HClO_4$, 1000 rpm, 100mV sec^{-1}, gold electrode

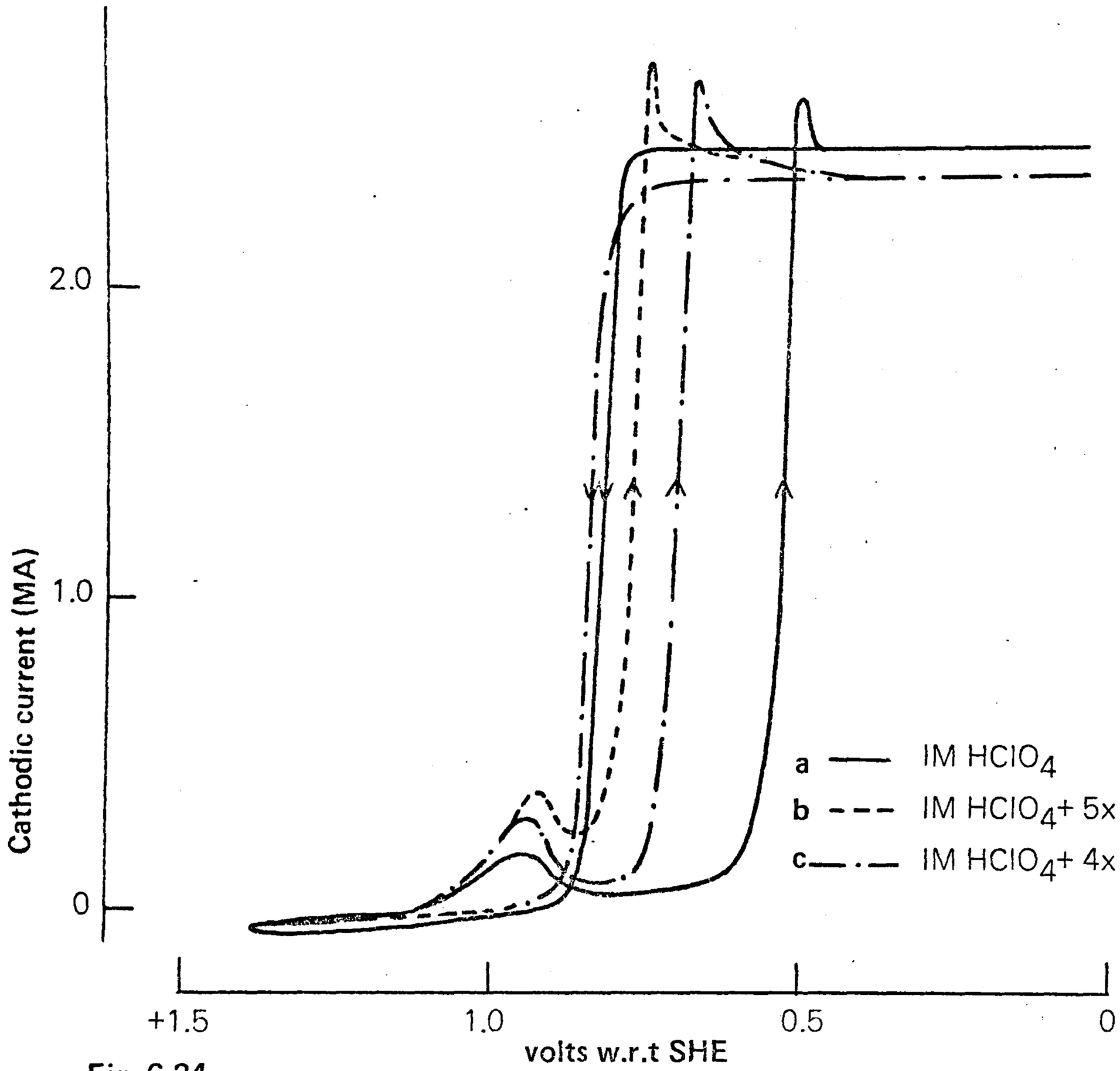

Fig. 6.24
CURRENT POTENTIAL RELATION, ETCHED GOLD ELECTRODE, $1x10^{-2}$M CrVI, IM $HClO_4$+ H_2SO_4, 1000 rpm, 100 mV sec^{-1}

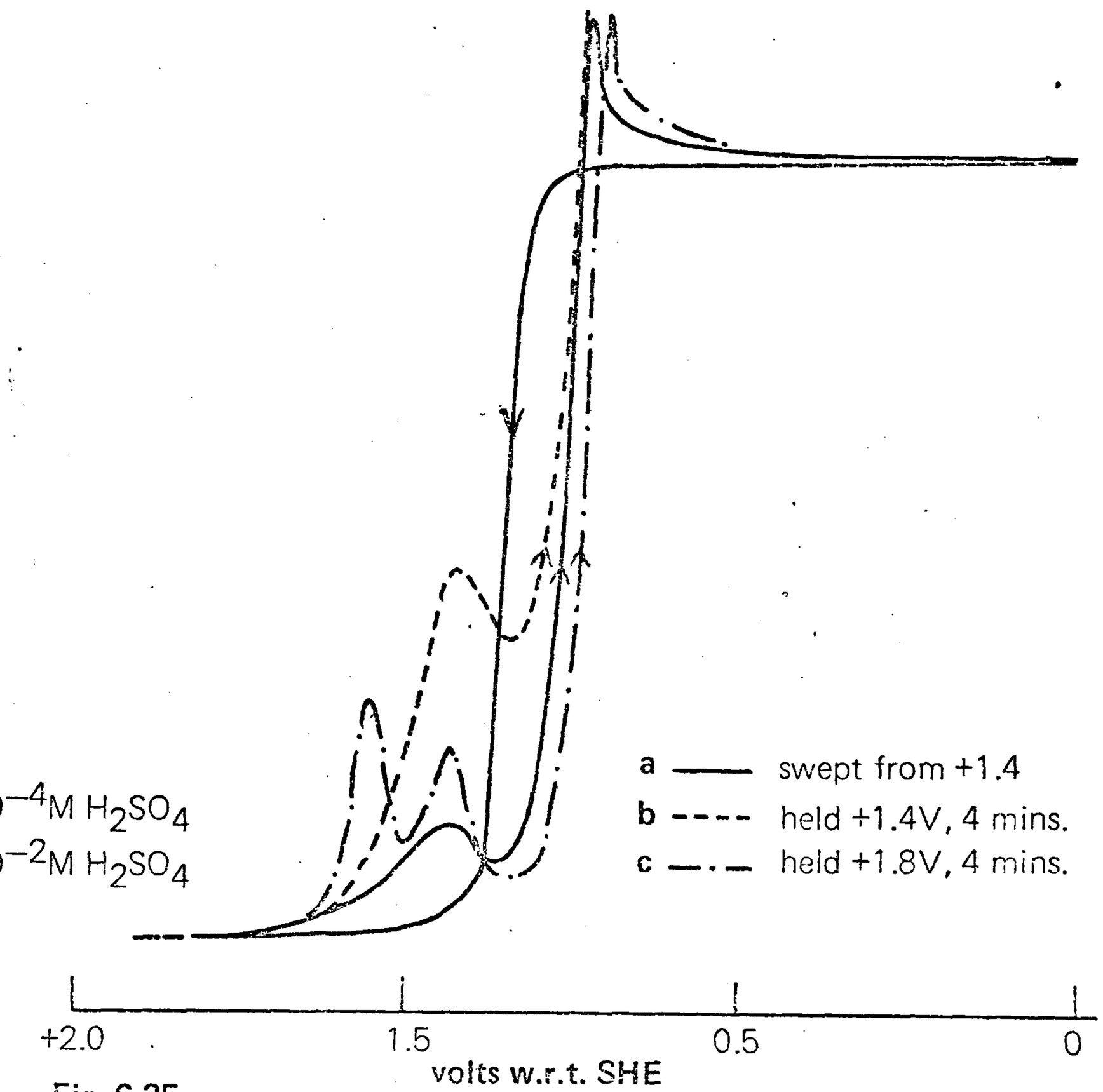

Fig. 6.25
CURRENT-POTENTIAL RELATION AFTER ANODIC PRETREATMENT ETCHED GOLD ELECTRODE, $1x10^{-2}$M CrVI, IM $HClO_4$, $5x10^{-4}$M H_2SO_4 1000 rpm, 100mV sec^{-1}

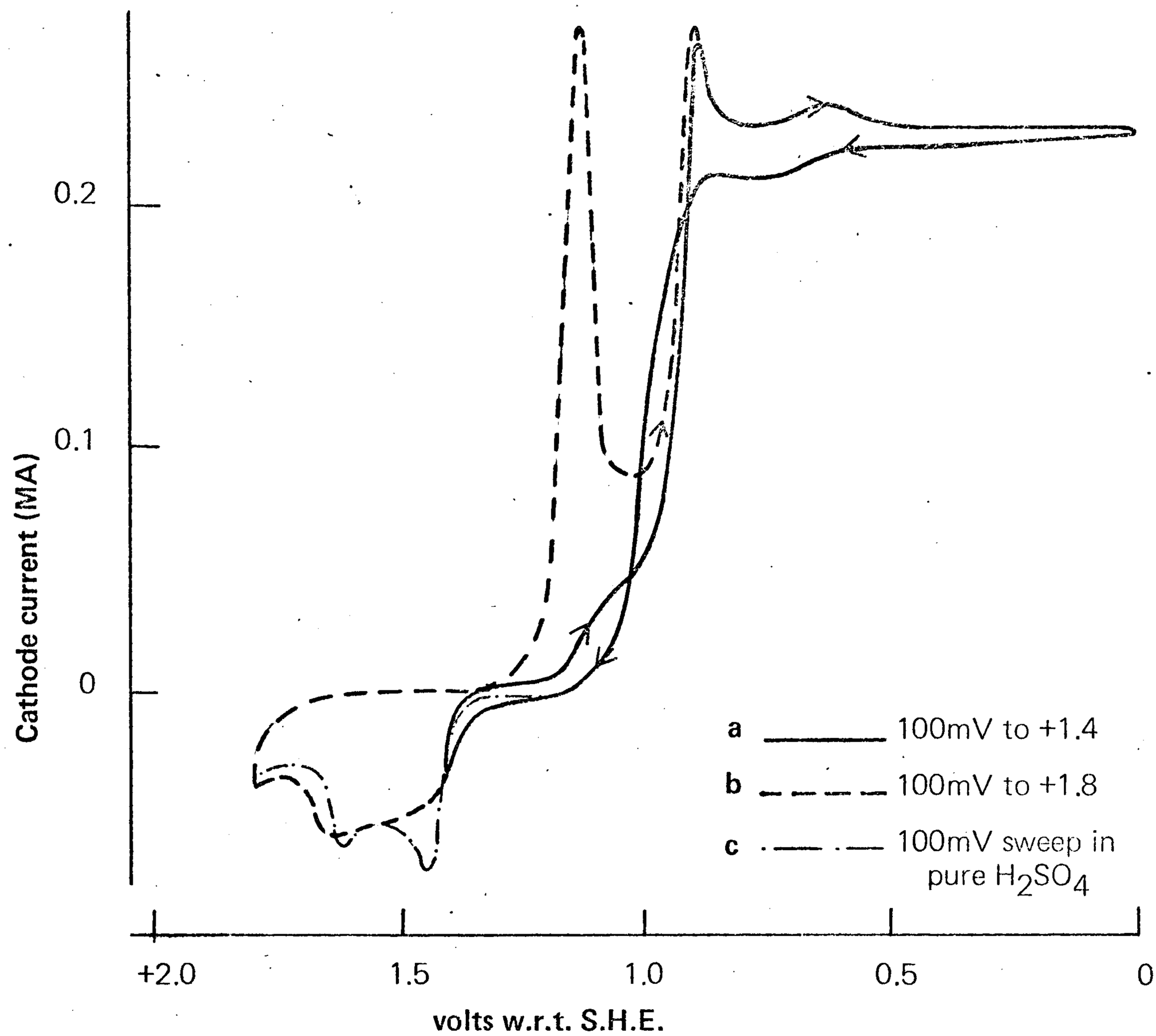

Fig. 6.26
CURRENT-POTENTIAL RELATION, ETCHED GOLD ELECTRODE, $1x10^{-3}$ M CrVI, 0.5M H_2SO_4, 1000 rpm, 100mV sec^{-1}

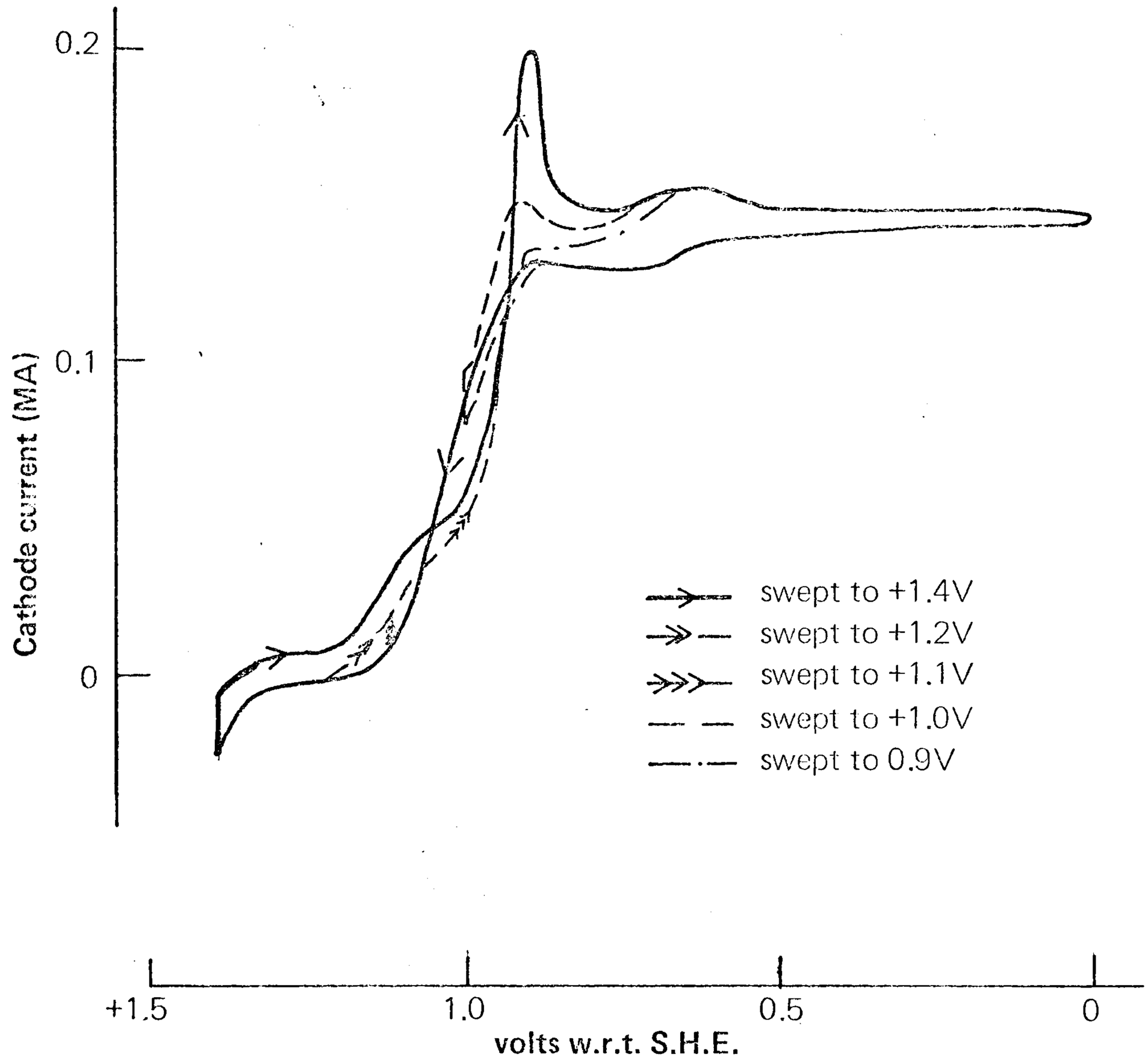

Fig. 6.27
CURRENT-POTENTIAL RELATION, ETCHED GOLD ELECTRODE
$1x10^{-3}$ M CrVI, 0.5M H_2SO_4, 250 rpm, 100 mV sec^{-1}

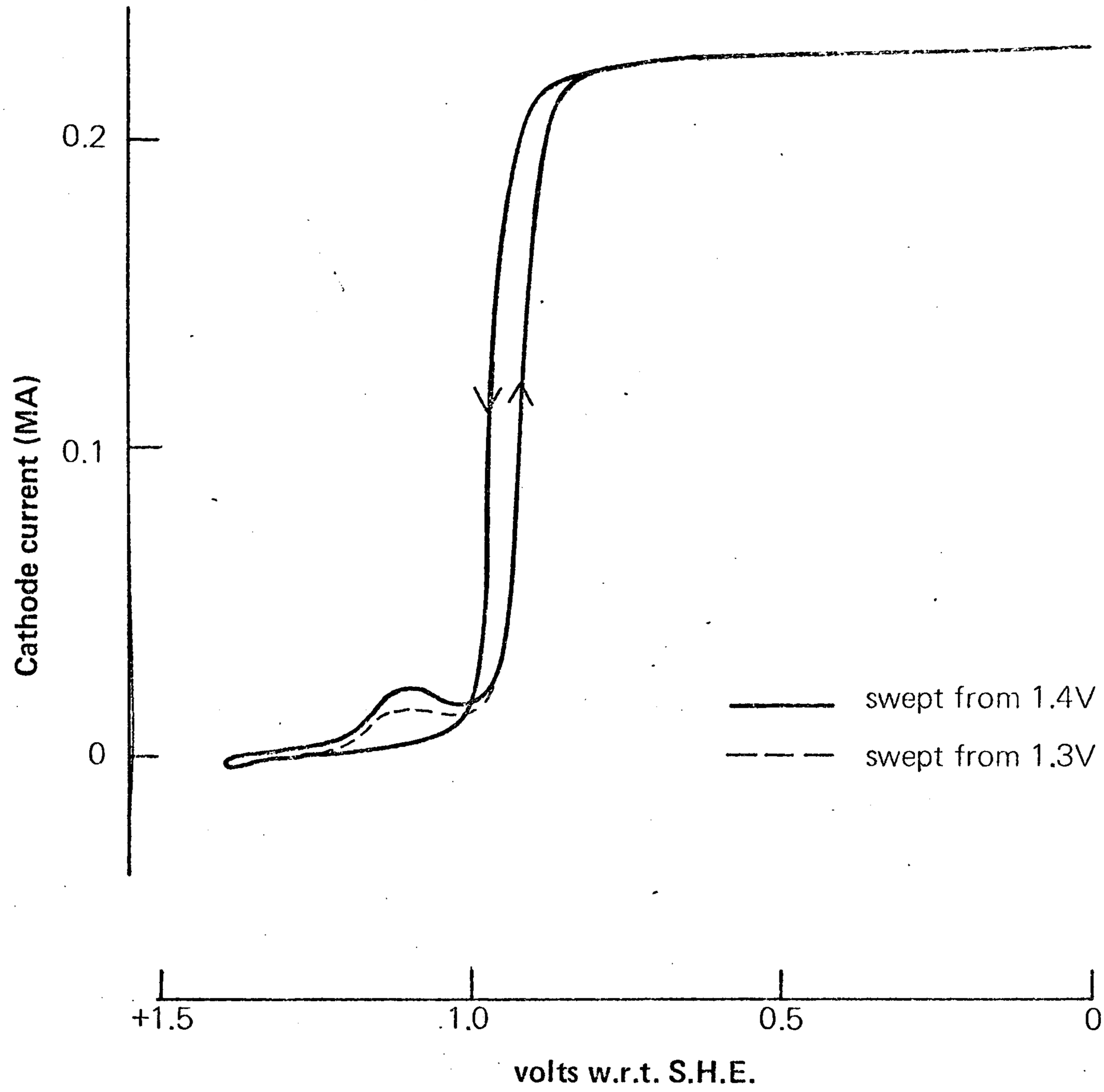

Fig. 6.28
CURRENT-POTENTIAL RELATION, ETCHED GOLD ELECTRODE, $1x10^{-3}$ M CrVI, 1000 rpm, 10mV sec^{-1}

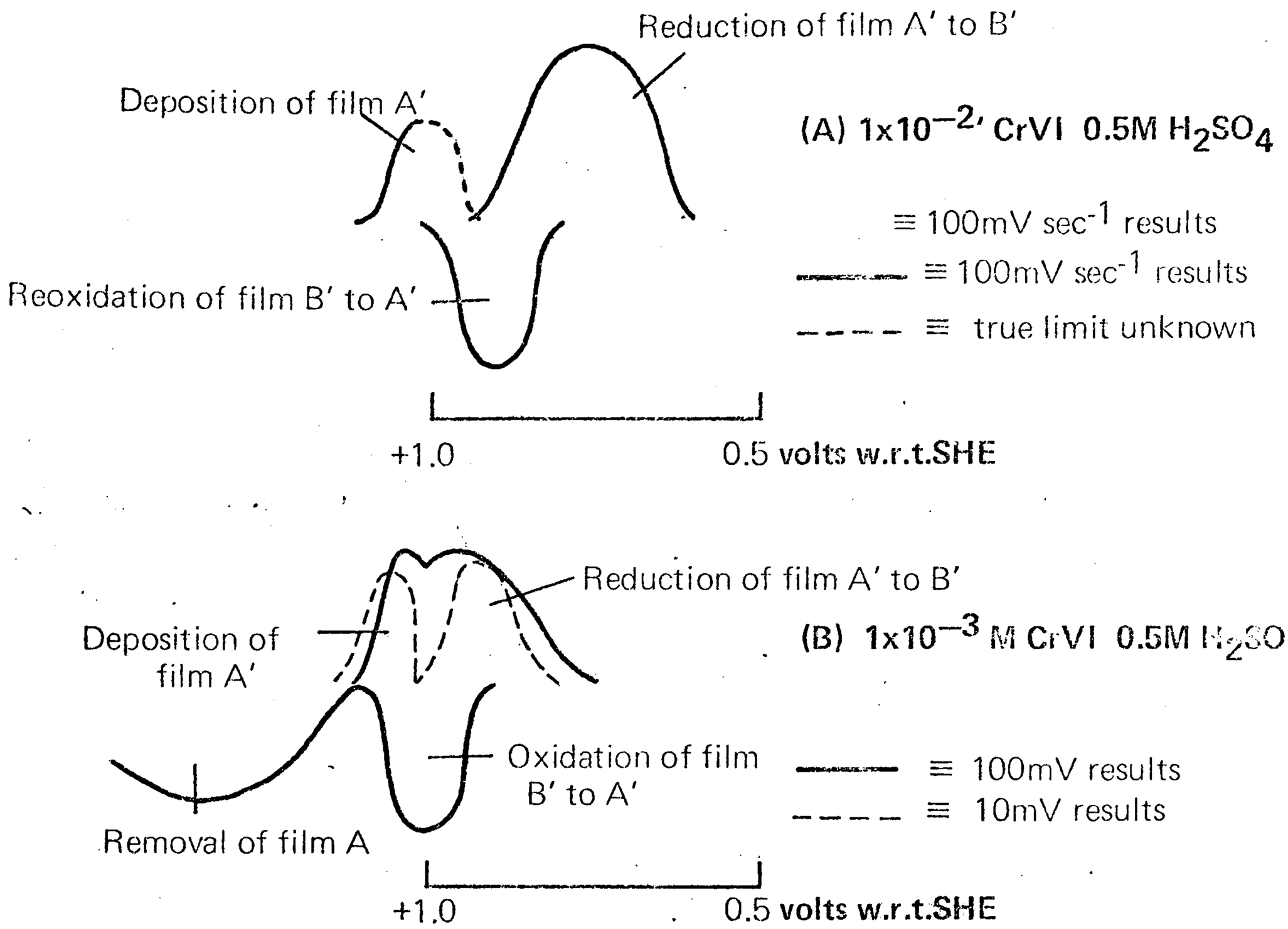

Fig. 6.29
SUMMARY OF CONDITION OF ELECTRODE SURFACE IN H_2SO_4 CONTAINING SOLUTIONS

Fig. 6.30
CURRENT-POTENTIAL RELATION, ETCHED GOLD ELECTRODE,
0.5M H_2SO_4, NO ROTATION

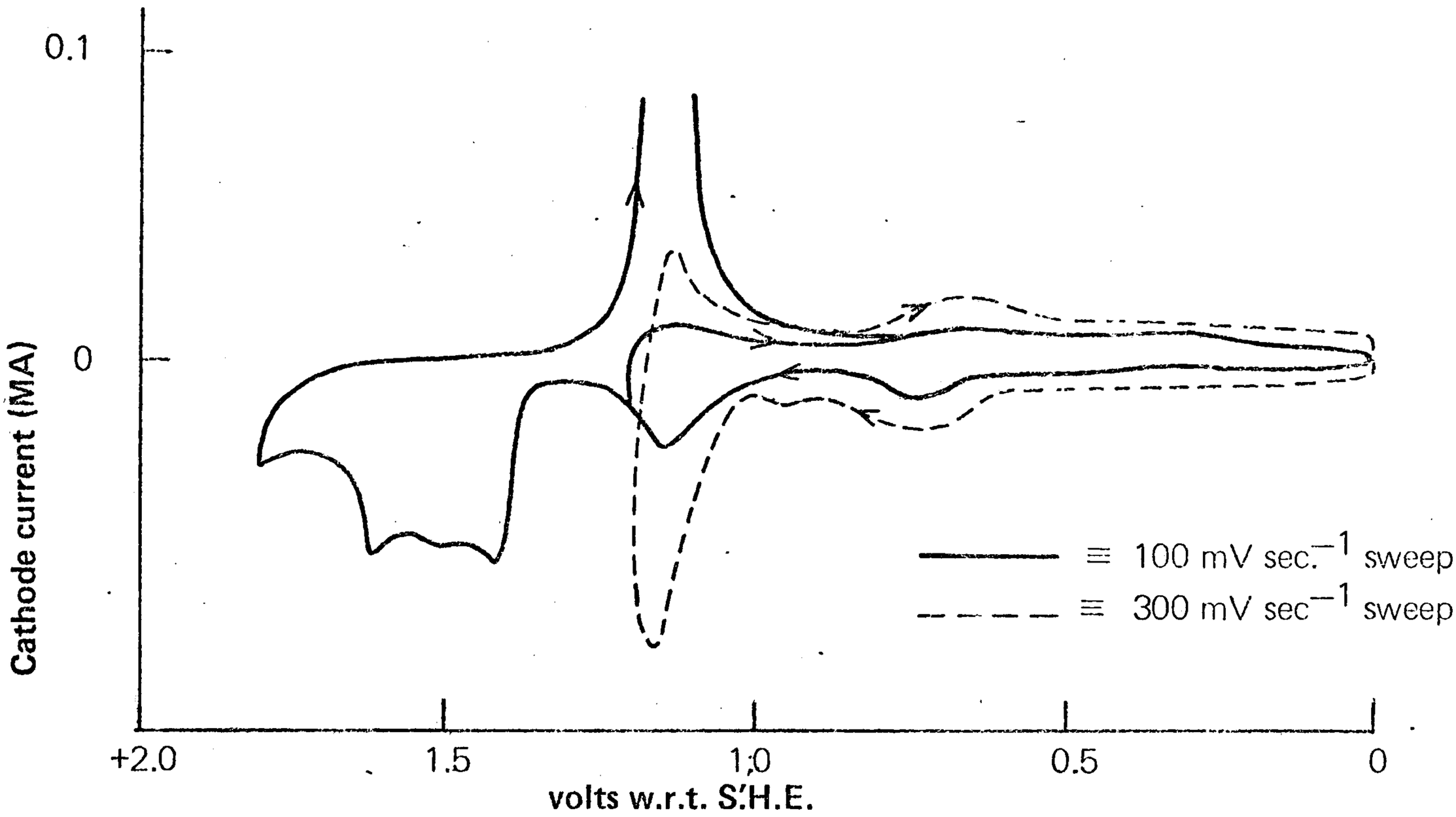

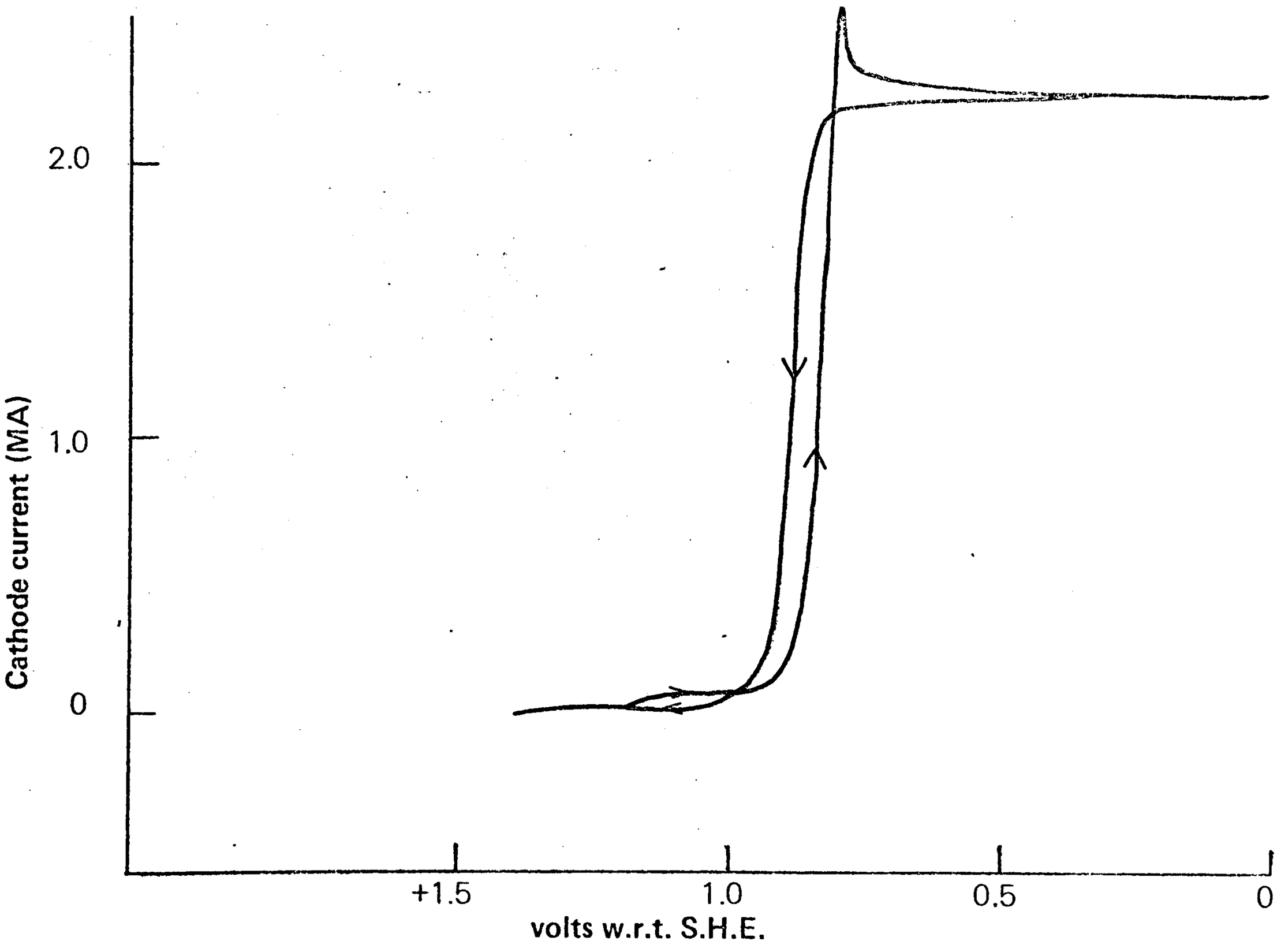

Fig. 6.31
CURRENT-POTENTIAL RELATION, ETCHED GOLD ELECTRODE,
$1x10^{-2}$M CrVI, 0.5M H_2SO_4, 1000 rpm, 100mV sec^{-1}

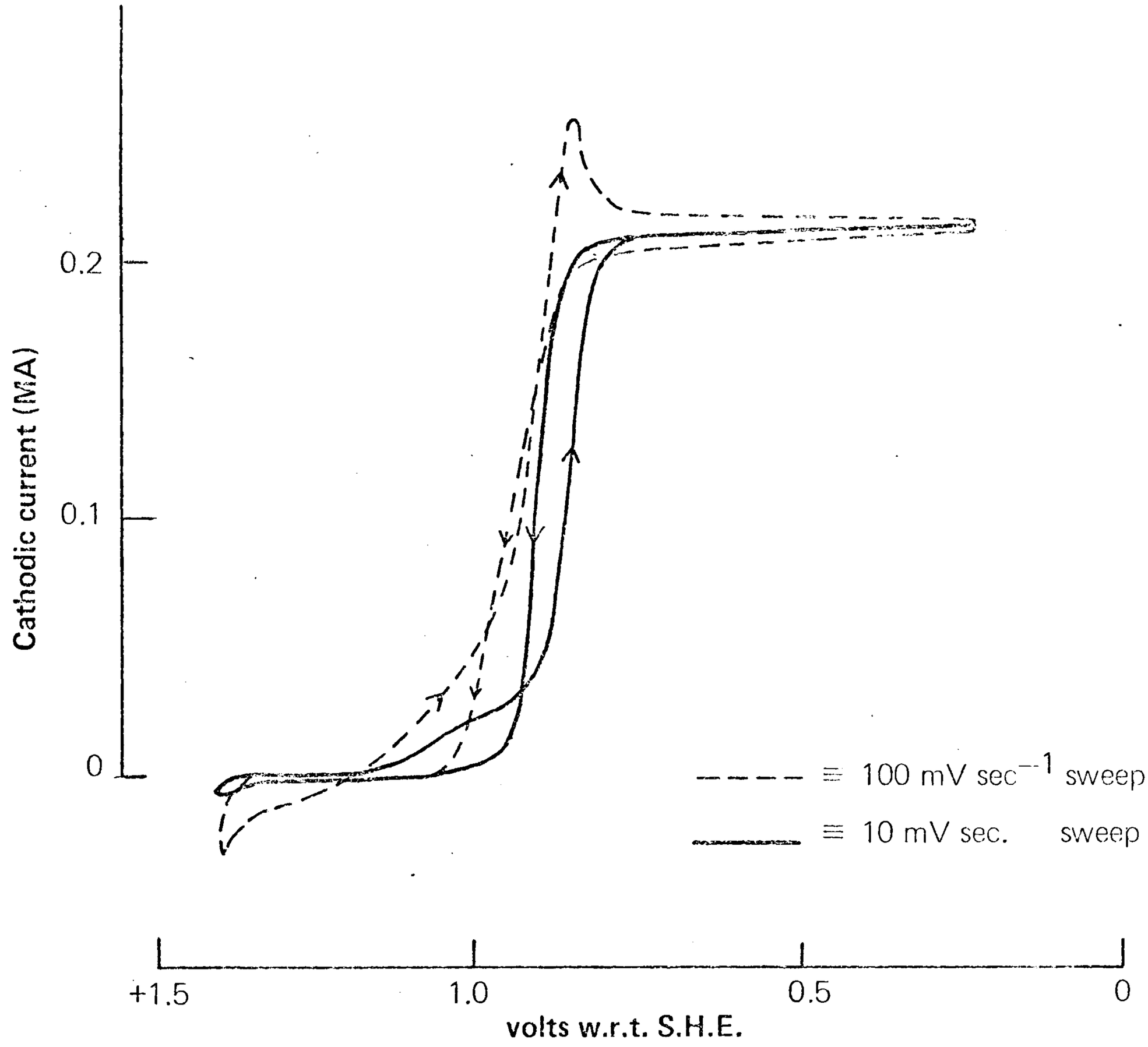

Fig. 6.32
CURRENT-POTENTIAL RELATION, ETCHED GOLD ELECTRODE,
1×10^{-2} M CrVI, 0.25M H_2SO_4, 0.25M Na_2SO_4, 1000 rpm

CHAPTER 7

THE ELECTROCHEMICAL BEHAVIOUR OF VARIOUS TYPES OF GRAPHITE IN PERCHLORIC AND SULPHURIC ACID SOLUTIONS

7.1 Introduction

These experiments were designed to assess the suitability of several types of graphite as electrode materials. Current-potential curves were obtained in the background electrolytes, to determine the potential ranges over which the graphites behaved as inert electrodes, and to study the ease of oxidation of the graphite surface. It was found that the insulating material used on the electrode sometimes affected the results obtained and thus a selection of insulators was examined.

Three types of graphite were employed, spectroscopically pure graphite (Johnson Matthey Ltd.), glassy carbon (Vitreous Carbons Ltd.) and pyrolytic graphite (Le Carbone Ltd.).

Spectroscopically pure graphite is amorphous and porous making it difficult to remove polishing material and reaction products from its surface. Glassy carbon is a hard amorphous material, capable of accepting a high polish. The surface of this material contains small closed pores which give rise to a high double-layer capacity and tend to retain reaction products and polishing materials. Pyrolytic graphite has a highly ordered structure, the hexagonal graphitic layers being arranged in almost parallel planes.

It is essentially non-porous at right angles to the layer planes but is permeable between the planes and excessive penetration by the solution can cause splitting. When the faces of the layer planes are used as the electrode surface, this material has the great advantage that a reproducible, fresh surface can be readily produced by removing a few layers of graphite. A reproducible, clean surface is very difficult to achieve with either spectroscopically pure graphite or glassy carbon.

Pyrolytic Graphite (PG)

This type of graphite is now a widely used electrode material. However, problems have been encountered in preparing a reproducible electrode surface.

Mamantov, Freeman, Miller and Zittel[7.1] have studied the behaviour of PG in 1.0 M H_2SO_4. These workers reported that oxidation of the electrode at potentials more positive than +1.2 V produced a cathodic peak at +0.4 V. This they suggested was caused by reduction of an oxide film although they could not detect its presence by electron diffraction. The method of surface preparation of the graphite was not described.

Panzer and Elving[7.2] have shown that the electrochemical behaviour of PG depends on the type (i.e. the supplier and method of manufacture) of graphite and the method of surface preparation. Bauer, Spritzer and Elving[7.3] also reached this conclusion and furthermore

reported extremely irreproducible double-layer capacitance measurements. Miller and Zittel[7.4] suggested that a reproducible surface could be obtained only by resurfacing the PG by cleaving off the old surface.

It appears likely[7.2,7.5,7.6] that the observed variation in the behaviour of PG is due to different numbers of edge planes being exposed to the solution. This is dependent upon the type and dur tion of the electrode surface preparation, which may also modify the number of oxidised reaction sites on the graphite surface[7.2].

PG obtained from the same manufacturers as that used in this work was found by Brennan and Brown[7.7] to have an apparent double layer capacitance of 1397 μF cm^{-2} (edges) and 109 μF cm^{-2} (faces - prepared by flaking-off a layer of graphite). These values dropped to 629 and 45 μF cm^{-2} respectively after cathodic polarisation at -0.8 V. The values reported are the averages of those obtained at sweep rates of 0.3, 1.0 and 3.0 V sec^{-1}. These workers also found that pyrolytic graphite with exposed edges was more active with respect to hydrogen evolution than the PG face surface.

Similarly Morcos and Yeager[7.8] reported that the edges were more active than the faces in promoting oxygen evolution.

<u>Glassy Carbon</u>

Brennan and Brown[7.7], using glassy (vitreous) carbon from the same source as used in this study,

report that its activity with respect to hydrogen evolution is similar to that observed with PG (edges). Its capacitance was 821 μF cm^{-2}, or 386 μF cm^{-2} following cathodic pretreatment. Measurement conditions were as described for PG.

Zittel and Miller[7.9] report a usable potential range of approximately +1.0 to -1.1 V for a glassy carbon electrode in 0.1 N H_2SO_4.

7.2 Results and Discussion

(i) Spectroscopically pure graphite

Reproducible current-potential relationships could not be obtained with this material even under steady-state conditions.

A typical steady-state current-potential curve in 1 M $HClO_4$ is however shown in Fig. 7.1. Hydrogen evolution begins at -0.8 V and oxygen evolution at +1.4 V. After anodic pretreatment a cathodic maximum was observed at +0.4 V. However since the curves were not reproducible, detailed work was not carried out using this electrode material.

(ii) Glassy Carbon

Fig. 7.2 shows the current-potential relation obtained in 1 M $HClO_4$, using a glassy carbon electrode insulated with Hostaflon. A sweep rate of 20 mV s^{-1} was employed and the solution purified with active charcoal. Hydrogen evolution occurs at potentials below about -0.9 V and oxygen evolution at about +1.6 V. Between 0.0 and +0.8 V, a fairly flat plateau is

present on the positive going sweep; a corresponding plateau is observed between 0.0 and -0.7 V on the negative going sweep. The plateau on the negative going sweep develops into a clear maximum by sweeping the potential to +1.5 V, Fig. 7.2, curve (b). Repeated sweeps to this potential, increase the height of the maximum, and a further maximum appears on the anodic side at +1.4 V. The quantity of electricity consumed on the anodic and cathodic sweeps is the same, and is 0.1 coulombs cm^{-2}.

All the maxima reported are independent of rotation speed but increase with sweep rate. They are therefore surface phenomena. It appears that the surface of glassy carbon may be oxidised at potentials more positive that 0 V, rapid oxidation occurring more positive than 1.0 V. Subsequent oxide reduction takes place at potentials more negative than +0.6 V, the process reaching a maximum rate at ~ -0.3 V.

The double-layer capacitance, calculated between 0.0 and -0.3 V is 1,200 $\mu F\ cm^{-2}$; Brennan and Brown[7.7] report a value of 821 $\mu F\ cm^{-2}$. The usable potential range of approximately +1.0 to -0.8 V (Fig. 7.2) compares well with that obtained by Zittel and Miller[7.9].

However the effect of the pores, causing a large double-layer capacity and contamination effects suggested that glassy carbon would be unsuitable for studying the reduction of CrVI.

(iii) Pyrolytic graphite in $HClO_4$ and H_2SO_4

The behaviour of pyrolytic graphite was found to depend on the nature of the insulator employed, the orientation of the graphite and the purity of both the solution and of the electrode surface.

The effect of solution/surface impurities is shown in Fig. 7.3. These results correspond to an electrode insulated with PTFE and only the layer planes of the pyrolytic graphite were exposed to the electrolyte. Curve a was obtained in a 1 M $HClO_4$ solution prepared from Aristar $HClO_4$ and triply distilled water. The anodic and cathodic peaks were independent of rotation speed but increased as the scan rate was increased. They therefore presumably correspond to the oxidation and reduction of some surface species.

The addition of purified active charcoal to the solution resulted in a marked reduction in the size of the peaks, Fig. 7.3 (curve b), while flaking the graphite to produce a fresh surface, gave a current-potential curve in this solution completely free from any peaks, Fig. 7.3 (curve c). Curve d, Fig. 7.3, illustrated a slightly better-defined result in pure solution at a higher scan rate. The peaks observed in curve a are therefore presumably caused by the oxidation and reduction of adsorbed impurities, which can be removed from the solution by active charcoal. Pre-electrolysis using platinum electrodes was not effective in this respect.

It may be concluded that in a pure solution, pyrolytic graphite (layer planes only exposed) behaves as a perfectly polarised electrode between +1.4 and -0.5 V.

Treatment at more positive potentials, however, does oxidise the graphite surface. Thus after sweeping to +1.8 V, Fig. 7.4, curve a, the negative going curve exhibits a peak at 1.5 V unaffected by rotation speed and the quantity of electricity being constant at different scan rates (given the same electrode pretreatment). The quantity of electricity passed during this peak is increased by extending the anodic treatment to more positive potentials and by holding the electrode at a given potential for longer times, Fig. 7.4, curve b. Limited oxidation produces no permanent change in the graphite surface (curve a) but prolonged oxidation causes the surface to disintegrate with a consequent increase in the double-layer capacity.

The behaviour of pyrolytic graphite, insulated with PTFE in 1 M H_2SO_4 was very similar to that observed in $HClO_4$ solutions. Current-potential curves obtained with a flaked graphite surface in a solution purified with active charcoal are shown in Fig. 7.5, curve a. At 40 mV sec^{-1} scan rate, the electrode is perfectly polarised between +1.5 and -0.4 V. After treatment at +1.8 V, reduction of surface oxide was observed at +1.7 V, Fig. 7.5, curve b. Prolonged treatment at such potentials again caused disintegration and increase in surface area.

The edges of the layer planes display lower hydrogen and oxygen overpotentials[7.8] than do the faces, Figs. 7.6 and 7.7 ($HClO_4$ and H_2SO_4 solutions respectively). The double-layer capacity and probably the true surface area is also greater. The various peaks and plateaux observed in these solutions may be due either to oxidation and reduction of the graphite surface or to impurities adsorbed onto the electrode surface. Marked oxidation of such a surface occurred at potentials more positive than +1.7 V. Reduction in 1 M $HClO_4$ took place at +1.6 V, in 1 M H_2SO_4 at +1.8 to +1.6 V.

Reproducible results with such a surface were very difficult to obtain, penetration of solution up the layer planes caused variable results, dependent on the length of time for which the electrode had been immersed. After anodic treatment some splitting was visible and the electrochemical behaviour then became even more variable.

As reported later, Chapter 8, in order to obtain a smooth electrode surface, machining followed in some cases by electrochemical pretreatment (holding at +0.8 V in 1 M $HClO_4$, 1 x 10^{-2} M CrVI) and finally polishing smooth on tissue, was used. A background sweep was always obtained after preparing the electrode to establish the condition of the electrode surface. Naturally following such treatment slight variability was obtained in the current-potential relation and double-layer

capacitance, but no significant deviation was encountered. As can be seen from Fig. 7.8, the hydrogen and oxygen overvoltages lie between those obtained with the faces and with the edges of the layer planes. The anodic and cathodic inflexions at +0.6 V were always present but involved only a very small quantity of electricity.

Such surfaces were very stable and gave no indication of solution seepage or splitting.

Oxygen reduction

Oxygen reduction occurred at potentials more negative than -0.2 V with no edges exposed and -0.1 V with exposed edges.

Hydrogen oxidation

This could not be detected on the graphite planes or edges.

The double layer capacities of the various types of pyrolytic graphite electrode surface, obtained from potential sweeps of 100 mV sec^{-1}, vary from 160 μF cm^{-2} (flaked surface layer planes only), to 830 μF cm^{-2} (edges only). The double layer capacity of a machined electrode surface varies from 300 μF cm^{-2} (machined, electrochemically treated and polished) to 800 μF cm^{-2} (machined and polished). The values reported by Brennan and Brown[7.7] are 109 and 1397 μF cm^{-2} on the faces (flaked surface) and edges respectively. Although the method of surface preparation has been found to modify slightly the behaviour of pyrolytic graphite as previously

reported[7.2,7.3,7.4], with care and under clean conditions the behaviour of the PG was found to be reproducible.

Effect of insulating material

The electrodes used in the early work were insulated with PTFE, but in order to prevent leakage of electrolyte between the graphite and insulator, the electrode material was recessed below the insulator surface. Slight leakage could be detected on the current-potential curve as the whole curve became tilted (in some cases to 45°) away from the zero current axis. Severe leakage caused further distortion of the current-potential relation.

A recessed electrode surface, however, does not satisfy the conditions for laminar flow of solution over the electrode surface. An electrode similar in design to that used for gold was not satisfactory because of cracking at the edges.when pressure was applied, and because the area changed as part of the cone-shaped graphite was removed to prepare a new surface. Since attractive designs of electrode are possible with other insulating materials, the effect of these materials on the background curves of pyrolytic graphite in 1 M $HClO_4$ was investigated.

Araldite

A moulded araldite insulator initially gave a fairly satisfactory curve, Fig. 7.9, curve a , but the curve obtained after two hours exposure to the solution (Fig. 7.9, curve b) was not satisfactory. The increased

slope of the curve is characteristic of leakage of electrolyte between the insulator and electrode material. The spurious maximum at 1.4 V (Fig. 7.9, curve b) is presumably caused by impurities adsorbed onto the electrode surface, while the higher, rotation dependent cathodic currents at potentials below -0.2 V can be attributed to impurities in the solution.

Laconite

Laconite (manufactured by Canning and Company, Birmingham), a resinous paint, contaminated the solution severely, as shown by the marked rotation dependence of the current at both anodic and cathodic potentials (Fig. 7.10).

Shrinkable tubing

Shrinkable polythene tubing also produced spurious maxima after moderate contact with the electrolyte. These could be almost removed by prolonged soaking in 1 M $HClO_4$ solution but the treatment was long and the results somewhat variable.

Shrinkable PTFE tubing (Helashrink Ltd.) did not adhere to the electrode sufficiently well to insulate the edges and substantial edge effects were observed.

Towards the end of the work "Flo-Tite" heat shrink PTFE tubing - Pope Scientific Inc., U.S.A. - became available. This consisted of an inner core of material which melted as the outer core shrunk. This material proved entirely satisfactory.

For all the kinetic work and the majority of the rest the use of PTFE moulded insulators, described in Section 3.6, was adopted. This provided a leak proof seal and gave identical curves to those obtained with only planes exposed to the solution.

Fig. 7.1
STEADY-STATE CURRENT-POTENTIAL CURVE, SPEC.PURE GRAPHITE, IM $HClO_4$, 1000 rpm

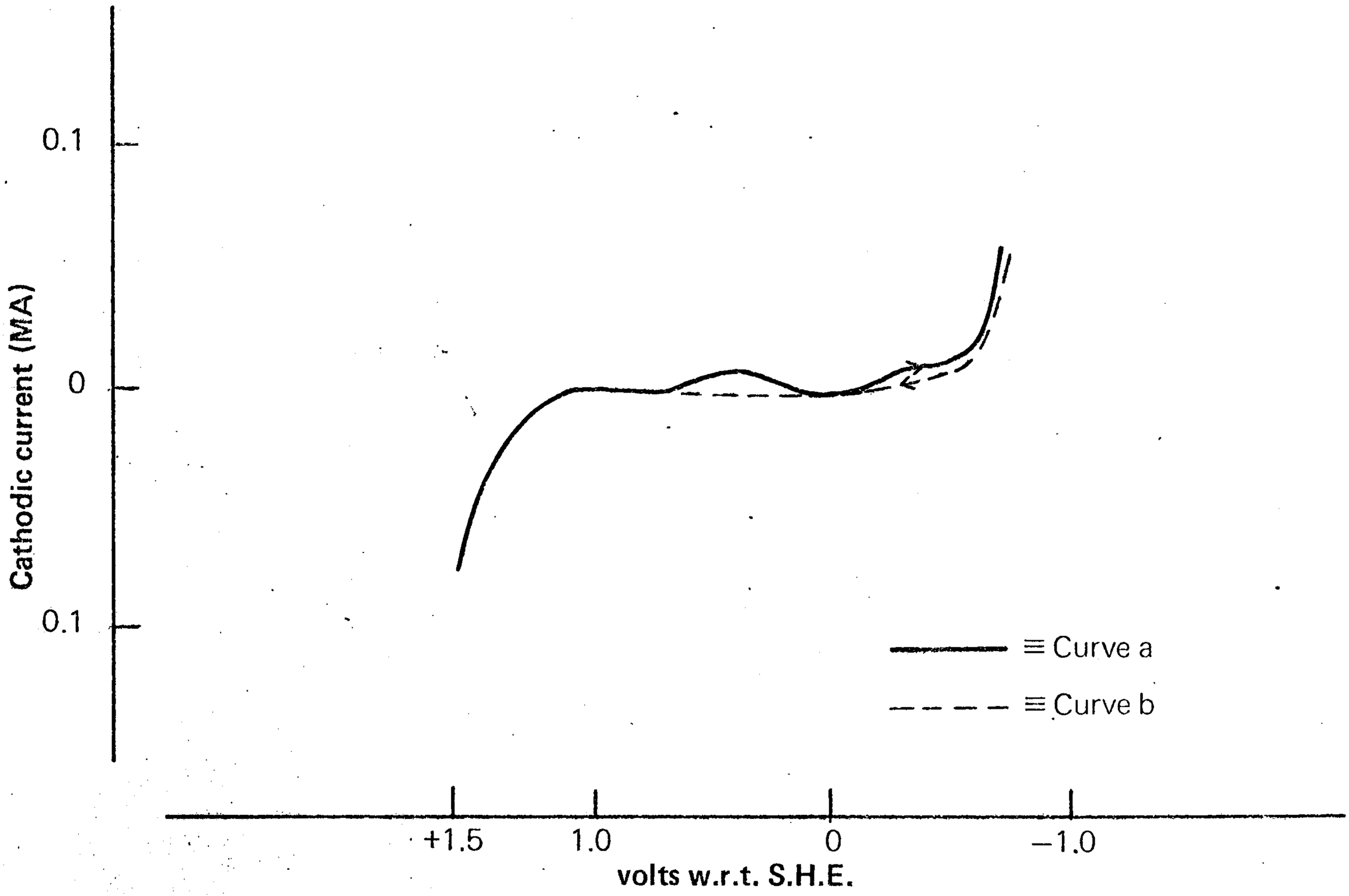

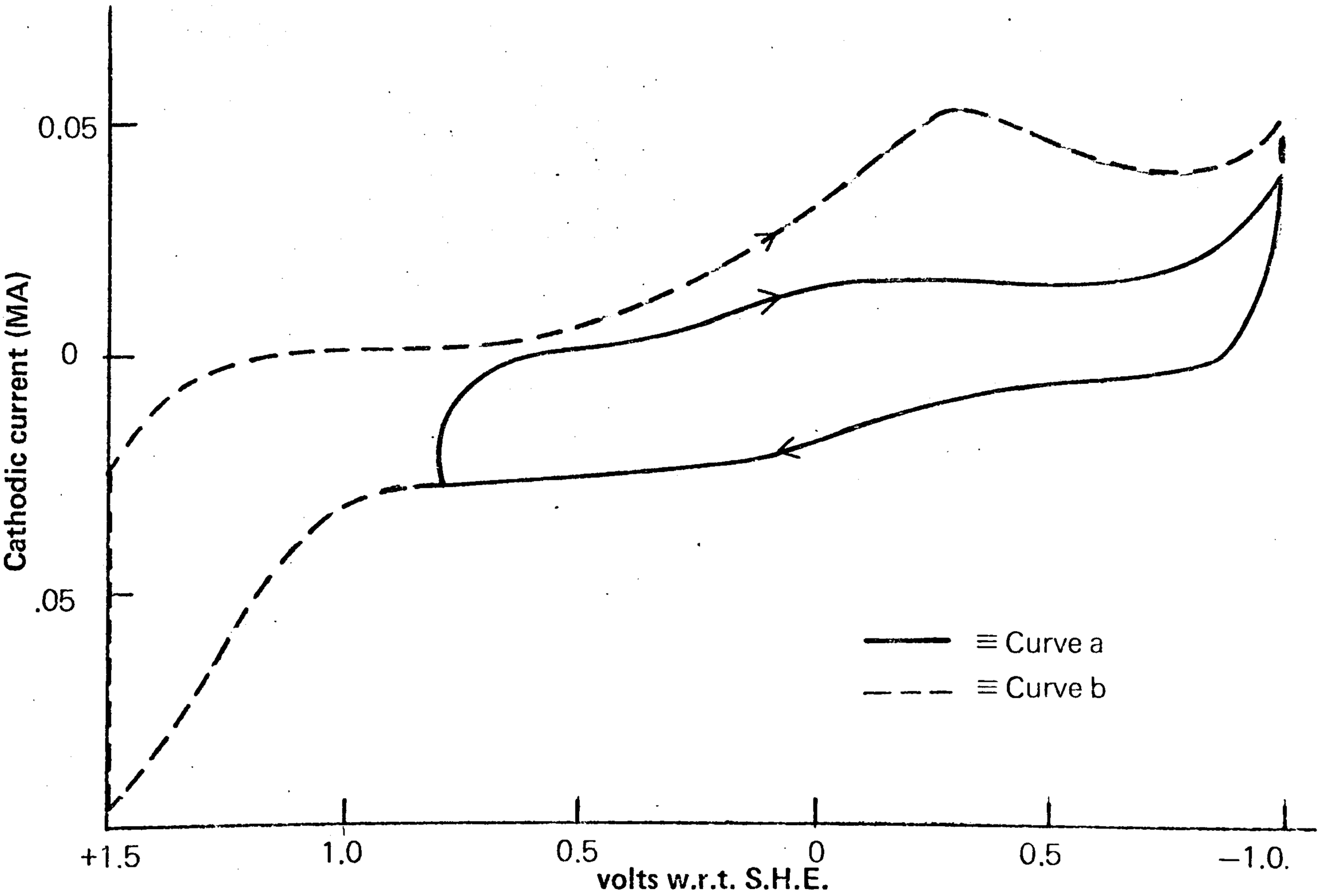

Fig. 7.2
CURRENT-POTENTIAL RELATION, GLASSY CARBON ELECTRODE (0.2cm DIAMETER), IM $HClO_4$, 1000 rpm, 20mV sec^{-1}

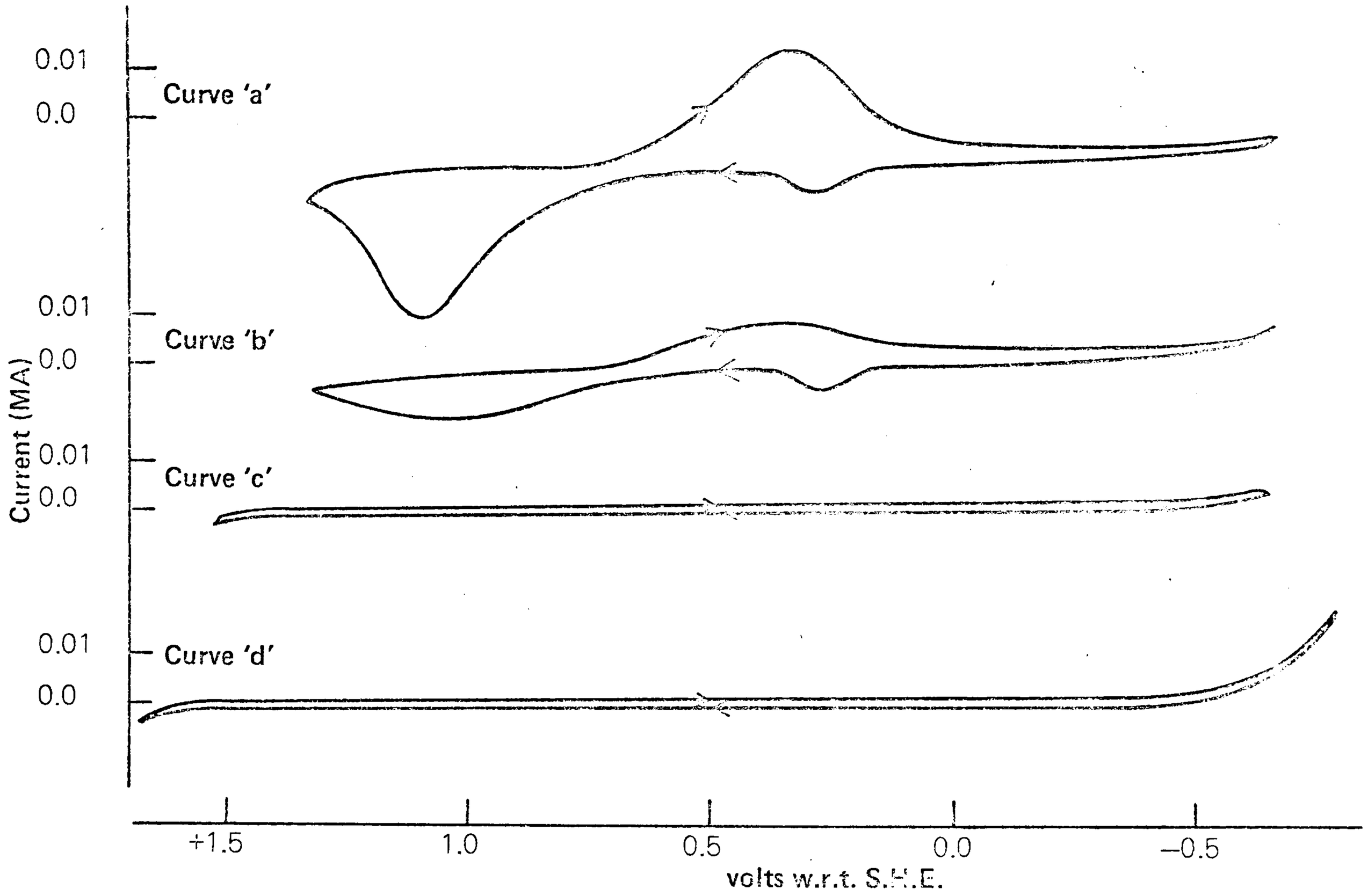

Fig. 7.3
CURRENT-POTENTIAL RELATION; FLAKED P.G.(FACES ONLY), IM $HClO_4$, 1000 rpm.
CURVES a,b,c, 20 $mVsec^{-1}$, CURVEd 40 $mVsec^{-1}$

Fig. 7.4
CURRENT-POTENTIAL RELATION, FLAKED P.G. (FACES ONLY),
IM $HClO_4$, 1000 rpm, 20 $mVsec^{-1}$

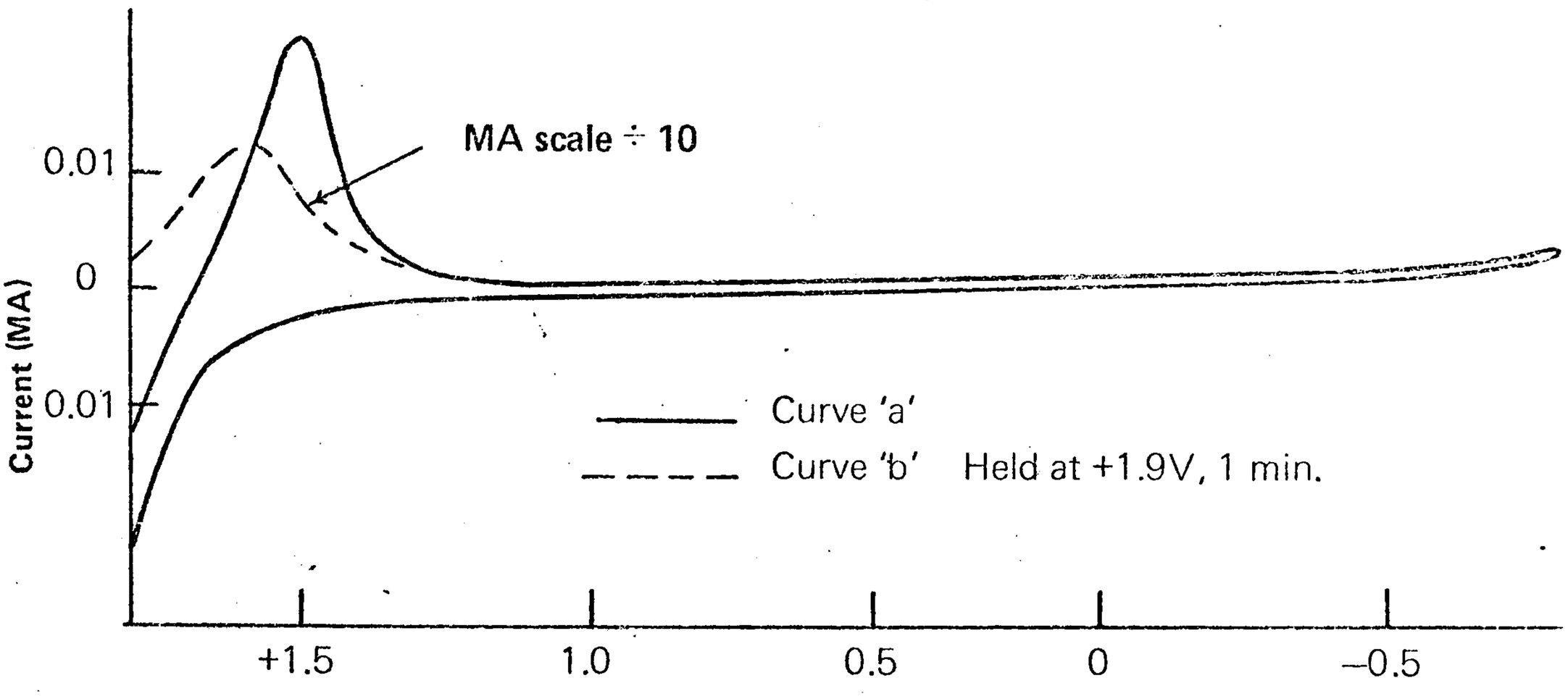

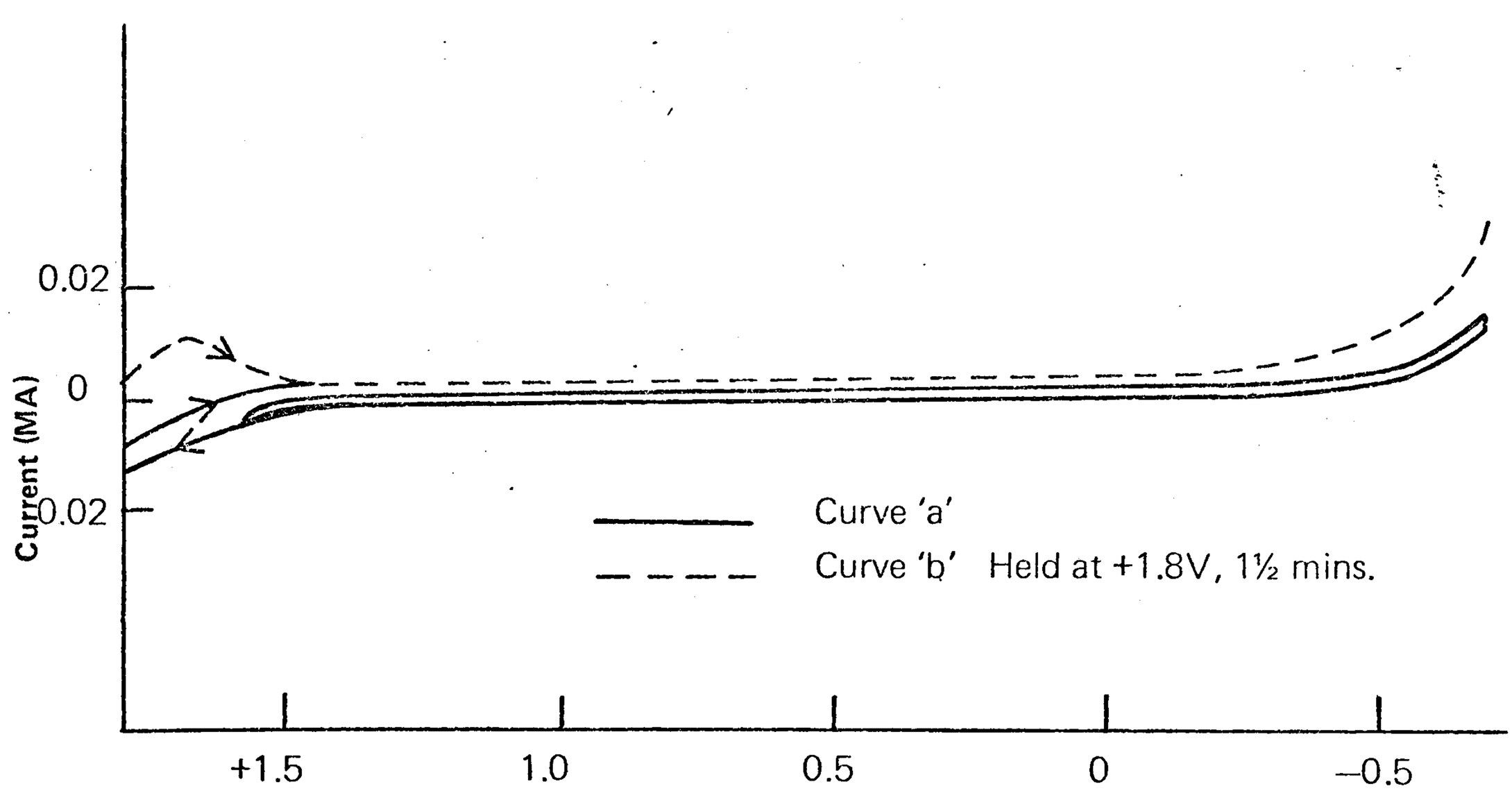

Fig. 7.5
CURRENT-POTENTIAL RELATION, FLAKED P.G.(FACES ONLY),
IM H_2SO_4, 100 rpm, 40 $mVsec^{-1}$

Fig. 7.6
CURRENT-POTENTIAL RELATION, P.G.(EDGES EXPOSED),
IM $HClO_4$, 1000 rpm, $40mVsec^{-1}$

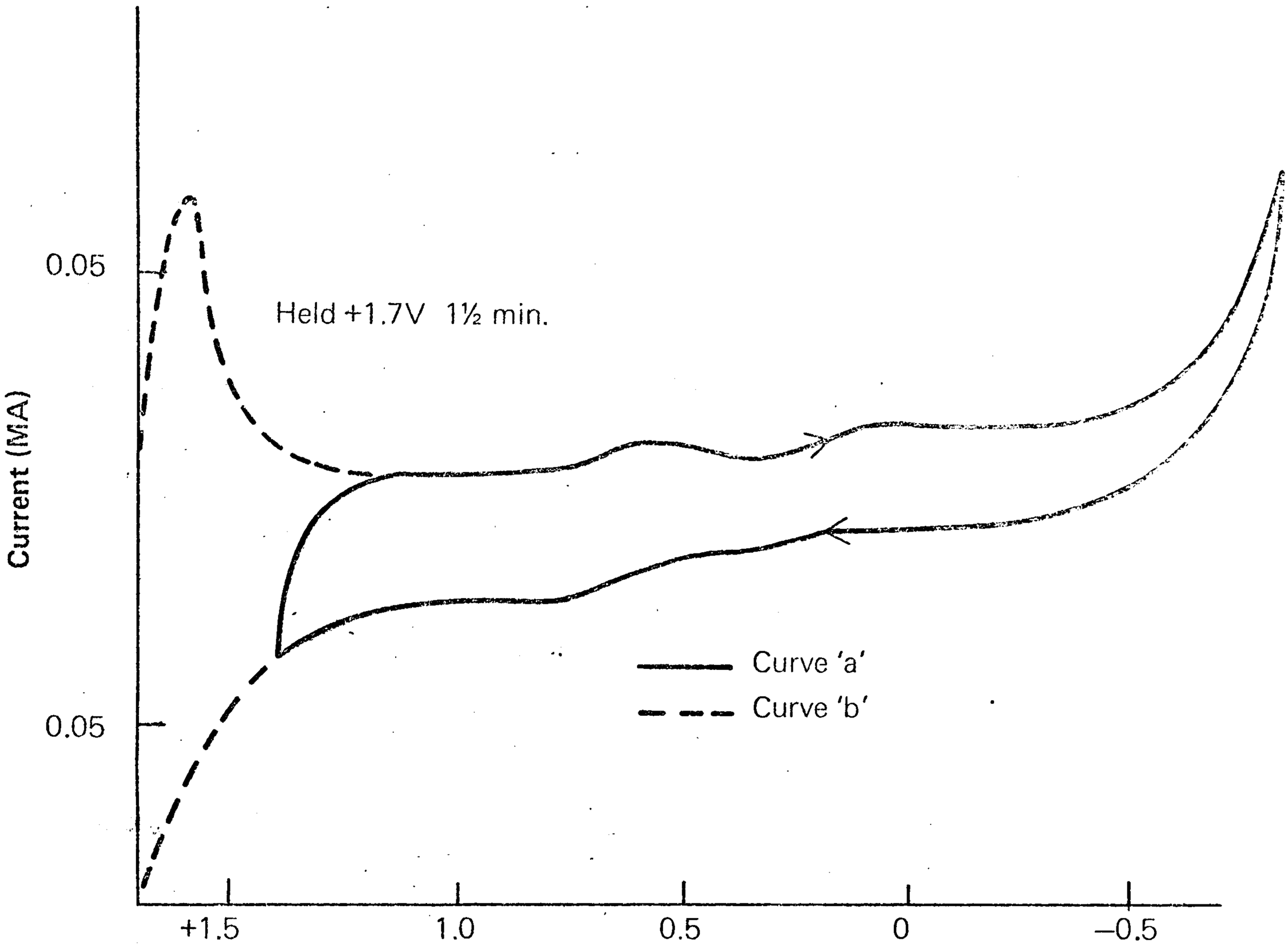

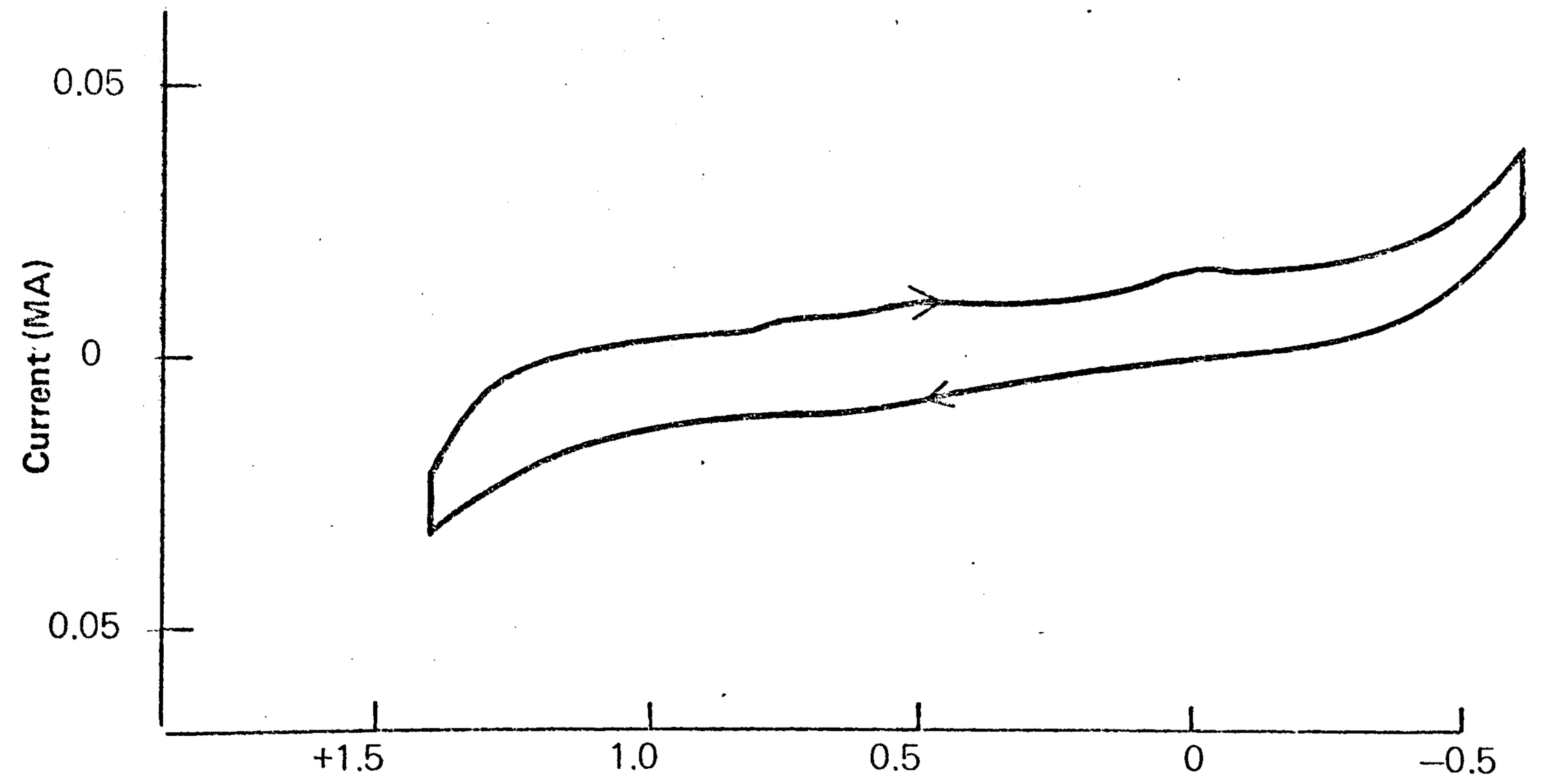

Fig. 7.7
CURRENT-POTENTIAL RELATION, P.G. (EDGES EXPOSED),
IM H_2SO_4, 1000 rpm, $40mVsec^{-1}$

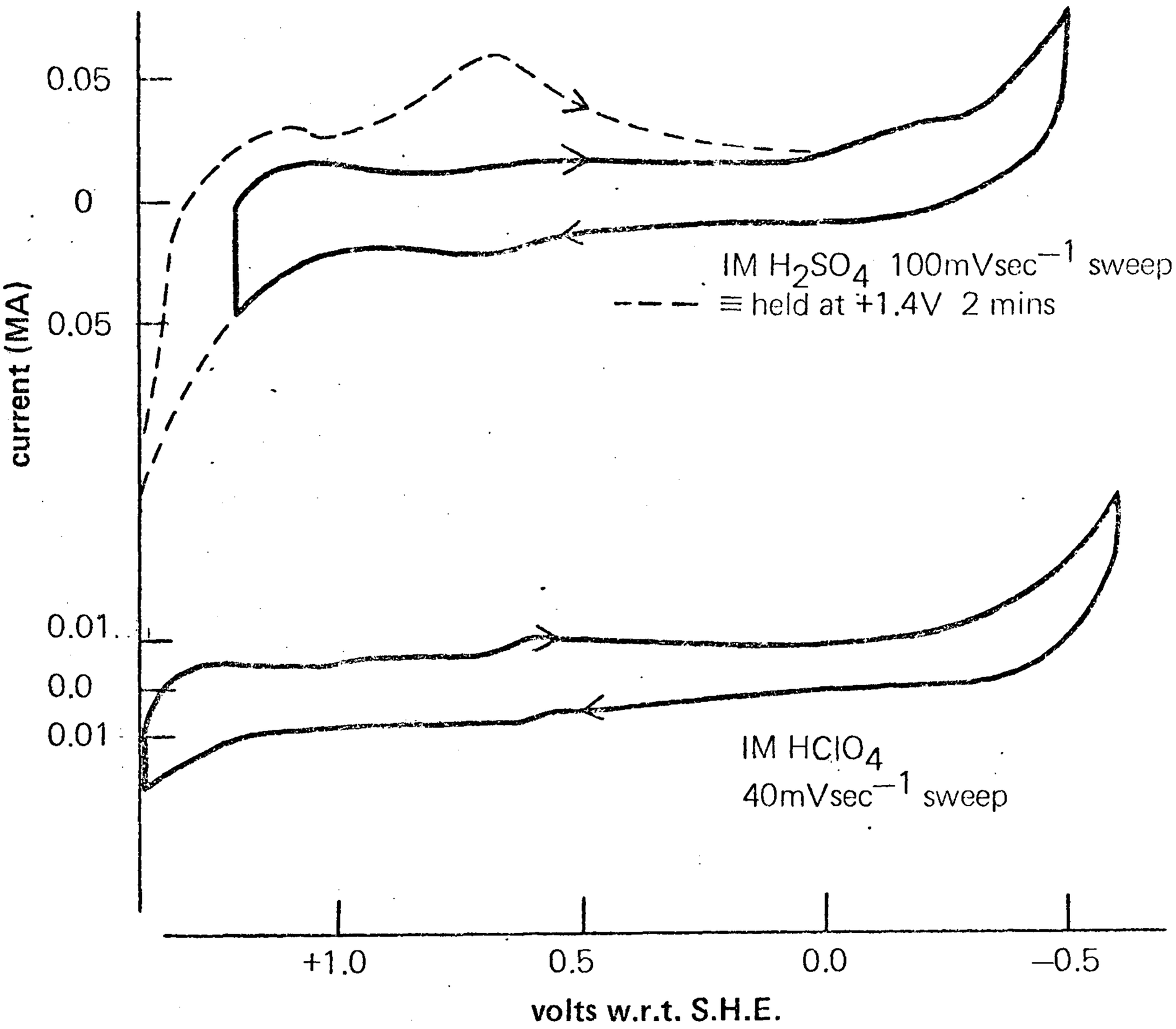

Fig. 7.8
CURRENT-POTENTIAL RELATION, P.G.(MACHINED THEN POLISHED) 1000rpm

Fig. 7.9
CURRENT-POTENTIAL RELATION, P.G.(FACES ONLY)
INSULATED BY ARALDITE, IM $HClO_4$, 1000rpm, $40mVsec^{-1}$

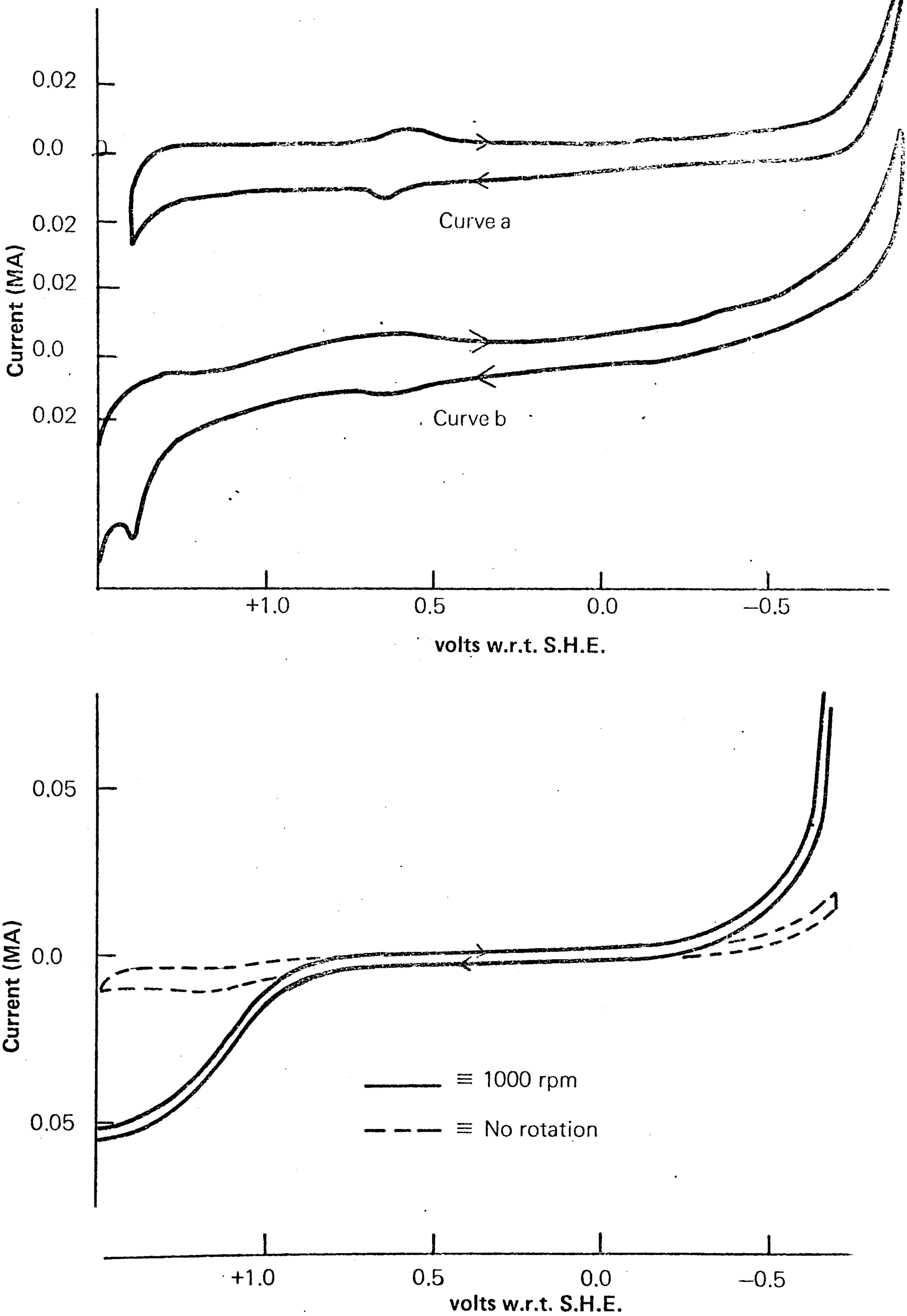

Fig. 7.10
CURRENT-POTENTIAL RELATION, P.G. (FACES ONLY),
INSULATED WITH LACONITE, IM $HClO_4$, $40mVsec^{-1}$

CHAPTER 8

REDUCTION OF CrVI IN PERCHLORIC AND SULPHURIC ACID SOLUTIONS ON A GRAPHITE ELECTRODE

8.1 Introduction

The object of this work was to study the kinetics and mechanism of the reduction of CrVI on a graphite electrode in solutions containing perchloric or sulphuric acid. The choice of perchloric acid was made in order to keep the number of CrVI containing solution species at a minimum. Due to film formation, however, it did not prove possible to investigate, in any detail, the kinetics of such a system. The presence of sulphuric acid, as found when using a gold electrode, minimised interference by films on the electrode surface.

Pyrolytic graphite was chosen as the electrode material because of the ease of obtaining a fresh, reproducible surface. Glassy carbon, although being capable of accepting a greater degree of polish, could not be used as it rapidly became inhibited due to film formation. Removal of these films necessitated mechanically abrading the electrode surface.

No work has been reported previously on a graphite electrode in $HClO_4$ solutions.

8.2 Experimental

The presence of ionic impurities was carefully avoided in these experiments by using the same methods of solution purification as described in Section 6.2.

A rotating, pyrolytic graphite electrode was used; its construction is described in Section 3.6. As reported in Section 3.6 both flaked and polished surfaces were employed for steady-state measurements. Although the current-potential relations obtained on the two types of surface were closely similar, the smoother surface resulting from polishing was more satisfactory when studying the rotation dependence of the current and was employed in all subsequent work.

8.3 Steady-state results in $HClO_4$ solutions

The current-potential relation obtained, with a flaked electrode, in 1 x 10^{-2} M CrVI, 1 M $HClO_4$, is shown in Fig. 8.1, curve a . In these measurements the potential was held at each value for no longer than 1 minute. On making the potential more negative a cathodic current is observed at potentials negative to 1.15 V. Between 0.8 and 0.6 V there is an inflexion in the curve prior to a smooth rise to a plateau at approximately 0.0 to -0.2 V. This behaviour is unaltered by polishing the electrode surface. On the positive-going measurements (curve b) the final plateau is extended to about 0.45 V prior to a sharp fall in current. This behaviour is slightly more emph-asised on a polished surface (curve c). At more positive potentials the inflexion between 0.8 and 0.6 V is still present, the current in this region being slightly below that of the negative-going curve.

True steady-state current-potential curves could not be obtained because the current fell with time in some potential regions, whereas in others it rose due to attack of the electrode surface. Thus at 0.9 V and more positive potentials the current fell with time (by a factor of 10 times in 15 minutes). Some reactivation occurred after holding at 1.2 V or switching the electrode to open circuit (potential $\approx$ 1.2 V). The current increased with time between 0.9 and 0.7 V but fell slowly at potentials more negative than 0.7 V (by 5% in 15 minutes). After holding at potentials between 0.9 and 0.7 V the electrode surface was found to have lost much of its original structure, being dark and non-reflective, Fig. 3.4. Mass spectrometry showed the surface to be covered by small particles of carbon and the double-layer capacitance, as obtained from sweep measurements was increased. Such attack did not take place at other potentials. It presumably results from oxidative attack of the graphite surface by an intermediate in the electrode reaction which was present at maximum concentration in this potential range.

Nature of the limiting current (i_p)

As described above, the value of the limiting current fell slowly with time. Satisfactorily reproducible results on the dependence of the current on rotation speed were obtained, however, by maintaining each rotation speed for no longer than 30 seconds. A typical

plot of $^{1}/i$ against $^{1}/w^{\frac{1}{2}}$ obtained with a freshly polished surface is shown in Fig. 8.2, line a. Essentially similar results were obtained at all potentials between 0.0 and -0.6 V. The graph is linear and has the same slope and intercept, when corrected for surface area, as obtained with a gold electrode in $HClO_4$ solutions. These results can therefore be interpreted as indicating that the plateau current is diffusion controlled but that as with gold a proportion of the graphite surface is blocked by a film. Additional evidence supporting these conclusions was obtained by varying the concentration of CrVI. After correcting for solution decomposition the plots of $^{c}b/_{i_p}$ against $^{1}/w^{1/2}$, obtained in solutions containing different concentrations of CrVI, superimposed and a first order dependence of i_p on CrVI concentration was obtained, Fig. 8.3

As mentioned earlier, a flaked graphite surface, although reproducibly clean, did not prove suitable for these investigations. The surface roughness resulted in the current increasing with rotation speed to a greater extent than predicted by the Levich theory. As a consequence graphs of i against $w^{\frac{1}{2}}$ curved upward, while those of $^{1}/i$ against $^{1}/w^{\frac{1}{2}}$ showed negative intercepts, Fig. 8.2, line b).

<u>Origin of the inflexion between 0.8 and 0.6 V</u>

As demonstrated in Section 8.4, a film formed on the electrode at more positive potentials undergoes

modification in this potential region. There is also evidence that this film inhibits the electrode reaction. While inhibition due to film modification may be the cause of this inflexion it is also possible that it results from

(i) a change in the number of electrons involved in the reduction

(ii) the CrVI species reduced at more positive potentials being different from that reduced at more negative potentials; the inflexion may then correspond to the limiting rate of reduction of the former species.

The coulometric experiments described in Chapter 4 show that the number of electrons involved in the reduction did not change with potential.

The second possibility was investigated by varying the CrVI concentration in the solutions employed. The current-potential curves obtained at a sweep rate of 10 mV sec^{-1} in 1 M $HClO_4$ containing different concentrations of CrVI is shown in Fig. 8.4. There was, however, no correlation between the ratio of the currents corresponding to the inflexion and the final plateau and the proportion of any CrVI species present. Since, unfortunately, an inflexion rather than a well defined plateau was obtained the true value of the first limiting current, if it exists, was not directly measurable. As a consequence no close correlation

would be expected. In Section 2.5.2 a method is described for determining the true limiting current under such conditions. This technique however requires data on the variation of current with rotation speed at potentials between the inflexion and the final plateau. In this potential range the currents were not sufficiently stable in $HClO_4$ solutions for meaningful results to be obtained. It has therefore not been possible to devise an adequate test of possibility (ii).

8.4 Sweep measurements in 1 M $HClO_4$ solutions

The current-potential relation obtained in 1 x 10^{-2} M CrVI, 1 M $HClO_4$ in repetetive sweeps at 100 mV and two rotation speeds is shown in Fig. 8.5. Curves of similar form but with larger maxima were obtained at higher sweep rates. The hysteresis became more pronounced with continued use of the electrode, possibly due to an increase in surface area caused by attack of the graphite as described previously. The curves show, on the negative-going sweep, a rise in current from 1.1 V, a maximum at 0.9 V (more clearly shown at the lower rotation speed) and a second maximum at 0.7 V. The current then rises to a third maximum at about 0.35 V, again more pronounced at the lower rotation speed, followed by a slight increase to -0.3 V. The positive-going curve consists of a fairly smooth fall to about 0.5 V, then two inflexions, the first occurring between 0.55 to 0.8 V, the second between 0.8 to about 1.1 V.

This behaviour and the results reported later can again be explained in terms of film formation and modification. The final conclusions reached are shown diagrammatically in Fig. 8.6. Reduction of CrVI begins at about 1.1 V and is seen to suffer inhibition from about 0.95 V as a result of the formation of film X; deposition of this film may however begin at more positive potentials. The peak at 0.9 V is attributed to the formation of this film. Reduction of X to Y which overlaps the former process, reaches a maximum value at 0.7 V. Subsequent reduction of Y to Z occurs at potentials more negative than about 0.55 V producing the final cathodic maximum observed. Reoxidation of Z to Y on the positive-going sweep is observed between 0.55 and 0.8 V and that of Y to X at potentials more positive than 0.8 V.

Holding the electrode between 1.0 and 1.4 V affects the first negative-going sweep as shown in Fig. 8.7. After holding the electrode at 1.0 V for 2 minutes the subsequent negative-going sweep has a very large maximum at 0.72 V as compared with that obtained when swept from 1.0 V. Similar behaviour is observed following 2 minutes electrolysis at 1.2 V. Both pretreatments produce a further peak at about 0.3 V. The sweep obtained after 2 minutes at 1.4 V shows higher currents between 1.2 and 1.0 V than observed after any of the previous treatments; no maximum at 0.7 V is obtained, a short plateau occurring. This is followed by a rise to a

larger maximum at 0.3 V than those observed following the other pretreatments. The next sweep from 1.4 V has a clear maximum at 0.7 V; that occurring at 0.3 V is however smaller than in the first sweep.

The large peaks observed at 0.7 V after pretreatment at 1.0 and 1.2 V correspond to the reduction of X to Y, and hence indicate that at these potentials X must be deposited on the electrode surface (or reoxidised from Y if this is present). Since under steady-state conditions (see Section 8.3) the current no longer fell with time at potentials negative to 0.9 V, the formation of X must be complete by this potential. After holding at 1.4 V most of film X must have been removed from the electrode since the initial current is higher and the peak at 0.7 V smaller than after the other pretreatments. Since subsequent sweeps from 1.4 V show lower initial currents and a higher peak for the reduction of X to Y it must be concluded that only part of film X, deposited during the previous sweep, is removed by sweeping to 1.4 V.

The anodic currents observed in the positive-going sweeps to 1.2 and 1.4 V are probably associated with both the conversion of Y to X (although this is believed to begin at about 0.8 V) and the removal of X. In accord with this, these anodic currents were larger after holding at 1.2 V than holding at 1.4 V; this would be expected since more material is present on the surface after the former pretreatment. That the

conversion of Y to X continues during sweeping to potentials more positive than 1.2 V is deduced from the fact that, if all of Y were oxidised to X by 1.2 V, the second negative-going sweep from 1.2 V should reproduce that obtained after holding at this potential.

The effect on the current-potential curve of sweeping to progressively more negative limits from 1.2 V is shown in Fig. 8.8. Between 1.2 and 1.1 V little extra film is deposited on the electrode. However by 1.0 V more film X must be deposited this being reflected in the lower current on the next negative-going sweep. By 0.9 V the inhibition caused by X results in a greater hysteresis. The inflexion on the positive-going sweep beginning at 0.85 V, caused by reoxidation of Y to X, becomes more marked as the sweep limit is extended to 0.6 V, that is, as more Y is produced on the electrode surface. As the potential is swept more negative than 0.6 V, the cathodic maximum at about 0.4 V (Y reduced to Z) develops and the corresponding dip on the positive-going curve, between 0.55 and 0.8 V where reoxidation of Z to Y occurs, becomes more obvious.

Additional information on the layer formation and modification processes was obtained by sweeping to progressively more positive limits from -0.3 V, Fig. 8.9. The peak for reduction of Y to Z becomes significantly larger after sweeping to 0.8 V and does not increase

further after sweeping to more positive potentials; this confirms that reoxidation of Z must be complete by 0.8 V. Similarly the maximum at 0.7 V (X to Y) does not develop until having swept more positive than 0.8 V, thus reoxidation of Y to X cannot occur prior to this. Removal of X must begin between 1.0 and 1.1 V since a clear maximum for its redeposition is obtained after sweeping to the latter but not the former potential.

Following polarisation for 5 minutes at 0.0 or -0.3 V, the current on the positive sweep is initially lower than with uninterrupted sweeping, Fig. 8.10, but the very flat plateau is maintained up to about 0.5 V prior to a steep fall. Although as Z accumulates it must gradually block the electrode surface, since the steady-state currents fell with time, the presence of film Z causes less inhibition than does Y because the limiting current is maintained until Z is oxidised to Y at about 0.5 V. The anodic contribution corresponding to Z being oxidised to Y is seen to be greater on the first sweep when more Z is present, confirming that oxidation of Z to Y occurs between 0.5 and 0.8 V. Under steady-state conditions, this oxidation process appears to begin at about 0.45 V (Fig. 8.1).

Confirmation of the conclusions reached above was obtained from the results of sweeps in 1 M $HClO_4$ following polarisation in 1 x 10^{-2} M CrVI, 1 M $HClO_4$. The condition of the electrode surface did not remain constant

throughout these experiments. Slight attack of the surface was noticed following those experiments in which a cathodic maximum at 0.7 V was observed in the background electrode (cf. steady-state results). However variation was minimised by polishing the surface with tissue after each run. The current-potential relations obtained in 1 M $HClO_4$ with a freshly prepared surface and one which had suffered severe attack are given in Fig. 8.11.

The result of holding the electrode at 1.0 V for 25 minutes in 1 x 10^{-2} M CrVI, 1 M $HClO_4$ on the sweep in 1 M $HClO_4$ alone is shown in Fig. 8.12, curve a. The height of the large cathodic peak at 0.73 V depends upon the time the electrode was held at 1.0 V in the CrVI containing solution and corresponds to the reduction of X to Y. Subsequent sweeps to 1.4 V show only a much smaller cathodic peak, Fig. 8.12, curve c. However following 15 minutes electrolysis in 1 M $HClO_4$ at 1.0 V the peak at 0.73 V again increased in height, Fig. 8.12, curve b. Thus under steady state conditions, in the background electrolyte, oxidation of Y to X occurs at 1.0 V. This behaviour was found to be independent of electrode rotation. When this electrode was then swept to 1.6 V, Fig. 8.13, with no rotation, an additional cathodic maximum was observed at 0.9 V, presumably corresponding to redeposition of X. If the electrode was rotated during this treatment, however, this maximum was not

observed. This indicates that oxidation of X produces a soluble material.

When a film-covered electrode was held at -0.3 V in the background electrolyte prior to recording the current-potential curve, an increased anodic current was obtained between 0.55 and 0.85 (Fig. 8.14); this maximum presumably corresponds to oxidation of Z to Y. Reduction of Y to Z must be a slow process, at least in the background electrolyte, since the above peak was only observed after holding the electrode at -0.3 V and was not present in repetitive sweeps.

Once film had been deposited on the electrode it was very difficult to remove from the surface. Normal behaviour in the background electrolyte could be restored only by either very prolonged washing and polishing with tissue or by machining a fresh surface.

Similar film deposition processes were found to occur also in more dilute CrVI containing solutions. The maxima in the current-potential curves, however, were much less well defined, making identification of the separate processes extremely difficult.

The presence of chromium on the electrode surface, following pretreatment in 1 x 10^{-2} M CrVI, 1 M $HClO_4$, has been demonstrated by analysis of X-rays emitted from the sample after excitation with an electron beam (Cambridge "Geoscan" or Scanning Electron Microscope). The results, which were qualitative only, due to surface roughness, showed chromium to be present on the electrode

surface following 30 minutes pre-electrolysis at 1.0, 0.7 or 0.0 V. With an unattacked electrode the chromium concentration on the surface did not vary markedly with potential, the surface coverage with chromium compounds being approximately 0.3% at 1.0 V and 0.2% at 0.0 V. When the surface had suffered severe attack, as was produced by holding at 0.7 V, the chromium count indicated a surface coverage of about 10% but this was almost certainly due to considerable inclusion of chromium compounds in the roughened surface. The appearance of a sample following 30 minutes pretreatment at 0.7 V in 1 x 10^{-2} M CrVI, 1 M $HClO_4$ in a scanning electron microscope detecting only X-rays emitted by chromium-containing compounds is shown in Fig. 3.4.

8.5 Conclusions

As reported in the case of gold electrodes, the results in $HClO_4$ solutions show that after suitable anodic pretreatment an essentially film-free surface can be produced. Reduction of CrVI takes place on this surface but film X is produced at more negative potentials. While this results in some inhibition, the severe inhibition as observed with gold does not occur. As the potential is made more negative film X is reduced to Y and then to the least inhibiting form, Z. Large quantities of Z or of another product do, however, cause some inhibition. Reoxidation of all three films takes place on making the potential more positive.

The inflexion between 0.8 and 0.6 V, present in the steady-state curves was not caused by a change in the number of electrons involved in the reduction. It was not, however, possible to decide whether it was due solely to film modification or to a change in the nature of the CrVI species being reduced.

8.6 The effect of addition of H_2SO_4 to $HClO_4$ containing solutions

The modification to the current-potential relation obtained in 1 x 10^{-2} M CrVI, 1 M $HClO_4$ caused by addition of H_2SO_4 is shown in Fig. 8.15. Making the solution only 0.04 M in H_2SO_4 causes a great reduction in the hysteresis between the positive and negative-going curves. The reduction is appreciably less inhibited at potentials positive to 1.0 V, this section of the curve resembling the first negative-going curve following anodic polarisation in 1 x 10^{-2} M CrVI, 1 M $HClO_4$. The maxima corresponding to the formation and modification of films, X, Y and Z, are largely removed. Further addition of H_2SO_4 enhances this effect.

The presence of sulphuric acid appears therefore to minimise film formation on pyrolytic graphite in perchloric acid solutions.

8.7 Sweep measurements in H_2SO_4 solutions

As mentioned in Section 8.1, film formation and modification appeared to be of minor importance in H_2SO_4 solutions. Because of this, the order of presentation adopted previously has been reversed here and the sweep

measurements, which showed that only very small amounts of film were present on the electrode surface, precede the steady-state results.

In sulphuric acid solutions the current-potential curves were very much more reproducible than in perchloric acid media and no attack of the electrode surface was observed. Typical curves, obtained at 100 mV sec^{-1} sweep rate, in CrVI concentrations of 1 x 10^{-2}, 1 x 10^{-3} and 1 x 10^{-4} M in 0.5 M H_2SO_4, 0.25 M H_2SO_4/ 0.25 M Na_2SO_4 and 0.05 M H_2SO_4/0.45 M Na_2SO_4, are shown in Figs. 8.16, 8.17 and 8.18. Compared with the sweep at 100 mV sec^{-1} in 1 M $HClO_4$, Fig. 8.5, the hysteresis between the positive and negative-going curves is greatly reduced. (This effect of H_2SO_4 was first demonstrated by addition of H_2SO_4 to 1 M $HClO_4$, Fig. 8.15.) Even at higher sweep rates no maxima or minima, corresponding to film deposition or modification, are observed.

In 1 x 10^{-2} M CrVI, 0.5 M H_2SO_4 cathodic currents are obtained at potentials negative to about 1.08 V. As the potential reaches more negative values two inflexions are observed in the curve, one at about 0.8 V, the other less distinct, between 0.3 and 0.4 V. At more dilute CrVI concentrations in 0.5 M H_2SO_4 the potential at which the current first rises moves more negative and the inflexions become indistinct. Decreasing the hydrogen ion concentration at constant CrVI concentration again moves the initial rise in current

towards more negative potentials, furthermore in 1×10^{-2} M CrVI the current corresponding to the first inflexion decreases in magnitude.

In contrast to the results obtained in perchloric acid, these curves show little evidence for film formation and modification. In more concentrated CrVI solutions however the hysteresis between the positive and negative-going sweeps decreases markedly at potentials more positive than 1.0 V and more negative than 0.0 V. Since this may indicate that the condition of the electrode varied with potential, the consequence of holding the electrode at various potentials prior to sweeping was investigated. Negative-going sweeps in 1×10^{-2} M CrVI solutions, following holding the electrode for 10 minutes at potentials between 1.0 and 0.5 V, were virtually identical with the curves obtained during continuous sweeping. Some evidence for the presence of a film on the surface was obtained by holding the electrode at more negative potentials and sweeping to positive values. The effect of this treatment was more pronounced as the pretreatment potential was made more negative (although little further change occurred in making the potential more negative than -0.3 V) and as the H_2SO_4 concentration was decreased. For purposes of comparison with Fig. 8.10 the sweep obtained after holding at -0.6 V for 5 minutes in 1×10^{-2} M CrVI, 0.5 M H_2SO_4 is shown in Fig. 8.19. A very much smaller effect is observed in the latter

case. The most pronounced effect was obtained in 1×10^{-4} M CrVI, 0.05 M H_2SO_4, 0.45 M Na_2SO_4, Fig. 8.20, where the anodic peak at about 0.25 V and the enhanced anodic current at potentials positive to 0.55 V, suggest that film modification processes are occurring. These effects persisted when the electrode was transferred to the background electrolyte and held at -0.3 V before being swept positive. The curves obtained in the various background electrolytes after pretreatment in 1×10^{-4} M CrVI solutions are compared in Fig. 8.21 It should be noted that the maxima were present only after holding the electrode at -0.3 V in the background electrolyte but were not observed if it was simply subjected to a cyclic sweep.

These results appear to indicate the presence of some film on the electrode following sufficiently negative pretreatment; the amount of film however is very much smaller than that found in $HClO_4$ solution. The potential at which the film is reoxidised becomes more positive as the H_2SO_4 concentration is increased. Reduction of the film appears to be very slow since no anodic peaks were observed unless the electrode was held at -0.3 V.

In contrast to the conclusions reached by Sternberg and Bagotskii[1.23], no evidence for "partial passivation" of the electrode has been obtained. It should however be noted that the former workers employed much more concentrated CrVI solutions and a different type of carbon as their electrode material.

8.8 Steady-state measurements in sulphuric acid solutions

The results described in the previous section indicate that the form of the current-potential curves obtained in sulphuric acid solutions was not determined primarily by film formation and modification processes. In accord with this, the curves obtained under steady-state conditions had the same shape as those obtained with a linear potential sweep. Moreover the current was essentially independent of time over most of the potential range; the currents obtained on making the potential progressively more negative, agreed to within 3% with those recorded on subsequently reversing the direction of potential change. In the more concentrated CrVI solutions the current fell slowly with time at potentials more positive than about 0.90 V on making the potential more negative, but rose slowly with time in the same potential range on making the potential more positive; under all conditions, the current at very negative potentials fell very slowly with time.

Typical steady-state current-potential curves obtained at a rotation speed of 1000 r.p.m. are shown for different CrVI concentrations in Figs. 8.22 (0.5 M H_2SO_4), 8.23 (0.25 M H_2SO_4, 0.25 M Na_2SO_4) and 8.24 (0.05 M H_2SO_4, 0.45 M Na_2SO_4). Other CrVI concentrations used, but not illustrated in the diagrams, were 3×10^{-3} and 3×10^{-4} M. As described in the case of the sweep measurements two inflexions are observed in the curve obtained in 1×10^{-2} M CrVI, 0.5 M H_2SO_4. The height

of the inflexions decreases as the sulphuric acid concentration is decreased and the curve moves toward more negative potentials. As the CrVI concentration is decreased in a given background solution, the curves again move to more negative potentials although this trend is reversed at potentials more negative than about 0.1 V.

As will be apparent later, interpretation of these curves necessitates a knowledge of the value and cause of the final limiting current.

In 0.5 M H_2SO_4 containing 1 x 10^{-2} M CrVI the graph of $^1/i$ against $^1/w^{\frac{1}{2}}$ at-0.6 V was linear and passed through the origin indicating that under these conditions the current is diffusion controlled. In accord with this, the value of the limiting current at 1000 r.p.m. was 5.40 mA in satisfactory agreement with the value of 5.43 mA obtained at the same rotation speed in 1 x 10^{-2} M CrVI in 1 M $HClO_4$. In solutions containing 1 x 10^{-4} M CrVI plots of $^1/i$ against $^1/w^{\frac{1}{2}}$ at 0.2 and 0.0 V were linear and parallel to each other but, as is to be expected for currents under partial kinetic control, showed marked intercepts at $w = \infty$. At more negative potentials the plots became curved probably due to concomitant hydrogen evolution, Fig. 8.25 (see Section 2.5.2). Such curvature was also apparent but less marked in 1 x 10^{-3} M CrVI solutions. Under these circumstances, as explained in Section 2.5.2, the true value of the diffusion-limited current is most readily determined by

plotting i against w , Fig. 8.26. As predicted by Equation 2.35 when the potential is sufficiently negative so that the reduction of CrVI is diffusion controlled, such a graph is linear but has an intercept equal to the rate of hydrogen evolution. At this potential the value of the diffusion-limited current at a given rotation speed can be found by subtracting the current due to hydrogen evolution, from the observed current. The values of $^{i}d/_{c_T}$ obtained by the most appropriate of these procedures were independent of C_T (the total concentration of CrVI, assuming only monomeric species to be present) in 0.5 M H_2SO_4 and in 0.25 M H_2SO_4, 0.25 M Na_2SO_4 and equalled 540 $\pm$ 5 mA mol^{-1}. In 0.05 M H_2SO_4, 0.45 M Na_2SO_4 $^{i}d/_{c_T}$ varied from 502 to 535 over the concentration range 1 x 10^{-2} to 1 x 10^{-4} M CrVI. It is possible that under these conditions the current is partially limited by the rate of diffusion of H^+.

8.8.1 Nature of the first plateau

The rather ill-defined first plateau, which is seen most easily in 10^{-2} M CrVI, 0.5 M H_2SO_4 occurs at potentials between 0.85 and 0.80 V. Although at somewhat more positive potentials the currents tended to change with time, perhaps suggesting that a layer was being formed on the electrode, the sweep measurements gave no evidence to suggest that the plateau was the result of inhibition by a layer. It seemed likely therefore that it corresponded to the limiting rate of reduction

of one or more of the chromium species present in the solution.

Although the plateau is rather ill-defined, and hence the true limiting current will be lower than the plateau current (see Section 2.5.2), it is possible to demonstrate that this first wave must result from the reduction of one of the dimeric species. Thus graphs of log [Cr] against log i_{p_1} (where i_{p_1} is the plateau current) are linear and have a slope close to unity, when [Cr] represents the concentration of either of the dimeric species (Fig. 8.27); linear plots but with a slope of $^1/_2$ are obtained when the concentration of any monomeric species is employed in such graphs. It follows therefore that i_{p_1} is directly proportional to the concentration of either of the dimeric species but depends on the square of the concentration of the monomeric species. This latter result is almost certainly a direct consequence of the fact that the concentration of any particular monomer is proportional to the square of the concentration of the dimers (see Fig. 1.1).

It is probable, therefore, that this first plateau is due to a limiting current resulting from reduction of one or both of the dimeric species. Since most ions have closely similar diffusion coefficients, it is likely that the diffusion coefficients of the dimeric species are near to those of the monomers. If this is

true the theoretical values of the diffusion limited current for the reduction of both dimers (i_d^d) may be calculated from the relation

$$\frac{i_d^d}{i_d} = \frac{2[\text{Dimer}]}{C_T} \qquad 8.1$$

where [Dimer] = total concentration of dimers

and i_d = the total diffusion limited current (5.40 mA in 1 x 10^{-2} M CrVI).

The resulting values of i_d^d are higher than the plateau currents. Thus in 1 x 10^{-2} M CrVI, 0.5 M H_2SO_4 i_d^d = 0.97 mA, whereas i_{p_1} = 0.90 mA, while in 1 x 10^{-2} M CrVI, 0.25 M H_2SO_4 0.25 M Na_2SO_4 i_d^d = 1.48 mA and i_{p_1} = 0.55 mA. Consequently the reduction of only one dimer must occur during this first wave. Providing this process does not suffer inhibition it may be concluded that the species involved is $HCr_2O_7^-$ since in 1 x 10^{-2} M CrVI, 0.25 M H_2SO_4, 0.25 M Na_2SO_4 the theoretical diffusion-limited currents are 1.14 mA for $Cr_2O_7^{2-}$ and 0.34 mA for $HCr_2O_7^-$. There may be a contribution from a preceding chemical step involving one of the other solution species whilst it is also possible that the plateau results from the adsorption of one or both dimers limiting the rate of the reaction (see Section 2.5).

8.8.2 Nature of the second plateau

The procedure used for the treatment of the first plateau was not satisfactory in this instance. Thus a

graph of log (total dimer concentration) against log i_{p_2} where i_{p_2} is the current corresponding to the second plateau, was linear and gave a reaction order with respect to dimers of 0.7 while graphs of log (monomer concentration) against log $(i_{p_2} - i_d^{HCr_2O_7^-})$ were also linear and gave a reaction order of 1.3 for each of the monomers. It is therefore not possible using this procedure to determine which chromium species is reduced in the second wave. The departure from first order dependence on all these plots is consistent with the true plateau height being appreciably smaller than i_{p_2} as is to be expected with an ill-defined plateau, see Section 2.5.2.

The alternative procedure described in Section 2.5.2 was therefore employed. This is based on the assumption that within a particular potential range the first and second waves become diffusion-limited and the process occurring in the final wave obeys the equation

$$i_3 = k_3 c_s$$

where k_3 is the potential-dependent rate constant for this process

and c_s is the surface concentration of the species undergoing reduction.

Consequently the observed current (i_m) is given by

$$i_m = i_{d_1} + i_{d_2} + i_3$$

Substitution of the equations for mass transport into the above expression and suitable rearrangement gives

$$\frac{i_m}{w^{\frac{1}{2}}} = B_1c_1 + B_2c_2 + \frac{k_3}{B_3}\left(\frac{i_d - i_m}{w}\right) \qquad \text{cf. Eqn. 2.34}$$

where c_1 and c_2 are the bulk concentrations of the species reduced in the first and second waves and i_d is the total diffusion-limited current for the whole wave.

If the foregoing assumptions are correct, graphs of $\frac{i_m}{w^{\frac{1}{2}}}$ against $\frac{i_d - i_m}{w}$ corresponding to different potentials should be linear and give the same intercept. Since

$$i_{d_1} + i_{d_2} = (B_1c_1 + B_2c_2)w^{\frac{1}{2}}$$

the sum of the true diffusion-limited currents corresponding to the first and second waves may be obtained from this intercept.

Inspection of Fig. 8.22 shows that the current is directly proportional to the CrVI concentration between 0.2 and 0.0 V indicating that the reaction is probably first order in CrVI over this potential range. As demonstrated later the process occurring in the last wave is in fact close to first order over a wider range of potentials. A typical graph of $\frac{i_m}{w^{\frac{1}{2}}}$ against $\frac{i_d - i_m}{w}$ is shown in Fig. 8.28. As required by the theory the lines obtained at sufficiently negative potentials all give the same intercept. The values of $i_{d_1} + i_{d_2}$ (i_d obs) obtained for solutions in 0.5 M H_2SO_4 from such graphs are listed in Table 8.1.

TABLE 8.1

CrVI concentration (M)	i_d obs.	i_d^d calc.	i_d (one dimer)
1×10^{-2}	0.98	0.968	0.49
3×10^{-3}	0.11	0.112	0.05
1×10^{-3}	0.014	0.0137	0.006
3×10^{-4}	0.001	0.00114	0.0005
1×10^{-4}	0.0001	0.00014	0.00006

Also included in the table are values of the diffusion-limited current i_d^d calculated using Equation 8.1. The good agreement between the observed and calculated values strongly suggests that both the first and second waves should be attributed to the reduction of the dimeric species. Since the first wave has already been attributed to the reduction of $HCr_2O_7^-$ the second presumably corresponds to reduction of $Cr_2O_7^{2-}$. It should be noted that the calculated values of i_d obtained from assuming that any other species or combination of species is reduced in the first two waves are in serious disagreement with i_d observed.

In 0.25 M H_2SO_4, 0.25 M Na_2SO_4 solutions comparable agreement between observed and calculated values of i_d^d was obtained. In the most dilute acid solution additional complications are apparently present and the interpretation of the current-voltage curves remains in doubt.

It should perhaps be stressed that the linearity of the graphs of $\frac{i_m}{w^{1/2}}$ against $\frac{i_d - i_m}{w}$ and the fact that the intercepts varied with the concentration of CrVI, is consistent only with the process occurring in the second wave becoming diffusion-limited. Thus as shown by Equations 2.48 and 2.44, Section 2.5.2, curved plots would be expected if adsorption of a reactant were rate determining or if a preceding chemical step were involved in the reduction. If adsorption of a product limited the rate, the intercept should be independent of the concentration of CrVI (see Equation 2.49).

As described in Section 1.1 there is some doubt as to whether $HCr_2O_7^-$ is present in solutions of CrVI. The values of i_d calculated on the assumption that only one dimeric species, that is $Cr_2O_7^{2-}$, is present are also shown in Table 8.1. They are not in agreement with values of i_d observed nor is it possible to reach agreement by assuming that the second wave corresponds to reduction of any of the other species present. It would seem therefore that both of the dimeric species are indeed present.

8.8.3 <u>Kinetics of processes occurring in last part of wave</u>

In the treatment described below, it has been assumed that;

(a) the first two waves are associated only with the reduction of dimers, the current for monomer reduction being obtainable by subtracting the diffusion limited

value of the dimer reduction current from the total current

$$\text{i.e.} \quad i_c = i_m - i_d^d$$

where i_m is the measured current,

i_d^d the diffusion limited value of the dimer reduction current, calculated on the basis of the concentration of dimers and the mean diffusion coefficient,

and i_c the corrected current, i.e. the current for monomer reduction.

This relation will hold at potentials sufficiently negative that the reduction of dimers is diffusion limited.

(b) Since an essentially smooth curve was obtained, that all the monomers behave as a single species.

The rate equation for monomer reduction can probably be generalised into an equation of the form

$i_c = k'(c_s)^p$ where p is the order of reaction

and c_s the concentration of monomers at the electrode surface.

Furthermore since

$$c_s = \left(\frac{i_d - i_m}{i_d}\right) c_T$$

where $c_T = 2c_b^d + c_b^m$ = total CrVI concentration in the bulk of the solution

$$\text{then} \quad i_c = k' \frac{(i_d - i_m)^p}{i_d} c_T$$

$$\text{and} \quad \log i_c = \log k' + p\log \frac{(i_d - i_m)}{i_d} c_T \qquad 8.2$$

Thus the order of reaction with respect to monomers, will be the slope of the plot of log i_c against log $\frac{(i_d - i_m)}{i_d} c_T$ at constant potential. Such graphs, corresponding to solutions in 0.5 M H_2SO_4 and 0.25 M H_2SO_4/0.25 M Na_2SO_4 are illustrated in Figs. 8.29 and 8.30. They show the order of reaction to be

<1 at negative potentials

≈ 1 at 0.3 V

>1 at positive potentials.

At more positive potentials, the points corresponding to the 1 x 10^{-2} M CrVI solutions deviate from the lines, presumably because the dimer reduction process is not diffusion limited and hence $i_c > i_m - i_d^d$.

The variation of reaction order with potential can also be seen by plotting the Tafel relation. Since if the reaction is simple and of first order,

$$i_c = kc_s \exp - \alpha nafE,$$

graphs of log i_c/c_s against E should be linear with a slope of $\frac{-\alpha F}{2.303\ RT}$ and graphs for all concentrations should superimpose. Such plots are illustrated in Figs. 8.31 and 8.32. In the most concentrated CrVI solution, the graph is almost linear at potentials more negative

than 0.3 V. At a Cr concentration of 1 x 10^{-4} M the graph is almost a smooth curve; the lines corresponding to intermediate concentrations fall between these two extremes. In 1 x 10^{-2} M CrVI, the curve has a very low slope,

$$\frac{dE}{d\log\left(i_{c/c_s}\right)} \gtrsim 500 \text{ mV/decade.}$$

Such a low slope is consistent with discharge occurring on a surface covered with some type of layer. This has been observed in the reduction of chlorine[8.1] and in the Ce^{3+}/Ce^{4+} reaction[8.2] on oxidised platinum, and for oxygen evolution on noble metal alloys[8.3]. It has therefore been assumed that in the most concentrated solution, the electrode is largely covered with a film of some sort over the whole of the potential range corresponding to monomer reduction; the reduction of monomers occurring on this covered surface.

In the most dilute solution, the "Tafel plot" becomes similar to that in the concentrated solution at negative potentials, where the current is high. It seems probable therefore that under these circumstances also, the electrode is largely covered with this film. At more positive potentials a much steeper slope is observed suggesting that a nearly film-free electrode is now obtained.

To accord with these results it is necessary to propose that the film is a product of the reduction reaction on a bare surface, but that the film can be removed by

some non-electrochemical process, probably normal dissolution. The coverage of the surface with film would then depend on the magnitude of the current, and with a sufficiently large current a surface coverage close to unity would be obtained.

The suggested mechanism is therefore

$$A + M + ne \xrightarrow{k_1} M\text{-}B \xrightarrow{k_2'} M + \text{Products} \qquad (1)$$

followed by

$$\text{either } A + M\text{-}B + ne \xrightarrow{k_3} M\text{-}B + \text{Products} \qquad (2a)$$

$$\text{or } A + M\text{-}B + ne \xrightarrow{k_4} M + \text{Products} \qquad (2b)$$

In this mechanism, A is the solution species undergoing reduction, and M-B the surface film, formed by the reduction process, which dissolves slowly into the electrolyte. Potential dependent rate constants are represented by k_1, k_3 and k_4; k_2 is potential independent.

The rate equations corresponding to these mechanisms are derived in Appendix 2. For mechanism (1) + (2a) we obtain

$$\frac{i_c}{nFA} = \frac{k_1 c_s (k_2 + k_3 c_s)}{k_1 c_s + k_2} \qquad A6$$

while for mechanism (1) + (2b)

$$\frac{i_c}{nFA} = \frac{k_1 c_s (k_2 + 2k_4 c_s)}{k_1 c_s + k_2 + k_4 c_s} \qquad A9$$

Equation A9 can be shown by the following argument to be unsatisfactory. A linear relation between log i/c_s and E, which can be obtained in concentrated solutions

at sufficiently negative potentials, Fig. 8.31 can be derived from Equation A9 only if

(i) k_2 is $\ll 2k_4c_s$ and $\ll k_1c_s$ and

(ii) either (a) $k_1 \gg k_4$, (b) $k_4 \gg k_1$ or

(c) k_1 and k_4 have the same potential dependence.

Thus if k_2 is negligibly small

$$\frac{i_c}{nFAc_s} = \frac{2k_1k_4}{k_1 + k_4}$$

If (ii) (a) applies, then in concentrated solutions at potentials $\lesssim 0.3$ V

$$\frac{i_c}{nFAc_s} = 2k_4$$

If the potential dependence of k_1 is different from that of k_4, and $k_1 \gg k_4$ when E $\lesssim 0.3$ V, then at some positive potential k_1 must equal k_4. When this is true

$$\frac{i_c}{nFAc_s} = \frac{k_1(k_2 + 2k_1c_s)}{2k_1c_s + k_2} = k_1 = k_4$$

Therefore, at all concentrations the graph of log i_c/c_s against E must pass through this point. Since however the graphs coincide only at one point, Figs. 8.31, 8.32, which falls on the line $\frac{i_c}{nFAc_s} = 2k_4$ this requirement cannot be satisfied. An analogous argument to that given above also shows that if (ii) (b) applies, the rate equation is again inapplicable.

To test this rate equation if (ii) (c) applies, suppose that $k_4 = Dk_1$ where D is a potential independent constant.

In concentrated solutions

$$\frac{i_{c'}}{nFAc'} = \frac{k_1(2k_4c')}{k_1c' + k_4 c'}$$

where $i_{c'}$ is the corrected current and c' the surface concentration in this solution

$$= \frac{2k_1^{\dot{2}}D}{k_1(1+D)} = \frac{2k_1D}{(1+D)}$$

whereas in dilute solutions

$$\frac{i_{c_d}}{nFAc_d} = \frac{k_1(k_2 + 2Dk_1c_d)}{k_2 + k_1c_d(1+D)}$$

where i_{c_d} is the corrected current and c_d the surface concentration in this solution.

$$\therefore \frac{i_{c_d/c_d}}{i_{c'/c'}} = \frac{k_1(k_2 + 2Dk_1c_d)}{[k_2 + k_1c_d\ (1+D)]} \frac{(1+D)}{2k_1D}$$

$$= \frac{k_2(1+D) + 2Dk_1c_d(1+D)}{k_2 2D + 2Dk_1c_d\ (1+D)}$$

Consequently if D is a constant, the ratio of i_{d/c_d} / $i_{c'/c'}$ must always lie between 1.0 and $\frac{1+D}{2D}$, the first limit applying when the term in k_1 dominates and the second when that in k_2 dominates. If D is large, therefore, the limits are 1.0 to 0.5 while if D is small the limits are 1.0 to ∞. In practice the ratio changes

from being less than 1.0 to larger than 1.0 which is not possible with this mechanism.

Equation A6 and hence the mechanism (1) + (2a) has been tested by evaluating the rate constants and thence obtaining calculated values for the current due to monomer reduction; these currents have then been compared with the observed currents.

It should be noted, however, that this mechanism is probably only an approximation to the true situation, since it ignores any processes accompanying dimer reduction. If, as is possible, these processes lead to the formation of a surface film they may influence the monomer reduction process. However in the most dilute solution, i_d^d is so low that no significant amount of film is likely to be produced. In the most concentrated solution, since log $i/c_s/$ E is linear over most of the potential range the surface coverage with the layer M-B is always close to unity. Consequently to a first approximation, if this mechanism is correct, the rate equation should give a reasonable fit to the data from 10^{-4} and 10^{-2} M solutions but may be less satisfactory with intermediate concentrations.

The values of the rate constants in the rate equation have been found in the following way.

Evaluation of k_3

In principle, k_3 can be obtained from the concentration dependence of the rate. This assumes that the rate equation is applicable over the whole concentration range which, as discussed above, may not be true.

Rearrangement of Equation A6 gives

$$\frac{nFAk_3c_s^2}{i_c} = c_s + \frac{k_2}{k_1} - \frac{k_2 c_s nFA}{i_c}$$

Designating $\frac{c_s^2}{i} = x$, $c_s = y$ and $\frac{c_s}{i} = z$

then if these quantities have values x_1, y_1, z_1; x_2, y_2, z_2; and x_3, y_3, z_3 at the same potential in three solutions of differing concentration

$$nFAk_3x_1 = y_1 + \frac{k_2}{k_1} - k_2z_1nFA \qquad 8.3$$

$$nFAk_3x_2 = y_2 + \frac{k_2}{k_1} - k_2z_2nFA \qquad 8.4$$

$$nFAk_3x_3 = y_3 + \frac{k_2}{k_1} - k_2z_3nFA \qquad 8.5$$

Subtracting 8.3 from 8.4 and rearranging gives

$$nFAk_3\frac{(x_2 - x_1)}{(z_2 - z_1)} = \frac{(y_2 - y_1)}{(z_2 - z_1)} - k_2nFA \qquad 8.6$$

while from 8.3 and 8.5 we obtain

$$nFAk_3\frac{(x_3 - x_1)}{(z_3 - z_1)} = \frac{(y_3 - y_1)}{(z_3 - z_1)} - k_2nFA \qquad 8.7$$

Subtracting 8.6 from 8.7 and rearranging gives

$$nFAk_3 = \frac{\left(\frac{y_3 - y_1}{z_3 - z_1}\right) - \left(\frac{y_2 - y_1}{z_2 - z_1}\right)}{\left(\frac{x_3 - x_1}{z_3 - z_1}\right) - \left(\frac{x_2 - x_1}{z_2 - z_1}\right)}$$

so that k_3 may be calculated at chosen potentials.

Such a calculation can be very sensitive to the experimental results. In order to avoid large errors, if the actual results did not fall on the linear plots for log i_c/log c_s, values falling on the line were used. The calculated values of k_3^* (= $nFAk_3$) corresponding to 0.5 M H_2SO_4 and 0.25 M H_2SO_4, 0.25 M Na_2SO_4 as background electrolytes, are shown as a function of potential in Fig. 8.33 and listed in Table 8.2. The values of k_3^* (Table 8.2) obtained at the more negative potentials are in accord with those obtained by assuming that at sufficiently negative potentials in the most concentrated solution, $i_c = k_3 c_s$ (see Appendix 2).

Since k_3^* is probably linearly dependent on potential, the values employed in evaluating k_1 and k_2 were those from the best straight line through the points in Fig. 8.33.

Evaluation of k_1

As shown in Appendix 2, k_1 is most important in determining the rate of reaction when θ is small, that is in dilute solutions and especially at positive potentials. Consequently only the results obtained in the most dilute solution have been employed in this calculation and greatest weight has been given to those obtained at the more positive potentials. Smoothed results (i.e. those lying on or interpolated from a linear log i_c against log c_s plot) have again been used.

TABLE 8.2

E	0.5 M H_2SO_4		0.25 M H_2SO_4 + 0.25 M Na_2SO_4	
	k_1'	$k_3^{\ddagger}$	k_1'	$k_3^{\ddagger}$
	(Amp cm^3 $mole^{-1}$)	(Amp cm^3 $mole^{-1}$)	(Amp cm^3 $mole^{-1}$)	(Amp cm^3 $mole^{-1}$)
0.7		103		40
0.6	25.5	166	10.3	65
0.5	76.0	270	37.5	105
0.4	225	435	110.3	170
0.3	670	700	340	270
0.2	2,050	1,120	1,040	440
0.1	6,000	1,810	3,150	710
0.0	18,000	2,930	9,600	1,150
-0.1	54,000	4,700	2,900	1,890
-0.2	155,000	7,600	88,000	3,000

The procedure employed is described in Appendix 3a. It is based on the assumption that $nFAk_1 = k_1^{\ddagger} \exp -\frac{\alpha n_a FE}{RT}$, where $k_1^{\ddagger}$ is independent of potential.

By the use of difference equations, the expression (Equation A17)

$$\exp - 2\ \alpha n_a f\Delta E \ + \ \frac{M}{L} \ = (\exp - \alpha n_a f\Delta E)\ \frac{N}{L}$$

is derived from the rate equation. In the above expression, L, M and N are functions of $k_3^{\ddagger}$, c_T, i_c and i_d^m ($= i_d - i_d^d$), while ΔE is some chosen potential interval (200 mV). When the values of M/L and N/L corresponding to different values of the electrode potential are plotted against one another, a graph of slope $\exp -\alpha n_a f\Delta E$ and intercept, when N/L = 0 equal to $-\exp -2\alpha n_a f\Delta E$ should be obtained. The resulting graphs for the two background electrolytes (0.5 M H_2SO_4 and 0.25 M H_2SO_4/0.25 M Na_2SO_4) satisfied this criterion; that obtained in 0.5 M H_2SO_4 is shown in Fig. 8.34. The values of αn_a may be obtained from these graphs; they were

αn_a = 0.278 in 0.5 M H_2SO_4 and

αn_a = 0.289 in 0.25 M H_2SO_4/0.25 M Na_2SO_4

These values of αn_a were then confirmed and $k_1^{\ddagger}$ determined by the procedure described in Appendix 3b. This involved using the expression

$$\log \frac{L}{X} = \log \frac{i_d}{c_T k_1^{\ddagger}} + \frac{\alpha n_a fE}{2.303} \qquad \text{A18}$$

where X depends on the same variables as L but is also dependent on exp $-\alpha n_a f \Delta E$. According to Equation 18, a graph of log L/X against E (the electrode potential) should be linear with slope equal to $\alpha n_a f/2.303$ and when E = 0.0 V, $L/X = i_d/c_T k_1^{\ddagger}$. The graphs obtained for the two background electrolytes are shown in Fig. 8.35. They are satisfactorily linear and give αn_a values in good agreement with those reported above. The actual values of αn_a and $k_1^{\ddagger}$ obtained were:

$\alpha n_a = 0.279$, $k_1^{\ddagger} = 17,705$ (Amp cm^3 $mole^{-1}$) in 0.5 M H_2SO_4, and

$\alpha n_a = 0.289$, $k_1^{\ddagger} = 9,636$ (Amp cm^3 $mole^{-1}$) in 0.25 M H_2SO_4/0.25 M Na_2SO_4.

The values of $nFAk_1 = k_1' = k_1^{\ddagger} \exp -\alpha n_a fE$ have also been calculated, using Equation A18, rearranged into

$$k_1' = k_1^{\ddagger} \exp -\alpha n_a fE = i_d X/c_T L.$$

The values obtained are reported in Table 8.2 and plotted as a function of potential in Fig. 8.33.

Evaluation of k_2

This constant has again been obtained from the results for the 1×10^{-4} M CrVI solution.

From Equation 8.3, when only one solution is involved,

$$nFAk_3 x = y + \frac{k_2}{k_1} - k_2 znFA$$

$$\therefore \quad nFAk_2 \left(\frac{1}{k_1'} - z\right) = k_3^{\ast} x - y$$

$$\therefore \quad nFAk_2 = \frac{(k_3^{\ast} x - y)}{\left(\frac{1}{k_1'} - z\right)} = \frac{A}{B}$$

The value of $k_2^{\ast} = nFAk_2$ was calculated at each of a number of potentials using this equation.

$k_2^{\ast}$ is found to be $\sim (3 \pm 0.3) \times 10^{-5}$ Amp (0.5 M H_2SO_4) and $\sim (4 \pm 0.3) \times 10^{-5}$ (0.25 M H_2SO_4/0.25 M Na_2SO_4.

We now know values of $k_1' = nFAk_1$, $k_2^{\ast} = nFAk_2$ and $k_3^{\ast} = nFAk_3$

since
$$\frac{i_c}{nFA} = \frac{k_1 c_s (k_2 + k_3 c_s)}{k_1 c_s + k_2}$$

$$i_c = \frac{nFAk_1 c_s (k_2 + k_3 c_s) nFA}{(k_1 c_s + k_2) nFA} = \frac{k_1' c_s (k_2^{\ast} + k_3^{\ast} c_s)}{k_1' c_s + k_2^{\ast}} \qquad 8.8$$

and also
$$c_s = \frac{(i_d^m - i_c)}{i_d} c_T \qquad 8.9$$

it is therefore possible to obtain theoretical values of the current due to monomer reduction and to test for the fit of theory to the results.

<u>Calculation of theoretical i_c values</u>

Rearranging Equation 8.8 gives

$$c_s + \frac{k_2^{\ast}}{k_1'} = \frac{k_2^{\ast} c_s}{i_c} + \frac{k_3^{\ast} c_s^2}{i_c}$$

and substituting from 8.9 for c_s produces

$$\frac{(i_d^m - i_c)}{i_d} c_T + \frac{k_2^*}{k_1'} = \frac{k_2^*}{i_c} \frac{(i_d^m - i_c)}{i_d} c_T + \frac{k_3^*}{i_c} \frac{(i_d^m - i_c)^2}{i_d} c_T^2$$

multiplying by i_d/c_T and rearranging gives

$$i_c^2 \frac{(1+k_3^* c_T)}{i_d} - i_c \left(\frac{2k_3^* c_T i_d^m}{i_d} + \frac{k_2^* i_d}{k_1' c_T} + k_2^* + i_d^m\right) + \frac{k_3^* c_T}{i_d} \times (i_d^m)^2 + k_2^* i_d^m = 0$$

i.e. $G\, i_c^2 - H\, i_c + K = 0$

where $G = 1 + \frac{k_3^* c_T}{i_d}$, $H = \left(\frac{2k_3^* c_T i_d^m}{i_d} + \frac{k_2^* i_d}{k_1' c_T} + k_2^* + i_d^m\right)$

and $K = \frac{k_3^* c_T}{i_d} (i_d^m)^2 + k_2^* i_d^m$ $\therefore$ $i_c = \frac{H \pm \sqrt{H^2 - 4GK}}{2G}$.

The theoretical values of i_c and i_c/c_s have been calculated in 0.5 M H_2SO_4 and 0.25 M H_2SO_4/0.25 M Na_2SO_4 backgrounds for 10^{-2} M and 10^{-4} M CrVI solutions. The lines in Figs. 8.31 and 8.32 correspond to these theoretical values of i_c/c_s.

The observed and calculated values of i_c/c_s vary with potential in a similar manner, and the agreement between the values is excellent, particularly in 0.25 M H_2SO_4/0.25 M Na_2SO_4. Serious discrepancies occur only in the 0.5 M H_2SO_4

(a) at the most negative potentials in 10^{-4} M CrVI, where the observed current may be enhanced by hydrogen evolution

(b) in 10^{-2} M CrVI at potentials more positive than 0.3 V.

The shape of the observed log $^{i}c/_{c_s}$ /E curve in 10^{-2} M Cr in 0.5 M H_2SO_4 at potentials more positive than 0.3 V is worthy of comment since a bump or inflexion is observed. This could indicate that the monomers are not all reduced as one species; one monomer being reduced at positive potentials and its rate of reduction becoming diffusion limited in the neighbourhood of 0.5 V. As shown by Table 1 (Appendix 1), however, the ratio of the concentrations of all the monomers to the total concentration of CrVI, increase as the concentration of CrVI is decreased, whereas the relative size of this bump (w.r.t. the actual values of $^{i}c/_{c_s}$) decreased as the concentration of CrVI was decreased. The cause of this bump is therefore not clear at present.

8.8.4 <u>Dependence of reaction rate on the composition of the background electrolyte</u>

As may be seen from Table 8.2 the values of both k_1' and k_3^* were larger at a given potential in 0.5 M H_2SO_4 than in 0.25 M H_2SO_4/0.25 M H_2SO_4; k_2^* was however rather smaller in the former than in the latter solution. Since the concentrations of a number of ions differ significantly between these two solutions, the cause of these changes in the rate constants is not obvious.

In an attempt to clarify this situation, measurements were also made in solutions of 0.05 M H_2SO_4, 0.45 M Na_2SO_4 and 0.025 M H_2SO_4, 0.45 M Na_2SO_4. Only the concentrations of H^+ and HSO_4^- alter significantly between these two solutions. Unfortunately, however, as described in Section 8.8, the results obtained with the more concentrated CrVI solutions in these background electrolytes suggested that the final current was partially limited by the rate of supply of hydrogen ions to the electrode. A complete analysis of these results to obtain the various rate constants was therefore not conducted. As shown in Fig. 8.36, however, the current-potential curves obtained using 10^{-4} M CrVI in these two background electrolytes have essentially the same form as observed in the other solutions. These curves show that over almost the whole potential range studied the order of reaction with respect to H_2SO_4 is close to unity.

To account for this result it must be assumed that hydrogen ions and/or bisulphate ions take part in each of the steps involved in the mechanism (1) + (2a). Thus, assuming that the hydrogen ion is the important species, the mechanism becomes

$$A + H^+ + M + ne \xrightarrow{k_1} M\text{-}B$$

$$M\text{-}B + H^+ \xrightarrow{k_2'} M + \text{Products}$$

$$A + H^+ + M\text{-}B + ne \xrightarrow{k_3} M\text{-}B + \text{Products}$$

when the resulting rate equation is

$$\frac{i}{nFA} = \frac{k_1 c_s [H^+] (k_2 + k_3 c_s)}{k_1 c_s + k_2}$$

as required.

Since, in spite of the increase in sulphuric acid concentration, $k_2^{\ddagger}$ was rather smaller in 0.5 M H_2SO_4 than in 0.25 M H_2SO_4/0.25 M Na_2SO_4, it must also be concluded that sulphate ions are involved in at least the second step in the above mechanism.

The proposed mechanism has a number of features in common with the mechanisms suggested (for a gold electrode) by previous workers. Thus as is generally agreed it is postulated that a film is formed on the electrode surface as a consequence of the reduction reaction. This film may participate in the reaction as suggested by Reinkowski and Knorr[1.16] and Gerischer and Käppel[1.15], if the third step in the above process is more complex than that considered. As proposed by Feigl and Knorr[1.13,1.20] it is probable that removal of this film (by the second step above) is promoted by both hydrogen ions and sulphate ions.

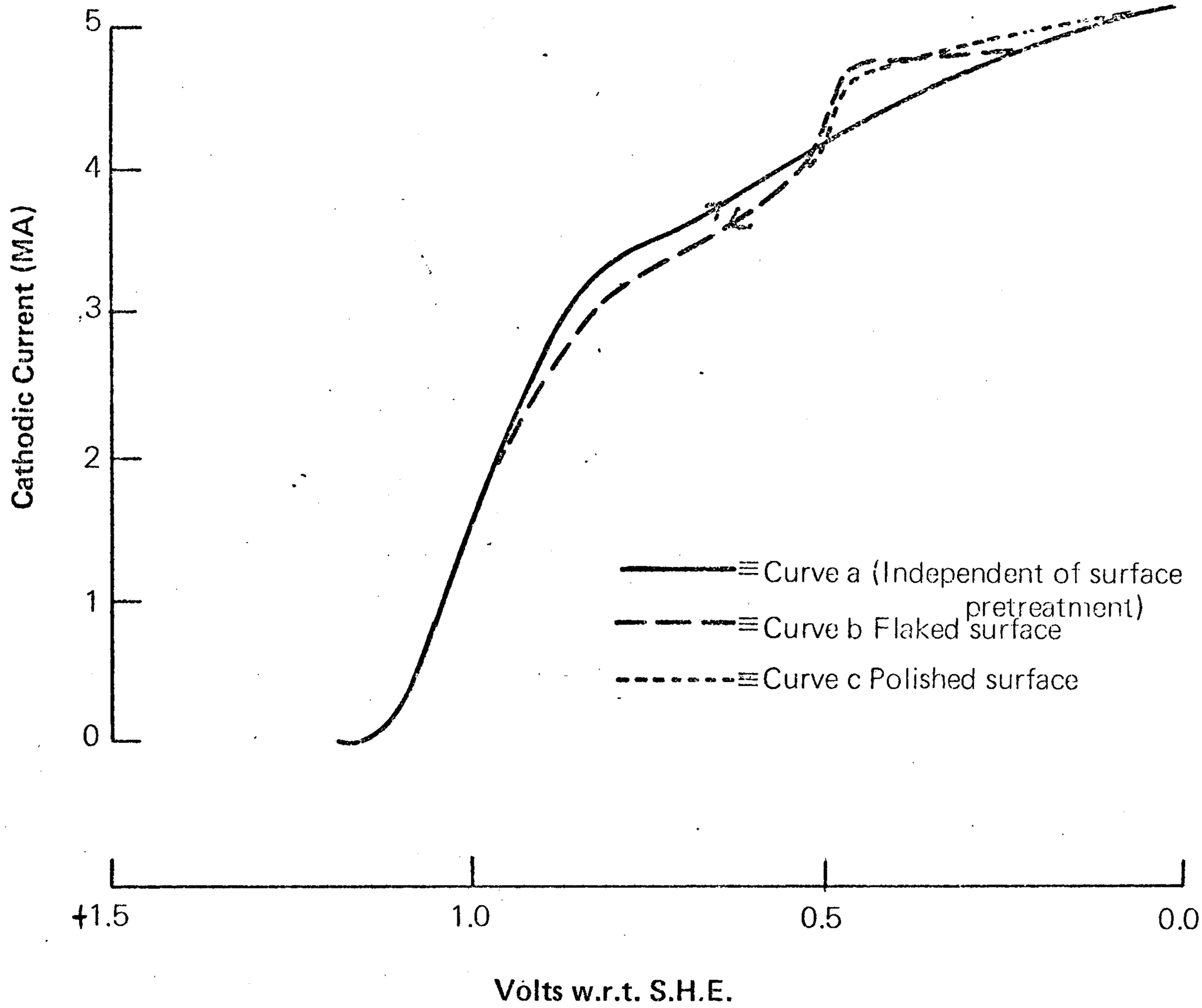

Fig. 8.1

CURRENT-POTENTIAL RELATION, P.G. ELECTRODE, 1 x 10^{-2}M CrVI, IM $HClO_4$, 1000 rpm

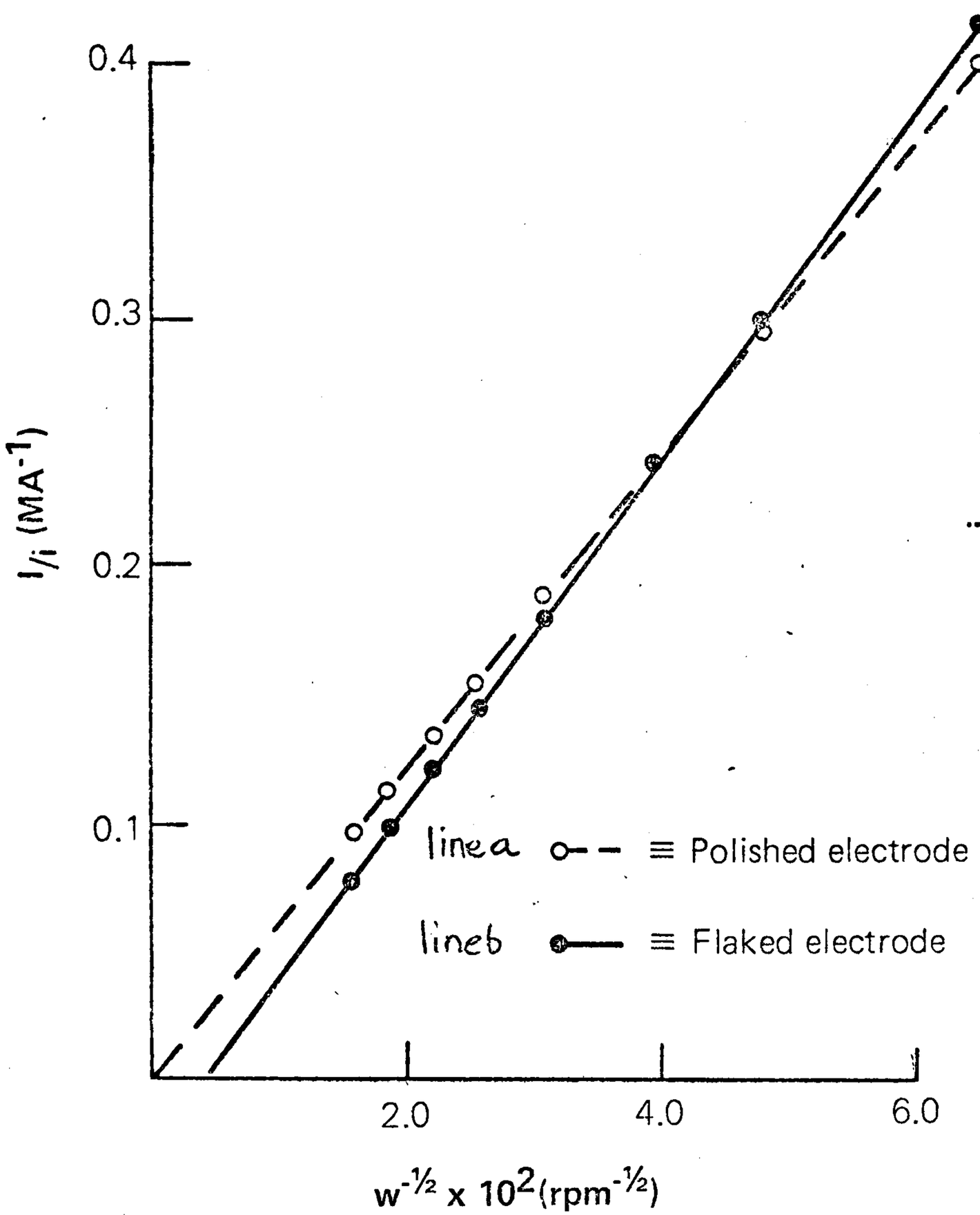

Fig. 8.2

PLOT OF I/i / $I_{w^{½}}$, P.G. ELECTRODE, 1x10-2 M Cr VI IM $HClO_4$

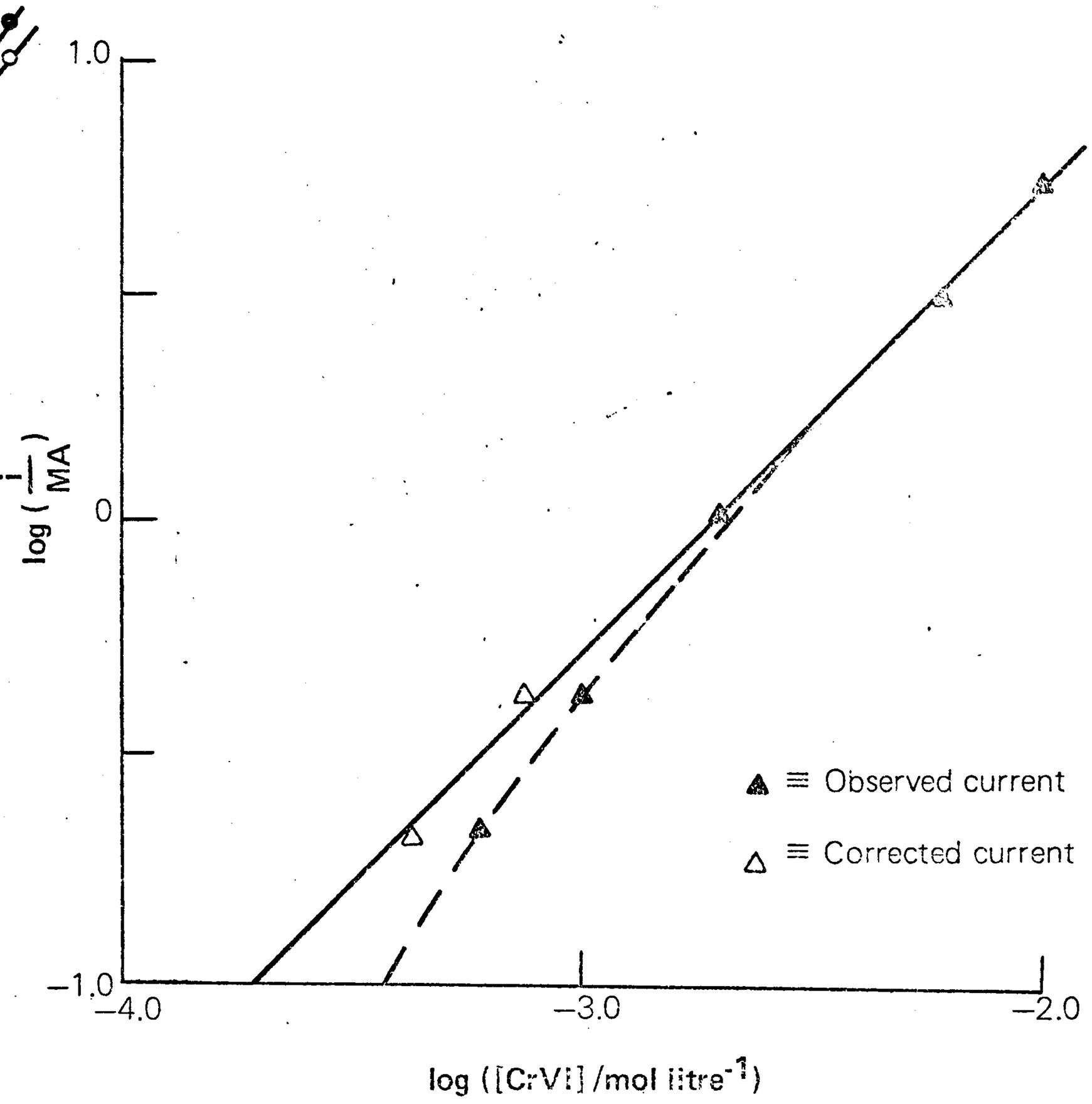

Fig. 8.3

REACTION ORDER P.G. ELECTRODE, IM $HClO_4$

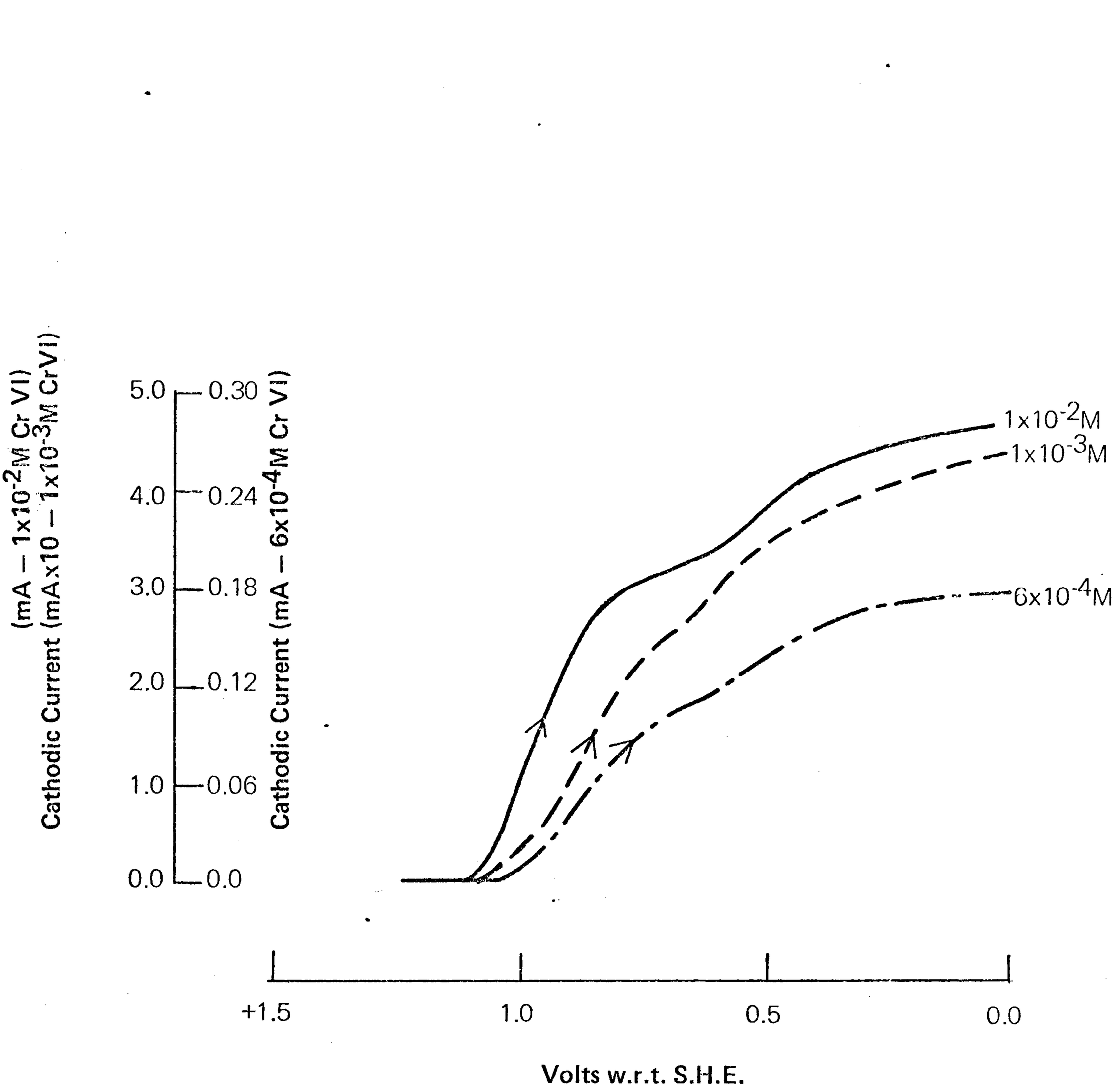

Fig. 8.4

CURRENT-POTENTIAL RELATION, POLISHED P.G. ELECTRODE, IM $HClO_4$, 1000 rpm, 10 $mVsec^{-1}$ (negative going sweep)

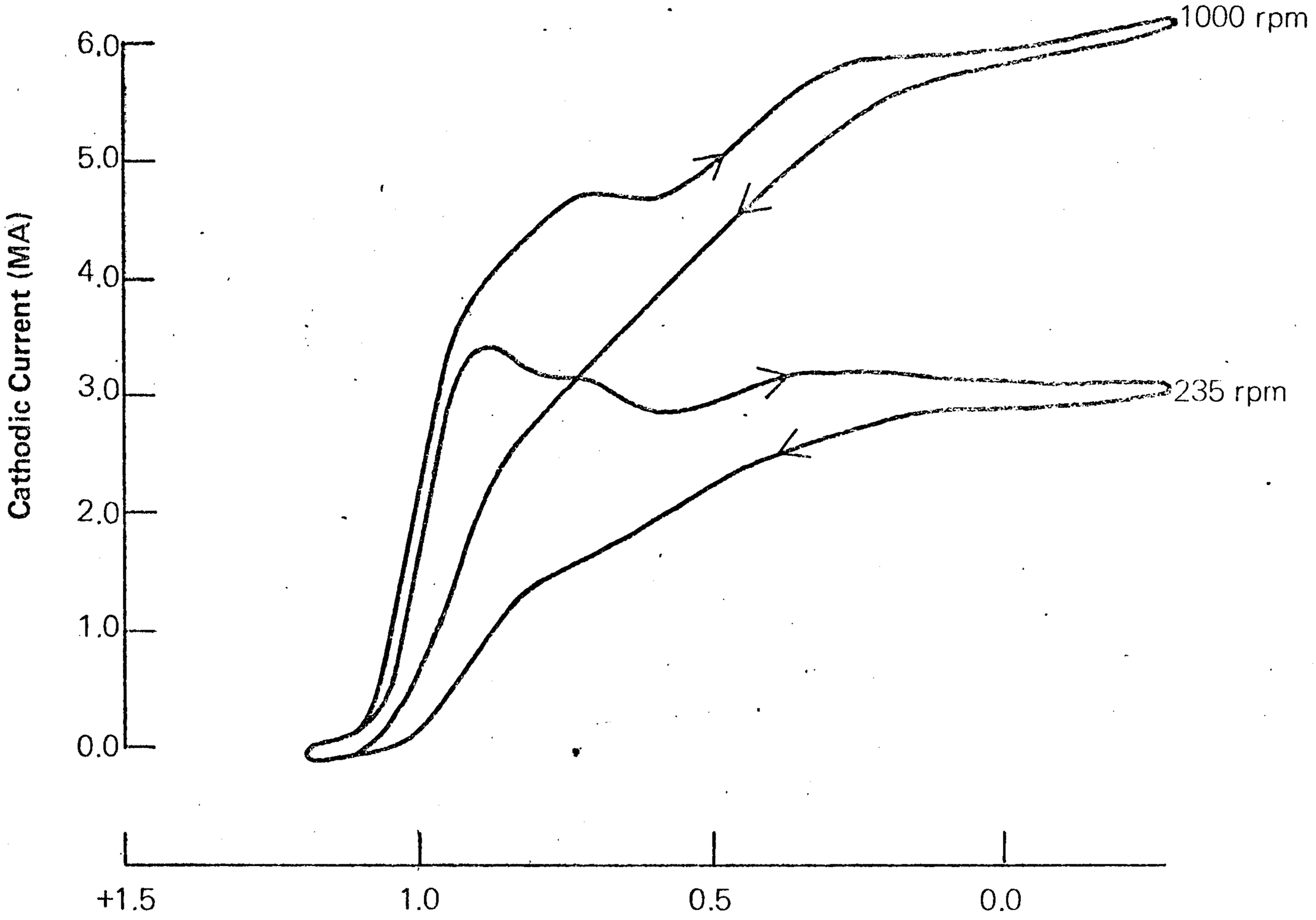

Fig. 8.5

CURRENT-POTENTIAL RELATION, POLISHED P.G. ELECTRODE, 1×10^{-2} M CrVI, IM $HClO_4$, 100mV sec^{-1}

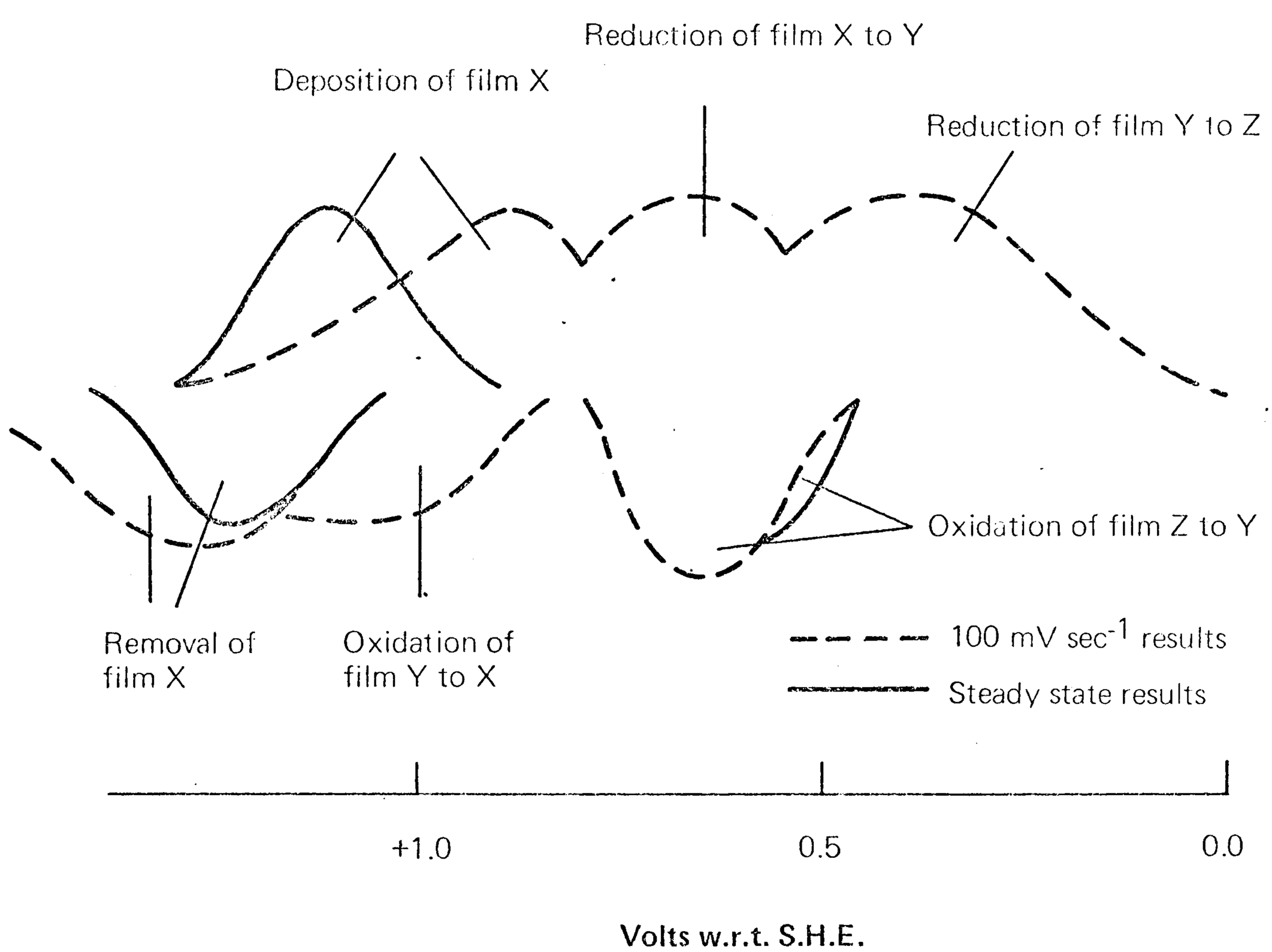

Fig. 8.6

DIAGRAMMATIC REPRESENTATION POTENTIALS OF FILM FORMATION AND MODIFICATION ON P.G. SURFACE IN 1 x 10^{-2}M CrVI, IM $HClO_4$

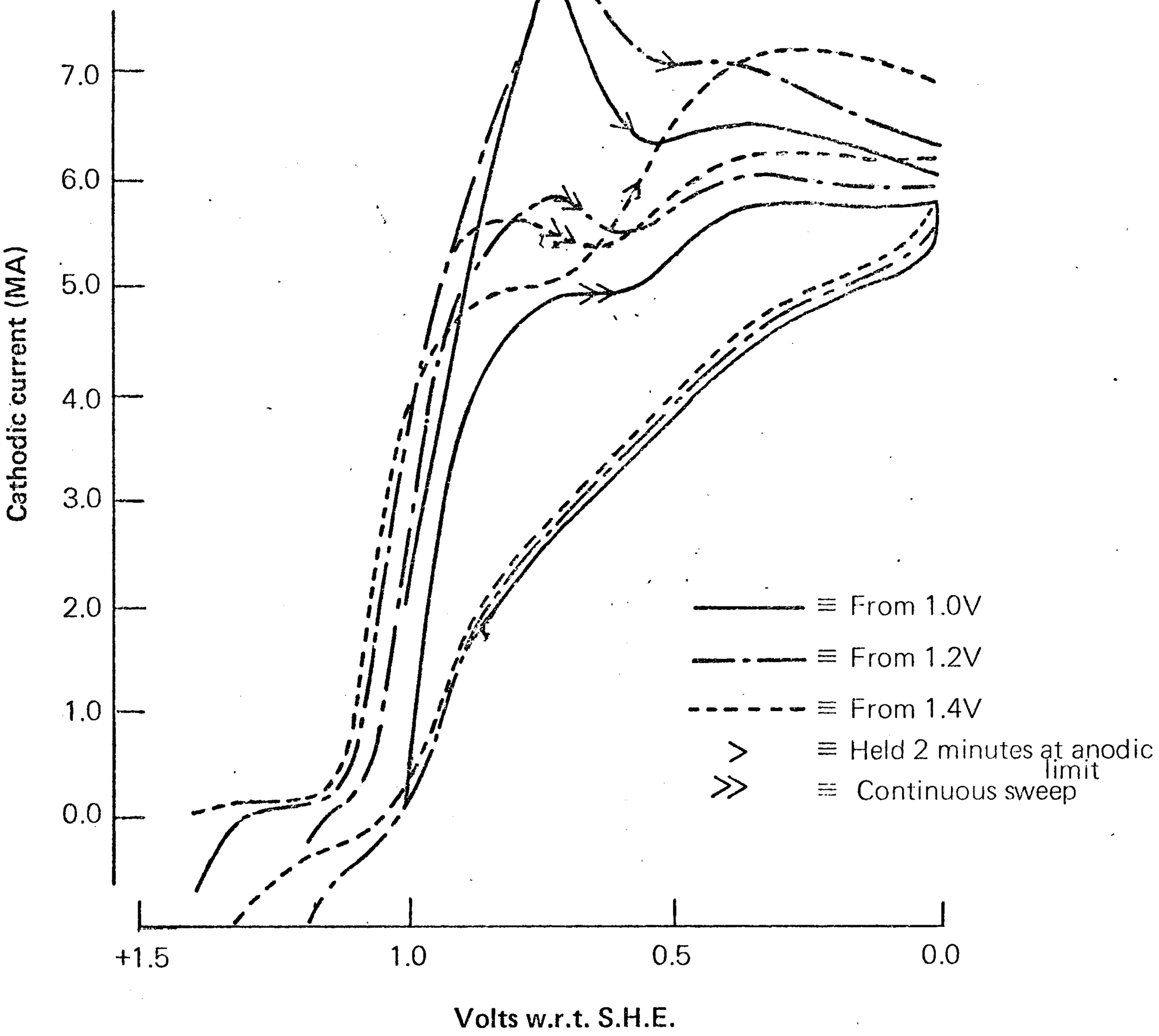

Fig. 8.7

CURRENT-POTENTIAL RELATION, POLISHED P.G. ELECTRODE, 1×10^{-2}M CrVI, IM $HClO_4$, 1000 rpm, 100 mV sec^{-1}

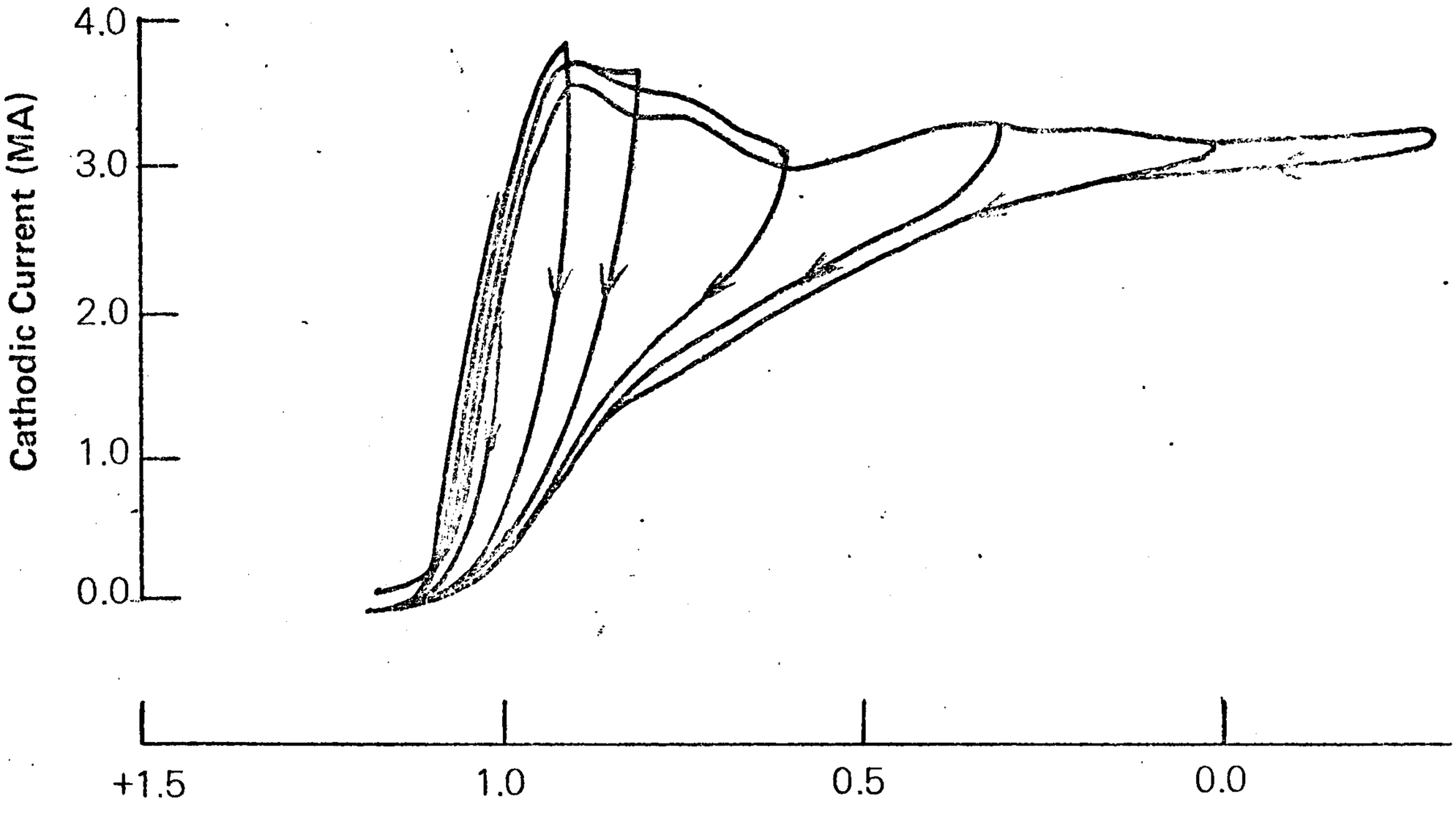

Fig. 8.8

CURRENT-POTENTIAL RELATION POLISHED P.G. ELECTRODE, 1×10^{-2}M CrVI, IM $HClO_4$, 235 rpm, 100 mV sec^{-1} EFFECT OF SWEEPING PROGRESSIVELY TO MORE NEGATIVE LIMITS

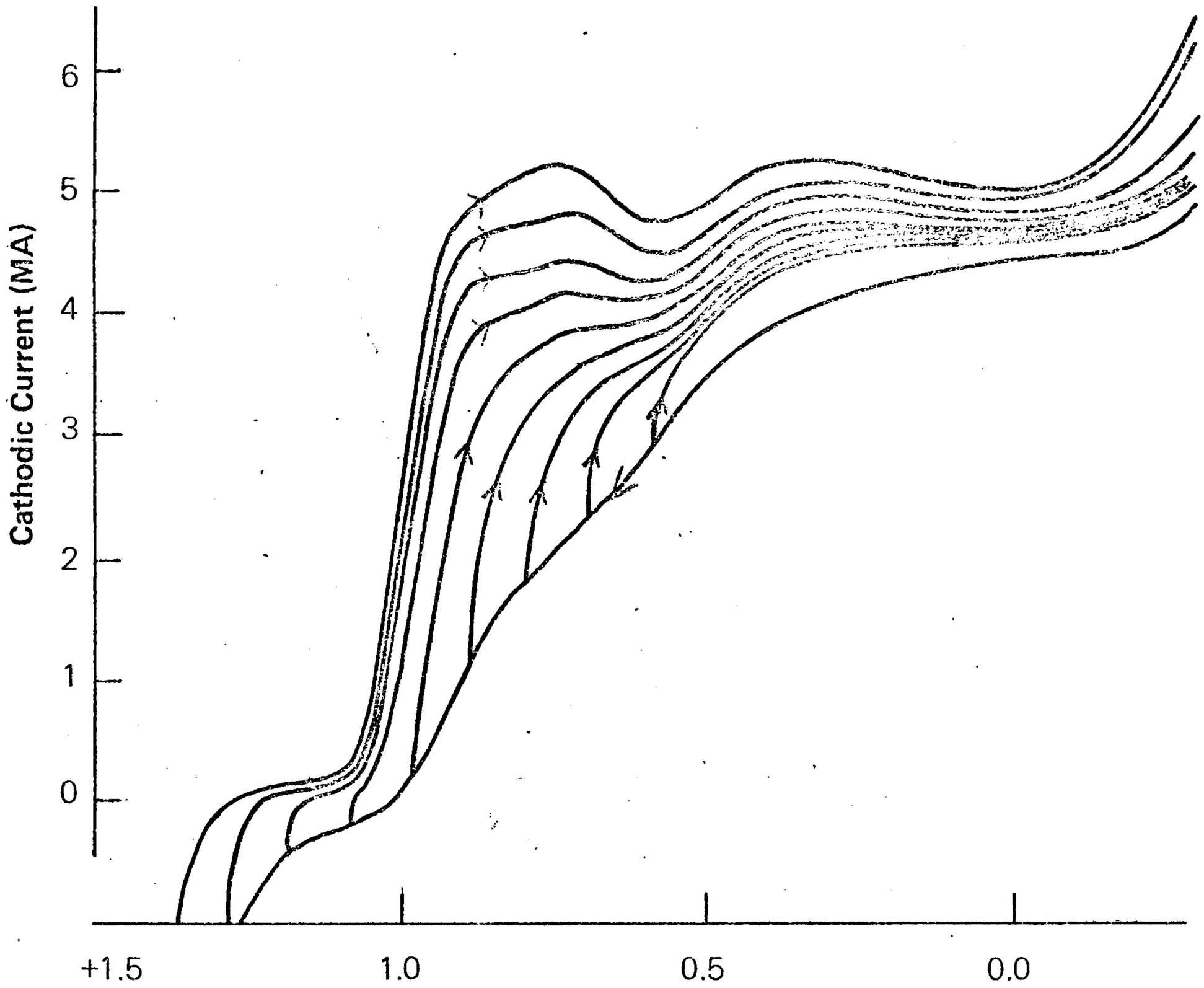

Fig. 8.9

CURRENT-POTENTIAL RELATION POLISHED P.G. ELECTRODE, $1x10^{-2}$M CrVI, IM $HClO_4$, 1000 rpm, 100 mV sec^{-1} EFFECT OF SWEEPING PROGRESSIVELY TO MORE POSITIVE POTENTIALS

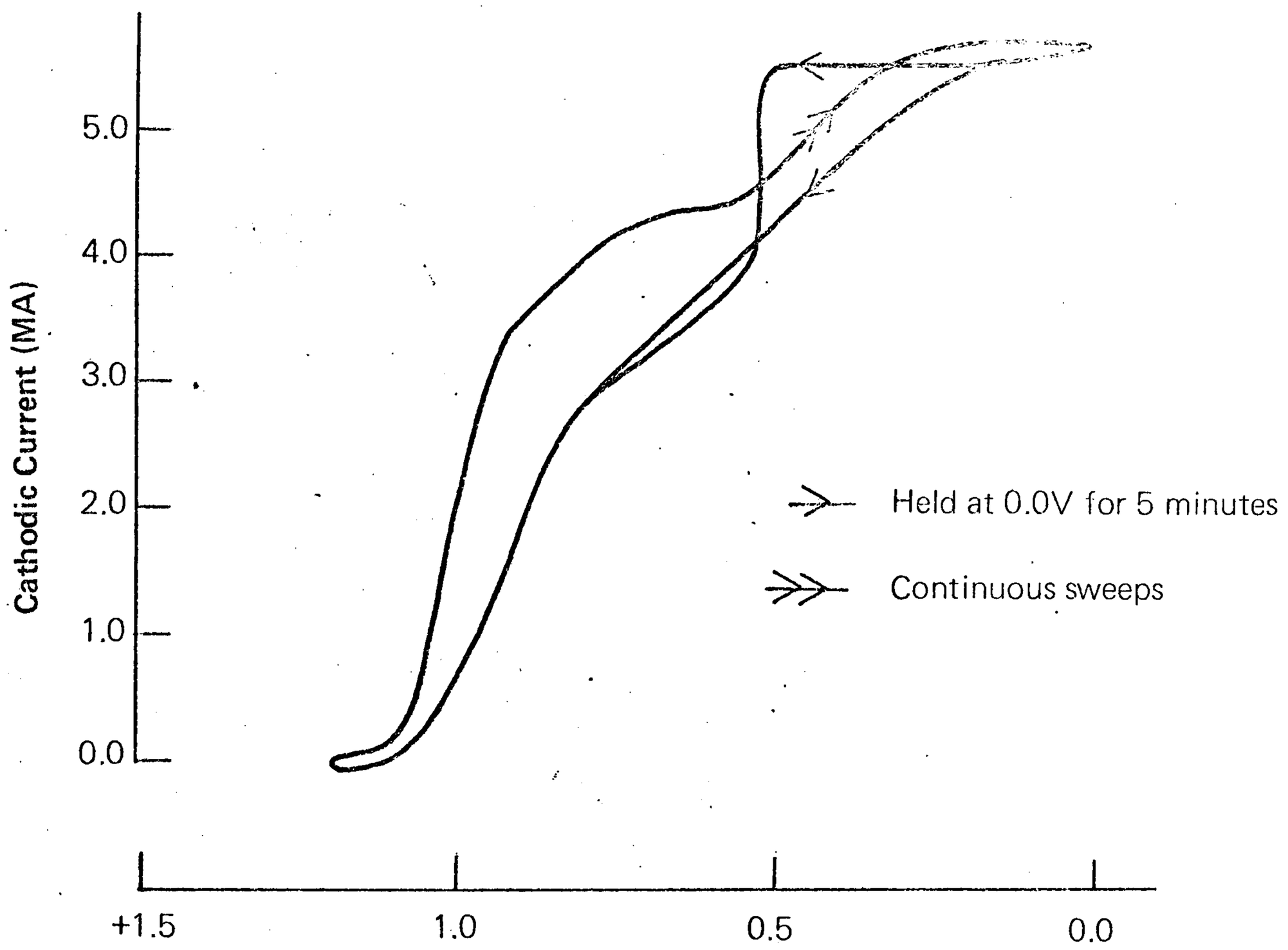

Fig. 8.10

CURRENT-POTENTIAL RELATION, POLISHED P.G. ELECTRODE, 1×10^{-2}M CrVI, IM $HClO_4$, 1000 rpm, 100mV sec^{-1}

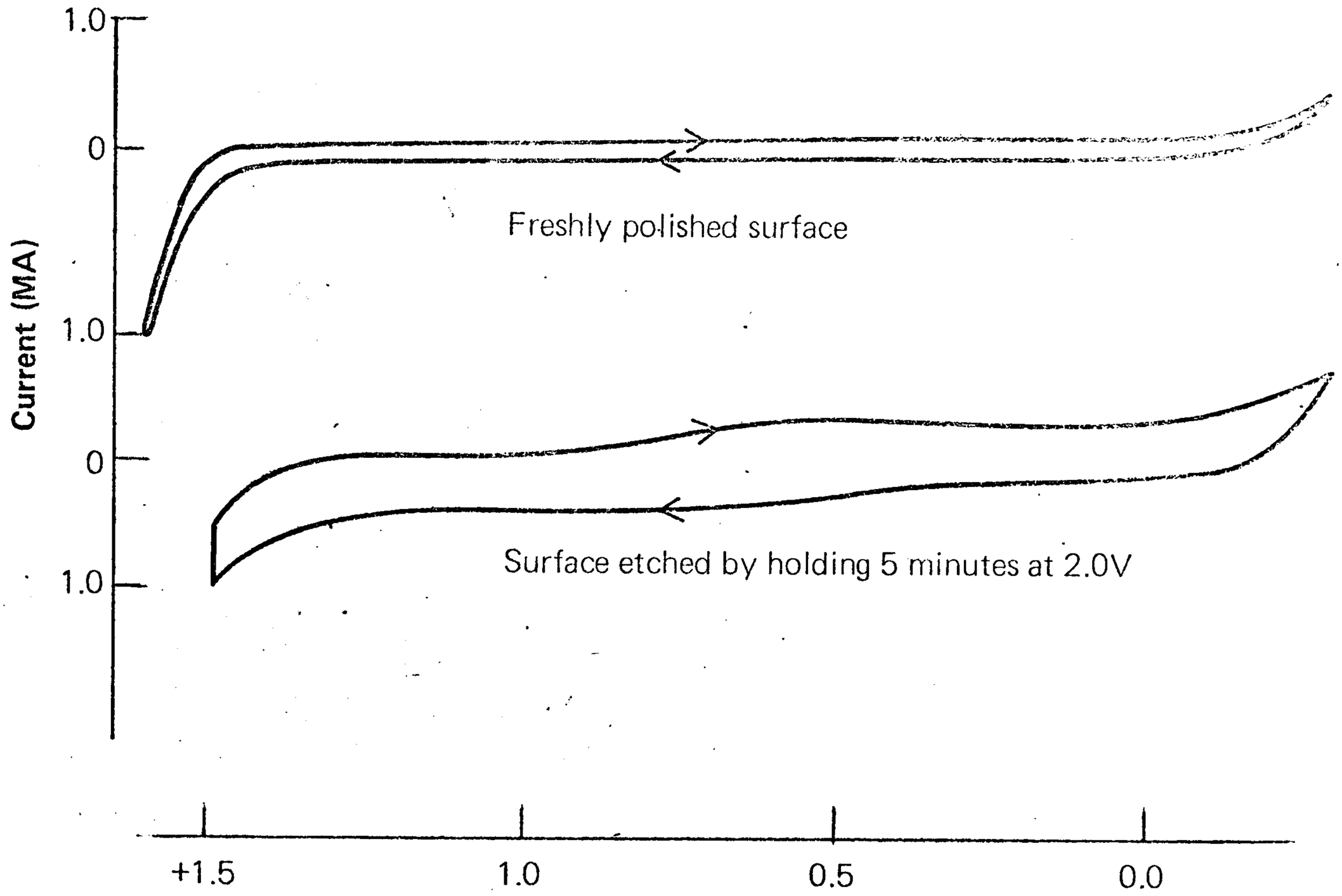

Fig. 8.11

CURRENT-POTENTIAL RELATION, P.G. ELECTRODE, IM $HClO_4$, 1000 rpm, 100 mV sec^{-1}

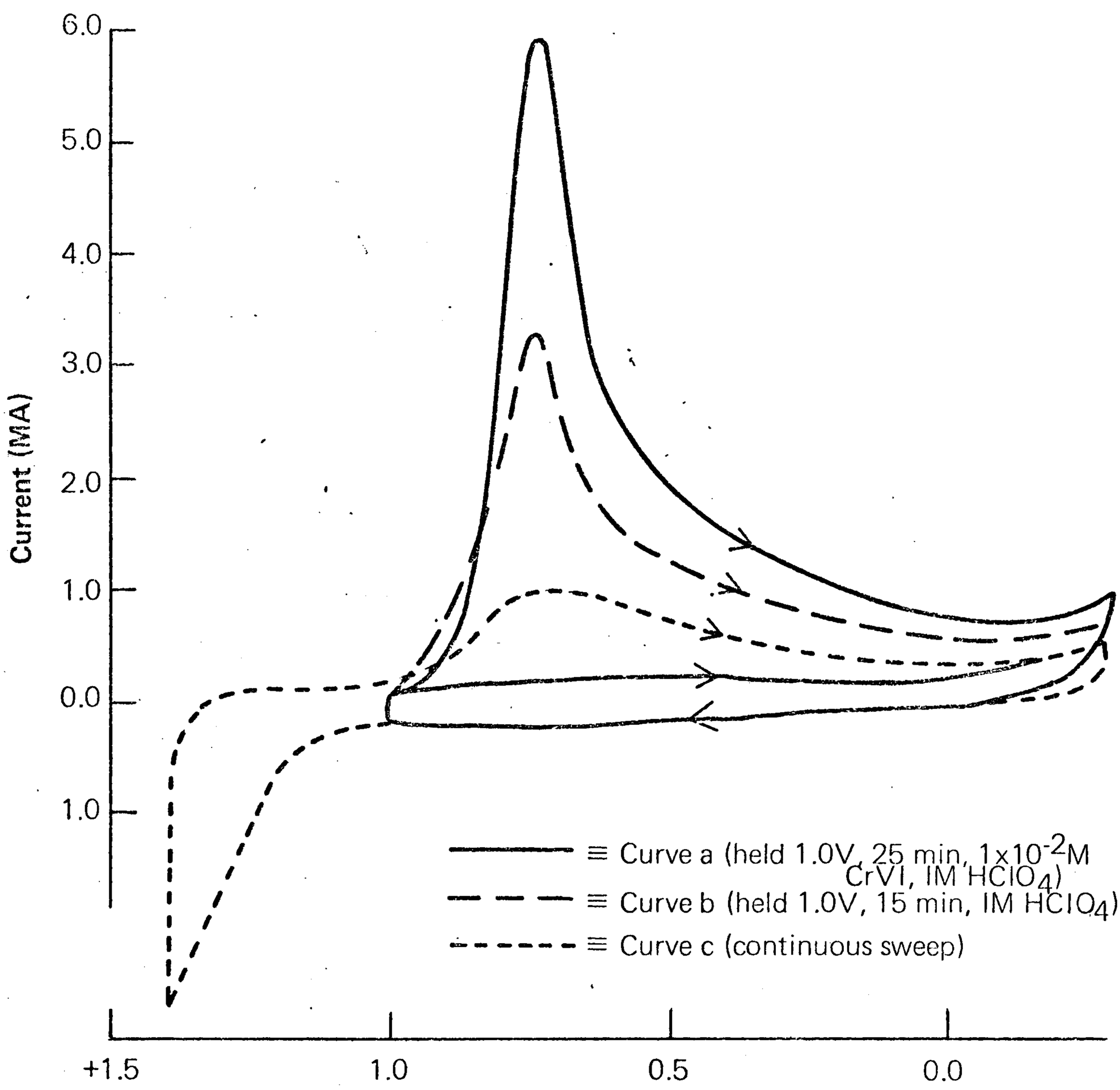

Fig. 8.12

CURRENT-POTENTIAL RELATION, POLISHED P.G. ELECTRODE, IM $HClO_4$, 1000 rpm, 100 mV sec^{-1}

Fig. 8.13

CURRENT-POTENTIAL RELATION, POLISHED P.G. ELECTRODE, IM $HClO_4$, NO ROTATION, 100mV sec^{-1}

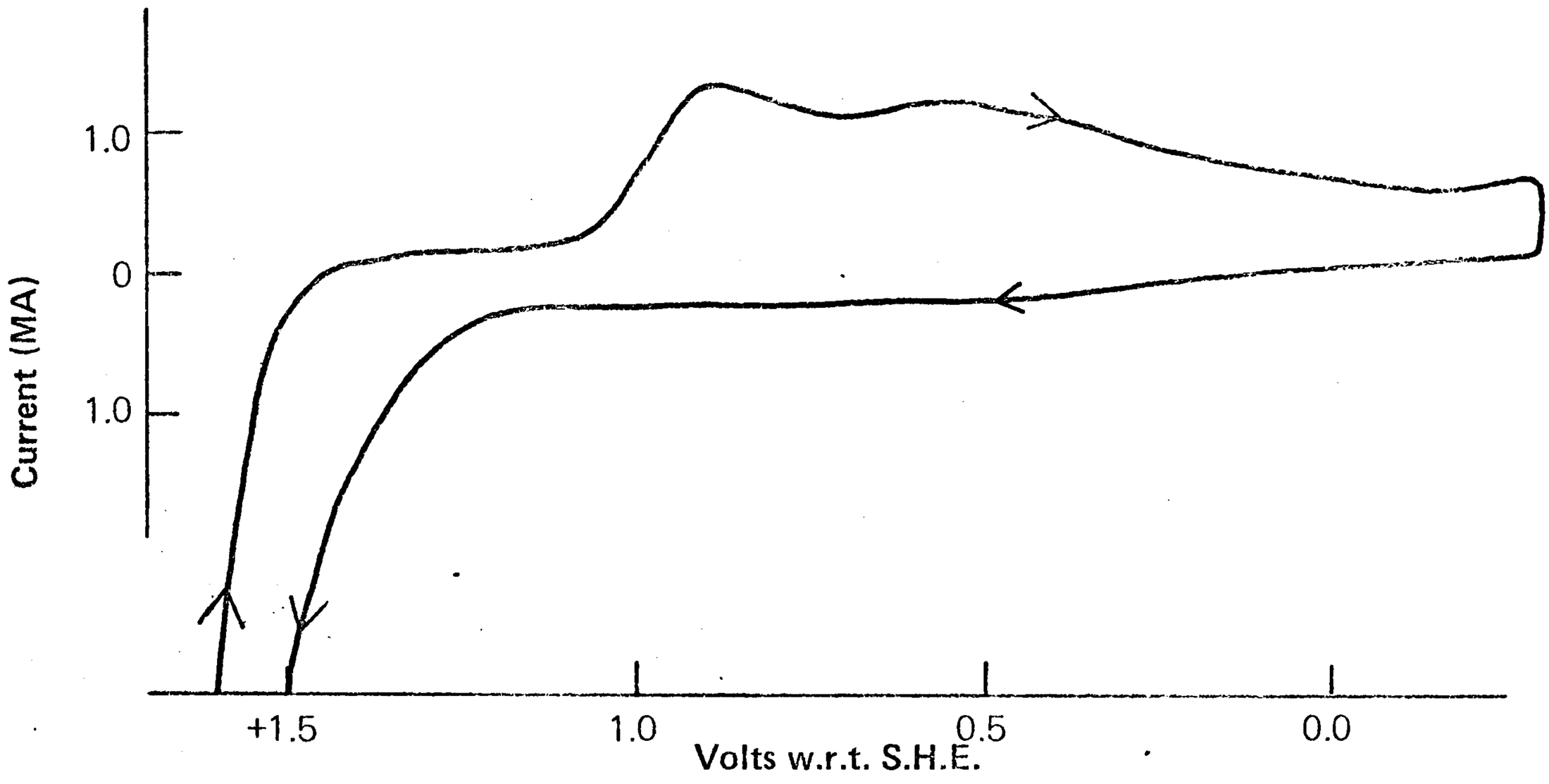

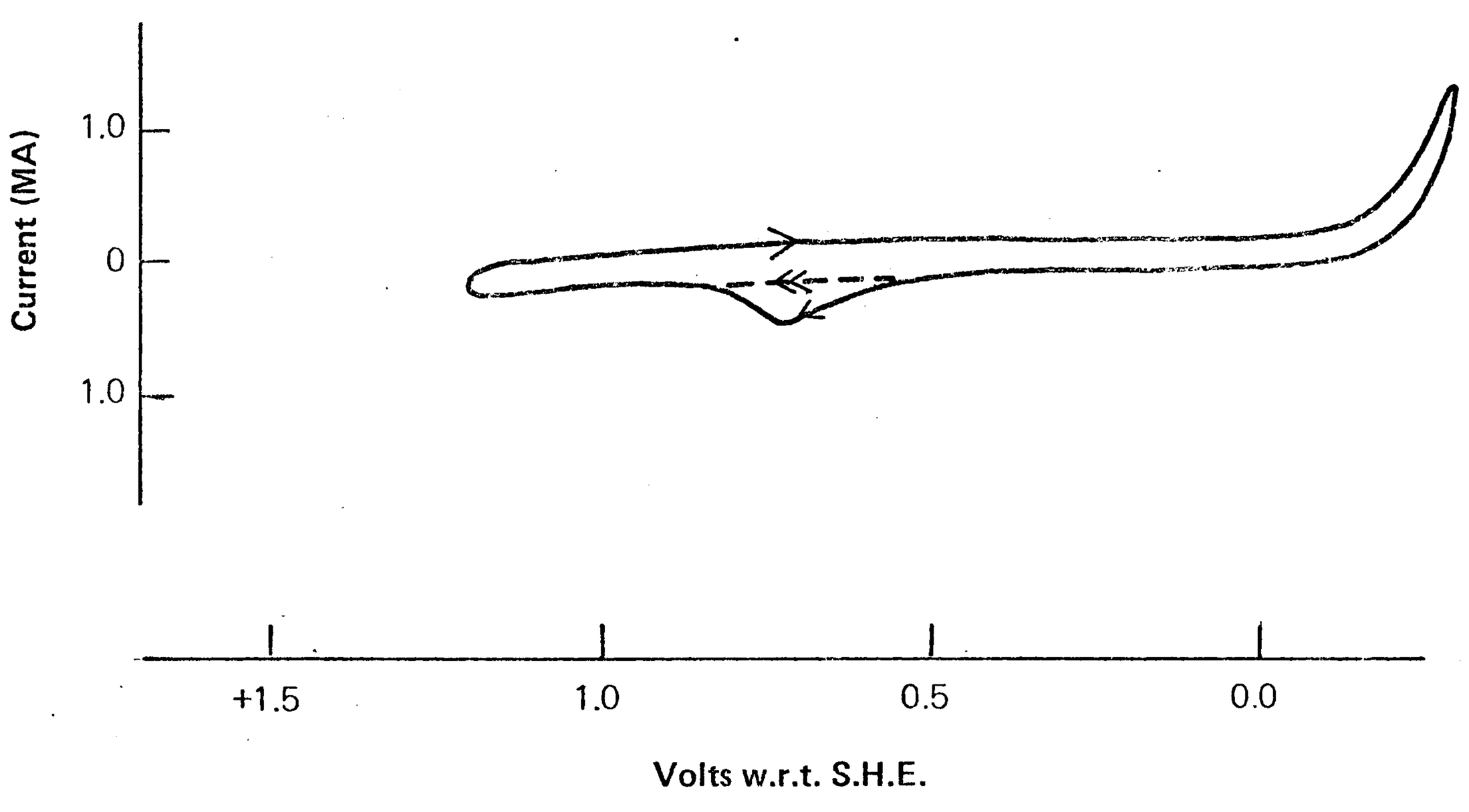

Fig. 8.14

CURRENT-POTENTIAL RELATION, POLISHED P.G. ELECTRODE, IM $HClO_4$, 1000 rpm, 100 mV sec^{-1}

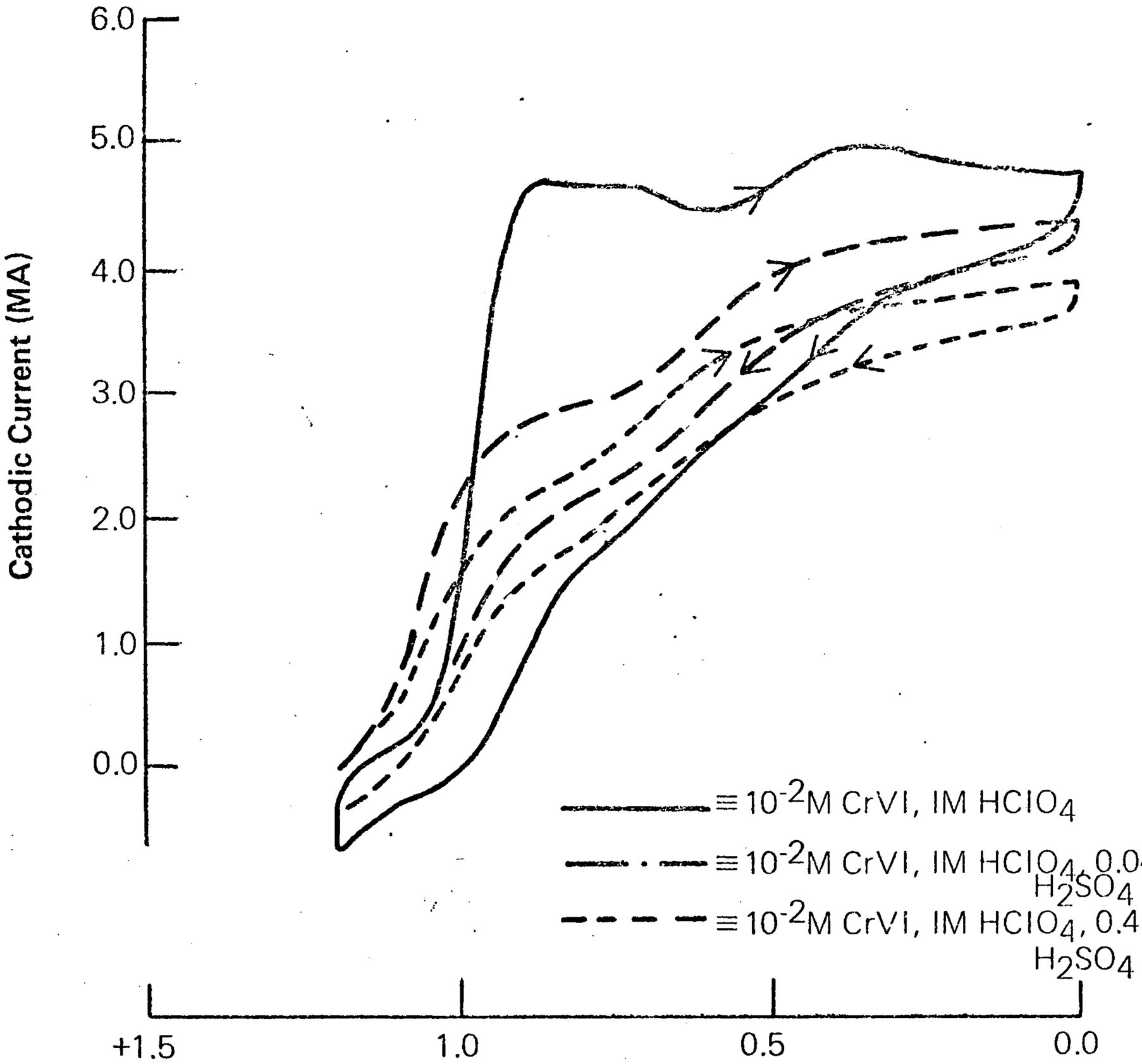

Fig. 8.15

CURRENT-POTENTIAL RELATION, POLISHED P.G. ELECTRODE, $1x10^{-2}$M CrVI, IM $HClO_4$, 1000 rpm, 100 mV sec^{-1}

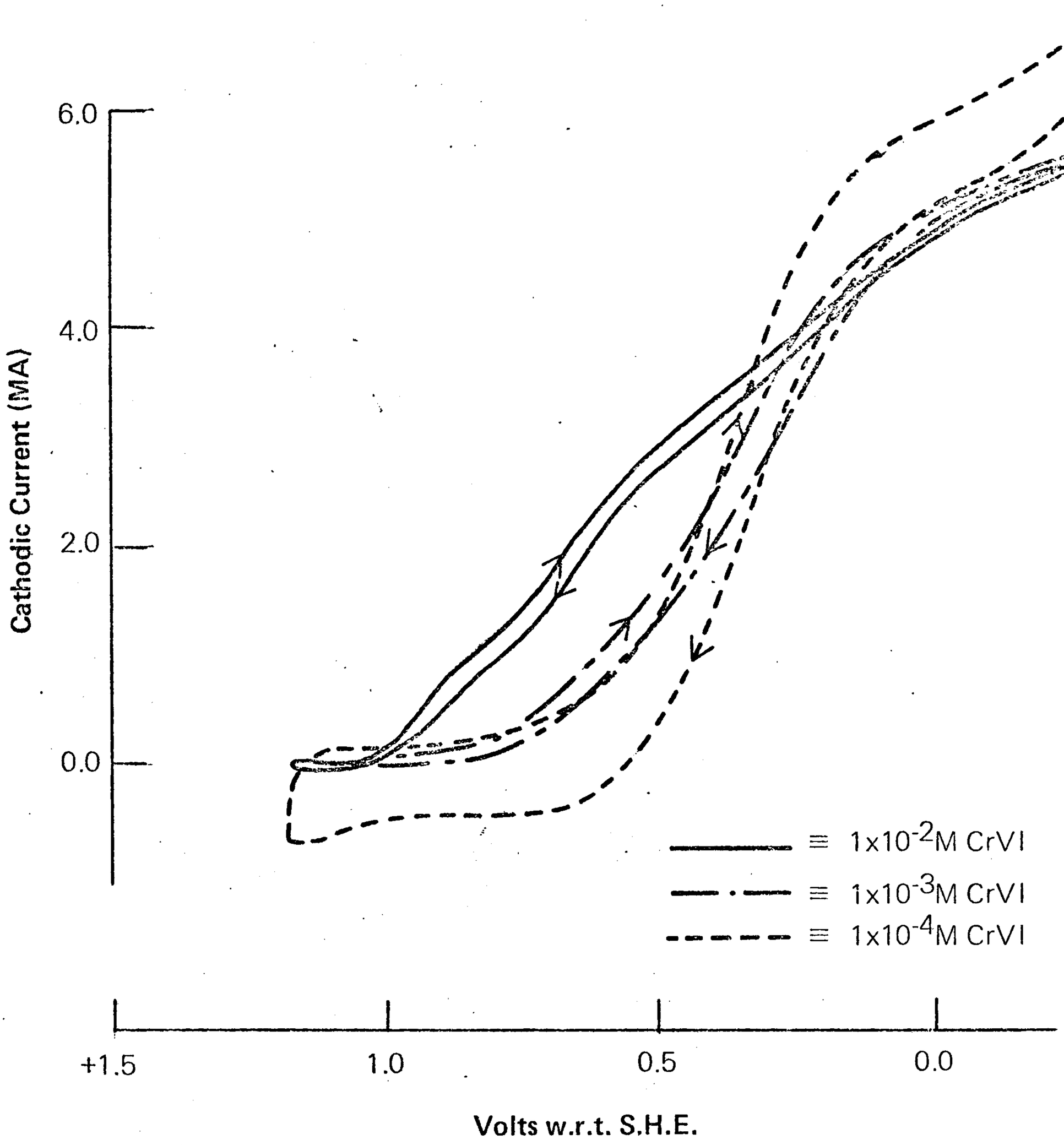

Fig. 8.16

CURRENT-POTENTIAL RELATION, P.G. ELECTRODE (machined), CrVI SOLUTIONS IN 0.5 MH_2SO_4, 1000 rpm, 100 mV sec^{-1}

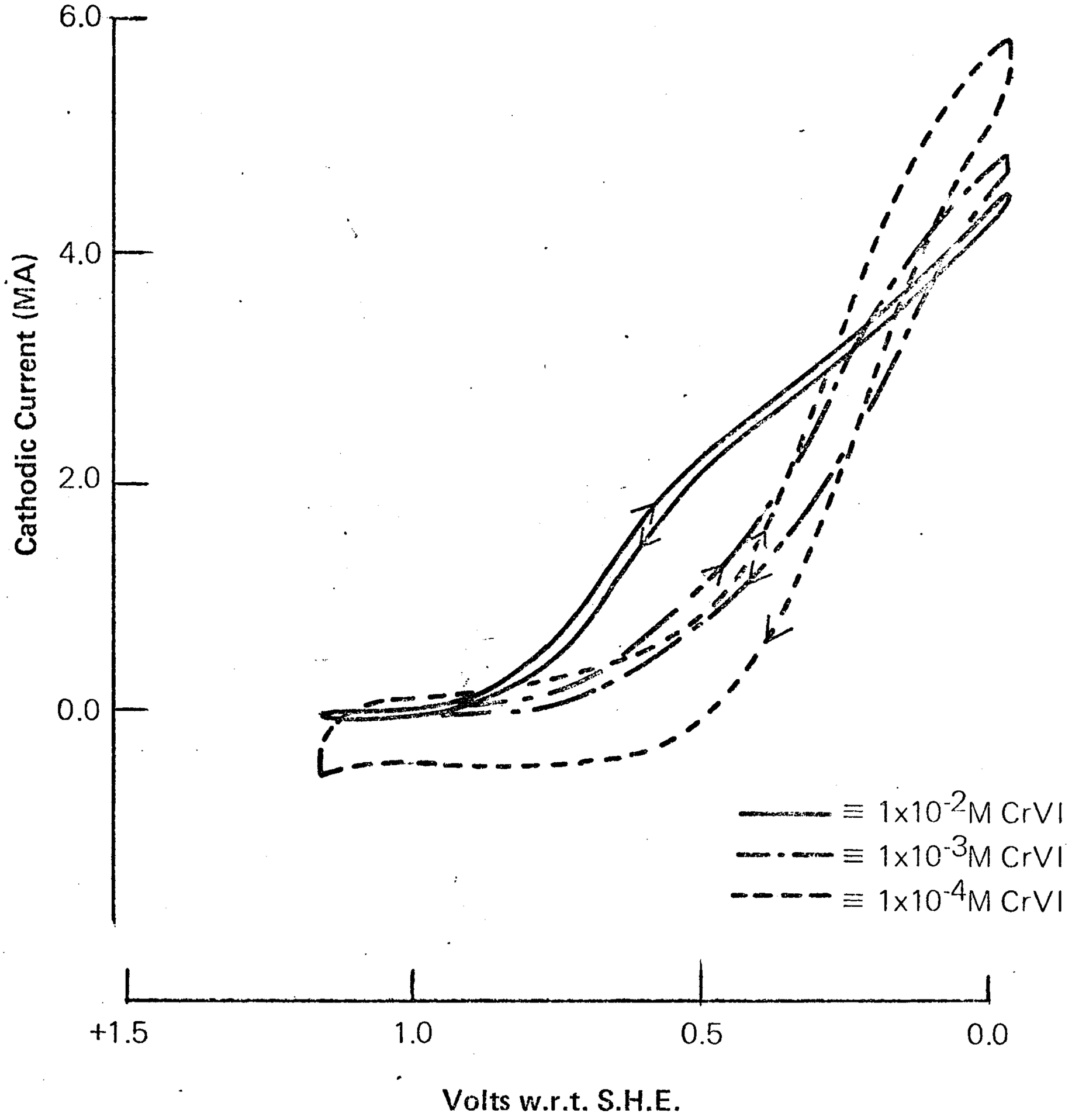

Fig. 8.17

CURRENT-POTENTIAL RELATION, P.G. ELECTRODE (machined), CrVI SOLUTIONS IN 0.25M H_2SO_4, 0.25M Na_2SO_4 1000 rpm, 100 mV sec^{-1}

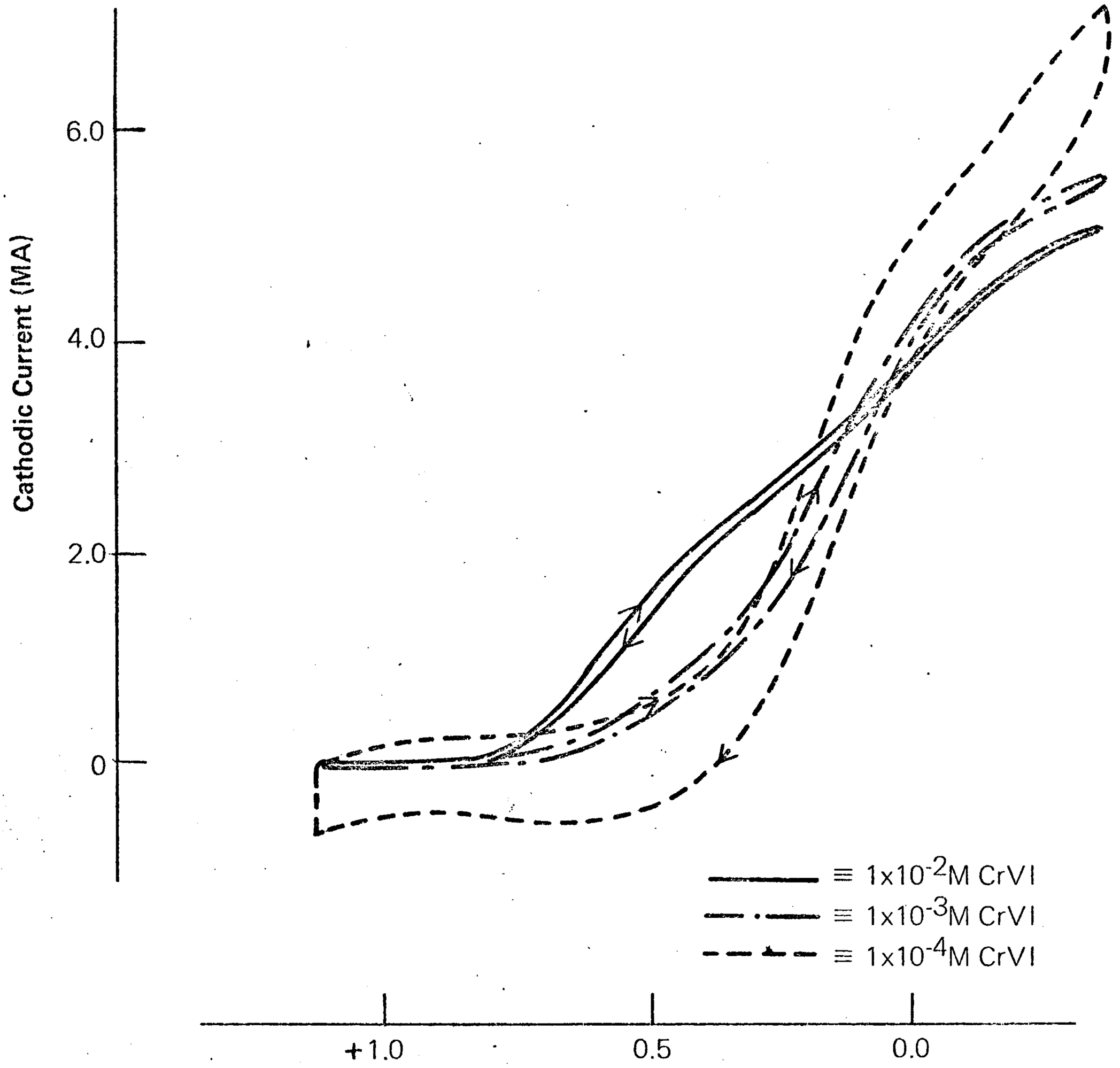

Fig. 8.18

CURRENT-POTENTIAL RELATION, P.G. ELECTRODE (machined) CrVI SOLUTIONS IN 0.05M H_2SO_4, 0.45M Na_2SO_4 1000 rpm, 100mV sec^{-1}

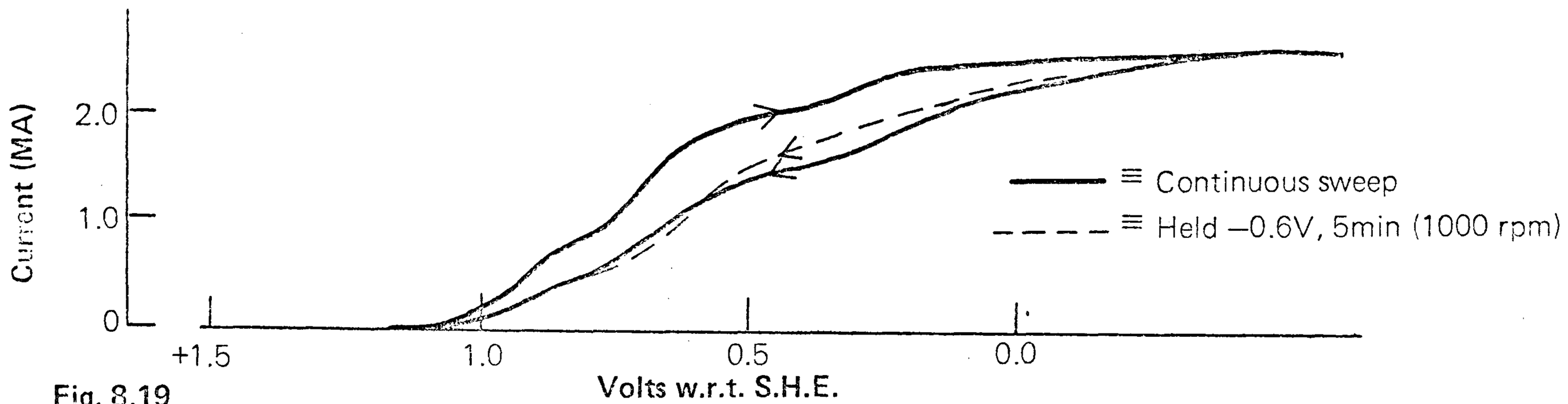

Fig. 8.19
CURRENT-POTENTIAL RELATION, P.G. ELECTRODE (machined), $1x10^{-2}$M CrVI, 0.5M H_2SO_4, 235rpm, 300 mV sec^{-1}

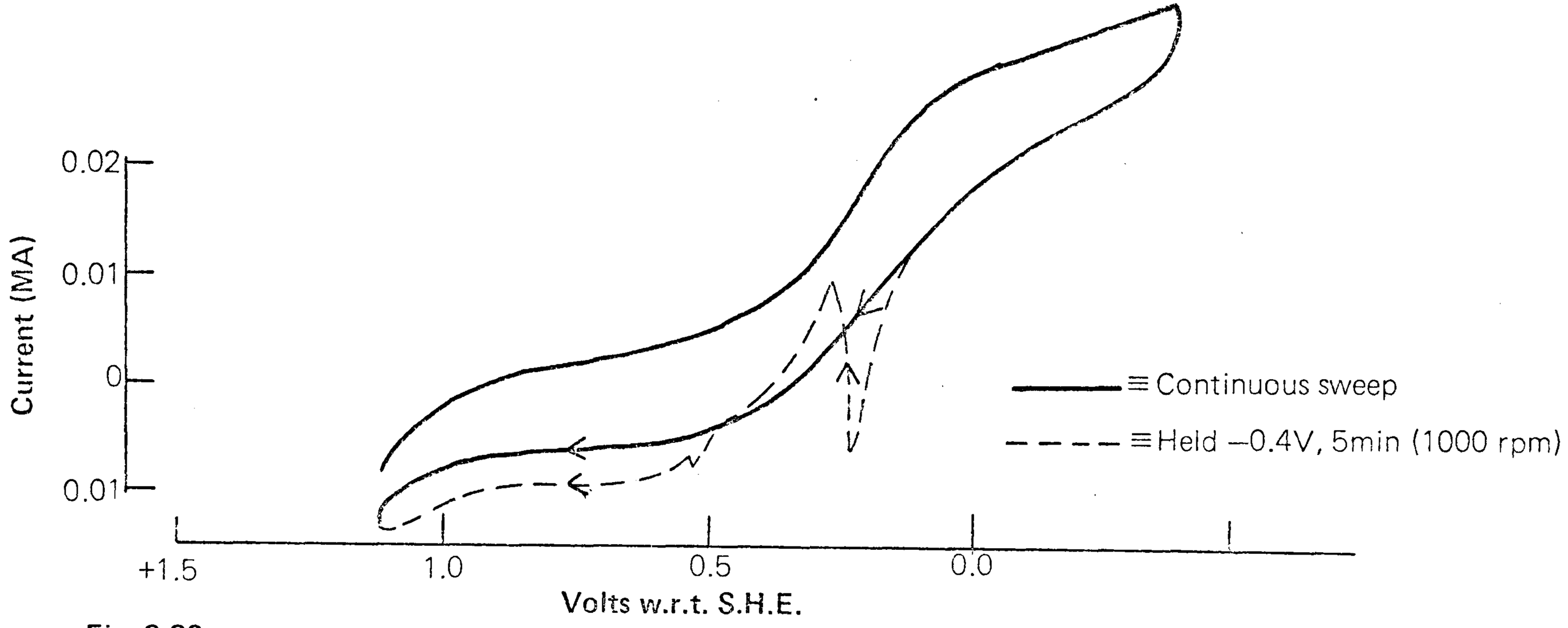

Fig. 8.20
CURRENT-POTENTIAL RELATION, P.G. ELECTRODE (machined), $1x10^{-4}$M CrVI, 0.05M H_2SO_4, 235rpm, 1000 mV sec^{-1}

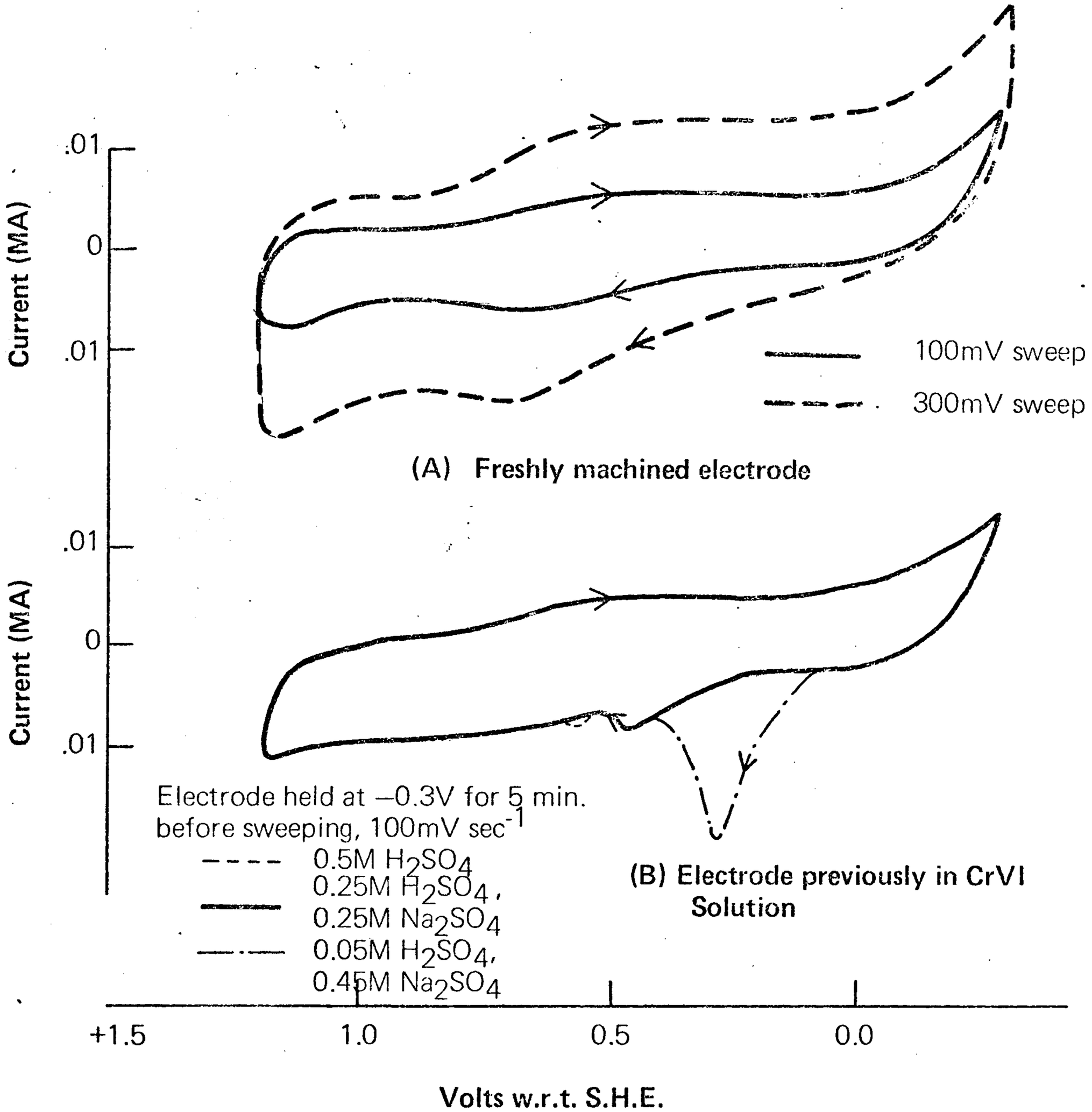

Fig. 8.21

CURRENT-POTENTIAL RELATIONSHIP, P.G. ELECTRODE (machined), BACKGROUND ELECTROLYTES, 1000 rpm

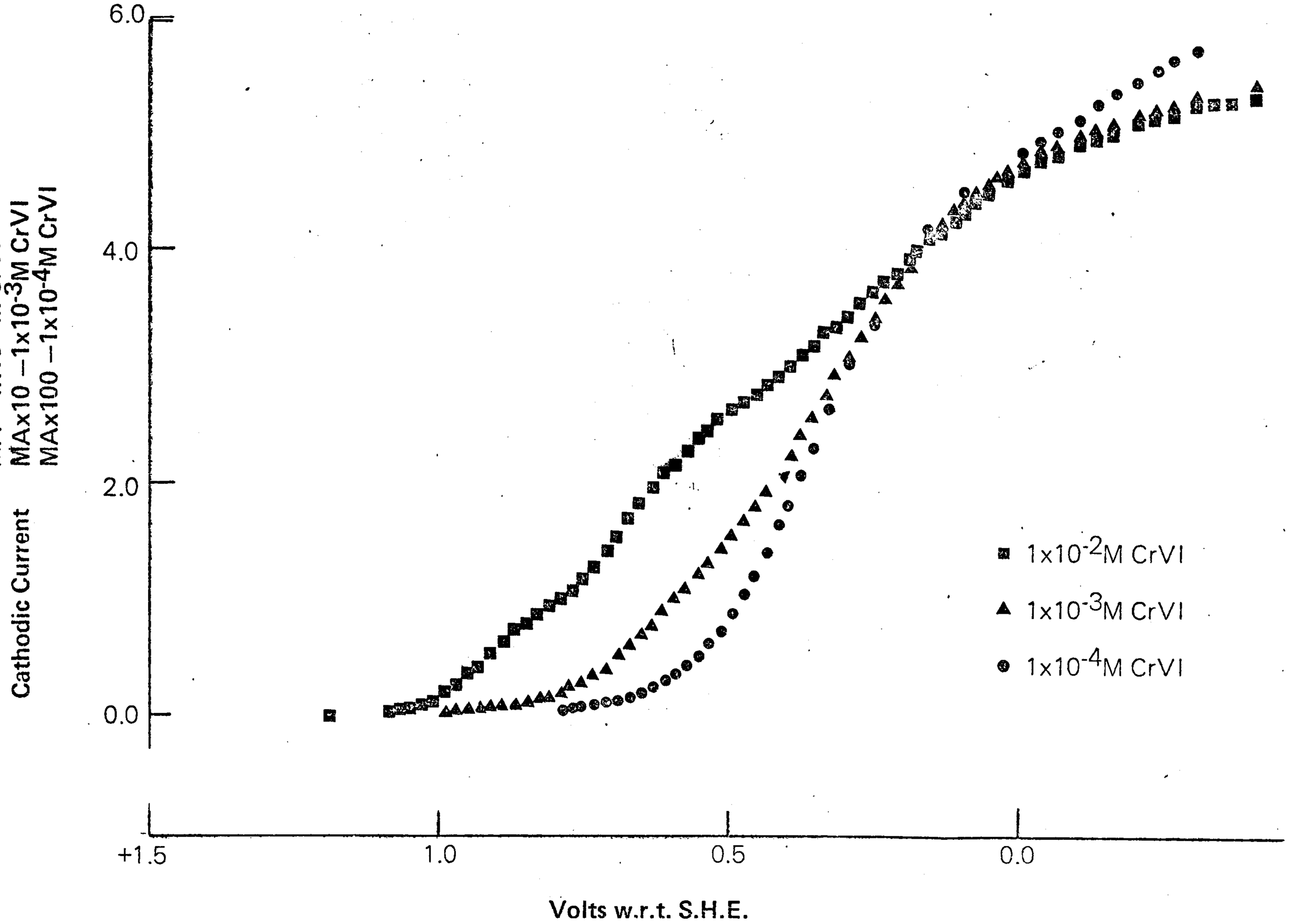

Fig. 8.22

STEADY-STATE CURRENT-POTENTIAL RELATION, P.G. ELECTRODE (machined), 0.5M H_2SO_4

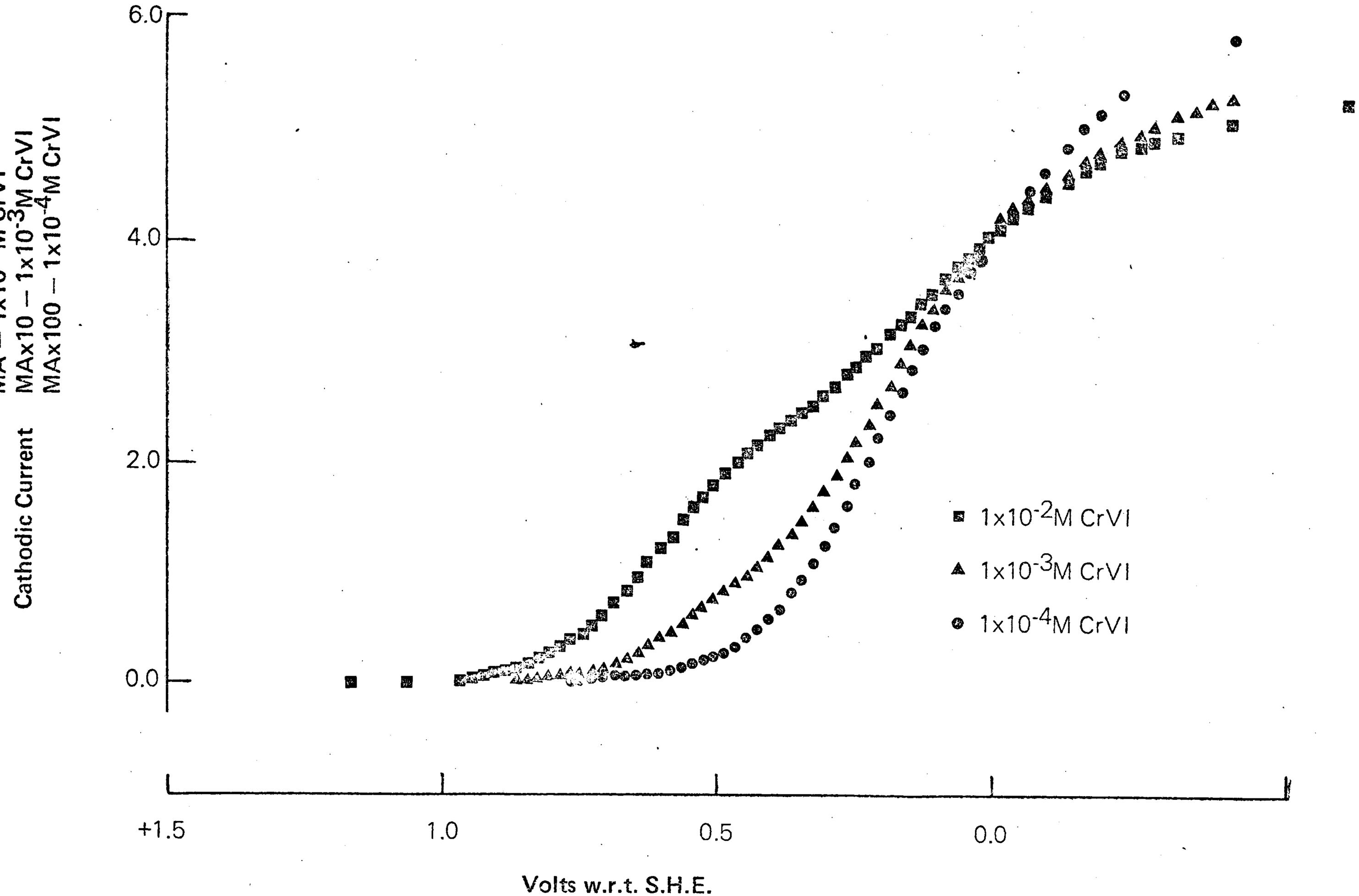

Fig. 8.23

STEADY-STATE CURRENT-POTENTIAL RELATION, P.G. ELECTRODE (machined), 0.25M H_2SO_4, 0.25M Na_2SO_4

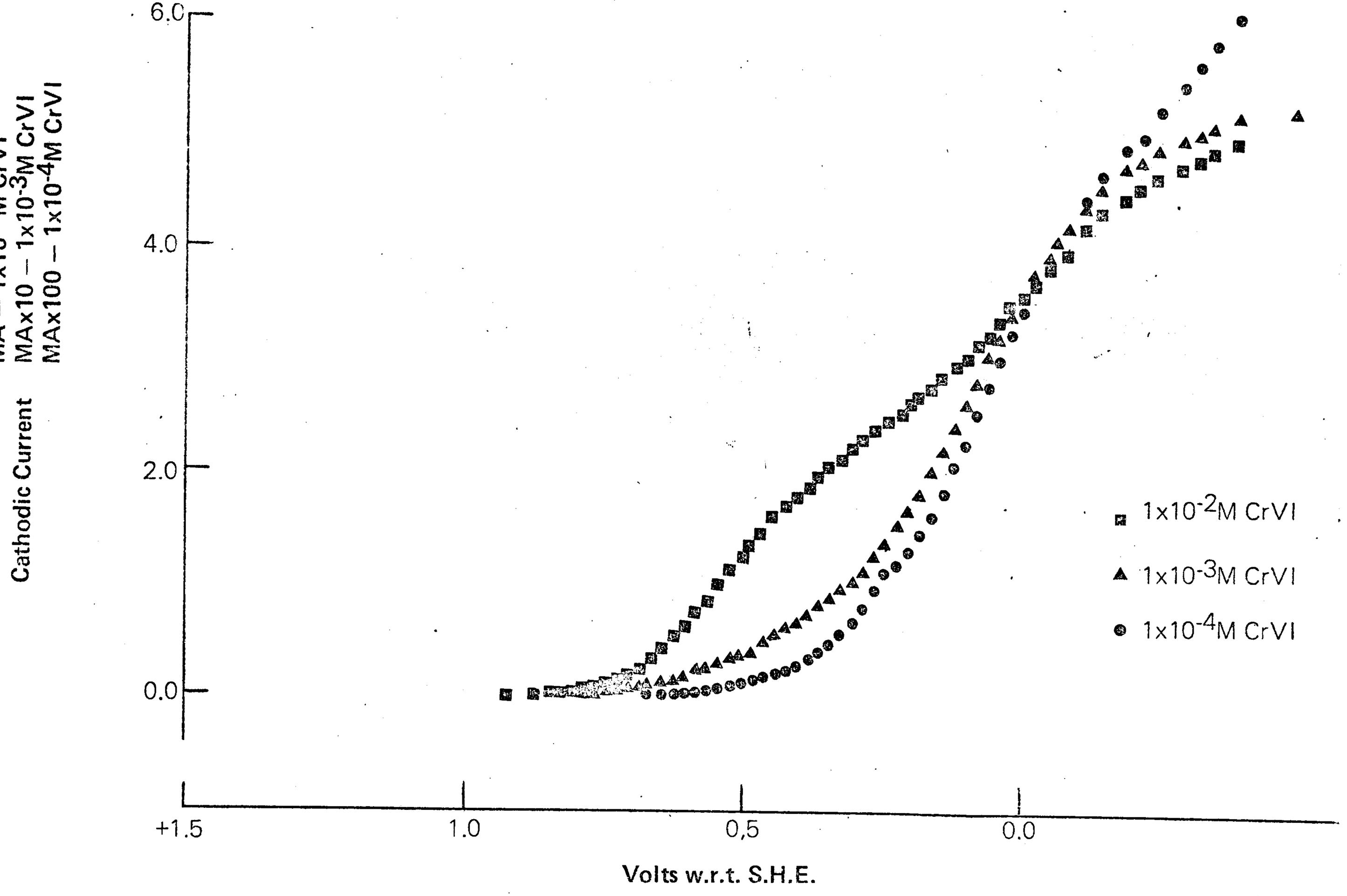

Fig. 8.24

STEADY-STATE CURRENT-POTENTIAL RELATION, P.G. ELECTRODE (machined), 0.05M H_2SO_4, 0.45M Na_2SO_4

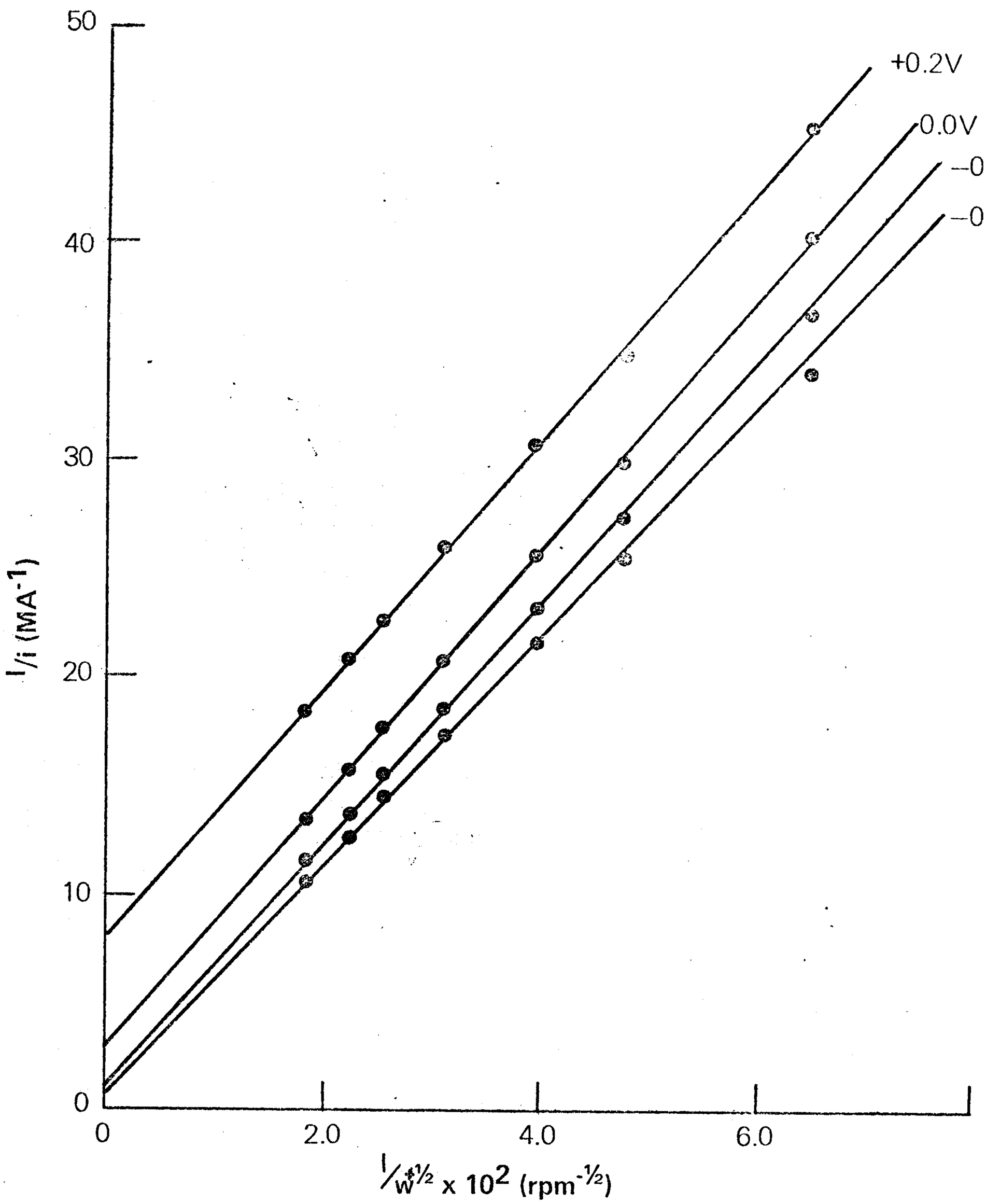

Fig. 8.25
PLOT OF I/i/ $I/w^{½}$, P.G. ELECTRODE (machined), $1x10^{-4}$M CrVI, 0.5M H_2SO_4

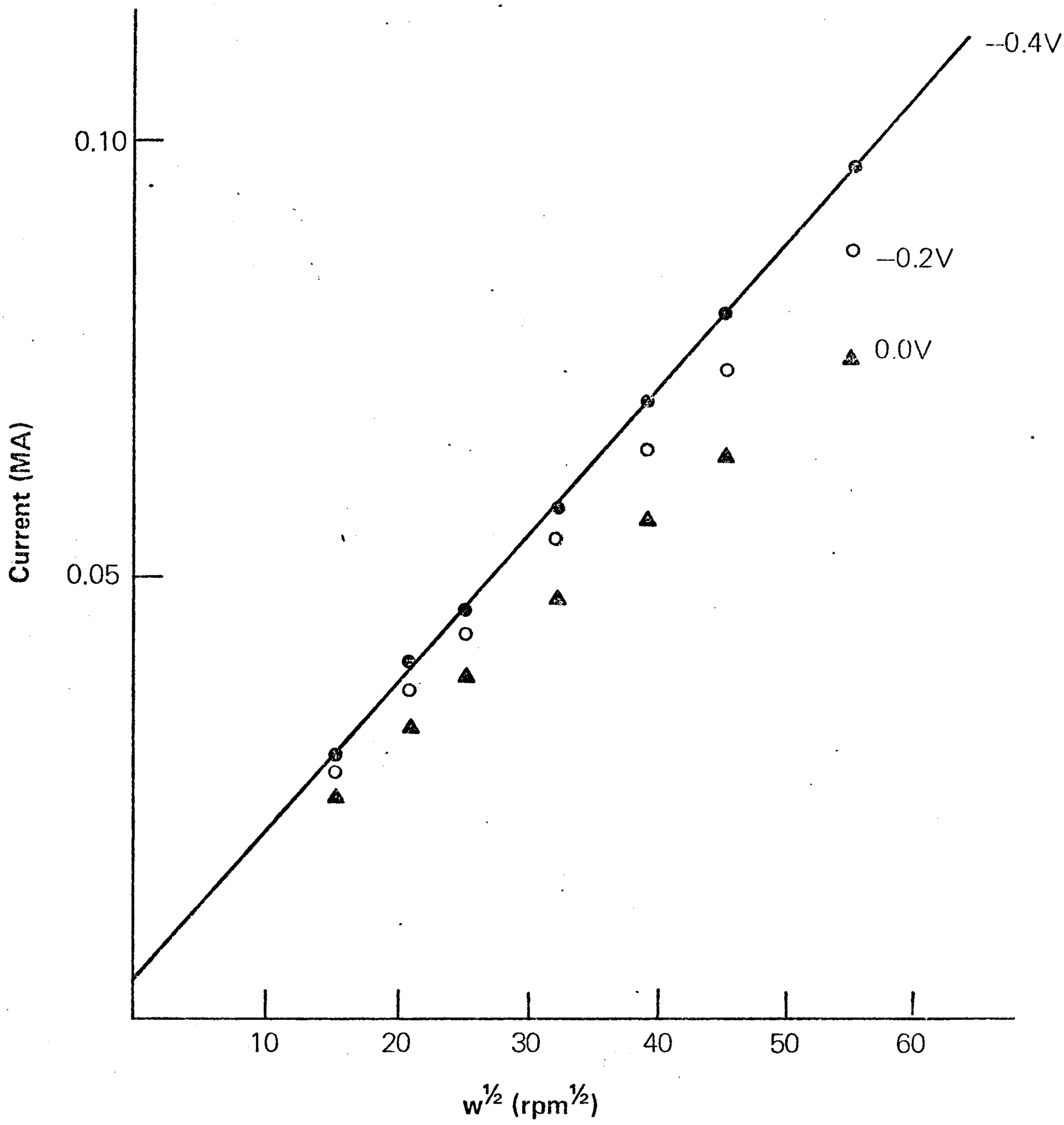

Fig. 8.26

PLOT OF $i/w^{1/2}$, P.G. ELECTRODE (machined), 1×10^{-4}M CrVI, 0.5M H_2SO_4

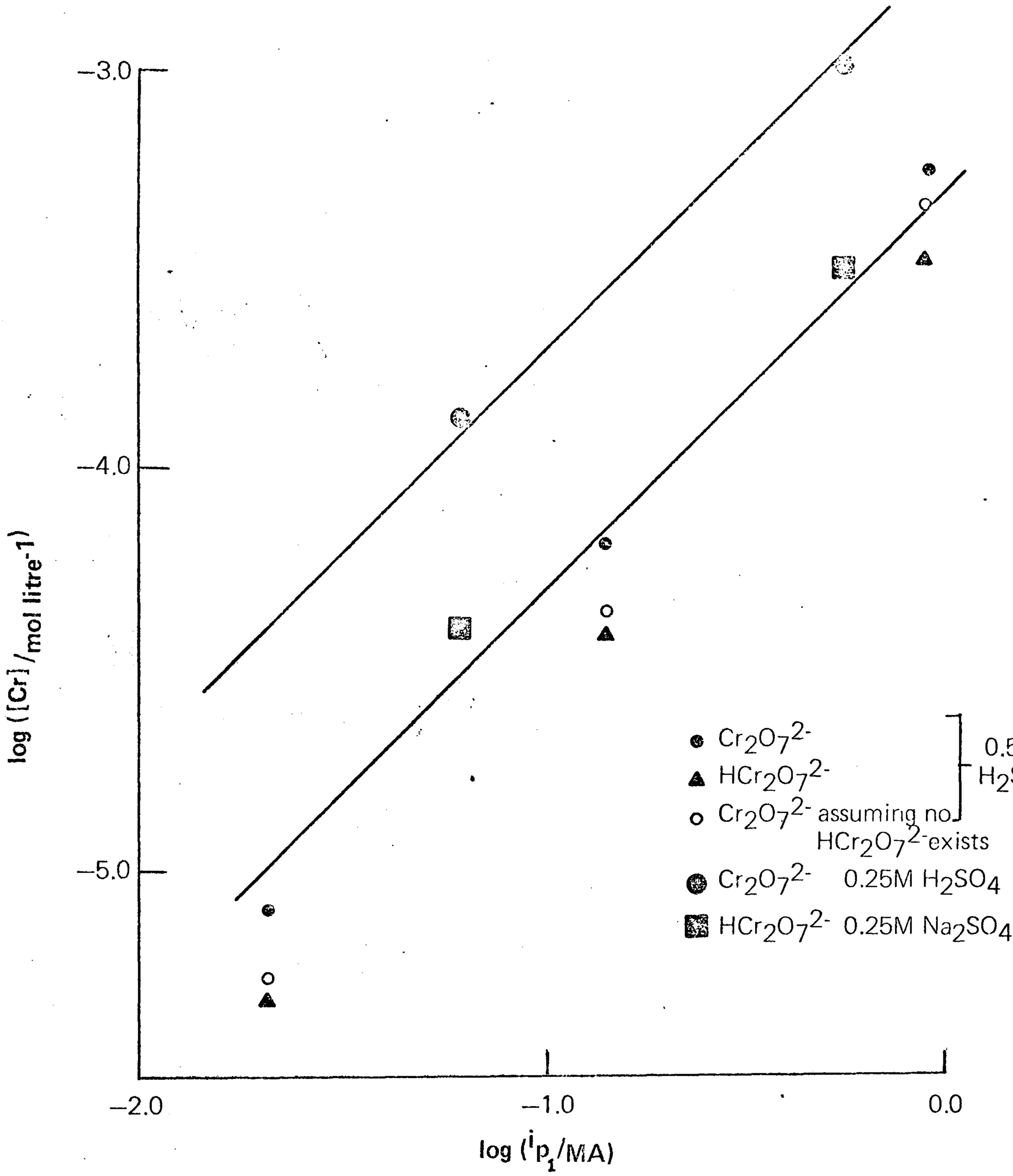

Fig. 8.27

PLOT OF LOG [Cr] /LOG i_{p_1}, 0.5M H_2SO_4 AND 0.25M H_2SO_4, 0.25M Na_2SO_4

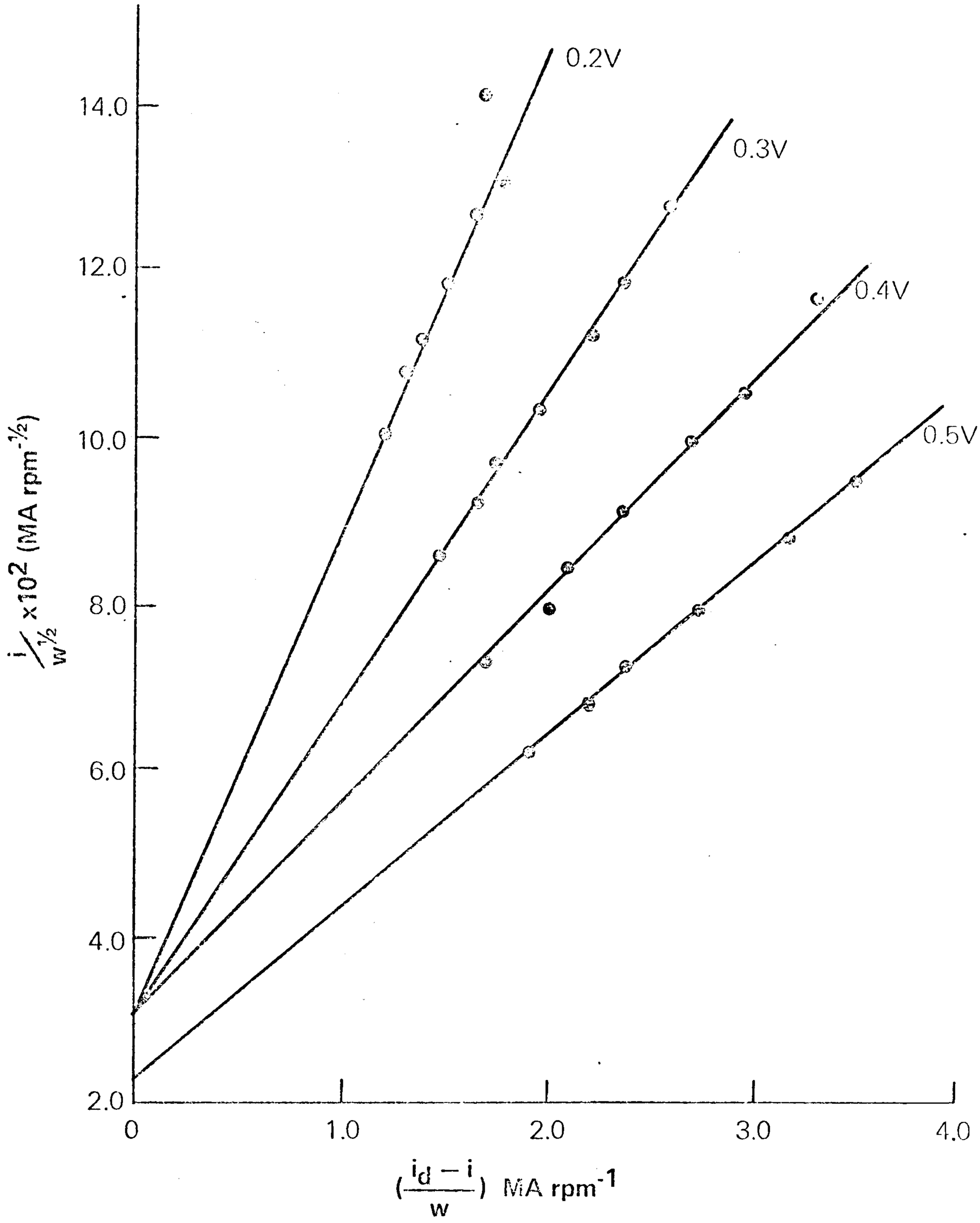

Fig. 8.28

PLOT OF $\frac{I_m}{w^{1/2}}$ / $\frac{I_d - I_m}{w}$, 1×10^{-2}M CrVI, 0.5M H_2SO_4

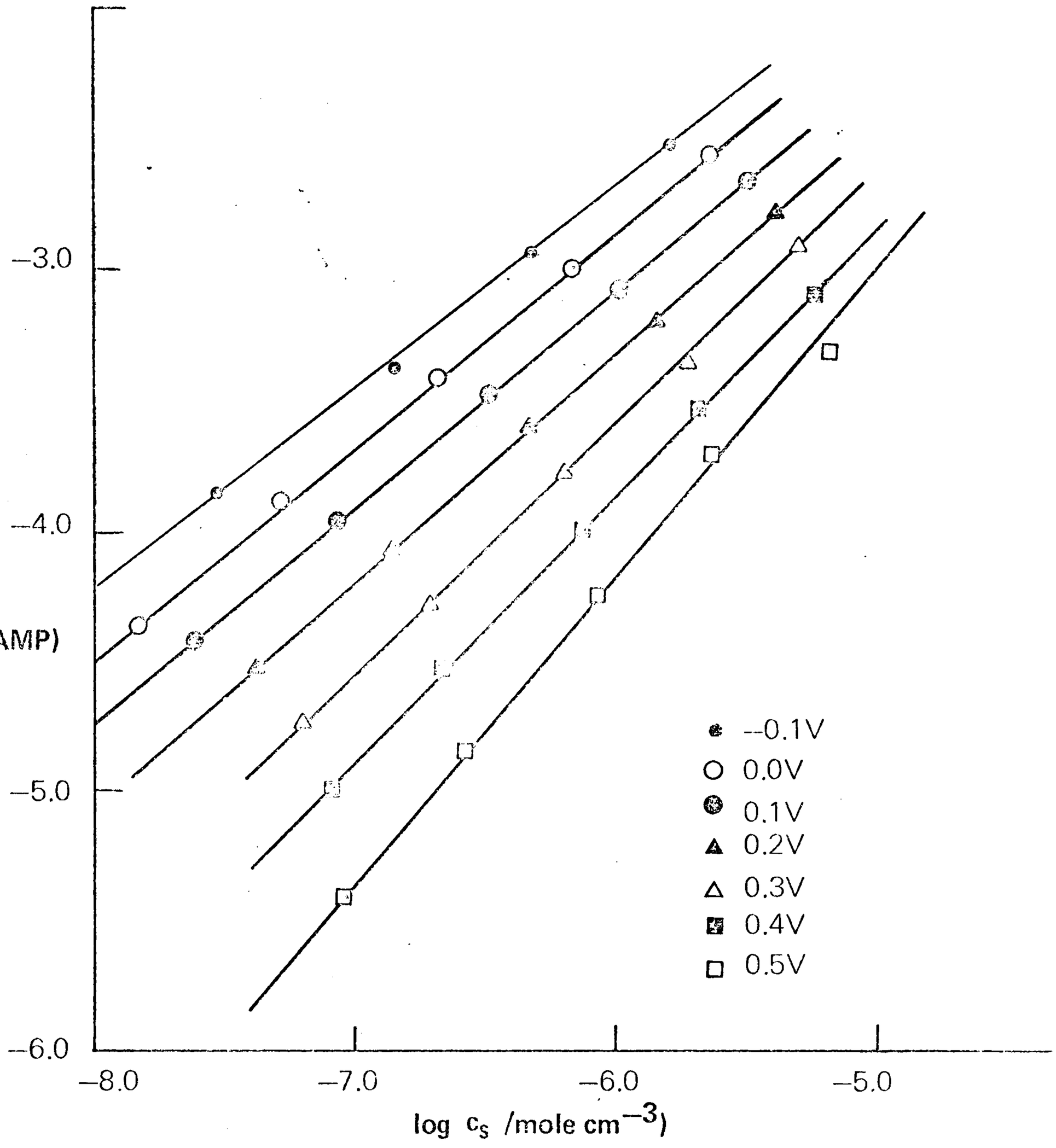

Fig. 8.29

ORDER OF REACTION IN 0.25 H_2SO_4, 0.25 M Na_2SO_4, P.G. ELECTRODE (MACHINED)

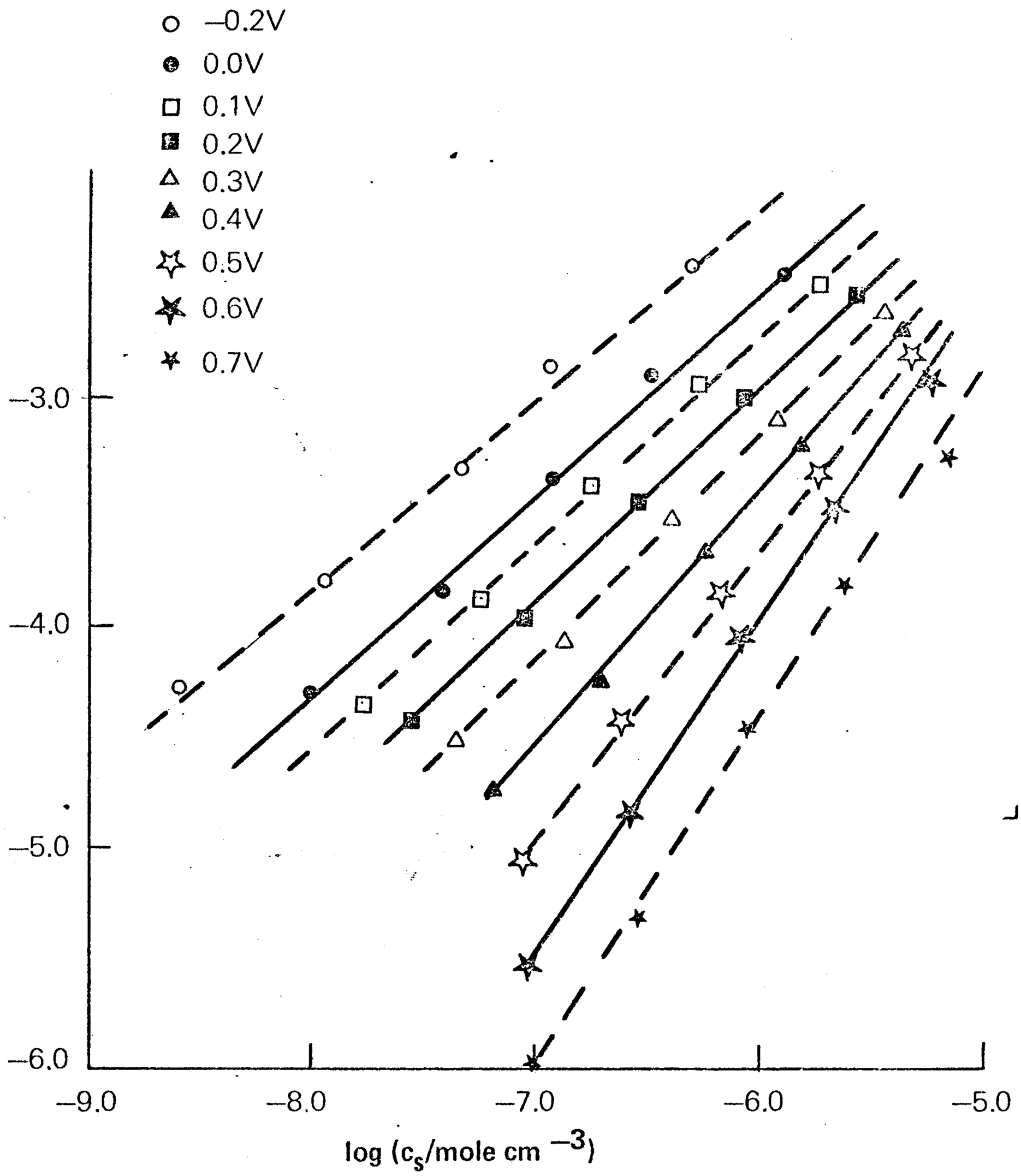

Fig. 8.30

ORDER OF REACTION IN 0.5M H_2SO_4, P.G. ELECTRODE (MACHINED)

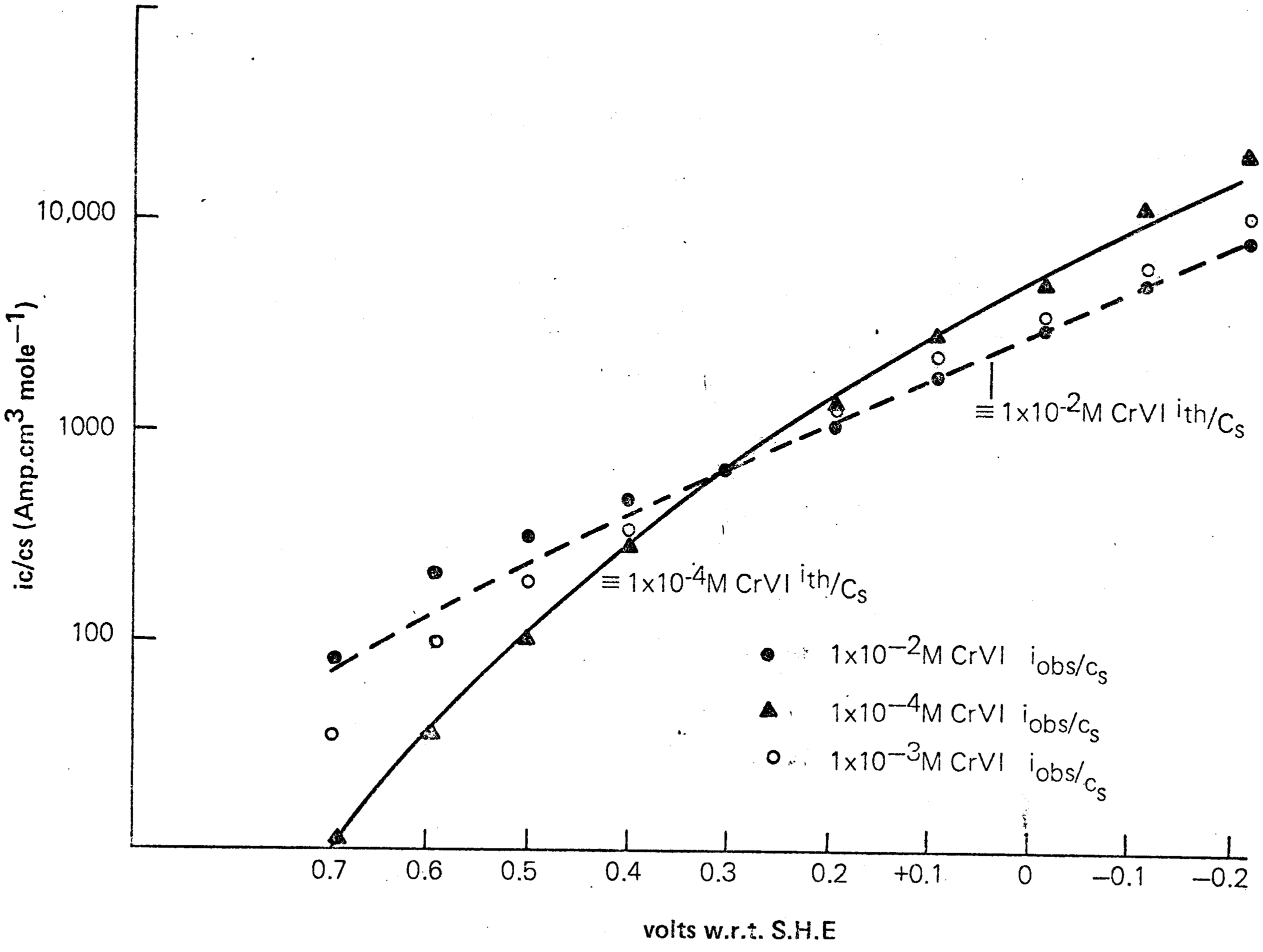

Fig. 8.31

POTENTIAL DEPENDENCE OF RATE OF REDUCTION OF CrVI IN 0.5M H_2SO_4 ON P.G. ELECTRODE; COMPARISON OF OBSERVED AND CALCULATED VALUES OF ic/cs

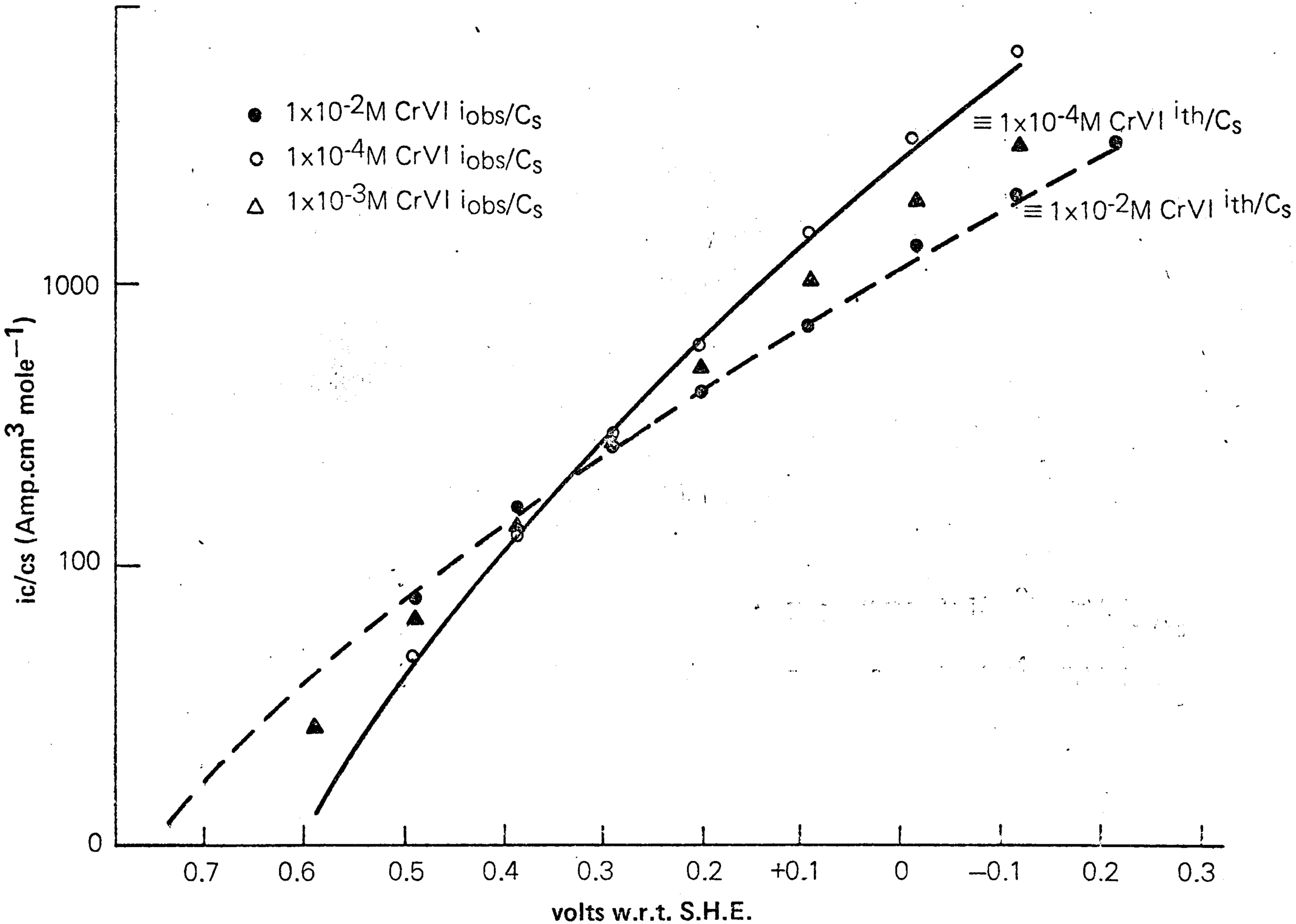

Fig. 8.32

POTENTIAL DEPENDENCE OF RATE OF REDUCTION OF CrVI IN 0.25M H_2SO_4, 0.25M Na_2SO_4 ON P.G. ELECTRODE; COMPARISON OF OBSERVED AND CALCULATED VALUES OF ic/cs

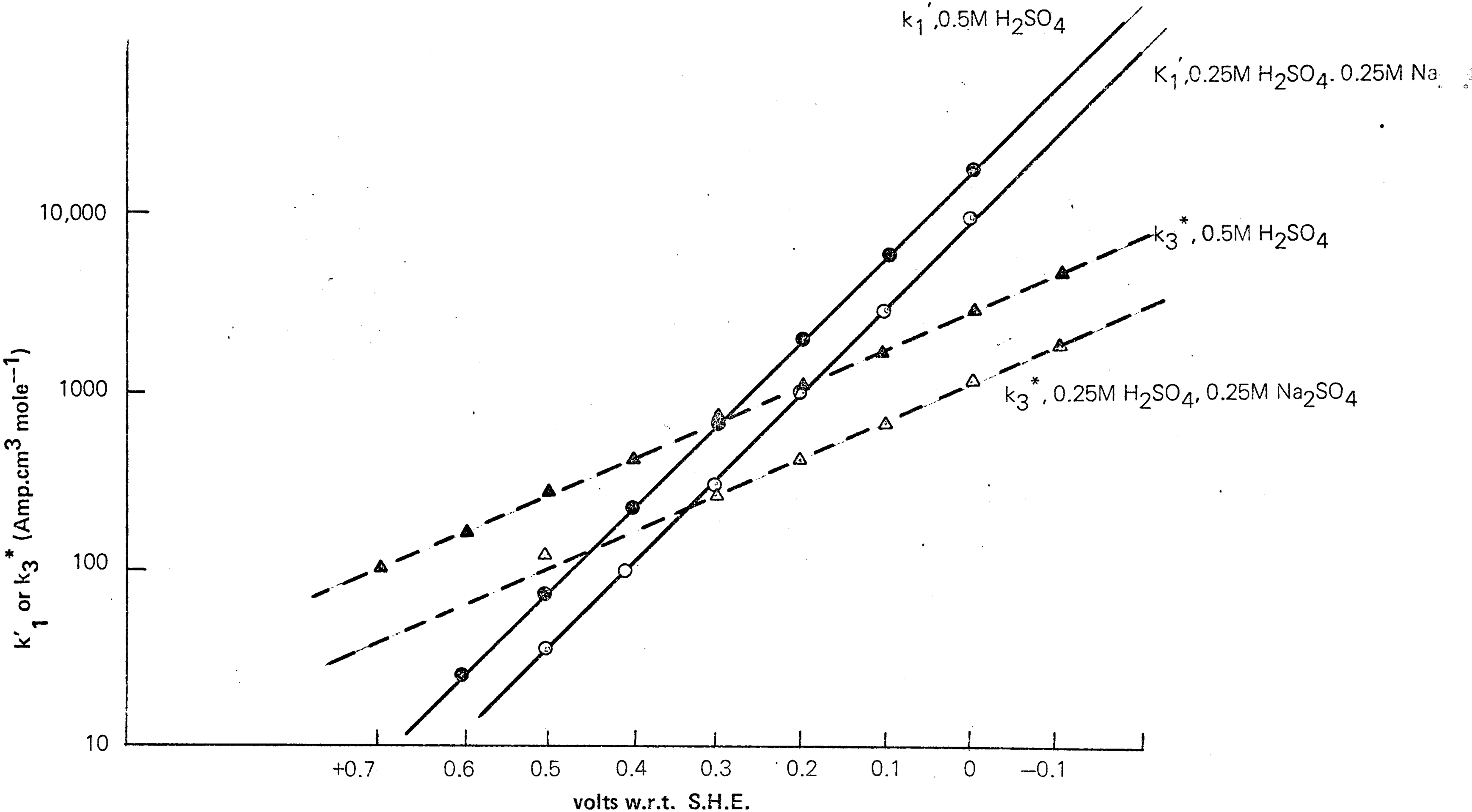

Fig. 8.33
VARIATION OF k'_1 AND k_3^* WITH POTENTIAL

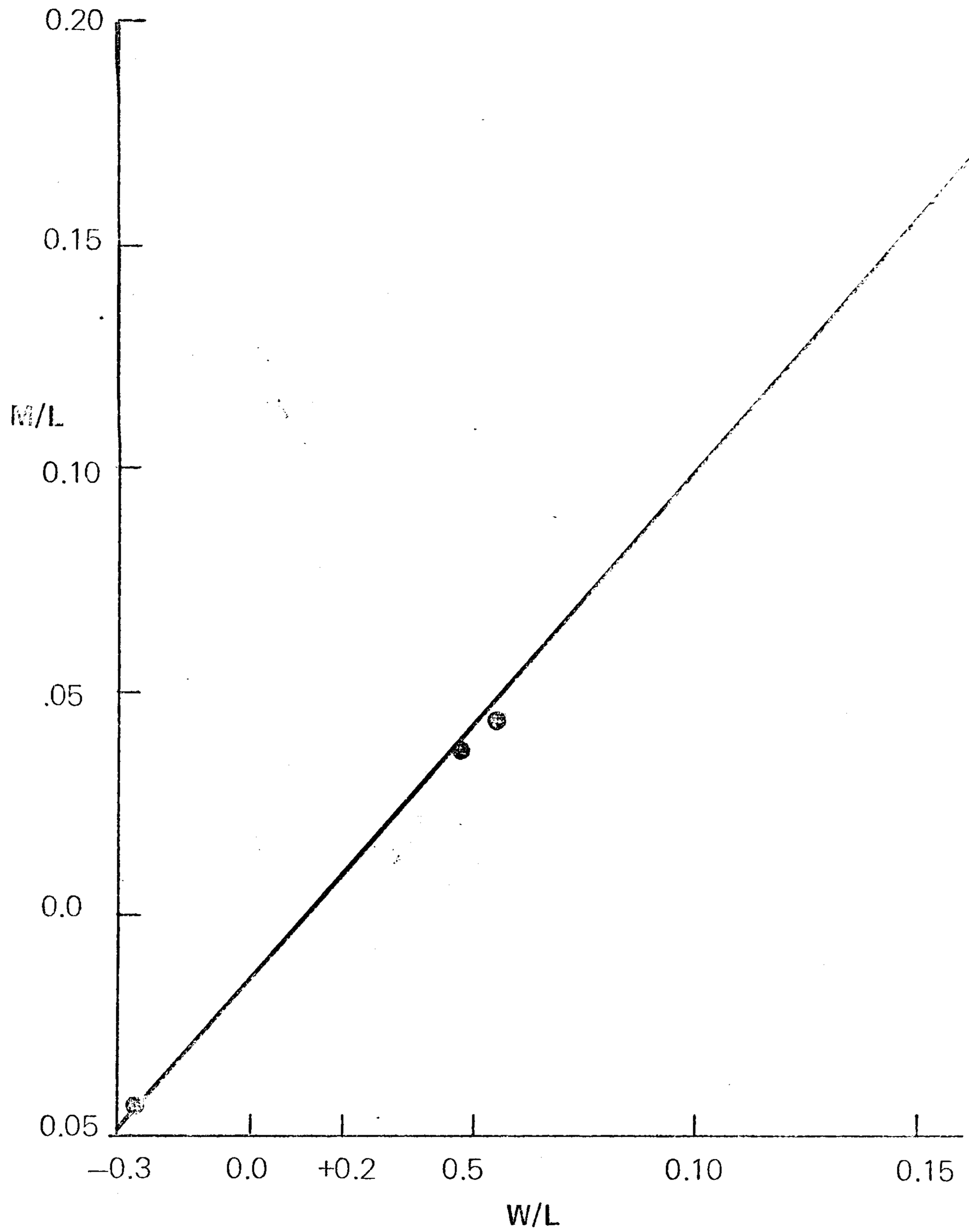

Fig. 8.34
GRAPH TO OBTAIN k_1 AND α, 0.5M H_2SO_4

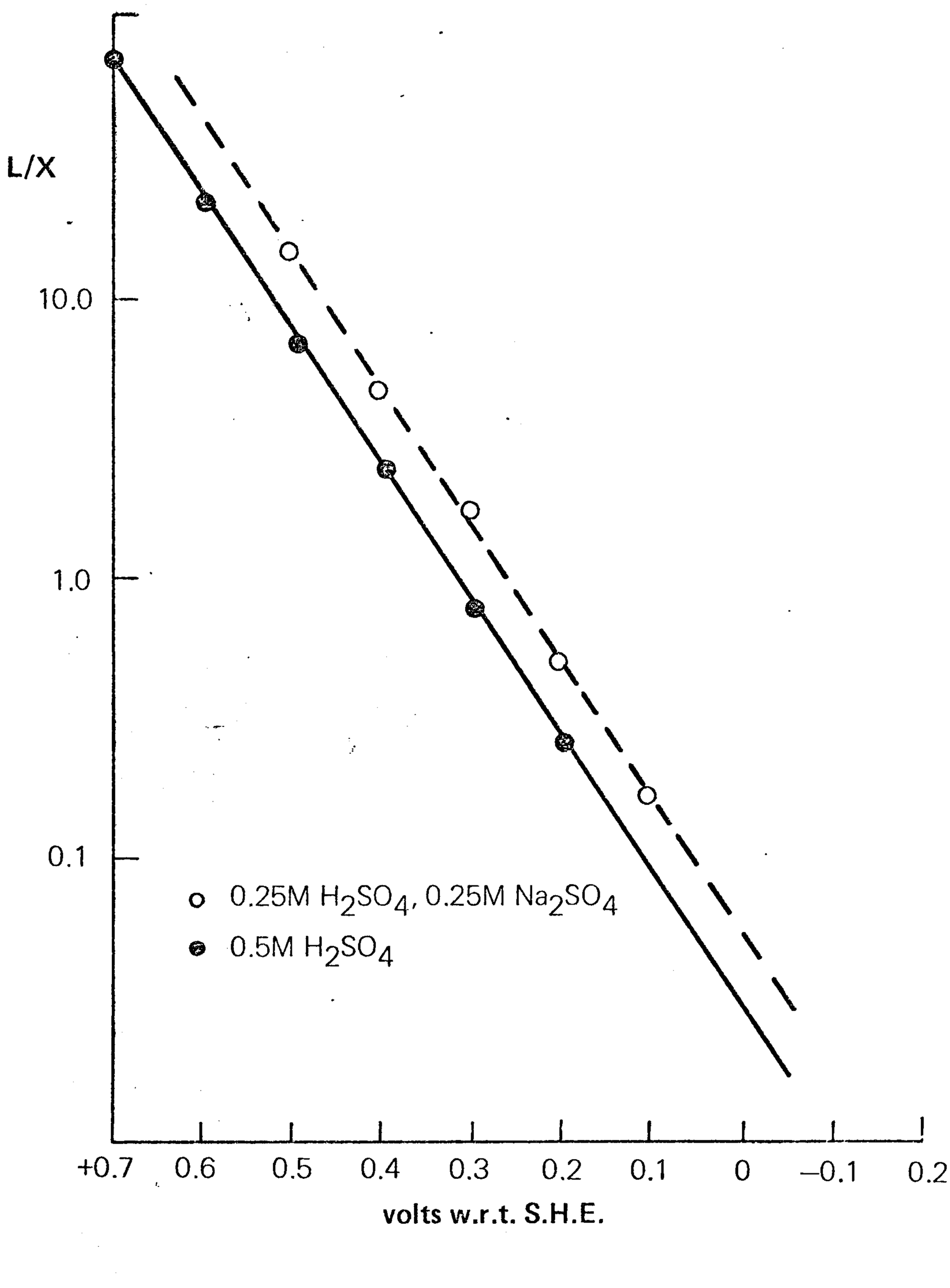

Fig. 8.35
DETERMINATION OF k_1^* AND α

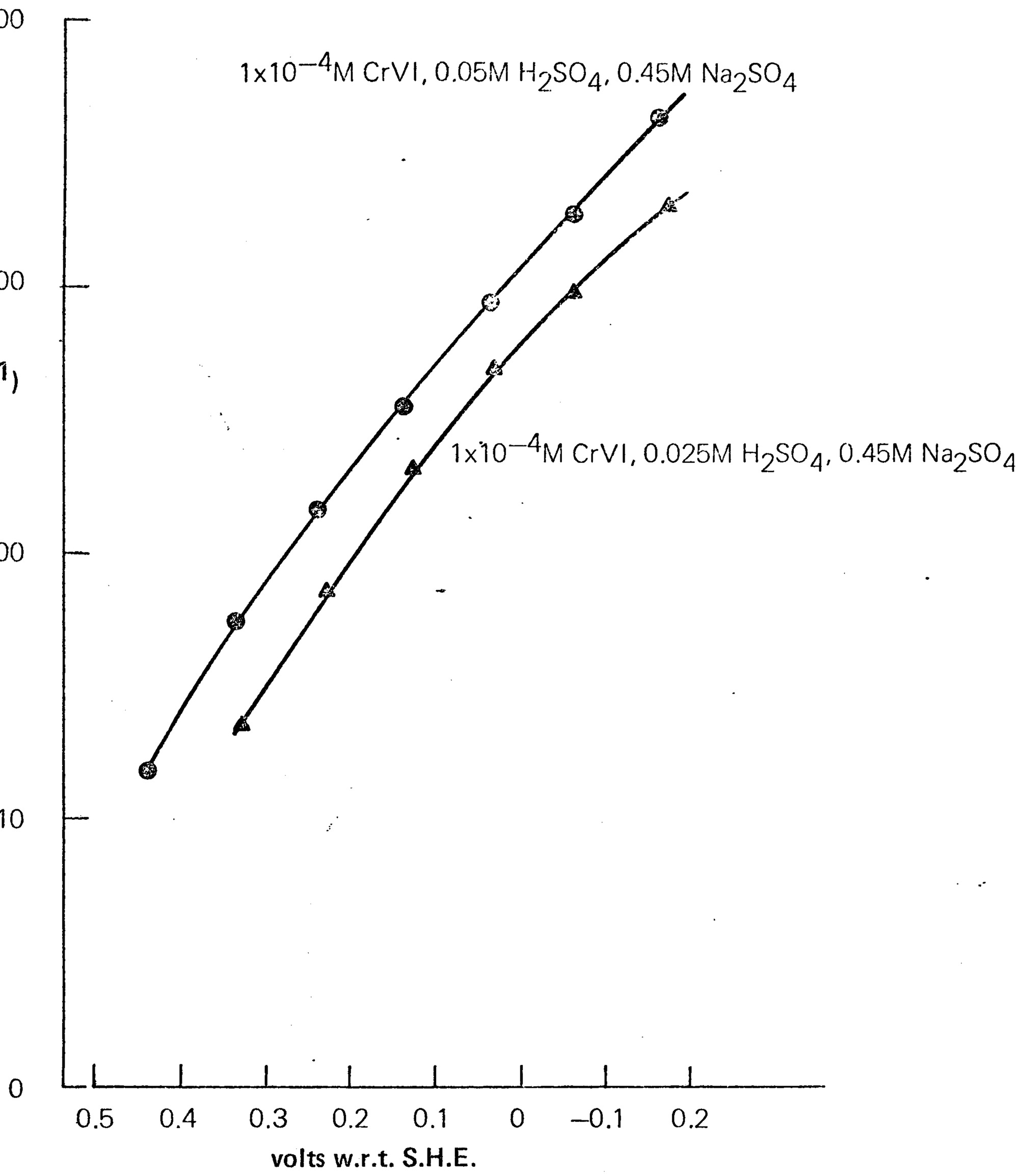

Fig. 8.36
POTENTIAL DEPENDENCE OF RATE OF REDUCTION OF CrVI ON P.G.ELECTRODE

APPENDIX 1

Equilibrium Concentrations of CrVI species in solutions of various acids

Table 1 - In 0.5 M H_2SO_4, assuming $HCr_2O_7^-$ present

Species	Concentration (mole $litre^{-1}$)				
[CrVI] total	1×10^{-2}	3×10^{-3}	1×10^{-3}	3×10^{-4}	1×10^{-4}
H_2CrO_4	1.007×10^{-3}	3.427×10^{-4}	1.196×10^{-4}	3.656×10^{-5}	1.224×10^{-5}
$HCrO_4^-$	2.392×10^{-3}	8.1370×10^{-4}	2.840×10^{-4}	8.680×10^{-5}	2.906×10^{-5}
$HCr_2O_7^-$	3.360×10^{-4}	3.890×10^{-5}	4.740×10^{-6}	3.962×10^{-7}	4.963×10^{-8}
$Cr_2O_7^{2-}$	5.605×10^{-4}	6.489×10^{-5}	7.946×10^{-6}	6.608×10^{-7}	8.277×10^{-8}
$CrSO_7^{2-}$	4.808×10^{-3}	1.6360×10^{-3}	5.711×10^{-4}	1.745×10^{-4}	5.843×10^{-5}

Table 2 - In 0.25 M H_2SO_4, 0.25 M Na_2SO_4, assuming $HCr_2O_7^-$ present

Species	Concentration (mole litre^{-1})				
[CrVI] total	1×10^{-2}	3×10^{-3}	1×10^{-3}	3×10^{-4}	1×10^{-4}
H_2CrO_4	6.904×10^{-4}	2.521×10^{-4}	9.058×10^{-5}	2.809×10^{-5}	9.457×10^{-6}
$HCrO_4^-$	3.278×10^{-3}	1.197×10^{-3}	4.355×10^{-4}	1.334×10^{-4}	4.490×10^{-5}
$HCr_2O_7^-$	3.156×10^{-4}	4.009×10^{-5}	5.441×10^{-6}	5.191×10^{-7}	5.924×10^{-8}
$Cr_2O_7^{2-}$	1.052×10^{-3}	1.337×10^{-4}	1.815×10^{-5}	1.731×10^{-6}	1.976×10^{-7}
$CrSO_7^{2-}$	3.295×10^{-3}	1.203×10^{-3}	4.2676×10^{-4}	1.340×10^{-4}	4.513×10^{-5}

Table 2 - In 0.25 M H_2SO_4, 0.25 M Na_2SO_4, assuming $HCr_2O_7^-$ present

Species	Concentration (mole litre^{-1})				
[CrVI] total	1×10^{-2}	3×10^{-3}	1×10^{-3}	3×10^{-4}	1×10^{-4}
H_2CrO_4	6.904×10^{-4}	2.521×10^{-4}	9.058×10^{-5}	2.809×10^{-5}	9.457×10^{-6}
$HCrO_4^-$	3.278×10^{-3}	1.197×10^{-3}	4.355×10^{-4}	1.334×10^{-4}	4.490×10^{-5}
$HCr_2O_7^-$	3.156×10^{-4}	4.009×10^{-5}	5.441×10^{-6}	5.191×10^{-7}	5.924×10^{-8}
$Cr_2O_7^{2-}$	1.052×10^{-3}	1.337×10^{-4}	1.815×10^{-5}	1.731×10^{-6}	1.976×10^{-7}
$CrSO_7^{2-}$	3.295×10^{-3}	1.203×10^{-3}	4.2676×10^{-4}	1.340×10^{-4}	4.513×10^{-5}

Table 3 - In 0.25 M H_2SO_4, assuming $HCr_2O_7^-$ present

Species	Concentration (mole litre^{-1})				
[CrVI] total	1×10^{-2}	3×10^{-3}	1×10^{-3}	3×10^{-4}	1×10^{-4}
H_2CrO_4	7.030×10^{-4}	2.564×10^{-4}	9.493×10^{-5}	2.876×10^{-5}	9.684×10^{-6}
$HCrO_4^-$	3.281×10^{-3}	1.1965×10^{-3}	4.43×10^{-4}	1.342×10^{-4}	4.519×10^{-5}
$HCr_2O_7^-$	3.247×10^{-4}	4.280×10^{-5}	2.91×10^{-6}	5.384×10^{-7}	6.105×10^{-8}
$Cr_2O_7^{2-}$	1.065×10^{-3}	1.403×10^{-4}	9.53×10^{-6}	1.765×10^{-6}	2.001×10^{-7}
$CrSO_7^{2-}$	3.238×10^{-3}	1.181×10^{-3}	4.372×10^{-4}	1.324×10^{-4}	4.460×10^{-5}

Table 4 - In 0.125 M H_2SO_4, 0.125 M Na_2SO_4 assuming $HCr_2O_7^-$ present

Species	Concentration (mole litre^{-1})				
[CrVI] total	1×10^{-2}	3×10^{-3}	1×10^{-3}	3×10^{-4}	1×10^{-4}
H_2CrO_4	4.380×10^{-4}	1.650×10^{-4}	6.189×10^{-5}	1.958×10^{-5}	6.636×10^{-6}
$HCrO_4^-$	3.995×10^{-3}	1.540×10^{-3}	5.777×10^{-4}	1.827×10^{-4}	6.194×10^{-5}
$HCr_2O_7^-$	2.386×10^{-4}	3.543×10^{-5}	4.988×10^{-6}	4.990×10^{-7}	5.700×10^{-8}
$Cr_2O_7^{2-}$	1.564×10^{-3}	2.323×10^{-4}	3.270×10^{-5}	3.272×10^{-6}	3.738×10^{-7}
$CrSO_7^{2-}$	1.971×10^{-3}	7.598×10^{-4}	2.851×10^{-4}	9.016×10^{-5}	3.056×10^{-5}

Table 5 - In 0.05 M H_2SO_4, 0.45 M Na_2SO_4 assuming $HCr_2O_7^-$ present

Species	Concentration (mole litre^{-1})				
[CrVI] total	1×10^{-2}	3×10^{-3}	1×10^{-3}	3×10^{-4}	1×10^{-4}
H_2CrO_4	1.756×10^{-4}	7.479×10^{-5}	2.981×10^{-5}	9.742×10^{-6}	3.340×10^{-6}
$HCrO_4^-$	4.630×10^{-3}	1.848×10^{-3}	7.188×10^{-4}	2.324×10^{-4}	7.931×10^{-5}
$HCr_2O_7^-$	1.217×10^{-4}	1.928×10^{-5}	2.990×10^{-6}	3.158×10^{-7}	3.700×10^{-8}
$Cr_2O_7^{2-}$	2.018×10^{-3}	3.348×10^{-4}	5.063×10^{-5}	5.292×10^{-6}	6.181×10^{-7}
$CrSO_7^{2-}$	9.145×10^{-4}	3.687×10^{-4}	1.441×10^{-4}	4.666×10^{-5}	1.604×10^{-5}

Table 6 - In 0.025 M H_2SO_4, 0.45 M Na_2SO_4 assuming $HCr_2O_7^-$ present

Species	Concentration (mole litre^{-1})		
[CrVI] total	1×10^{-2}	1×10^{-3}	1×10^{-4}
H_2CrO_4	8.141×10^{-5}	1.597×10^{-5}	1.845×10^{-6}
$HCrO_4^-$	4.807×10^{-3}	7.823×10^{-4}	6.786×10^{-5}
$HCr_2O_7^-$	5.459×10^{-5}	1.743×10^{-6}	2.259×10^{-8}
$Cr_2O_7^{2-}$	2.265×10^{-3}	5.998×10^{-5}	7.553×10^{-7}
$CrSO_7^{2-}$	4.732×10^{-4}	7.828×10^{-5}	2.874×10^{-5}

Table 7 - In 0.5 M H_2SO_4, assuming $HCr_2O_7^-$ absent

Species	Concentration (mole litre^{-1})				
[CrVI] total	1×10^{-2}	3×10^{-3}	1×10^{-3}	3×10^{-4}	1×10^{-4}
$CrSO_7^{2-}$	4.319×10^{-3}	1.380×10^{-3}	4.698×10^{-4}	1.420×10^{-4}	4.744×10^{-5}
H_2CrO_4	2.628×10^{-3}	8.400×10^{-4}	2.858×10^{-4}	8.639×10^{-5}	2.886×10^{-5}
$Cr_2O_7^{2-}$	4.523×10^{-4}	4.622×10^{-5}	5.351×10^{-6}	4.889×10^{-7}	5.456×10^{-8}
$HCrO_4^-$	2.148×10^{-3}	6.868×10^{-4}	2.335×10^{-4}	7.06×10^{-5}	2.36×10^{-5}

Table 8 - In 0.25 M H_2SO_4, 0.25 M Na_2SO_4 assuming $HCr_2O_7^-$ absent

Species	Concentration (mole litre^{-1})				
[CrVI] total	1×10^{-2}	3×10^{-3}	1×10^{-3}	3×10^{-4}	1×10^{-4}
$CrSO_7^{2-}$	3.725×10^{-3}	1.331×10^{-3}	4.760×10^{-4}	1.469×10^{-4}	4.940×10^{-5}
H_2CrO_4	2.181×10^{-4}	7.789×10^{-5}	2.786×10^{-5}	8.600×10^{-6}	2.956×10^{-6}
$Cr_2O_7^{2-}$	1.246×10^{-3}	1.589×10^{-4}	2.033×10^{-5}	1.937×10^{-6}	2.190×10^{-7}
$HCrO_4^-$	3.565×10^{-3}	1.649×10^{-3}	4.555×10^{-4}	1.406×10^{-4}	4.721×10^{-5}

Table 9 - In 0.05 M H_2SO_4. 0.45 M Na_2SO_4 assuming $HCr_2O_7^-$ absent

Species	Concentration (mole litre^{-1})				
[CrVI] total	1×10^{-2}	3×10^{-3}	1×10^{-3}	3×10^{-4}	1×10^{-4}
$CrSO_7^{2-}$	9.425×10^{-4}	3.806×10^{-4}	1.480×10^{-4}	4.786×10^{-5}	1.635×10^{-5}
H_2CrO_4	5.738×10^{-5}	2.317×10^{-5}	9.012×10^{-6}	2.913×10^{-6}	9.954×10^{-7}
$Cr_2O_7^{2-}$	2.155×10^{-3}	3.514×10^{-4}	5.317×10^{-5}	5.556×10^{-6}	6.486×10^{-7}
$HCrO_4^-$	4.690×10^{-3}	1.895×10^{-3}	6.555×10^{-4}	2.381×10^{-4}	8.136×10^{-5}

Table 10 - In 0.025 M H_2SO_4, 0.45 M Na_2SO_4 assuming $HCr_2O_7^-$ absent

Species	Concentration (mole litre^{-1})				
[CrVI] total	1×10^{-2}	3×10^{-3}	1×10^{-3}	3×10^{-4}	1×10^{-4}
$CrSO_7^{2-}$	4.876×10^{-4}	2.009×10^{-4}	7.955×10^{-5}	2.602×10^{-5}	8.931×10^{-6}
H_2CrO_4	2.975×10^{-5}	1.226×10^{-5}	4.853×10^{-6}	1.587×10^{-6}	5.448×10^{-7}
$Cr_2O_7^{2-}$	2.312×10^{-3}	3.926×10^{-4}	6.155×10^{-5}	6.585×10^{-6}	7.757×10^{-7}
$HCrO_4^-$	4.858×10^{-3}	2.002×10^{-3}	7.924×10^{-4}	2.592×10^{-4}	8.897×10^{-5}

Table 11 - In $HClO_4$ solutions, assuming $HCr_2O_7^-$ absent

	Species	CrVI total		
		1×10^{-2}	1×10^{-3}	1×10^{-4}
0.1 M $HClO_4$	H_2CrO_4	1.2×10^{-4}	2.0×10^{-5}	2.3×10^{-6}
	$HCrO_4^-$	4.9×10^{-3}	8.4×10^{-4}	9.6×10^{-5}
	$Cr_2O_7^{2-}$	2.5×10^{-3}	4.9×10^{-4}	9.1×10^{-7}
1.0 M $HClO_4$	H_2CrO_4	1.1×10^{-3}	1.7×10^{-4}	1.9×10^{-5}
	$HCrO_4^-$	4.6×10^{-3}	7.2×10^{-4}	7.9×10^{-5}
	$Cr_2O_7^{2-}$	2.2×10^{-3}	5.6×10^{-5}	1.2×10^{-6}
2 M $HClO_4$	H_2CrO_4	2.1×10^{-3}	3.0×10^{-4}	3.2×10^{-5}
	$HCrO_4^-$	4.3×10^{-3}	6.2×10^{-4}	6.7×10^{-5}
	$Cr_2O_7^{2-}$	1.8×10^{-3}	3.8×10^{-5}	4.6×10^{-7}

APPENDIX 2

Derivation of the rate equations

The mechanisms considered are;

$$A + M + ne \xrightarrow{k_1} M\text{-}B \xrightarrow{k_2'} M + \text{Products} \qquad (1)$$

followed by

$$\text{either } A + M\text{-}B + ne \xrightarrow{k_3} M\text{-}B + \text{Products} \qquad (2a)$$

$$\text{or } A + M\text{-}B + ne \xrightarrow{k_4} M + \text{Products} \qquad (2b).$$

Since the reduction of CrVI to CrIII involves three electrons, and it is unlikely that they will all be transferred in a single step, the detailed mechanism is likely to be more complex than those shown above. It is also possible that the values of n may differ in the three processes shown above; any such differences can however be incorporated in the rate constants.

If the fraction of the electrode surface covered by B is θ, the theoretical rate equations may be derived as below.

1) <u>For mechanism (1) + (2a)</u>

The rate of reducing monomers (mole s^{-1}) is

$$\frac{-dN}{dt} = Ak_1c_s(1 - \theta) + Ak_3c_s\theta ,$$

where A is the area of the electrode (cm^2), k_1 and k_3 are potential dependent rate constants (cm s^{-1}) and c_s is the concentration of reducible species at the electrode surface (mole cm^{-3}). Consequently the current for monomer reduction (^ic/Amp) is given by

$$i_c = -nF\frac{dN}{dt} = nFAk_1c_s(1-\theta) + nFAk_3c_s\theta \qquad A3$$

where n is the number of electrons involved in each of the steps and F the Faraday constant.

The rate of formation of adsorbed molecules of B (mole s^{-1}) is

$$\frac{dn_B}{Ldt} = Ak_1c_s(1-\theta) - Ak_2'\frac{n_B}{L}$$

where n_B is the number of molecules of B adsorbed on unit area of the electrode surface and L the Avogadro constant; k_2' has units of s^{-1}.

Hence $$\frac{d\theta}{dt} = \frac{dn_B}{n_t dt} = \frac{LAk_1c_s}{n_t}(1-\theta) - Ak_2'\frac{n_B}{n_t} \qquad A4$$

where n_t is the total number of molecules of B which could be adsorbed on unit area of the electrode surface.

Since $n_B/n_t = \theta$, and in the steady-state $d\theta/dt = 0$, substitution of these values into equation A4 and rearranging gives

$$\theta = \frac{k_1c_s}{k_1c_s + k_2} \qquad A5$$

where $k_2 = k_2' n_t/L$ and has units of mole s^{-1} cm^{-2}.

Substituting for θ in equation A3 from equation A5 gives

$$\frac{i_c}{nFA} = \frac{k_1c_s(k_2 + k_3c_s)}{k_1c_s + k_2} \qquad A6$$

The process will therefore become first-order when $k_2 \ll k_1c_s$ and $\ll k_3c_s$. Under these conditions we obtain

$$\frac{i_c}{nFA} = k_3 c_s \ .$$

From equation A5 it follows that for θ to be large $k_1 c_s$ must be much larger than k_2. This is likely to apply at negative potentials (since k_1 will increase but k_2 remain constant as the potential is made more negative) or at high concentrations. Similarly for θ to be small, $k_1 c_s$ must be much smaller than k_2. This is likely at positive potentials and in dilute solutions. As $\theta \longrightarrow 1$, equation A3 shows that $i_c \longrightarrow nFAk_3 c_s$ while as $\theta \longrightarrow 0$, $i_c \longrightarrow nFAk_1 c_s$.

2) <u>For mechanism (1) + (2b)</u>

An analogous treatment to that given above gives

$$\frac{i_c}{nFA} = k_1 c_s (1 - \theta) + k_4 c_s \theta \qquad \text{A7}$$

and

$$\frac{d\theta}{dt} = k_1 c_s (1 - \theta) - k_2 \theta - k_4 c_s \theta = 0$$

Consequently

$$\theta = \frac{k_1 c_s}{k_1 c_s + k_2 + k_4 c_s} \qquad \text{A8}$$

and

$$\frac{i_c}{nFA} = \frac{k_1 c_s (k_2 + 2k_4 c_s)}{k_1 c_s + k_2 + k_4 c_s} \qquad \text{A9}$$

APPENDIX 3

Method used to obtain k_1

3(a) Initially α is determined in $nFAk_1 = k_1^{\ddagger} \exp -\alpha f F$, where $f = \frac{F}{RT}$, then $k_1^{\ddagger}$ is obtained.

We start with equation A6, i.e.

$$\frac{i_c}{nFA} = \frac{k_1 c_s (k_2 + k_3 c_s)}{k_1 c_s + k_2} \qquad A6$$

which on rearrangement gives

$$c_s + \frac{k_2}{k_1} = \frac{nFAk_2 c_s}{i_c} + \frac{k_3 c_s^2}{i_c} nFA \qquad A10$$

As shown previously

$$c_s = \left(\frac{i_d - i_m}{i_d}\right) c_T = \frac{i_d^m - i_c}{i_d} c_T$$

where i_d^m $(= i_d - i_d^d)$ is the diffusion limited value of the current for monomer reduction,

i_d is the total diffusion limited current,

and c_T is the total CrVI concentration in the bulk of the solution.

Substituting for c_s in equation A10 gives

$$\left(\frac{i_d^m - i_c}{i_d}\right) c_T + \frac{k_2}{k_1} = \frac{nFAk_2(i_d^m - i_c)}{i_c i_d} c_T + \frac{nFAk_3(i_d^m - i_c)^2}{i_c i_d^2} c_T^2$$

Multiplying by $\frac{i_d}{c_T}$ and rearranging gives

$$nFAk_2 \left(\frac{i_d}{nFAk_1c_T} + 1 - \frac{i_d^m}{i_c}\right) = \frac{nFAk_3c_T}{i_d}\frac{(i_d^m - i_c)^2}{i_c} - (i_d^m - i_c)$$

$$= \frac{nFAk_3c_s}{i_c}(i_d^m - i_c) - (i_d^m - i_c)$$

$$= (i_d^m - i_c)\left(\frac{k_3^{\ddagger}c_s}{i_c} - 1\right)$$

$$= a \qquad \text{A11}$$

Knowing k_3, a can be evaluated at each potential. If at a potential E_1 the values of a and i_c are a_1 and i_1 while at $(E_1 - \Delta E)$ they are a_2 and i_2, and at $(E_1 - 2\Delta E)$ they are a_3 and i_3, then the corresponding forms of equation A11 become

$$nFAk_2 \left(\frac{i_d}{c_Tk_1^{\ddagger}\exp-\alpha n_a FE_1} + 1 - \frac{i_d^m}{i_1}\right) = a_1 \qquad \text{A12}$$

$$nFAk_2 \left(\frac{i_d}{c_Tk_1^{\ddagger}\exp-\alpha n_a f(E_1-\Delta E)} + 1 - \frac{i_d^m}{i_2}\right) = a_2 \qquad \text{A13}$$

$$nFAk_2 \left(\frac{i_d}{c_Tk_1^{\ddagger}\exp-\alpha n_a f(E_1-2\Delta E)} + 1 - \frac{i_d^m}{i_3}\right) = a_3 \qquad \text{A14}$$

Dividing A12 by A13, eliminates $nFAk_2$ and on multiplying out gives

$$a_2 + \frac{a_2i_d}{c_Tk_1^{\ddagger}\exp-\alpha n_a fE_1} - \frac{a_2i_d^m}{i_1} = a_1 + \frac{a_1i_d}{c_Tk_1^{\ddagger}\exp-\alpha n_a f(E_1-\Delta E)} - \frac{a_1i_d^m}{i_2}$$

Rearranging gives

$$a_2 - a_1 + i_d^m \left(\frac{a_1}{i_2} - \frac{a_2}{i_1}\right) = \frac{i_d}{c_T k_1^{\ddagger}} \left(a_1 \exp \alpha n_a f(E_1 - \Delta E) - a_2 \exp \alpha n_a f E_1\right) \quad A15$$

Similarly, dividing A12 by A14, multiplying out and rearranging gives

$$a_3 - a_1 + i_d^m \left(\frac{a_1}{i_3} - \frac{a_3}{i_1}\right) = \frac{i_d}{c_T k_1^{\ddagger}} \left(a_1 \exp \alpha n_a f(E_1 - 2\Delta E) - a_3 \exp \alpha n_a f E_1\right) \quad A16$$

Dividing A15 by A16 eliminates $k_1^{\ddagger}$ and exp $\alpha n_a f E_1$, to give

$$\frac{(a_2 - a_1) + i_d^m \left(\frac{a_1}{i_2} - \frac{a_2}{i_1}\right)}{(a_3 - a_1) + i_d^m \left(\frac{a_1}{i_3} - \frac{a_3}{i_1}\right)} = \frac{a_1 \exp -\alpha n_a f \Delta E - a_2}{a_1 \exp -2\alpha n_a f \Delta E - a_3}$$

$$\therefore \quad a_1 \exp -2\alpha n_a f \Delta E \left[(a_2 - a_1) + i_d^m \left(\frac{a_1}{i_2} - \frac{a_2}{i_1}\right)\right] - a_3 a_2 + a_1 a_3 - a_3 i_d^m \left(\frac{a_1}{i_2} - \frac{a_2}{i_1}\right) =$$

$$a_1 \exp -\alpha n_a f \Delta E \left[(a_3 - a_1) + i_d^m \left(\frac{a_1}{i_3} - \frac{a_3}{i_1}\right)\right] - a_3 a_2 + a_1 a_2 - a_2 i_d^m \left(\frac{a_1}{i_3} - \frac{a_3}{i_1}\right)$$

Dividing by a_1 and rearranging gives

$$\exp-2\alpha n_a f\Delta E\ [(a_2 - a_1) + i_d^m\ (\frac{a_1}{i_2} - \frac{a_2}{i_1})] + (a_3 - a_2) + i_d^m\ (\frac{a_2}{i_3} - \frac{a_3}{i_2})$$

$$= \exp-\alpha n_a f\Delta E\ [(a_3 - a_1) + i_d^m\ (\frac{a_1}{i_3} - \frac{a_3}{i_1})]$$

i.e. $L \exp-2\alpha n_a f\Delta E + M = N \exp-\alpha n_a f\Delta E$

where $L = [(a_2 - a_1) + i_d^m\ (\frac{a_1}{i_2} - \frac{a_2}{i_1})]$

$M = [(a_3 - a_2) + i_d^m\ (\frac{a_2}{i_3} - \frac{a_3}{i_2})]$

$N = [(a_3 - a_1) + i_d^m\ (\frac{a_1}{i_3} - \frac{a_3}{i_1})]$

$$\therefore \quad \exp-2\alpha n_a f\Delta E + \frac{M}{L} = (\exp-\alpha n_a f\Delta E)\ \frac{N}{L} \qquad \text{A17}$$

Thus values of $\frac{M}{L}$ and $\frac{N}{L}$ can be obtained corresponding to different values of E_1.

A graph of $\frac{M}{L}$ against $\frac{N}{L}$ should have slope = $\exp-\alpha n_a f\Delta E$ and intercept (when $\frac{N}{L} = 0$) = $-\exp-2\alpha n_a f\Delta E$.

3 (b) The value of α may now be confirmed and k_1^* determined by the following procedure.

Equation A15 may be rewritten as

$$(a_2 - a_1) + i_d^m\ (\frac{a_1}{i_2} - \frac{a_2}{i_1}) = \frac{i_d}{c_T k_1^*}\ \exp\alpha n_a fE\ (a_1 \exp-\alpha n_a f\Delta E - a_2)$$

i.e. $$L = \frac{i_d}{c_T k_1^*}\ \exp\alpha n_a fE\ (a_1 \exp-\alpha n_a f\Delta E - a_2)$$

$$\therefore \quad \log \frac{L}{(a_1 \exp -\alpha n_a f \Delta E - a_2)} = \log \frac{i_d}{c_T k_1^{\ddagger}} + \frac{\alpha f E}{2.303}$$

$$\text{i.e.} \quad \log \frac{L}{X} = \log \frac{i_d}{c_T k_1^{\ddagger}} + \frac{\alpha f E}{2.303} \qquad \text{A18}$$

$\therefore$ a graph of $\log \frac{L}{X}$ against E should be linear with slope $= \frac{\alpha f}{2.303}$ and when E = 0.0 V, $\frac{L}{X} = \frac{i_d}{c_T k_1^{\ddagger}}$.

REFERENCES

CHAPTER 1

1.1 J. D. Neus and W. Reiman III, J. Amer. Chem. Soc., 56, 2238 (1934).

1.2 W. G. Davies and J. E. Prue, Trans. Far. Soc., 51, 1045 (1955).

1.3 H. G. Linge and A. L. Jones, Aust. J. Chem., 21, 1445 (1968).

1.4 J. Y. Tong and E. L. King, J. Amer. Chem. Soc., 75, 6180 (1953).

1.5 J. Y. Tong, Inorg. Chem., 3, 1804 (1964).

1.6 G. P. Haight Jr., D. C. Richardson and N. H. Coburn, Inorg. Chem., 3, 1777 (1964).

1.7 J. R. Howard, U. S. K. Nair and G. H. Nancollas, Trans. Far. Soc., 54, 1034 (1958).

1.8 J. J. Lingane and I. M. Kolthoff, J. Amer. Chem. Soc., 62, 852 (1940).

1.9 J. H. Green and A. Walkley, Aust. J. Chem., 8, 51 (1955).

1.10 J. J. Tondeur, A. Dombret and L. Gierst, J. Electroanal. Chem., 3, 225 (1962).

1.11 N. V. Nickolaeva-Fedorovich, G. E. Titova and N N. Zung, Elektrokhimiya, 4, 392 (1968).

1.12 R. M. Issa, B. A. Abd-el-Nabey and H. Sadek, Electrochim. Acta, 13, 1827 (1968).

1.13 H. Fiegl and C. A. Knorr, Z. Elektrochem, 63, 239 (1959).

1.14 E. Müller, Z. Elektrochem., 49, 16 (1943).

1.15 H. Gerischer and M. Käppel, Z. Elektrochem., 61, 463 (1957).

1.16 D. Reinkowski and C. A. Knorr, Z. Elektrochem., 58, 709 (1954).

1.17 R. Weiner, Metalloberfläche, 14, 7 (1960).

1.18 I. M. Kolthoff and A. M. Shams El Din, J. Phys. Chem., 60, 1564 (1956).

1.19 H. Okada, K. Nakamura and T. Ishida, Nature, 185, 377 (1960).

1.20 H. Feigl, L. Kandler and I. Reinhold, Metalloberfläche, 17, 229 (1963).

1.21 A. N. Sysoev, N. T. Drobahtseva and O. A. Platonina, Zh. Priklad. Khim., 33, 372 (1960).

1.22 R. Weiner and C. Schiele, Z. Phys. Chem. N.F., 26, 248 (1960).

1.23 I. V. Sternberg and V. S. Bagotskii, Dok. Akad. Nauk. SSSR, 115, 568 (1957).

1.24 E. Liebreich, Z. Elektrochem., 27, 94 (1921).

1.25 M. Kabasakaloglu and S. Üneri, Comm. Faculte Sciences de l'Universite D'Ankara, 14B, 59 (1967).

1.26 M. Kabasakaloglu and S. Üneri, Comm. Faculte Sciences de l'Universite D'Ankara, 15B, 5 (1968).

1.27 R. Weiner and C. Schiele, Metalloberfläche, 14, 357 (1960).

1.28 J. C. Saiddington and G. R. Hoey, J. Electrochem. Soc., 117, 1011 (1970).

1.29 H. Okada and K. Yamamoto, Electrochem. Technology, 6, 389 (1968).

1.30 Z. A. Soloveva, Yu. S. Petrova and N. L. Klimasenko, Zh. Priklad. Khim., 35, 1806 (1962).

1.31 H. Gerischer and M. Käppel, Z. Elektrochem., 64, 235 (1960).

CHAPTER 2

2.1 P. Delahay, "Double Layer and Electrode Kinetics", Interscience (1954).

2.2 S. Glasstone, K. J. Laidler and H. Eyring, "The Theory of Rate Processes", McGraw-Hill (1941) p. 516.

2.3 A. C. Riddiford in "Advances in Electrochemistry and Electrochemical Engineering", Vol. 4, Ed. P. Delahay, Interscience (1966).

2.4 D. P. Gregory and A. C. Riddiford, J. Chem. Soc., 3756 (1956).

2.5 P. Delahay, "New Instrumental Methods in Electrochemistry", Interscience (1954), p. 92.

CHAPTER 3

3.1 D. H. Angell, Ph.D. Thesis, Newcastle University, 1968.

3.2 O. R. Brown, Electrochim. Acta, 13, 317 (1968).

3.3 A. C. Riddiford in "Advances in Electrochemistry and Electrochemical Engineering", Vol. 4, Ed. P. Delahay, Interscience (1966) p.47.

3.4 J. Newman, J. Electrochem. Soc., 113, 501 (1966).

3.5 D. H. Angell, T. Dickinson and R. Greef, Electrochim. Acta, 13, 120 (1968).

3.6 S. Popoff, A. H. Kunz and R. D. Snow, J. Phys. Chem., 32, 1056 (1928).

3.7 R. W. Powers, General Electric Research Lab. Report No. 63-RL-(3128M) 1963.

3.8 P. A. Thiessen and K. Herrman, Z. Elektrochem., 43, 66 (1937).

CHAPTER 4

4.1 D. L. Fuhrman and G. W. Latimer, Jnr., Talanta, 14, 1199 (196).

4.2 J. Y. Tong and E. L. King, J. Amer. Chem. Soc., 75, 6180 (1953).

CHAPTER 5

5.1 G. Armstrong, F. R. Himsworth and J. A. V. Butler, Proc. Roy. Soc. (London), A143, 89 (1934).

5.2 G. Deborin and B. Ershler, Acta. Physicochim., 13, 347 (1940).

5.3 A. Hickling, Trans. Faraday Soc., 42, 518 (1946).

5.4 S. E. S. El Wakkad and A. M. Shams El Din, J. Chem. Soc., 3098 (1954).

5.5 K. J. Vetter and D. Berndt, Z. Elektrochem., 62, 378 (1958).

5.6 D. Clark, T. Dickinson and W. N. Mair, Trans. Faraday Soc., 55, 1937 (1959).

5.7 F. G. Will and C. A. Knorr, Z. Elektrochem., 64, 270 (1960).

5.8 H. A. Laitinen and M. S. Chao, J. Electrochem. Soc., 108, 726 (1961).

5.9 S. B. Brummer and A. C. Makrides, J. Electrochem. Soc., 111, 1122 (1964).

5.10 G. Gruneberg, Electrochim. Acta, 10, 339 (1965).

5.11 G. M. Schmid and R. N. O'Brien, J. Electrochem. Soc., 111, 832 (1964).

5.12 R. S. Sirohi and M. A. Genshaw, J. Electrochem. Soc., 116, 910 (1969).

5.13 W. E. Reid and J. Kruger, Nature, 203, 402 (1964).

5.14 J. P. Hoare, Electrochim. Acta, 9, 1289 (1964).

5.15 J. P. Hoare, J. Electrochem. Soc., 110, 245 (1963).

5.16 T. Takamura, K. Takamura, N. Nippe and E. Yeager, J. Electrochem. Soc., 117, 62 5 (1970).

CHAPTER 6

6.1 F. Scheller, R. Landsberg and H. Wolf, Z. Phys. Chem., 243, 345 (1970).

CHAPTER 7

7.1 G. Mamantov, D. B. Freeman, F. J. Miller and H. E. Zittel, J. Electroanal. Chem., 9, 305-310 (1965).

7.2 R. E. Panzer and P. J. Elving, J. Electrochem. Soc., 119, 865 (1972).

7.3 H. H. Bauer, M. S. Spritzer and P. J. Elving, J. Electroanal. Chem., 17, 299 (1968).

7.4 F. J. Miller and H. F. Zittel, Anal. Chem., 35, 1866 (1963).

7.5 J. P. Randin and E. Yeager, J. Electrochem. Soc., 118, 711 (1971).

7.6 J. P. Randin and E. Yeager, J. Electroanal. Chem., 36, 257 (1972).

7.7 M. J. P. Brennan and O. R. Brown, J. Applied Electrochem., 2, 43 (1972).

7.8 I. Morcos and E. Yeager, Electrochim. Acta, 6, 953 (1970).

7.9 H. E. Zittel and F. J. Miller, Analyt. Chem., 37, 200 (1965).

CHAPTER 8

8.1 T. Dickinson, R. Greef and W. F. K. Wynne-Jones, Electrochim. Acta, 14, 467 (1969).

8.2 M. Spiro, Electrochim. Acta, 9, 1531 (1964).

8.3 B. E. Conway and J. J. MacDonald, Proc. Roy. Soc., A269, 419 (1962).

ACKNOWLEDGEMENTS

I wish to offer my sincere thanks to my supervisor, Dr. T. Dickinson, for his encouragement and help with this work.

I should also like to thank the Ministry of Defence (Admiralty) for financing the project, and Miss Heather B. Carr who typed the thesis.